



**HAL**  
open science

# Réponse des sols et des structures aux séismes : des données pour mieux estimer le risque

Clotaire Michel

► **To cite this version:**

Clotaire Michel. Réponse des sols et des structures aux séismes : des données pour mieux estimer le risque. Géophysique [physics.geo-ph]. Communauté Université Grenoble Alpes, 2017. tel-01505738

**HAL Id: tel-01505738**

**<https://theses.hal.science/tel-01505738>**

Submitted on 11 Apr 2017

**HAL** is a multi-disciplinary open access archive for the deposit and dissemination of scientific research documents, whether they are published or not. The documents may come from teaching and research institutions in France or abroad, or from public or private research centers.

L'archive ouverte pluridisciplinaire **HAL**, est destinée au dépôt et à la diffusion de documents scientifiques de niveau recherche, publiés ou non, émanant des établissements d'enseignement et de recherche français ou étrangers, des laboratoires publics ou privés.

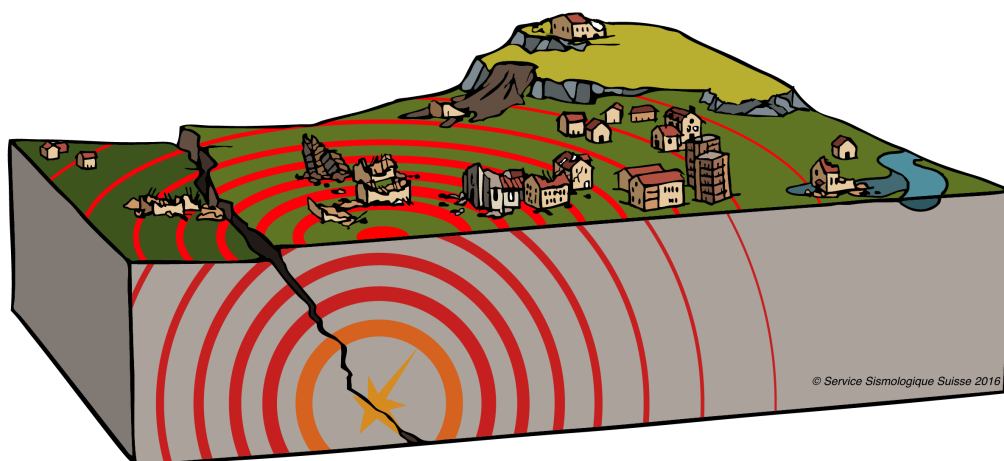
---

# Réponse des sols et des structures aux séismes : des données pour mieux estimer le risque

Habilitation à Diriger les Recherches

Université de Grenoble - Sciences de la planète

---



**Clotaire MICHEL**

Soutenue le 3 janvier 2017 à Grenoble devant le jury composé de :

**Frédéric Dufour**

**Françoise Courboux**

**Fabrice Cotton**

**Guido De Roeck**

**Helle Pedersen**

**Professeur INP Grenoble**

**Directeur de recherche Géoazur Nice**

**Professeur GFZ Potsdam**

**Professeur KU Leuven**

**Physicien OSUG Grenoble**

**Président du jury**

**Rapporteur**

**Rapporteur**

**Rapporteur**

**Examineur**

# Table des matières

<b>Introduction</b>	<b>4</b>
<b>1 Avancées dans l'estimation des effets de site</b>	<b>6</b>
1.1 Enregistrer le mouvement sismique . . . . .	7
1.1.1 Avant l'instrumentation sismologique . . . . .	7
1.1.2 Premières estimation de l'accélération . . . . .	7
1.1.3 Débuts de l'accélérométrie . . . . .	8
1.1.4 L'accélérométrie moderne . . . . .	9
1.1.5 L'accélérométrie en France et en Suisse . . . . .	10
1.1.6 Futur de l'accélérométrie . . . . .	10
1.2 Prédire le mouvement sismique . . . . .	11
1.2.1 Mesures d'intensité du mouvement du sol . . . . .	11
1.2.2 Modèles de prédiction du mouvement sismique . . . . .	12
1.3 Effets de la géologie locale sur le mouvement sismique et leur estimation . . . . .	15
1.4 Extraire l'effet de la géologie locale des enregistrements de séismes (Edwards <i>et al.</i> , 2013) . . . . .	19
1.5 Extraire l'effet de la géologie locale des enregistrements de vibrations ambiantes (Michel <i>et al.</i> , 2014a) . . . . .	32
1.6 Combiner la caractérisation géophysique des sites aux observations sous séisme pour cartographier l'amplification (Michel <i>et al.</i> , 2016) . . . . .	51

1.7	Perspectives . . . . .	66
<b>2</b>	<b>Avancées dans la compréhension de la réponse des structures de génie civil aux séismes</b>	<b>68</b>
2.1	Enregistrer les vibrations des structures . . . . .	68
2.2	Prédire le mouvement des structures sous séisme : Problématique . . . . .	70
2.3	Comprendre le comportement linéaire des structures . . . . .	71
2.3.1	Comportement des bâtiments et point de départ linéaire pour l'analyse de vulnérabilité sismique . . . . .	71
2.3.2	Comportement des ponts et identification structurale sous vibrations ambiantes . . . . .	72
2.4	Comprendre le comportement non-linéaire des structures . . . . .	73
2.4.1	Chute de fréquence sous séisme (Michel <i>et al.</i> , 2011b) . . . . .	74
2.4.2	Déplacement maximal sous séisme (Michel <i>et al.</i> , 2014b) . . . . .	90
2.5	Perspectives . . . . .	110
<b>3</b>	<b>Données sismologiques pour l'analyse post-sismique</b>	<b>111</b>
3.1	La multidisciplinarité en mission post-sismique . . . . .	112
3.2	Contribution de l'enregistrement de vibrations ambiantes en mission post-sismique (Régnier <i>et al.</i> , 2013) . . . . .	113
3.3	Analyse post-sismique rapide grâce à l'instrumentation de bâtiments (Goulet <i>et al.</i> , 2015) . . . . .	121
3.4	Perspectives . . . . .	137
	<b>Conclusions et perspectives générales</b>	<b>138</b>
	<b>Activités scientifiques</b>	<b>141</b>
	Encadrement d'étudiants . . . . .	141
	Enseignement et formations . . . . .	141

<i>TABLE DES MATIÈRES</i>	3
Responsabilités administratives . . . . .	142
Autres activités . . . . .	142
Publications . . . . .	142
<b>Remerciements</b>	<b>148</b>
<b>Bibliographie</b>	<b>148</b>
<b>Annexe : le spectre de réponse</b>	<b>155</b>

# Introduction

L'invention de la sismologie est intimement liée à l'avènement des premiers instruments permettant d'enregistrer les vibrations du sol, à la fin du XIX<sup>e</sup> siècle. Cependant, il existait alors déjà une large connaissance des tremblements de terre, de leurs effets et des moyens de s'en protéger, peu à peu organisée en savoir scientifique, notamment par Robert Mallet (1810-1881). La sismologie de l'ingénieur est née de la volonté de quantifier l'amplitude des mouvements du sol, à travers la mesure et la modélisation, pour une utilisation rationnelle des protections contre les tremblements de terre, en particulier dans la construction. Cette volonté s'est exprimée parallèlement au développement de l'instrumentation sismologique, notamment par John Milne (1850-1913). Après lui, de nombreux scientifiques, en particulier au Japon et en Californie (on peut citer notamment Fusikachi Omori, John Freeman, Mishio Ishimoto, Georges Housner, Kiyoshi Kanai, Mihailo Trifunac) ont développé de l'instrumentation, collecté et interprété des enregistrements de vibrations du sol et de structures (fortes et faibles) et proposé des méthodes de prédiction des mouvements forts et de la réponse des structures de génie civil à ces mouvements.

Les modèles empiriques font aujourd'hui peu à peu place à des modèles fondés sur la physique, sur des domaines de plus en plus grands et sur des maillages de plus en plus petits, grâce à l'augmentation de la puissance de calcul et l'optimisation des algorithmes. En parallèle, le déploiement de nouveaux réseaux, les améliorations dans la chaîne d'acquisition des données, des capacités de stockage et de communication et les grands projets de collaboration dans la communauté scientifique mettent à disposition des quantités de données en augmentation exponentielle. L'avènement, voire la banalisation de la modélisation numérique en dynamique du sol et des structures ne doit cependant pas faire oublier, d'une part, que son objectif primaire est d'être en mesure de reproduire les observations et, d'autre part, que les nombreux paramètres d'entrée nécessaires à une telle modélisation seront choisis de manière bien plus adéquate après une campagne de mesure *in situ* qu'à la lecture d'une table de valeurs génériques issue d'une compilation d'autres sites. En effet, en géosciences, mais aussi en génie civil, les **propriétés mécaniques** de nombreux matériaux mais aussi la **géométrie** des structures sont très incertaines, voire inconnues et doivent donc être mesurées. Il ne s'agit pas (seulement) d'améliorer la précision des modèles de prédiction mais bien de leur permettre de livrer les bons ordres de grandeur, il en va donc de leur pertinence même. Enfin, si des modèles entièrement basés sur la physique des phénomènes sont souhaitables puisqu'ils sont les seuls à permettre une extrapolation objective à des situations qui ne se sont jamais produites, les modèles « empiriques », combinant physique des phénomènes et observations sous forme statistique sont toujours nécessaires. Ils sont en général plus simples à mettre en œuvre, moins précis mais souvent plus justes et permettent des calculs sur des domaines plus grands, avec plus d'éléments.

L'objectif de ma recherche est de proposer de nouvelles méthodes pour intégrer des observations sismologiques dans des modèles de prédiction du mouvement du sol et de la réponse des structures puis d'appliquer ces méthodes à des cas réels, typiques, afin de diriger les recherches méthodologiques

futures vers les maillons de la chaîne de l'analyse du risque qui peuvent bénéficier d'améliorations. Il s'agit également, suite à un événement destructeur, de comprendre l'origine des dommages observés et d'aider à l'analyse de la sécurité à court et à long terme.

Un objectif supplémentaire de ce document est de rendre accessible les problématiques actuelles de la sismologie de l'ingénieur et de la dynamique des structures à un plus large public et d'améliorer la compréhension mutuelle entre ces deux disciplines.

Il est structuré en trois parties : l'étude des effets de la géologie locale sur l'amplification des ondes sismiques, l'étude de la réponse des structures de génie civil, en particulier les bâtiments et enfin la sismologie de l'ingénieur dans le contexte de l'après-séisme. Chaque partie contient une sélection de deux à trois articles en anglais publiés dans des revues scientifiques, ainsi qu'un résumé en français des principales idées contenues dans chaque article. La première partie détaille l'histoire de l'observation des mouvements forts, quelques repères à propos de leur modélisation, en particulier en ce qui concerne les effets de site puis les approches que j'ai suivies pour améliorer leur connaissance : sous séisme et à l'aide de mesures géophysiques ainsi que la comparaison de ces deux approches. La deuxième partie propose également deux sections introductives sur l'enregistrement en structure et la modélisation de leur mouvement puis deux sections de recherche personnelle : sur le comportement dynamique linéaire puis non-linéaire des structures. La troisième partie introduit tout d'abord le contexte des missions post-sismiques puis les études que j'ai réalisées avec des données sismologiques pour comprendre les dommages et aider à la détermination de l'habitabilité. Chaque partie comporte un paragraphe détaillant les perspectives de ces recherches et le document se termine par des perspectives générales sur les recherches que je souhaite mener dans les années à venir concernant l'analyse du risque sismique.

# Chapitre 1

## Avancées dans l'estimation des effets de site

Un aspect fondamental pour l'estimation du risque sismique est la prédiction de l'amplitude des mouvements du sol redoutés que l'on désigne généralement par le terme d'aléa sismique. Le dimensionnement des constructions neuves et l'analyse sismique du bâti existant se fondent sur le mouvement sismique du sol attendu avec une certaine probabilité. Pour l'analyse du risque sismique, la connaissance de l'aléa est aussi un préalable. Or, le mouvement sismique dépend de la source, de la propagation des ondes et de l'effet de la géologie de subsurface sur le mouvement sismique. Nous nous intéressons ici plus particulièrement à ce dernier avec pour objectifs de montrer que de grandes quantités de données locales peuvent et doivent être collectées et de proposer des méthodes et des procédures pour les utiliser au mieux, c'est-à-dire pour déterminer les paramètres nécessaires et suffisants pour estimer l'amplification des ondes sismiques par la géologie locale. Contrairement à la source sismique, ces « effets de site » sont relativement bien compris depuis plusieurs décennies mais la quantification de leur variabilité a été négligée faute de données suffisantes.

Pour comprendre le contexte et les enjeux de la problématique des effets de site, l'histoire et l'état de l'art des enregistrements de mouvements forts sont tout d'abord présentés puis la thématique de la prédiction du mouvement sismique et des effets de site. Nous proposons ensuite une nouvelle méthode pour extraire l'amplification due à la géologie de surface à partir d'enregistrements de séismes sur le réseau suisse (article Edwards *et al.*, 2013). Cette méthode est complémentaire de l'analyse géophysique de la sub-surface qui permet également de mesurer les propriétés physiques du sous-sol afin de prédire son effet sur le mouvement sismique. Nous avons montré la convergence de ces deux approches et fait ressortir quelles étaient les propriétés importantes à déterminer pour évaluer les effets de site (article Michel *et al.*, 2014a). Enfin, la grande quantité de données disponible dans la région de Bâle (Suisse) est revisitée à travers ces approches afin de proposer un modèle d'amplification à haute résolution (article Michel *et al.*, 2017a).



## 1.1 Enregistrer le mouvement sismique

### 1.1.1 Avant l'instrumentation sismologique

Le mouvement sismique constitue la partie sensible des « tremblements de terre », ce que chacun peut observer, mais aussi la principale source de dégâts aux constructions et donc de victimes (75% des décès lors de tremblements de terre sur la période 1900-1999 sont dus à l'effondrement de bâtiments (Coburn et Spence, 2002)). C'est pourquoi les premières études scientifiques des tremblements de terre se sont intéressées aux effets des secousses, au premier rang desquels on trouve les dommages aux constructions (bâtiments, monuments), mais aussi le ressenti des personnes, les effets sur les objets et les effets sur l'environnement (fissures dans le sol, liquéfaction, etc.). Les premières collectes de données sur les effets des secousses que l'on peut qualifier de scientifiques remontent au milieu du XVIII<sup>e</sup> siècle, notamment suite aux séismes de Lima 1746, Lisbonne 1755 et de Calabre 1783 (Guidoboni et Ebel, 2009). Cette dernière étude dirigée par Michele Sarcone (1731-1797) est la première pour laquelle une commission d'experts relèvent exhaustivement les dégâts aux bâtiments. L'intensité des secousses a ensuite été formalisée à l'aide d'échelles « d'intensité macrosismique » afin de la quantifier. La première est généralement attribuée à Egen (1828) créée pour le séisme de Tienen-Tirlemont (Belgique) (Gisler *et al.*, 2008). De nombreuses autres ont suivi, en particulier celles de Mallet (1862) et de Rossi-Forel (Forel, 1884). Cette dernière est la première utilisée à l'international, proposée par Michele Stefano de Rossi (1834-1898) de Rome (Italie) et François-Alphonse Forel (1841-1912) de Morges (Vaud, Suisse). Cette dernière a ensuite été modifiée plusieurs fois par Giuseppe Mercalli (1850-1914), Adolfo Cancani (1856-1904), August Sieberg (1875-1945) et d'autres, donnant naissance aux échelles MCS, MMI et EMS-98 (Grünthal *et al.*, 1998) utilisées aujourd'hui. Rétrospectivement, les séismes historiques ont ensuite été étudiés à l'aide de ces outils. Ces études ont surtout permis de produire des catalogues de sismicité (date, localisation et estimation de la magnitude) à partir des effets observés.

Pour remonter à l'intensité du mouvement du sol depuis les effets observés, il faut prendre en compte leur fréquence d'occurrence (le témoignage d'une seule personne ne suffit pas) et la vulnérabilité des objets considérés. Ainsi, pour les plus faibles secousses, le ressenti des personnes va dépendre de leur localisation (dans un bâtiment, dehors) et de leur activité (endormi, en mouvement etc.) alors que les dégâts aux constructions va dépendre de leur qualité et de leur sensibilité aux secousses sismique (leur « vulnérabilité sismique »). Seules les échelles les plus récentes, en particulier l'EMS-98, prennent en compte ces facteurs. Cette dernière est la seule à considérer toute la distribution des observations et pas seulement les effets les plus forts. Quoi qu'il en soit, l'intensité macrosismique ne peut informer sur les secousses que de manière grossière et en moyenne sur une grande surface (en général une commune). L'intensité macrosismique ne permet pas de remplacer la mesure directe des vibrations du sol.

### 1.1.2 Premières estimation de l'accélération

Alors que la sismologie de l'ingénieur a pour but d'étudier les caractéristiques des mouvements forts, la sismologie « classique » s'intéresse à la source des tremblements de terre et à l'utilisation des ondes sismiques pour déterminer les propriétés de l'intérieur de la Terre. C'est pourquoi les sismographes développés à partir de 1841 (Ben-Menahem, 1995) ont pour objectif d'enregistrer des mouvements du sol d'origine lointaine de plus en plus faibles mais ils « saturent » lorsque ceux-ci deviennent violents : en particulier, le stylet chargé de transcrire le mouvement casse. Les ingénieurs du génie civil expriment la nécessité dès la fin du XIX<sup>e</sup> siècle de connaître les valeurs des forces d'inertie qui s'appliquent sur les

structures (bâtiments, ponts, barrages. . .) lors d'un fort tremblement de terre, et donc de l'accélération du sol, afin de calculer la taille et la résistance des éléments stabilisateurs à intégrer dans leurs structures (Freeman, 1932).

Les premiers sismographes, mécaniques, permettaient d'enregistrer les déplacements du sol. Cependant, pour les ingénieurs et les sismologues de l'époque, c'est l'accélération horizontale du sol qui contrôle les forces qui s'appliquent sur une structure et donc les dommages. Au Japon, dès 1884, Milne et Sekiya estiment l'accélération  $A$  du sol à partir du déplacement  $D$  mesuré par leur sismographe en supposant un mouvement harmonique ( $A = \omega^2 D$ ) (Otani, 2008). Ils estiment la période des ondes destructrices entre 0.5 et 1 s en comptant les passages à zéro sur les sismogrammes. Holden (1888) utilise les valeurs fournies par ces chercheurs pour établir une conversion entre l'intensité macrosismique (échelle Rossi-Forel) et l'accélération du sol, exprimée en fraction de l'accélération de la gravité  $g$ . De nombreuses autres relations semblables, aujourd'hui appelées *Ground Motion to Intensity Conversion Equation* (GMICE) suivront.

Outre le déplacement des sismographes, Milne s'appuie sur les dimensions de murs ayant basculé, ou non, lors d'un séisme pour estimer l'accélération du sol à partir d'une formule simple, dite formule de West (Otani, 2008). Kikuchi (1904) affirme que le premier enregistrement *strong motion* a été effectué par Fusakichi Omori (1868-1923) le 20 juin 1894 avec un sismographe « mouvement fort » à Tokyo lors d'un séisme ayant fait des dégâts mineurs. L'accélération maximale aurait atteint  $0.4 \text{ m/s}^2$ . Cependant, la majorité des ingénieurs reste sceptique quant à l'intérêt pratique d'estimer les forces à attendre lors d'un tremblement de terre jusqu'à la fin des années 1920 et peu de développements ont lieu (Trifunac, 2009).

### 1.1.3 Début de l'accélérométrie

En 1931, soit près de 45 ans après l'enregistrement d'Omori, l'américain Freeman et le japonais Suyehiro s'étonnent que l'accélération durant les forts tremblements de terre n'ait toujours pas été mesurée directement et décident de lancer un projet à l'*U.S. Coast and Geodetic Survey* (USCGS) pour créer un instrument capable de cette mesure (Brady, 2009; Trifunac, 2009). En parallèle, au Japon, Mishio Ishimoto (1892-1940) développe également un accélérographe en 1931. Les sismographes mécaniques permettent, en théorie tout du moins, de livrer l'accélération du sol en dessous de leur fréquence de résonance qui dépend de la masse et du ressort utilisés. Durant le projet de l'USCGS, des modifications du sismomètre Wood-Anderson sont réalisées notamment afin d'augmenter sa fréquence de résonance, ce qui aboutit à l'accélérographe standard de l'USCGS (Brady, 2009). Il faut cependant noter que la gamme d'amplitudes pouvant être enregistrée reste limitée, par la sensibilité de l'instrument d'une part et par la taille du support d'écriture d'autre part. Ces limitations sont toujours valables pour les accéléromètres digitaux aujourd'hui (bruit instrumental et *full-scale recording range*). Le déploiement de cet accélérographe en Californie en 1932 porte ses fruits dès 1933 : les premiers enregistrements de l'histoire de l'accélérométrie sont obtenus au cours du séisme de 1933 à Long Beach (magnitude 6.4), près de Los Angeles où 3 stations avaient été installées. L'accélération du sol la plus forte mesurée (*Peak Ground Acceleration* PGA) est alors de  $2.8 \text{ m/s}^2$  (après corrections intervenant dans les années 1970). En 1940, l'un de ces accélérographes enregistre le séisme d'Imperial Valley à El Centro à proximité (17 km) de la faille à l'origine du tremblement de terre de magnitude 6.9. Cet enregistrement, d'une valeur maximale de  $3.6 \text{ m/s}^2$ , sera le plus utilisé pour la modélisation dynamique des structures en génie parasismique. Il n'est pas rare de trouver, 75 ans après, des études utilisant encore cet enregistrement malgré sa qualité limitée (c'est seulement le sixième enregistrement accélérométrique de l'histoire) par rapport aux enregistrements modernes. Ces enregistrements cali-

forniens sont particulièrement utilisés par la communauté grâce à leur diffusion libre via les rapports de l'Earthquake Engineering Research Laboratory (EERL) dans les années 1970, ce qui n'est pas la politique de toutes les institutions. Le Japon ne déploiera ses premiers accélérographes qu'à partir de 1952 (Trifunac, 2009) mais exploite aujourd'hui le réseau plus important et celui livrant le plus données de mouvements forts dans le monde. La Nouvelle-Zélande lancera à son tour un réseau au milieu des années 1960 (Trifunac, 2009).

#### 1.1.4 L'accélérométrie moderne

La qualité d'une station accélérométrique est déterminée par la résolution des données enregistrées et la dynamique de l'instrument (rapport entre le mouvement le plus fort et le plus faible potentiellement enregistrés). Le mouvement le plus fort pouvant être enregistré par une station accélérométrique est défini par l'utilisateur (*full-scale recording range*). Une étape cruciale dans l'amélioration de la qualité des données enregistrées a été le passage progressif d'enregistrements analogiques à des enregistrements numériques dans les années 1980. Le numérique a permis une amélioration déterminante de la dynamique des enregistrements. Dès lors, les objectifs de l'accélérométrie ont été étendus : les instruments sont en mesure d'enregistrer des séismes locaux de faible magnitude (de l'ordre de 3 et supérieure) et peuvent donc être déployés dans des zones à sismicité modérée afin de collecter des données avant un possible séisme destructeur. La numérisation des accélérogrammes analogiques a été un casse-tête dans les années 1970 aux Etats-Unis, ainsi, on a par la suite privilégié l'installation d'un grand nombre d'instruments numériques, considérant que la masse de données ainsi collectées rendrait rapidement les anciennes données analogiques inutiles. On peut cependant noter que certains accélérographes (analogiques) ont continué à opérer jusque dans les années 2000.

Un palier dans la qualité des instruments a été atteint au début des années 2000, notamment avec l'accéléromètre FBA Episensor de Kinematics et les numériseurs 24 bits. Dès lors, des efforts ont été entrepris pour remplacer les anciens instruments, passer à l'enregistrement, à la transmission et au contrôle continu, vérifier et améliorer leur installation (encastrement, en anglais *housing*) et surtout mieux caractériser leur site d'implantation (voir partie 1.5). Avec ces stations installées la plupart du temps dans des zones urbaines, les vibrations ambiantes du sol sont enregistrées au dessus d'environ 1 Hz (bruit instrumental pour les fréquences plus basses) et donc tous les événements dépassant le niveau des vibrations ambiantes sont enregistrés dans la gamme de fréquence la plus importante pour la sismologie urbaine (1-10 Hz). L'augmentation exponentielle des données collectées par les réseaux accélérométriques est donc due à la densification des réseaux, à l'augmentation de la dynamique des instruments et, à partir du milieu des années 2000, au passage progressif aux enregistrements continus qui ont permis de ne manquer aucun événement et de contrôler le bon fonctionnement des appareils en temps réel. Cette explosion des données ne doit cependant pas cacher que ce sont essentiellement des données de séismes faibles qui sont collectées par ces réseaux.

Si le développement de modèles de prédiction du mouvement du sol constitue l'application la plus importante des enregistrements accélérométriques comme détaillé dans la partie 1.2, elle n'est de loin pas la seule. Les enregistrements en champ libre sont utilisés pour l'étude de la réponse de modèles dynamiques de structures de génie civil, l'inversion de la source sismique (détermination de l'histoire de la rupture d'une faille lors d'un grand séisme) ou encore la localisation d'événements.

### 1.1.5 L'accélérométrie en France et en Suisse

En France, les premiers accélérographes ont été installés en Guadeloupe en 1977 par le Service Géologique des Antilles mais sans permettre d'enregistrement jusqu'en 1984 conduisant à une restructuration du réseau (Bertil, 2013). Le premier enregistrement de mouvement fort en France est celui d'un séisme de magnitude 6.5 enregistré en Guadeloupe en 1985 à 115 km de l'épicentre avec une accélération maximale de  $2.2 \text{ m/s}^2$  dans le quartier Bergevin à Pointe-à-Pitre (enregistrement aujourd'hui disparu). Hormis une réplique de ce séisme, aucun autre événement n'est enregistré jusqu'en 1994 et le déploiement d'un réseau digital plus sensible (Bertil, 2013). En métropole, les premiers instruments (digitaux) ont été installés dans les Alpes à partir de 1994 à la faveur des améliorations techniques décrites précédemment. Le Réseau Accélérométrique Permanent (RAP) s'est ensuite structuré en 2000 autour de réseaux régionaux pilotés par les différents acteurs de la sismologie de l'ingénieur et centralisé par l'Observatoire de Grenoble, chargé notamment de l'archivage et de la distribution des données. Outre les Antilles, des sous-réseaux sont également déployés en Nouvelle-Calédonie et à Mayotte depuis 2006. Le réseau compte environ 150 stations sur le territoire national. Les principales données de mouvements forts ont été enregistrées lors des séismes des Saintes (Guadeloupe, 21/11/2004, magnitude 6.4) et de Nord-Martinique (29/11/2007, magnitude 7.3) (Schlupp *et al.*, 2008).

Les premières stations accélérométriques en champ libre sont installées en Suisse en 1989 en guise de test par des compagnies privées et le Service Sismologique Suisse (Smit, 1996). Le pays décide l'installation d'un réseau accélérométrique en 1990 et en confie la réalisation au Service Sismologique Suisse qui débute en 1991 avec une première station dans la zone épiscopale du séisme de Vaz-Obervaz du 20/11/1991 ( $M_w=4.7$ ) et dure 2 ans pour l'installation de 41 stations numériques en mode déclenché. Le Swiss Strong Motion Network (SSMNet) a ensuite été étendu progressivement à la faveur de différents projets européens et nationaux (Clinton *et al.*, 2011). A partir de 2005, des stations modernes comprenant un numériseur 24 bits enregistrant et envoyant les données en continu et temps réel et accéléromètres de grande dynamique, sont installées. En 2009, un projet de renouvellement et d'extension du réseau s'est donné pour objectif d'installer 100 nouvelles stations modernes et en champ libre dans tout le pays en 10 ans. J'ai mené à bien la première phase de ce projet avec l'installation de 30 nouvelles stations (voir partie 1.5) et participe activement à la seconde phase. En 2019, le réseau devrait compter près de 150 stations, ce qui en fait depuis quelques années l'un des réseaux nationaux les plus denses du monde. Les données de mouvements réellement forts ( $PGA > 1 \text{ m/s}^2$ ) sont cependant rares : il s'agit d'un enregistrement de la station SLTM (Linthal GL) d'un séisme de magnitude 3.4 et de 3 km de profondeur dont l'épicentre était situé à moins de 1 km (17/03/2001, PGA de  $2.1 \text{ m/s}^2$ ) et des enregistrements du séisme de Vallorcine ( $M_w=4.4$ , 08/09/2005) aux stations SMAV (PGA de  $1.3 \text{ m/s}^2$ ) et EMV (accéléromètre, le capteur large-bande ayant saturé) située à 3 km de l'épicentre (PGA de  $0.9 \text{ m/s}^2$ ). Cependant, l'intérêt d'un tel réseau ne se limite de loin pas aux mouvements forts et l'exploitation des enregistrements de séismes faibles (magnitude 2.5 et supérieure), potentiellement ressentis par la population, permet d'améliorer notre compréhension du mouvement sismique et de sa prédiction (voir partie 1.4 et suivantes). Une vingtaine se produit en Suisse chaque année. Par ailleurs, par sa densité, il est complémentaire du réseau large bande pour la localisation de ces événements et d'événements plus petits.

### 1.1.6 Futur de l'accélérométrie

Pour l'enregistrement de mouvements forts, il existe une forte complémentarité entre l'accélérométrie et le GPS. Si un accéléromètre bien implanté permet d'enregistrer ces mouvements jusqu'à de

très basses fréquences, l'enregistrement simultané des données GPS permet d'étendre cette bande de fréquence jusqu'au déplacement statique. Dans Psimoulis *et al.* (2014), nous avons comparé les données accélérométriques et de stations GPS pour le séisme de Tohoku de 2011 (Mw=9.0) et montré que les données GPS permettait d'obtenir les paramètres dont la sismologie de l'ingénieur a besoin pour les périodes de 3 s et plus. Les données GPS montrent ainsi parfaitement l'amplification des ondes à longue période dans les grands bassins sédimentaires du Japon. Les instruments colocalisés restent cependant rares mais devraient se multiplier dans les zones à forte sismicité.

Les réseaux accélérométriques se développent désormais plus lentement et se situent plutôt dans une phase de consolidation. A l'avenir, il seront sans doute complétés par des réseaux plus denses de capteurs à bas-coûts, notamment les systèmes microélectromécaniques (MEMS). De nombreuses applications de tels réseaux déployés dans les zones urbaines sont envisageables (voir par exemple Bowden *et al.* (2015) et l'application en structures que nous avons proposée dans Goulet *et al.* (2015), partie 3.3).

## 1.2 Prédire le mouvement sismique

### 1.2.1 Mesures d'intensité du mouvement du sol

Si les instruments permettent d'enregistrer les formes d'ondes complètes, il est naturel d'essayer de caractériser ce mouvement par des paramètres plus simples. Ces paramètres, appelés mesures d'intensité (IM pour *Intensity Measure* en anglais) ou encore indicateurs de nocivité, servent de mesure pour classer les mouvements enregistrés et pour prédire les mouvements redoutés. Une mesure d'intensité est particulièrement intéressante si elle peut être utilisée comme paramètre d'entrée pour un modèle (simplifié) de structure de génie civil. Si les formes d'ondes complètes sont utiles pour les analyses dynamiques (linéaires ou non-linéaires), la plupart des modèles utilisés pour le dimensionnement ou l'analyse du bâti existant sont fondés sur ces mesures d'intensité.

La mesure la plus naturelle est l'accélération maximale du sol ou Peak Ground Acceleration (PGA). Selon les auteurs, il peut s'agir du maximum des composantes horizontales, du maximum de la norme L2 des formes d'onde (racine carrée de la somme des carrés) ou du maximum obtenu par rotation des enregistrements horizontaux. Elle est exprimée en  $\text{m/s}^2$  (unités SI), mais on la trouve souvent exprimée en  $g$  ( $1 g = 9.81 \text{ m/s}^2$ ), en  $\text{cm/s}^2$ , ou en gal ( $1 \text{ gal} = 1 \text{ cm/s}^2$ ). Le PGA est aussi la mesure la plus utilisée en ingénierie malgré ses inconvénients : elle n'est, en particulier, représentative que du mouvement sismique à haute fréquence.

La vitesse maximale du sol (Peak Ground Velocity PGV) obtenue après intégration des accélérogrammes est une mesure qui est bien corrélée avec les dommages observés et donc avec l'intensité macrosismique (Faenza et Michellini, 2010; Lesueur *et al.*, 2013). En conséquence, elle est utilisée comme paramètre physique principal pour les ShakeMaps (Worden *et al.*, 2010; Cauzzi *et al.*, 2015), ce qui a provoqué un récent regain d'intérêt pour cette mesure au sein de la communauté travaillant sur les mouvements forts. Elle est donnée en  $\text{m/s}$  (unités SI), mais on la trouve souvent exprimée en  $\text{cm/s}$ .

Le déplacement maximal du sol (Peak Ground Displacement PGD) est encore peu utilisé et en général approximé par le spectre de réponse en déplacement à 10 s (DRS(10 s) ou SD(10 s), voir paragraphe suivant) (Cauzzi et Faccioli, 2008). Outre le fait que ce paramètre est peu pertinent pour

les séismes modérés (magnitude inférieure à 7), il est difficile à obtenir à l'aide d'enregistrements accélérométriques qui doivent être exempts de bascule (*tilt*). En revanche, il peut être obtenu à l'aide d'enregistrements GPS pour les plus gros événements (Psimoulis *et al.*, 2014).

Le spectre de réponse (voir annexe) est construit à partir de la valeur maximale atteinte par des oscillateurs linéaires à un degré de liberté à différentes périodes  $T$  et un amortissement donné  $\xi$  et soumis au mouvement sismique considéré. On considère le plus souvent le spectre de réponse en accélération SA (en fait souvent le pseudo-spectre PSA, voir annexe), mais aussi en déplacement SD, plus rarement en vitesse. Le premier est défini comme l'accélération maximale absolue de l'oscillateur (et inclue donc l'accélération du sol) et les deux autres comme le déplacement et la vitesse maximaux relatifs de l'oscillateur. Ils sont exprimés dans les unités d'accélération, de déplacement et de vitesse comme détaillé précédemment. En termes simples, ces mesures constituent une bonne approximation de la réponse maximale linéaire attendue pour des bâtiments ayant les périodes de résonance  $T$  et l'amortissement  $\xi$ . Si l'on suppose que la structure se déforme selon son mode fondamental uniquement, le spectre de réponse en déplacement correspond à sa déformation, le spectre de réponse en accélération correspond au coefficient sismique, c'est-à-dire à la force élastique qui s'applique sur la structure, mais aussi à la valeur maximale enregistrée par un accéléromètre situé au sommet de la structure. Le spectre de réponse a été proposé par Biot en 1932 mais n'a été réellement utilisé en génie parasismique qu'à partir des années 1970 (Trifunac, 2008). Une valeur d'amortissement de  $\xi = 5\%$  est arbitrairement le plus souvent utilisée. Elle correspond à ce que le génie parasismique considère historiquement comme la valeur correspondant aux structures de génie civil bien que cette question soit largement débattue.

D'autres mesures d'intensité qui expliquent mieux la réponse des structures ont été proposées. Certains auteurs s'intéressent en particulier à l'intensité d'Housner modifiée qui consiste en la moyenne du spectre de réponse entre deux périodes, par exemple la période fondamentale de la structure et un multiple de celle-ci (p. ex. De Biasio *et al.*, 2014). Elle trouve une application en particulier lorsque des spectres réalistes (et non des spectres de Newmark, c.-à-d. des spectres de normes) sont utilisés, pour lesquels l'accélération spectrale peut fortement varier d'une période à l'autre.

## 1.2.2 Modèles de prédiction du mouvement sismique

Le mouvement sismique, qui dépend à la fois du temps et de l'espace, doit être simplifié pour permettre des calculs. La discrétisation de l'espace est généralement imposée par le problème étudié (analyse d'un barrage, d'un ensemble de bâtiments ou encore d'une région représentée par une grille régulière). En ce qui concerne l'aspect temporel, si l'idéal est d'utiliser des formes d'ondes complètes, elles imposent des coûts de calculs assez importants et ce d'autant plus qu'une analyse probabiliste, nécessaire car deux événements ne sont jamais identiques, impose la prise en compte de nombreuses formes d'ondes. C'est pourquoi l'aspect temporel du mouvement sismique est généralement réduit à une seule mesure d'intensité ou, plus rarement, à un vecteur de mesures. Chaque mesure d'intensité peut être considérée comme une variable aléatoire prenant en compte les caractéristiques de la source sismique (localisation, magnitude, radiation...), de sa propagation dans la croûte (atténuations géométrique et anélastique) et les effets de la géologie locale (effets de sites).

L'atténuation de l'amplitude du mouvement du sol avec la distance est connue depuis les débuts des observations de tremblements de terre. En revanche, on peut associer la première modélisation de cette atténuation à la définition de la magnitude par Richter (1935). Il remarque en effet que le logarithme de l'amplitude des ondes mesurées en fonction de la distance représente des courbes parallèles pour chaque séisme. Il définit la magnitude comme  $M = \log(A) + 3 \log(D) - 3.37$ , avec  $A$

l'amplitude maximale en mm sur le sismographe Wood-Anderson et  $D$  la distance en km. Si on inverse cette relation, on peut prédire l'amplitude (la vitesse) à partir de la magnitude et de la distance. On notera cependant la circularité de ce raisonnement, seulement récemment complètement rompue par l'utilisation de la magnitude de moment à la place de la magnitude locale (dite de Richter). Les premières équations de prédiction de l'accélération du sol à partir de la magnitude sont proposées dans les années 1960 (Douglas et Edwards, 2016). Les données enregistrées deviennent ainsi le fondement de nombreuses études statistiques permettant de développer des relations empiriques adaptées à différents contextes et régions du globe (voir [www.gmpe.org.uk](http://www.gmpe.org.uk)). Outre la magnitude et la distance, ces relations dépendent également d'autres paramètres définissant la source (en général le type de faille) et du site (classe de sol ou  $V_{s,30}$ , voir partie 1.3). Les réseaux accélérométriques ont donc permis grâce à leurs enregistrements, de développer ce qu'on appelait des « lois d'atténuation », terme aujourd'hui abandonné pour le terme « relation de prédiction du mouvement du sol » (*Ground Motion Prediction Equation* GMPE en anglais).

Des centaines de modèles prédisant le logarithme de différentes mesures d'intensité  $Y$  avec leurs incertitudes  $\sigma$  ont été publiés (Douglas et Edwards, 2016) et ont généralement la forme suivante (Edwards et Fäh, 2014) :

$$\ln(Y) = f_{Source}(M) + f_{propagation}(M, R) + f_{site}(V_{s,30}, \dots) + \epsilon\sigma$$

avec  $f_{Source}$  une fonction représentant la source sismique et dépendant de  $M$  la magnitude, en général la magnitude de moment  $M_w$ ;  $f_{propagation}$  une fonction représentant l'atténuation notamment en fonction de  $R$  la distance à la source (de nombreuses définitions possibles);  $f_{site}$  une fonction du site;  $\epsilon\sigma$  représente la variabilité. Elles concernent le plus souvent le PGA et le spectre de réponse à différentes périodes pour un amortissement de 5% pour le mouvement horizontal (p. ex. Akkar *et al.*, 2014b). Le mouvement vertical est quant à lui le plus souvent prédit à travers son rapport avec le mouvement horizontal (rapport V/H) (p. ex. Akkar *et al.*, 2014a). L'incertitude qui est associée à ces relations est l'écart-type du logarithme, c'est-à-dire que le mouvement sismique est implicitement considéré comme suivant une loi lognormale. Cet écart-type correspond à l'incertitude aléatoire (variabilité) mais n'inclue pas les incertitudes épistémiques, liées aux hypothèses de la modélisation. De plus en plus, la corrélation des incertitudes entre les différentes périodes (p. ex. Akkar *et al.*, 2014a) et entre les différentes distances (corrélation spatiale) sont également estimées (Esposito et Iervolino, 2012). Ces valeurs sont nécessaires pour une estimation probabiliste rigoureuse des dommages et du risque sismique.

**Modèles empiriques** Les modèles développés à partir d'une régression statistique des observations sont dits empiriques. Les régressions sont fondées sur des fonctions relativement simples, souvent polynomiales, mais en général sans lien avec la physique des phénomènes.

Ainsi,  $f_{Source}$  est souvent un polynôme du second degré en  $M$  ajouté à une constante dépendant du type de faille. Les modèles utilisant une fonction linéaire en  $M$  sont désormais considérés comme obsolètes (Edwards et Fäh, 2014), en particulier car ils ne permettent pas de bien représenter à la fois les petits et les grands séismes. La constante associée au type de faille est plus grande pour les failles inverses et plus petite pour les failles normales.

$f_{propagation}$  est plus débattue dans la littérature. Elle comprend une somme de l'atténuation géométrique (répartition de l'énergie dans l'espace à mesure de la propagation) et de l'atténuation anélastique (pertes d'énergies). L'atténuation géométrique est typiquement une fonction linéaire de la magnitude multipliée au logarithme de la distance. L'atténuation anélastique est typiquement proportionnelle à la distance. Le champ proche (courtes distances) est parfois traité séparément.

$f_{site}$  est traité de manière différente par chaque auteur, ce qui ne permet pas de comparaison d'un modèle à l'autre. La prise en compte de la géologie locale reste en général simpliste et se limite à la classe de sol ou à la valeur  $V_{s,30}$  (voir partie 1.3), faute d'une caractérisation systématique et précise des sites d'implantations de stations accélérométriques. L'atténuation anélastique de la géologie locale est rarement prise en compte explicitement (Douglas et Edwards, 2016). Pourtant, l'effet de la géologie locale sur le mouvement sismique, en comparaison des termes de source et de propagation, est relativement accessible grâce à la possibilité de mesurer les propriétés de la sub-surface à l'aide de méthodes géophysiques à la surface ou en forage (voir partie 1.3). Cette prise en compte simpliste conduit à une augmentation évitable des incertitudes des modèles de prédiction et permet plus difficilement de prédire la répartition spatiale du mouvement sismique, largement contrôlée par la géologie locale.

Comme ces modèles sont fondés sur une régression statistique et non sur la physique, ils ne peuvent être utilisés pour prédire le mouvement sismique en dehors des gammes de valeurs de paramètres (magnitude, distance,  $V_{s,30}$ ) pour lesquelles ils ont été développés.

**Modèles simulés** Les modèles dits « simulés » sont fondés sur un modèle physique de la source sismique et permettent de générer les formes d'ondes complètes, pas seulement leurs mesures d'intensité. Si les modèles numériques peuvent être utilisés pour des scénarios donnés afin d'estimer ces formes d'ondes (p. ex. Baumann et Dalguer, 2014), le spectre de Fourier d'un enregistrement (en accélération, vitesse ou déplacement) constitue une grandeur plus facile à modéliser de manière physique. A partir du spectre de Fourier, des accélérogrammes synthétiques peuvent être générés à l'aide d'un signal avec des phases aléatoires. Ces modèles sont alors dits « stochastiques ». Le spectre de réponse peut même être directement calculé sans passer par les accélérogrammes grâce à la *Random Vibration Theory* (voir Edwards et Fäh, 2014). Des modèles de prédiction du mouvement du sol peuvent donc être générés à partir de ces méthodes dès que les paramètres d'entrée du modèle sont contrôlés par des données objectives. Une question centrale vient de l'estimation des incertitudes qui peut être réalisée à partir des incertitudes sur les paramètres d'entrée (et de leur covariance) ou à partir des résidus des valeurs médianes par rapport aux observations (voir Edwards et Fäh, 2014).

Si l'on exclut les simulations numériques, le modèle de source le plus souvent utilisé est le modèle de Brune (1970) qui utilise notamment comme paramètres le moment sismique, la fréquence-coin (qui permettent de calculer la chute de contrainte) et le coefficient de radiation (point source). Différentes méthodes existent pour simuler une source étendue. La modélisation de l'atténuation est simple au premier ordre : l'atténuation géométrique s'effectue en  $1/R$  (sphère) et l'atténuation anélastique est une exponentielle décroissante dépendant de la fréquence et du facteur  $\kappa$ . Cependant, ces modèles peuvent être affinés et calibrés selon les régions, la distance et le site. C'est pour la modélisation de l'effet de la géologie locale que les méthodes simulées apportent le plus d'avantages. En effet, outre les simulations numériques, les effets de sites sont généralement modélisés par une fonction de transfert qui peut être naturellement multipliée au spectre de Fourier simulé. Cette fonction d'amplification peut être obtenue par modélisation spectrale (voir partie 1.4) ou par estimation de la réponse des sites à partir de données géophysiques (voir partie 1.5).

La modélisation numérique de la propagation des ondes dans la croûte terrestre et à la subsurface est de plus en plus accessible en 3D grâce à l'optimisation des méthodes de calcul et l'augmentation de la puissance de calcul. Les fréquences atteintes dépendent de la taille de la maille et le mouvement sismique doit en général être combiné avec une méthode stochastique qui apporte les hautes fréquences (typiquement au-delà de quelques hertz) (voir Douglas et Edwards, 2016). Ces modèles sont également limités par la quantité et la qualité des informations sur les sites étudiés : la géométrie des couches et leur rigidité (voir partie 1.3 et 1.5).



Afin de bien prendre en compte les effets de site, le site de référence doit être bien défini (p. ex. Poggi *et al.*, 2011). Une problématique actuellement déterminante pour la modélisation du mouvement sismique est de savoir comment transposer des modèles obtenus pour une région à une autre région avec des sites de référence différents, c'est-à-dire avec des caractéristiques de rigidité de la croûte et d'atténuation anélastique différents (ajustements  $V_s$ - $\kappa$ ). Une difficulté majeure vient de l'incertitude d'estimation de l'atténuation représentée par le paramètre  $\kappa$ , qui intègre en outre des effets sur le trajet des ondes et de la géologie locale (Edwards *et al.*, 2015). Plus généralement, la thématique de la dépendance régionale des modèles est toujours d'actualité.

Enfin, la prédiction probabiliste simultanée de plusieurs mesures d'intensité du mouvement du sol ou la prédiction en des points distribués dans l'espace, conduit à s'intéresser à des distributions à plusieurs variables. Il s'agit donc de travailler sur la corrélation entre les incertitudes de ces équations de prédiction. Elles ont un impact sur l'étude du risque sismique, où plusieurs mesures d'intensité en plusieurs sites sont calculées pour calculer le risque porté par un ensemble d'éléments (bâtiments, infrastructures, biens mobiliers...).

### 1.3 Effets de la géologie locale sur le mouvement sismique et leur estimation

Les premiers sismologues avaient déjà reconnu l'importance du sous-sol sur l'amplitude du mouvement sismique. Ainsi, John Milne note après le séisme de Nohbi (Nagoya, Japon) en 1891 que les bâtiments situés sur les sols mous, c'est-à-dire en général les plaines, ont plus souffert que ceux situés sur des sols plus compacts, par exemple sur les collines (Field, 1996; Otani, 2008). Les différents phénomènes physiques qui expliquent les « effets de site » sont les suivants :

- la diminution de la vitesse de propagation des ondes vers la surface augmente, par conservation de l'énergie, son amplitude ;
- un contraste de rigidité (c.-à-d. de vitesse de propagation) important entre une couche superficielle et le rocher sous-jacent empêche les ondes de quitter la couche superficielle, les piégeant et augmentant ainsi l'amplitude et la durée à des fréquences particulières (résonance 1D) ;
- dans certaines conditions, le même effet peut se produire dans des structures géologiques 2D/3D générant la résonance de toute la structure avec des amplitudes encore plus fortes (résonance 2D/3D) ;
- certaines géométries locales (p. ex. bord de bassin) peuvent favoriser la génération et le piégeage d'ondes de surface qui contribuent à augmenter l'amplitude et la durée du mouvement sismique.

L'atténuation anélastique, c'est-à-dire les pertes d'énergie en particulier dans les sous-sols plus mous, ne permet en général pas de compenser ces phénomènes d'amplification et a un effet seulement à haute fréquence. La topographie (géométrie locale et/ou résonance) joue également un rôle dans le mouvement sismique mais de second ordre par rapport à la présence de couches géologiques de faible vitesse comme l'ont montré Burjánek *et al.* (2014). On trouve donc en premier lieu de forts effets de site là où existent des contrastes de vitesse importants comme dans les bassins sédimentaires récents (p. ex. Fig. 1.1), avec des facteurs pouvant atteindre 20 par rapport au rocher sain. Cependant, des amplifications non négligeables, avec des facteurs 2 à 3 peuvent aussi avoir lieu sur des sites composés de roches altérées : la Fig. 1.2 montre l'amplification maximale entre les stations du réseau large-bande suisse (SDSNet) composé de stations « au rocher » calculée avec la méthode décrite dans la partie 1.4. Comme on peut s'y attendre, cette amplification maximale décroît avec la période (les longues

périodes traversent une croûte relativement homogène à l'échelle du pays). Pourtant cette amplification atteint toujours un facteur 5 à une période de 2s. Par ailleurs, dans les couches non-consolidées, lors de mouvements forts, on peut observer un comportement non-linéaire qui, selon les cas, peut diminuer ou augmenter l'amplitude du mouvement du sol et créer d'autres désordres comme la liquéfaction.

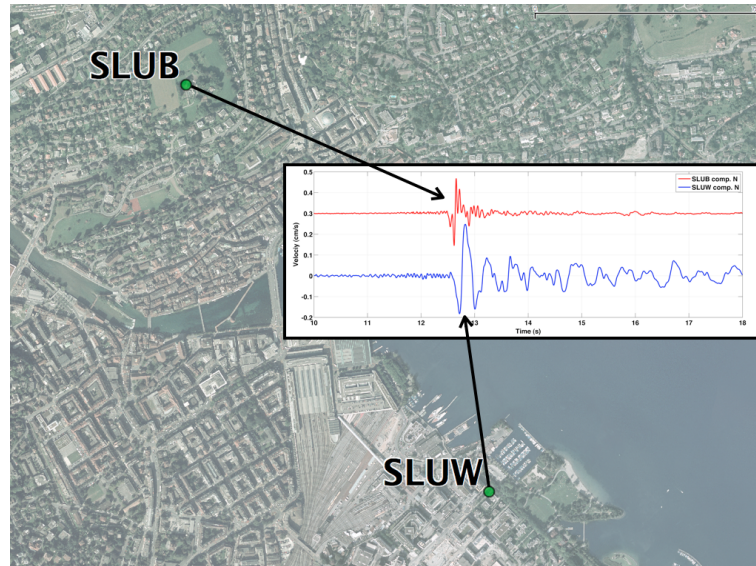


**Figure 1.1** – Sismogrammes du séisme de Zoug (11/02/2012  $M_L = 4.2$ ) enregistrés à Lucerne à 21 km de l'épicentre par deux stations installées lors de la phase 1 du renouvellement du SSMNet (voir partie 1.5). Les accélérogrammes ont été intégrés en vitesse afin de bien montrer les ondes de surface générées à la station SLUW. SLUB est située sur une colline au rocher (équivalent au rocher suisse de référence), SLUW au coeur du bassin sédimentaire du lac des Quatre-Cantons.

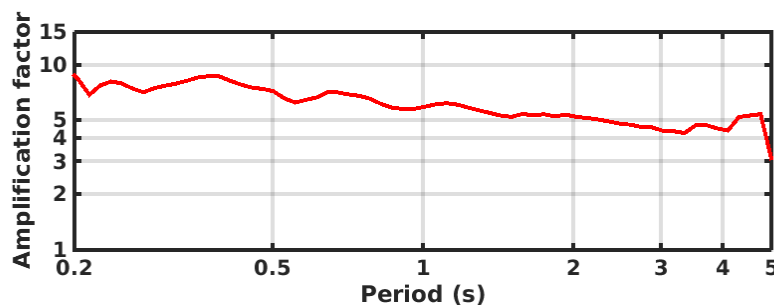


**Figure 1.2** – Amplification maximale entre les stations dites « au rocher » du réseau large-bande suisse (SDSNet) calculées à partir de la méthode ESM (voir partie 1.4).

Hormis la non-linéarité des sols, qui n'est pas traitée dans ce document, les phénomènes d'effets de site sont bien connus et modélisés avec des méthodes plus ou moins complexes. Cependant, dans la plupart des cas, les données d'entrée collectées localement manquent pour pouvoir proposer des estimations réalistes. Ces données sont constituées de la répartition spatiale de la vitesse des ondes S, des ondes P, de la densité et du facteur de qualité. Selon la géométrie, la répartition avec la profondeur peut suffire (profil 1D), pour les sites les plus complexes, la géométrie 2D voire 3D peut être nécessaire. Un rocher géophysique, en dessous duquel cette géométrie a une influence négligeable pour les estimations liées au risque, peut en général être défini. Son interface avec les couches sus-jacentes est à l'origine de la fréquence fondamentale de résonance du site. Dans la partie 1.5, nous proposons et validons une

procédure qui fournit les vitesses des ondes P et S sur un profil 1D et permet de déterminer si des effets 2D/3D ont lieu.

Un aspect important lorsque l'on définit l'amplification des ondes sismiques due à la géologie locale est de définir une référence. Cette référence peut être définie localement par le choix d'un site « au rocher » ou à partir d'un profil de vitesse des ondes S générique (ou d'une valeur unique). Dans nos travaux, les amplifications ont toujours pour référence le modèle suisse de Poggi *et al.* (2011) défini à partir de 27 sites instrumentés et caractérisés (Fig. 1.3). Il a pour vitesse moyenne sur les 30 premiers mètres  $V_{s,30}=1100$  m/s, ce qui correspond à un rocher altéré du plateau molassique suisse. Par comparaison, le rocher « ingénieur » équivaut en général à une vitesse de 800 m/s et certaines références pour l'aléa de centrales nucléaires à 2000 voire 3000 m/s. Les amplifications correspondantes ne peuvent donc pas être comparées directement (voir partie 1.4 pour la correction).

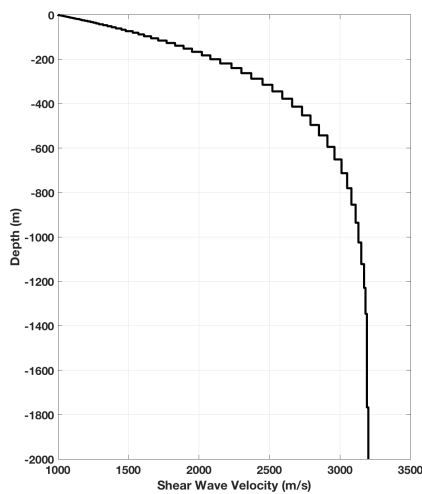


**Figure 1.3** – Profil de vitesse des ondes S en profondeur du rocher de référence pour la Suisse défini par Poggi *et al.* (2011).

Les propriétés moyennes des terrains traversés par les ondes sismiques peuvent être très différentes selon les longueurs d'onde de ces ondes. Les effets de site sont donc intrinsèquement dépendants de la fréquence. Pourtant, par souci de simplification ou par manque de données, ils sont souvent pris en compte à l'aide de paramètres uniques, qui ne peuvent rendre compte que partiellement de cette dépendance à la fréquence. Le premier type de paramètres consiste en une classification géologique ou géotechnique (classes de sol), utilisée notamment pour les normes de construction. Le second type de paramètre simple est la vitesse moyenne des ondes S sur les Z premiers mètres, Z étant souvent égal à 30 m ( $V_{s,30}$ ). La fréquence fondamentale du site  $f_0$  peut aussi être utilisée comme paramètre explicatif de l'amplification, souvent en combinaison avec  $V_{s,Z}$ .

Les informations géologiques et topographiques permettent de classer les terrains sur une grande échelle, en fonction de leur susceptibilité à amplifier le mouvement sismique. En particulier, la corrélation entre la pente des terrains et le paramètre  $V_{s,30}$  a montré des résultats intéressants en Californie (Wald et Allen, 2007), mais une faible corrélation en Europe (Lemoine *et al.*, 2012). Pour quantifier l'amplification, des mesures géophysiques ou géotechniques sont absolument nécessaires. La fréquence de résonance du site est le paramètre le plus accessible car il peut être obtenu à l'aide d'enregistrements de quelques dizaines de minutes de vibrations ambiantes à l'aide d'une seule station sismique et de la technique des rapports spectraux H/V (Nakamura, 1989). La vitesse des ondes S en profondeur (profil ou valeur moyenne  $V_{s,Z}$ ), en revanche, demande des mesures sismiques actives ou passives, à la surface ou en forage avec plusieurs capteurs. Dès lors que ces mesures sont disponibles, il est regrettable de se contenter d'un seul paramètre comme  $V_{s,30}$ .

On peut classer les mesures géophysiques par le type de source qu'elles utilisent (active ou passive), la nécessité ou non d'un ou plusieurs forages (invasive ou non invasive) ou encore par le fait qu'elles utilisent les ondes de volume ou les ondes de surface (Fig. 1.4). Les mesures passives non-invasives présentent l'intérêt de leur simplicité et de leur faible coût de mise en œuvre. Le *benchmark* INTERPacific a montré que la reproductibilité des profils de vitesse obtenus n'était pas supérieure avec les méthodes invasives, malgré leur coût élevé, par rapport aux méthodes de surface (Garofalo *et al.*, 2016a,b). La sismique en forage est plus précise pour définir les interfaces importantes mais les incertitudes liées aux vitesses sont similaires à celles des méthodes de surface (Garofalo *et al.*, 2016b). Par ailleurs, les méthodes invasives avec un seul forage ne permettent de déterminer les propriétés du sous-sol qu'en un point précis alors que les méthodes non-invasives opèrent naturellement une moyenne de ces propriétés sur un volume du sous-sol, comme le font les ondes sismiques.

L'analyse des ondes de surface est complémentaire de l'analyse des ondes de volume. Ces dernières nécessitent une source active qui doit être très puissante pour atteindre de grandes profondeurs. Par ailleurs, la résolution spatiale (horizontale et verticale) dépend du nombre de capteurs. Un grand nombre rend ces mesures rapidement coûteuses. Seuls les temps d'arrivée sont utilisés en général, mais les formes d'onde complètes peuvent aujourd'hui également être inversées. Le problème inverse est le plus souvent linéarisé et relativement simple à résoudre si l'on suppose des variations de vitesses continues. Les ondes de surface, notamment celles composant les vibrations ambiantes, échantillonnent le sous-sol jusqu'à de grandes profondeurs. La profondeur maximale obtenue ne dépend alors que de la taille du réseau de stations utilisé. Les techniques permettant de déterminer leurs caractéristiques de dispersion (ondes de Love et de Rayleigh) et d'ellipticité (ondes de Rayleigh) sont nombreuses : analyse fréquence nombre d'onde (FK) et ses dérivés (Poggi et Fäh, 2010), corrélation et ses dérivés (SPAC, Bettig *et al.*, 2001), inversion complète du champ d'onde (WaveDec, Maranò *et al.*, 2012 ; MUSIQUE Hobiger *et al.*, 2016). Pour l'analyse des ondes de surface, le seul avantage des mesures actives (MASW, Park *et al.*, 1999) sur les mesures passives est d'apporter de l'énergie à haute fréquence qui peut manquer dans les vibrations ambiantes afin de mieux résoudre les couches les plus superficielles. Une fois ces propriétés déterminées, le problème inverse est plus complexe à résoudre à cause de la non-unicité de la solution et du nombre de paramètres à inverser (Wathelet, 2008). Il est donc souvent limité à une seule dimension spatiale et nécessite de faire des hypothèses simplificatrices, en particulier en ce qui concerne la présence de zones à faible vitesse en profondeur. Mon travail est principalement fondé sur l'analyse des ondes de surface des vibrations ambiantes (mesures passives) et décrit dans la partie 1.5.

Les vibrations ambiantes du sol sont composées essentiellement d'ondes de surface, Love et Rayleigh dans des proportions variables d'un site à l'autre. Elles sont créées par des phénomènes naturels pour les fréquences inférieures à 1 Hz et par les activités humaines pour les plus hautes fréquences (Bonney-Claudet *et al.*, 2006). Le premier et le second pics microsismiques, à des périodes de 5 et 15 s, ainsi que *hum* à une période de 30 s et plus, sont produits par l'interaction entre les vagues océaniques et la croûte terrestre et sont observables sur la Terre entière. Arduin *et al.* (2015) ont explicité les mécanismes générant ces vibrations : le mécanisme générant le premier pic microsismique, lié à l'interaction entre les vagues, est différent de celui générant les vibrations à plus longues périodes (interaction avec le fond océanique). Les activités humaines génèrent des vibrations ambiantes avec un pic autour de 10-20 Hz, d'amplitude de plusieurs ordres de grandeurs aux vibrations naturelles dans les zones urbaines. En dehors de ces sources principales, d'autres sources peuvent localement avoir un effet important. Quoi qu'il en soit, des vibrations ambiantes peuvent être enregistrées partout et dans toutes les bandes de fréquences à l'aide de sismomètres. Même si leur origine est inconnue, tant que leur source se situe suffisamment loin du réseau de stations utilisé, on peut supposer qu'il s'agit d'ondes planes et mesurer les différences de phases entre ces ondes enregistrées à différentes stations et donc leur vitesse de propagation dans le milieu à l'aide des méthodes listées dans le paragraphe précédent.

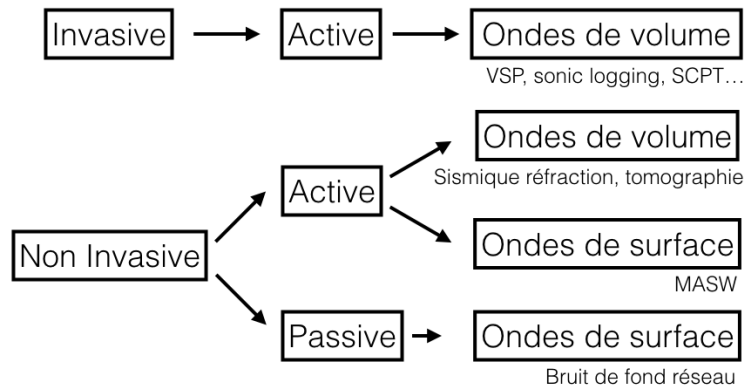


**Figure 1.4** – Classification des mesures géophysiques de sub-surface permettant de déterminer le profil des ondes  $S$  avec exemples (non exhaustif).

Nous avons analysé les ondes de surface des vibrations ambiantes à Bucarest (Roumanie) dans Manea *et al.* (2016) et nous avons montré que l'on pouvait les caractériser avec ces techniques jusqu'à des fréquences très faibles (des périodes longues - ici jusqu'à 7s) afin d'imager la profondeur, pour autant que l'on dispose d'un réseau de stations suffisamment grand (35 km d'ouverture ici). Nous avons ainsi proposé un nouveau modèle de vitesse pour la région de Bucarest qui sera utilisé dans des simulations numériques afin de mieux prédire le mouvement sismique dans la capitale roumaine. Les modèles actuels n'ont en effet permis de reproduire les ondes de surface à basse fréquence générées par les grands séismes, notamment celui de 1977 ( $M=7.4$ ).

## 1.4 Extraire l'effet de la géologie locale des enregistrements de séismes (Edwards *et al.*, 2013)

Dans Edwards *et al.* (2013), nous proposons une procédure d'estimation des effets de site pour chaque site d'implantation d'une station du réseau suisse (accélérométrique et large-bande) à partir des enregistrements de séismes ayant un rapport signal sur bruit suffisant. Cette estimation automatique est continuellement mise à jour dès l'enregistrement de nouveaux événements. Elle permet de déterminer l'amplification par rapport au rocher de référence défini par Poggi *et al.* (2011) (Fig. 1.3).

La méthode est fondée sur la modélisation spectrale des enregistrements à partir d'un modèle simple de source et de propagation comme dans les modèles simulés (partie 1.2.2). Les paramètres de la source (magnitude, chute de contrainte), les amplifications moyennes et l'atténuation anélastique sont ajustés aux données. Pour éviter la compensation de paramètres, l'amplification moyenne a été fixée préalablement à 27 stations du réseau par Poggi *et al.* (2011) qui définissent ainsi le rocher suisse de référence. Les résidus de cette modélisation par rapport aux enregistrements à chaque station constituent l'amplification en fonction de la fréquence. On peut donc ensuite reconstruire l'amplification élastique en multipliant l'amplification moyenne à sa composante dépendant de la fréquence, puis l'amplification anélastique en lui multipliant un terme en exponentielle décroissante fonction du paramètre  $\kappa$ . Une estimation statistique fondée de nombreux événements permet de s'affranchir des effets de sources et d'estimer les incertitudes sur l'amplification.

Dans Edwards *et al.* (2013), nous validons cette approche en la comparant aux rapports spectraux site sur référence, aux rapports H/V et avec la fonction de transfert des ondes SH déterminée à partir de modèles de vitesse 1D (voir aussi les parties 1.5 et 1.6).

# Determination of Site Amplification from Regional Seismicity: Application to the Swiss National Seismic Networks

by Benjamin Edwards, Clotire Michel, Valerio Poggi, and Donat Fäh

*Online Material:* Supplemental figures and tables.

## INTRODUCTION

The propagation of energy released by an earthquake through the uppermost crust has a significant impact on the ground motion that is observed at the surface. Knowledge of this site amplification effect can significantly reduce the uncertainty involved in the determination and application of stochastic or empirical predictive ground-motion equations and therefore reduce the uncertainty in subsequent hazard calculations. However, due to the heterogeneity of the upper crust, the site amplification effect is highly variable over scales of kilometers or less (e.g., Boore, 2004).

It is important to characterize site amplification at seismic instrument locations in order to correct or account for data from several recording sites, such that a common reference (e.g., Poggi *et al.*, 2011) is defined in ground-motion prediction equations (GMPEs). State of the art GMPEs take advantage of site characterization based on broad classes, such as National Earthquake Hazards Reduction Program (NEHRP) soil class (BSSC, 2003; Akkar and Bommer, 2010), or the average shear-wave velocity of the uppermost 30 m ( $V_{S30}$ ; e.g., Abrahamson and Silva, 2008). However, despite the use of this simple characterization, recent work has shown the importance of considering site-to-site amplification variability in the estimation of ground-motion prediction uncertainty (Atkinson, 2006; Al Atik *et al.*, 2010). This highlights that the strong variability of site amplification, even within a single NEHRP or  $V_{S30}$  class, contributes significantly to the uncertainty of ground-motion prediction.

Developers of GMPEs typically make an assumption of ergodicity; that is, that the variability over space is treated as an uncertainty in time. Spatial variability (beyond simple site classification) is therefore assumed to be zero. In order to minimize the influence of site-to-site variability in single-site hazard analyses, Atkinson (2006) introduced the concept of single-site sigma (uncertainty). Its use can lead to reduced site-specific hazard due to the fact that, contrary to the ergodic assumption, the uncertainty of ground motion observed at a single site is

lower than that over a range of sites. The single-site sigma approach is particularly applicable in seismic hazard analyses of sensitive facilities due to the fact that, in such cases, extensive site characterization studies are undertaken. Given such knowledge, the site-to-site component of uncertainty buried in the sigma of GMPEs is clearly superfluous.

One approach taken to isolate the influence of site-to-site variability in GMPE development, and subsequently obtain single-site sigma, is through direct regression, or, alternatively, residual analysis (e.g., Al Atik *et al.*, 2010). However, statistical analyses, particularly of small datasets coupled with GMPEs with high degrees of freedom, are sensitive to trade-off problems. Furthermore, the site-of-interest may not share the characteristics of any of the recording sites used to construct the GMPE. This makes it difficult to assign a particular single-site sigma to the hazard analysis. A more thorough approach, which we explore in this article, is to consider the site amplification at recording instrumentation sites based on the physical properties of the site (e.g., the measured velocity profile). Given such information, we facilitate a uniquely referenced site-specific GMPE that could easily be adapted to an arbitrary target site for hazard analysis.

Of course, there is reasoning behind the use of simple site characterization approaches in GMPE development; typically, even basic  $V_{S30}$  characterization may not exist for a given site. One potential candidate for site-specific amplification determination is the horizontal to vertical (H/V) spectral ratio. H/V spectral ratios extracted from ambient vibrations have been proposed as a simple easy-to-derive proxy for site amplification (e.g., Nakamura, 1989; Atkinson and Boore, 2006). However, other authors (e.g., Scherbaum *et al.*, 2003; Bonnefoy-Claudet *et al.*, 2006) have showed the limitations and incorrectness of its use; while it can be shown that the frequencies at which resonance occurs, for instance due to strong impedance contrasts at depth (Fäh *et al.*, 2001), the amplitude of H/V ratios are not representative of ground-motion amplification. This is simply because the vertical component of motion itself undergoes unknown amplification and cannot therefore be considered a suitable reference.

Often 1D modeling is used to compute the theoretical elastic SH-transfer function (SHTF) based on known or inferred shear wave velocity profiles (e.g., Fähr *et al.*, 2003; Poggi *et al.*, 2012). However, obtaining a detailed estimate of the velocity profile to a sufficient depth for such computations might be impractical due to high implementation costs in the case of borehole logging or high-resolution active seismic techniques. Even when low-cost, non-invasive measurement techniques such as array analysis of the natural ambient vibration wavefield are used (e.g., Fähr *et al.*, 2008; Poggi and Fähr, 2010), problems exist. For such measurements, sites with smooth topography and low lateral variability over an area comparable to the expected penetration depth are required in order to acquire data that allows for the reconstruction of the velocity profile. This may not be possible, particularly in regions of complex or laterally heterogeneous geology, such as at the edge of sedimentary basins. When high quality 1D shear-wave velocity profiles are available, 1D site amplification modeling methods do not consider the lateral complexity of the near surface and topography and therefore neglect 2D and 3D amplification effects often observed in Alpine valleys (e.g., Roten *et al.*, 2008; Thompson *et al.*, 2012). Finally, in the case of anelastic SHTF, uncertainties are particularly high due to the uncertainty of attenuation information, with  $Q$  typically estimated based on geology.

The standard spectral ratio (SSR) method (Borcherdt, 1970) has, for many years, been considered the only reliable technique to derive site amplification that include such effects. However, it assumes the absence of local effects at the reference site and that the same rock profile can be found below the reference and the target site. Moreover, SSR refers to a rock reference that is relevant only at the local scale, with the variations in the local rock reference properties from  $V_{S30}$  around 700–2500 m/s. Finally, the cost of installing an additional reference station to a strong-motion station on soil is high, and often no rock outcrop is available close to the site of interest.

In this article we present an alternative method through empirical spectral modeling (ESM) that can be used to obtain site amplification at instrument locations of a permanent or temporary seismic network given sufficient recordings of small or moderate earthquakes. In practice the method is a combination of physical modeling and statistical approach. The methodology is based on an established approach of separating source, path, and site effects, for example, through a generalized inversion (Field and Jacob, 1995). In our implementation, we compare recorded seismograms' spectra with those expected from a Brune (1970, 1971)  $\omega^2$  source model, accounting for geometrical decay and path attenuation (Edwards *et al.*, 2008; Edwards and Fähr, 2013) on an event-by-event basis. Subsequent determination of magnitude following Edwards *et al.* (2010) and residual analysis for consistent site effects over all recorded events facilitates the determination of referenced amplification. Each new event is processed individually, with the resulting event-specific amplification added to the statistical representation of the database site-response functions, leading to increasingly robust results with time. This allows us to avoid

both the limitations of the simple 1D amplification function, and the limitations of non-physical parametric analysis (as in the case of most GMPEs).

The proposed technique is employed within the routine monitoring of the Swiss Seismological Service (SED). The SED produces automatic hypocenter determination solutions of regional seismicity, with a magnitude ( $M_L$ ) of completeness of at least 2.0 over the entire Switzerland. These hypocenter solutions are used to trigger the automatic creation or update of a site-response function database for all stations with continuous recording within the networks operated by the SED. A web interface is employed to allow for visualization and interpretation, providing an illustration of amplification phenomena immediately after the earthquake is recorded. This proves particularly useful in the case of newly installed sites relating to the rapidly expanding Swiss Strong-Motion Network (Clinton *et al.*, 2011).

In order to test our approach we show a number of examples of empirical amplification and compare it to site-to-reference spectral ratios (SSR), 1D SH-wave modeling and single station H/V of ambient vibration recordings. Comparisons account for reference corrections in order to cope with the limitations of locally referenced methods.

## EARTHQUAKE RECORDINGS

The expanding earthquake waveform database of the SED was used as a basis for our work. This comprises the broadband Swiss Digital Seismic Network (SDSNet; Deichmann *et al.*, 2010) and the Swiss Strong Motion Network (SSMNet; Clinton *et al.*, 2011). We use recordings starting from January 2010. Automated trace-windowing and quality control of the resulting spectra are performed following Edwards *et al.* (2010) to ensure only reliable data are included in this inversion; the minimum and maximum frequencies considered are 0.1–30 Hz, although the included bandwidth of individual spectra depends on the relative noise level. Our analysis window comprises the 5%–95% energy integral around the direct  $S$  wave and coda. The noise estimate, taken from the waveform prior to the  $P$ -wave arrival, is artificially increased until it intersects the signal spectrum at its lowest and highest frequencies. The conservative noise estimation prevents subsequent modeling being influenced by the noise, and is reasonable for small to moderate earthquakes, as at very low or high frequencies the signal is typically dominated by background noise. Finally, the maximum bandwidth over which the signal is at least three times greater than the noise is selected. If the frequency range covers at least an order of magnitude, the record is retained and, given three or more stations per event fulfilling the quality check, the data are passed through to the inversion stage.

## SITE AMPLIFICATION FROM BROADBAND SPECTRAL FITTING

Given instrument corrected data, the Fourier velocity spectrum  $\Omega_{ji}$ , observed at a station  $j$  originating from an earthquake  $i$  is represented by



$$\Omega_{ij}(f, r) = 2\pi f E_i(f, M_{0i}, f_{ci}) B_{ij}(f, t_{ij}^*) S_{ij}(r, r_{0\dots n-1}, \lambda_{1\dots n}) \times T_j(f, A_j, \Delta\kappa_j) T_{\text{Ref}}(f, A_{\text{Ref}}, \kappa_{\text{Ref}}), \quad (1)$$

for which  $f$  is the frequency,  $r$  is the hypocentral distance,  $E_i(f, M_{0i}, f_{ci})$  is the source model,  $B_{ij}(f, t_{ij}^*)$  is the intrinsic attenuation along the ray path,  $S_{ij}(r, r_{0\dots n-1}, \lambda_{1\dots n})$  is the frequency independent amplitude decay with distance, and  $T_j(f, A_j, \Delta\kappa_j)$  is the site-response function at the station relative to the reference  $T_{\text{Ref}}(f, A_{\text{Ref}}, \kappa_{\text{Ref}})$  with  $A_{\text{Ref}} = 1$ . The source spectrum  $E_i$  is a [Brune \(1970, 1971\)](#)  $\omega^2$  spectrum with event-specific corner frequency  $f_c$  and long-period spectral plateau defined by the seismic moment,  $M_{0i}$ .  $B_{ij}$  is given by the model according to [Anderson and Hough \(1984\)](#), with path attenuation operator  $t^*$ .

The geometrical spreading function  $S_{ij}$ , is described by a piecewise function comprising two segments of constant exponential decay in the form  $R^{-\lambda}$ : initial spherical decay ( $\lambda_1 = 1.0$ ) followed by trapped surface wave (cylindrical,  $\lambda_2 = 0.5$ ) spreading after  $r_1 = 150$  km ([Atkinson and Mereu, 1992](#)). Finally, local site amplification, relative to a regional reference (including local attenuation) is given by

$$T_j(f) = A_j a_j(f) e^{-\pi f \Delta\kappa_j}, \quad (2)$$

for which  $A_j$  is the average site amplification (the average amplification over all frequencies),  $\Delta\kappa_j$  is a constant, site-related attenuation operator ([Anderson and Hough, 1984](#)) and  $a_j(f)$  is the frequency-dependent site amplification function. The relative site attenuation operator  $\Delta\kappa_j$  is related to absolute site attenuation  $\kappa_j$  by

$$\Delta\kappa_j = \kappa_j - \kappa_{\text{Ref}}, \quad (3)$$

for which  $\kappa_{\text{Ref}}$  is the local attenuation of the reference site.

A modification of the method of [Edwards et al. \(2008, 2010\)](#) is followed to deconvolve equation (1) for a single earthquake. We first determine the combined path attenuation term at each site  $t_j^* + \kappa_j$ , the event-common source corner frequency  $f_c$ , and a spectral amplitude parameter termed the signal moment for each spectrum. Here we do not define a regional attenuation model to pre-determine  $t_j^* + \kappa_j$  because this requires simultaneous inversion of the full dataset (rather than the event-by-event application) and may bias results due to model simplification ([Edwards et al., 2010](#)). The misfit of the spectral model to the data is minimized in the log-log space with the  $L_2$  norm. Using the resulting minimum misfit model, the residuals are then assumed to be an estimate of the frequency-dependent elastic component of the site function  $a_j(f)$ . If an existing estimate of this is available from previous events, the existing function is updated assuming a log-normal distribution of the estimates.

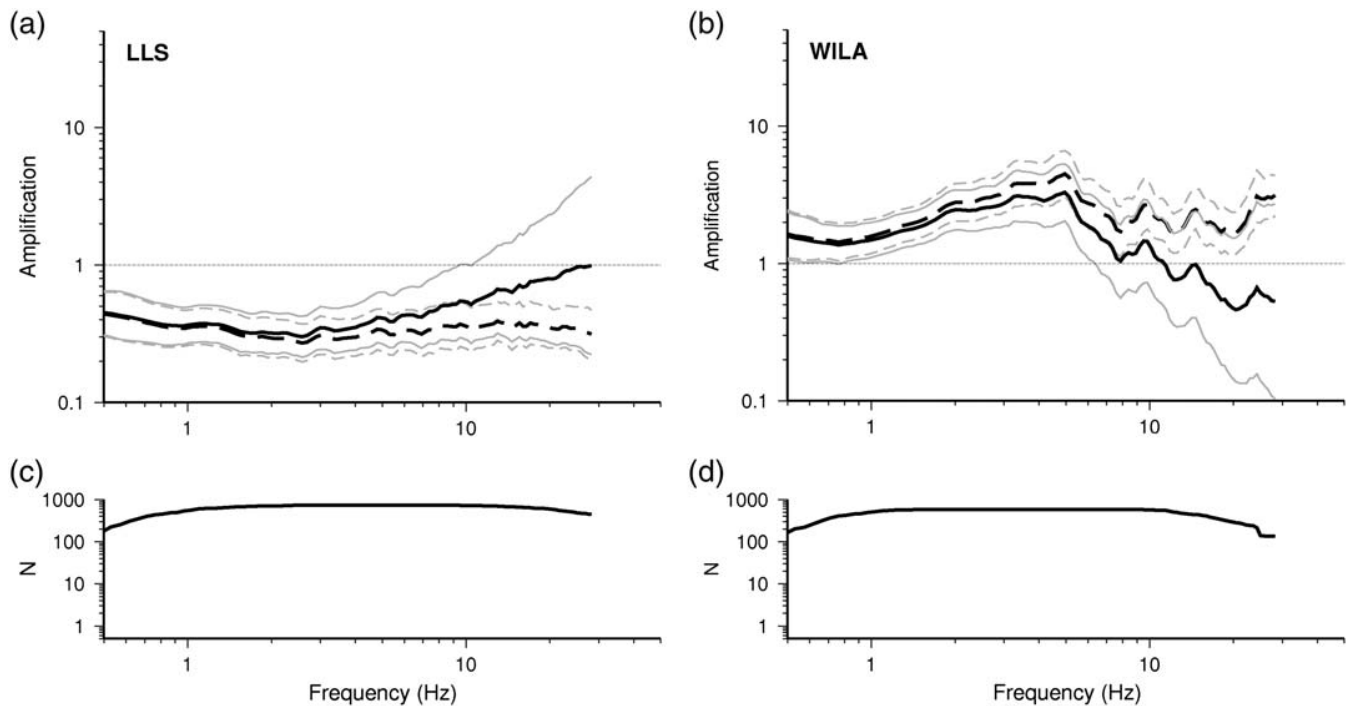
By correcting for the geometrical decay function  $S_j$  the frequency-independent component of the modeled spectra, the signal moments, can be split into a single seismic moment  $M_0$ , and average site amplification terms  $A_j$  relative to the

common reference. Clearly a strong trade-off exists between the moment and average amplification. However, in [Poggi et al. \(2011\)](#), 17,300 records from 585 earthquakes occurring in Switzerland with  $M_L > 2.0$  were used simultaneously to determine  $A_j$  and  $a_j(f)$  for 77 instrumentation sites in Switzerland. Of these, 27 with available shear-wave velocity profiles were used to define the Swiss generic rock reference model. Our inversion is constrained by fixing the known 77  $A_j$  values, based on the Swiss generic rock reference model, and using the corresponding  $a_j(f)$  from the same study as a starting model, weighted by the number of observations used in their derivation ([Edwards et al., 2011; Poggi et al., 2011](#)). This enforces any subsequently derived amplification (i.e., for newly installed sites) to be defined as amplification relative to the Swiss rock reference, providing at least one recording at a station with predefined amplification is available in the inversion. The parameters defining the Fourier spectra of recordings used for the sites in this study are provided in [Table S1](#). The parameters defined by [Poggi et al. \(2011\)](#) for the data prior to 2010 can be found in [Table S2](#). Both [Tables S1 and S2](#) can be found in the electronic supplement to this article.

For the anelastic ESM amplification function the absolute site attenuation term  $\kappa$  must be determined. To separate  $\kappa$  from the whole-path terms ( $t_j^* + \kappa_j$ ) obtained during the spectral inversion we use the model of [Edwards et al. \(2011\)](#) to estimate the contribution from crustal attenuation  $t^*$  along the path. Because ESM amplification is with reference to a regional velocity profile, we must also account for the local attenuation at the reference using equation (3). The site attenuation at the rock reference of [Poggi et al. \(2011\)](#) was given by [Edwards et al. \(2011\)](#) as  $\kappa_{\text{Ref}} = 0.016$  s. Finally, the elastic or anelastic ESM amplification functions can be reconstructed from the product of  $A_j$  and  $a_j(f)$  or  $A_j$ ,  $a_j(f)$  and  $\exp(-\pi f \Delta\kappa_j)$  respectively (equation 2). An example of the elastic and anelastic ESM amplification functions is shown in [Figure 1](#). Swiss foreland site WILA ( $V_{S30} = 683$  ms $^{-1}$ ) exhibits moderate elastic amplification of up to around a factor four with respect to the reference profile ( $V_{S30} = 1105$  ms $^{-1}$ ) due to its lower shear-wave velocity. On the other hand, alpine site LLS ( $V_{S30} = 3011$  ms $^{-1}$ ) shows constant deamplification of around 0.4 due to shear-wave velocities much higher than those of the reference profile. For the anelastic functions, LLS shows high-frequency amplification, while WILA shows deamplification. This is due to the fact that LLS has site attenuation lower than the reference  $\Delta\kappa_{\text{LLS}} < 0$ , and WILA has attenuation higher than at the reference profile  $\Delta\kappa_{\text{WILA}} > 0$ .

The standard deviation of the ESM amplification functions is determined through the propagation of errors in individual components. Assuming no covariance between the parameters and given a log-normal distribution in the uncertainty of  $A_j$  and  $a_j(f)$  [ $\sigma_A$  and  $\sigma_a(f)$  respectively] and a normal distribution in  $\Delta\kappa_j$  ( $\sigma_\kappa$ ) we obtain the log-normal error in  $T_j(f)$ :

$$\sigma_T = \sqrt{\sigma_A^2 + \sigma_a^2 + \pi f \sigma_\kappa^2}. \quad (4)$$



▲ **Figure 1.** Example of the dynamic ESM amplification functions displayed on the web interface for two SDSNet stations. (a) LLS, with attenuation lower than the reference. (b) WILA, with attenuation higher than the reference of 0.016 s. Solid lines show the anelastic functions, and dashed lines show the elastic functions. Black lines show mean amplification, and gray lines show standard deviation. (c) Number of records used for the determination of amplification for LLS. (d) Number of records used for the determination of amplification for WILA.

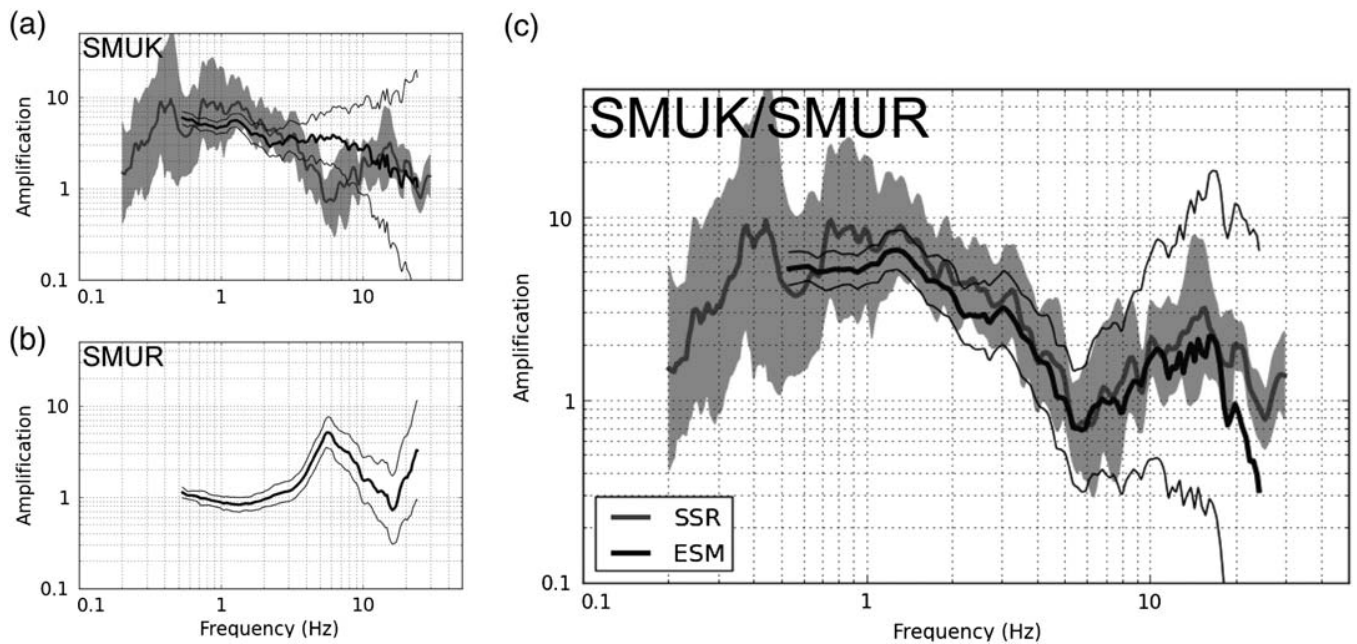
## COMPARISON OF EMPIRICAL SITE AMPLIFICATION WITH SITE-TO-REFERENCE SPECTRAL RATIOS

In a first-stage validation, the proposed approach to retrieve site amplification was compared to the classical SSR approach (Borcherdt, 1970). In the SSR approach the horizontal spectra of earthquake recordings at the target site are divided by the spectra at a reference station. The reference station is typically chosen to be as close to a “non-amplifying rock site” as possible, often through the analysis of H/V spectral ratios to rule out sites exhibiting resonance. The reference station must, however, still be near to the target site in order to satisfy the assumption that source and path effects are cancelled by the spectral ratio. One such example, in the case of a target site installed in a sedimentary basin, is outcropping bedrock at the basin edge. Given a close reference and target site with respect to the recording distance, this approach has the advantage of almost completely removing any source and propagation effects through the spectral division. However, one disadvantage is that, contrary to the proposed method, the reference velocity structure as well as the attenuation is not the same for all sites (Steidl *et al.*, 1996). Furthermore, the selected local rock reference can be quite dissimilar to the expected bedrock below the target site, including some residual site effect due to weathering

of the rock or shallow sediments, especially visible at high frequencies.

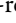
For the calculation of the SSR, spectra are computed for each horizontal component using the Fourier transform of  $S$  waves and coda, which are then smoothed following the Konno and Ohmachi (1998) procedure with a  $b$ -value of 80. Only the bandwidth of the spectra with sufficient signal-to-noise ratio is used (SNR larger than 3). Consistent with geometrical mean ground-motion estimation, the mean and standard deviation are computed in the log-space over all recording components available at both target and reference sites. For the ESM amplification, we use the anelastic version [the product of  $A_j$ ,  $a_j(f)$  and  $\exp(-\pi f \Delta \kappa_j)$ ] as the SSR also includes relative differences in the local attenuation with respect to the reference.

Figure 2 shows a comparison of SSR amplification with that from spectral modeling for station SMUK, located in the center of the deeply filled Rhone valley, proximate to the city of Monthey. The retrieved ESM amplification of the reference station used (SMUR) shows a clear peak at 5 Hz for this “rock” site that makes a direct comparison between the ESM and SSR methods difficult. This highlights a typical, though extreme, issue with the SSR approach; the results being highly dependent on having a non-amplifying local reference site. In order to make a meaningful comparison, rather than directly



▲ **Figure 2.** (a) Standard spectral ratio SMUK/SMUR (gray) compared to ESM amplification at site SMUK (black). (b) ESM amplification of the reference site SMUR. (c) Comparison of the SSR SMUK/SMUR (gray) with the ratio of the ESM amplifications (black) between site and reference (SMUK/SMUR) finally selected for comparison.

compare amplification estimates, the SSR amplification functions were compared to the ratio of ESM amplifications at site and reference (Fig. 2). This approach completely negates the influence of the local reference site for the SSR and is used for all further comparisons.

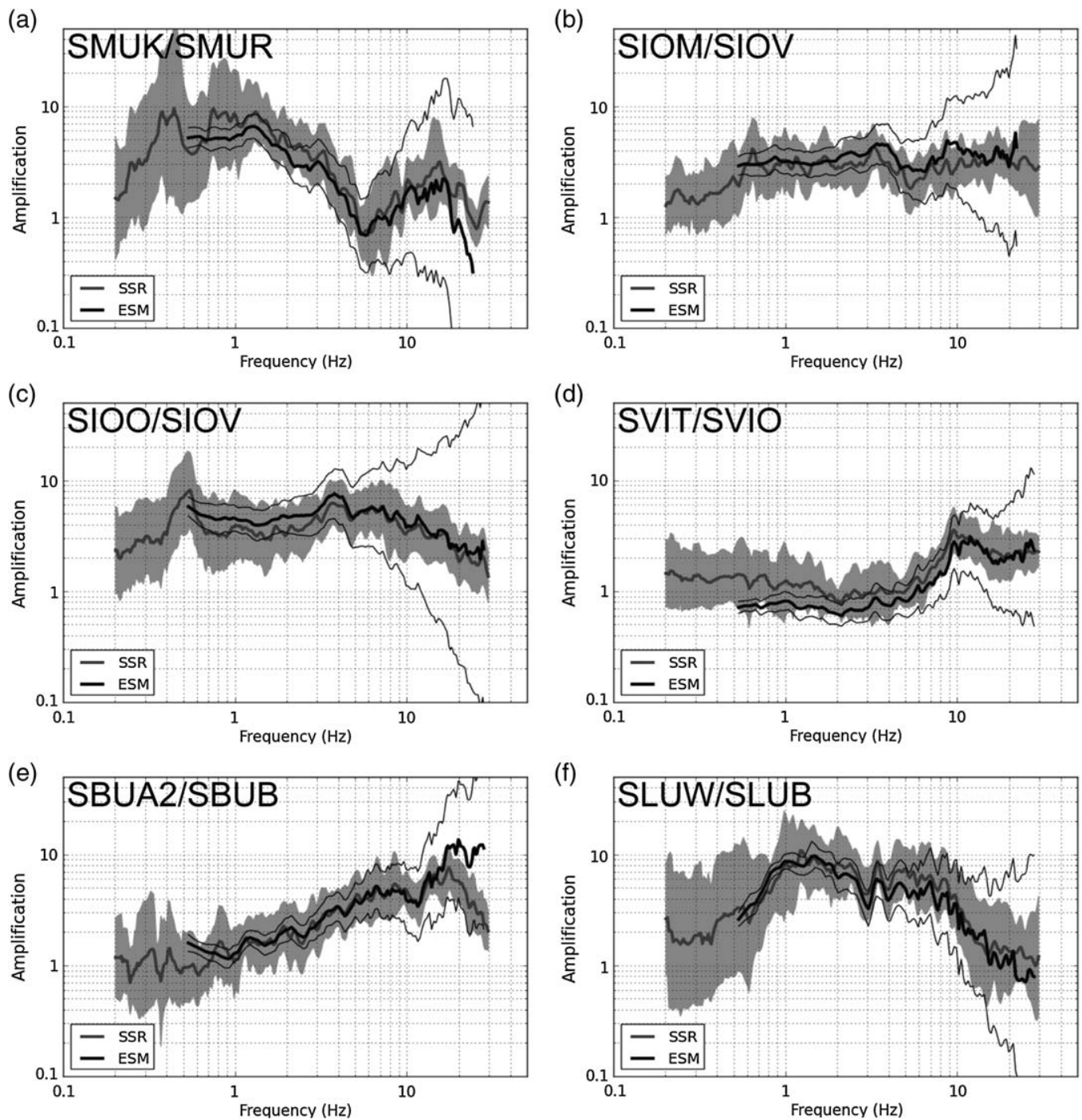
Six pairs of stations are studied, the results of which are presented in Figure 3. The absolute amplification at the six non-reference sites is shown in the  electronic supplement as Figure S1. The six target stations were chosen because they all have a nearby “local reference rock” site. Four of the pairs are located in the Rhone Valley (Valais, Switzerland), an area previously studied by [Roten et al. \(2006, 2008\)](#) and known to produce 2D amplification effects. One of the four pairs is located in Monthey (SMUK/SMUR), two in Sion (SIOM/SIOV and SIOO/SIOV) and one in Visp (SVIT/SVIO). In Sion, reference station SIOV is located on a hard rock outcrop located 1.5 km to the west of station SIOO and 700 m north of station SIOM. SIOM is located at the edge of a deep part of the basin, whereas SIOO is located in the center of the valley. In Visp, only a small number of recordings were available in the Rhone basin. Only station SVIT, located on a shallow alluvial fan adjacent to the valley, is presented here. Reference station SVIO is located on a rock outcrop, 350 m to the west of SVIT in the old town of Visp. A fifth pair of sites is located at the edge of the Rhine Valley (St. Gallen, Switzerland) in Buchs (SBUA2/SBUB), having a relatively distant hard rock reference at 3 km to the west. The last pair of sites (SLUW/SLUB) is located in Lucerne. Station SLUW is located on a lacustrine basin described in detail by [Poggi et al. \(2012\)](#). The reference station SLUB is located on a Molasse hill 1.5 km northwest from station SLUW. SLUB provides ESM amplification close

to unity and is therefore assumed to be close to the reference rock for Switzerland used in this study.

Stations SIOM, SBUB, SBUA2, SLUB and SLUW were installed between 2010 and 2012 and characterized in the framework of the SSMNet renewal project ([Michel et al., 2012](#)), whereas stations SVIO and SVIT were installed as part of the COGEAR project in 2010 ([Fäh et al., 2012](#)). Therefore, the number of recorded events with sufficient signal-to-noise ratio is still limited, especially at low frequencies. Nevertheless, the overall agreement between ESM amplification and SSR is excellent, despite very different sites being presented, with amplifications ranging from close to unity in some frequency bands, up to 10. In some frequency ranges, the small features of the spectra are also reproduced. However, inconsistencies at low frequencies (below 1 Hz) can be noticed, where the ESM amplification is much smoother than the SSR amplification, leading to loss of resolution. One such example can be seen in the fundamental frequency of the Rhone basin at SIOO, which is 0.5 Hz. This is due to the fact that we use the multi-taper algorithm to obtain smooth Fourier spectra for the ESM. Along with the duration-limited analysis signal this may lead to a loss of resolution at low frequencies. At high frequencies ( $f > 10$  Hz), the mean ESM amplification ratio is again very close to the SSR, despite an obvious increase in uncertainty due to the sensitivity to the determination of  $\Delta\kappa$ .

## COMPARISON OF EMPIRICAL SITE AMPLIFICATION WITH 1D SH-WAVE MODELING

The previous analysis showed that the ESM approach produces results consistent with those from SSR in the case in which



▲ **Figure 3.** Comparison of Standard Spectral Ratios (gray) with ratios of ESM amplifications (black) for six station pairs of SSMNet.

nearby reference sites existed. However, in contrast to the SSR approach, the application of the ESM approach is not only limited to such cases. In order to show the advantage of the spectral modeling technique over other commonly applied methods in site-response analysis, we compared the elastic ESM amplification functions with modeled one-dimensional, elastic SH-wave transfer functions (Knopoff, 1964) at several specific target sites of the SSMNet. The velocity profiles for these sites

were obtained from surface-wave analysis of ambient vibration array recordings (Havenith *et al.*, 2007; Fäh *et al.*, 2009; Michel *et al.*, 2012). As mentioned, the ESM amplification always refers to a common rock reference velocity profile, which in the case of Switzerland has a gradient form with velocity increasing from around 1 to 3.2 km/s, as described in Poggi *et al.* (2011). In the case of an analytical 1D SH-amplification function, however, the reference is generally local. This can be based

on either real outcropping bedrock or the deep portion of the bedrock, virtually outcropped by removing the top sediment cover from the velocity profile. As with the SSR approach, comparing the SHTF and ESM approaches without accounting for the differences in the reference may result in large deviations.

In order to correct the SH transfer functions (with local reference) to the Swiss reference (target), we apply a method that is based on the use of the quarter-wavelength approach (Joyner *et al.*, 1981). In this method, a correction function is computed as the square root of the ratio between seismic impedances ( $Z$ ) between the two references (local and target). Average seismic impedances are calculated using the quarter-wavelength method, which makes this parameter frequency dependent. The correction function is based on the original formulation by Joyner *et al.* (1981) and is given by

$$C(f) = \sqrt{\frac{Z_{\text{Target}}^{\text{Qwl}}(f)}{Z_{\text{Local}}^{\text{Qwl}}(f)}} = \sqrt{\frac{V_{S_{\text{Target}}}^{\text{Qwl}}(f)\rho_{\text{Target}}^{\text{Qwl}}(f)}{V_{S_{\text{Local}}}^{\text{Qwl}}(f)\rho_{\text{Local}}^{\text{Qwl}}(f)}}, \quad (5)$$

where  $V_S$  is the shear-wave velocity,  $\rho$  is density, and Qwl indicates averaging using the quarter-wavelength approach.

A simplification of equation (5) can be obtained through two considerations:

1. The difference in density has little impact in the final correction function; we can therefore neglect this parameter, assuming equal density between the two profiles.
2. For the transfer function modeling, the last layer of the discrete velocity profile is usually assumed as the reference. Therefore, being a layer of constant velocity, its quarter-wavelength expression will also be constant (frequency independent).

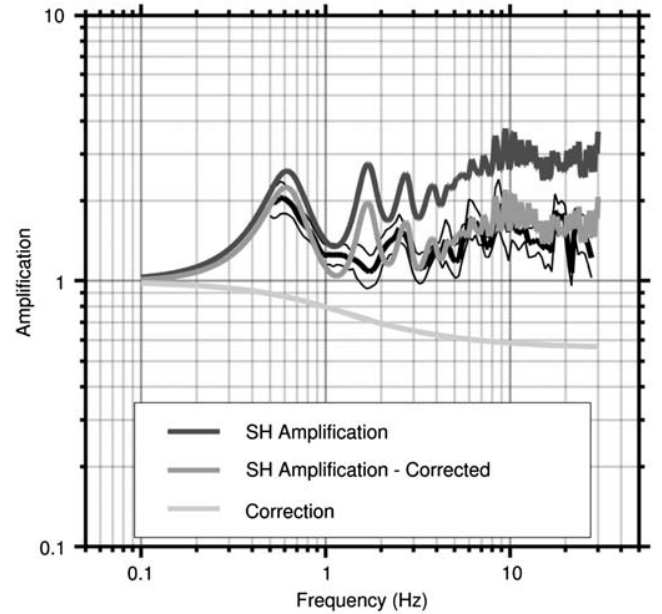
In this case equation (5) can be simplified to

$$C(f) = \sqrt{\frac{V_{S_{\text{Target}}}^{\text{Qwl}}(f)}{V_{S_{\text{Local}}}}}, \quad (6)$$

where  $V_{S_{\text{Local}}}$  is the velocity of the local reference: the lowermost (base) layer of the local site's shear-wave velocity profile. The reference corrected amplification function  $A_{\text{SH}}^{\text{Corr}}(f)$  can then be obtained by multiplication with the local correction function

$$A_{\text{SH}}^{\text{Corr}}(f) = C(f)A_{\text{SH}}(f). \quad (7)$$

Figure 4 shows an example of correcting the analytical elastic SH amplification function with local reference at the station SCUG to the Swiss generic rock reference. The correction to the common Swiss reference pulls the high frequency part down, making it comparable with the ESM amplification determined in this study. The main advantage of this correction method is its simplicity, as it gives the possibility to correct existing amplification functions without recomputing the whole transfer function to the target reference. Such an approach, nevertheless, must be regarded as an approximation,



▲ **Figure 4.** Example of correcting the elastic amplification from SH-wave transfer function modeling at the SSMNet station SCUG to the common reference by applying the proposed correction function. Comparison with the ESM amplification function proposed in this paper (black).

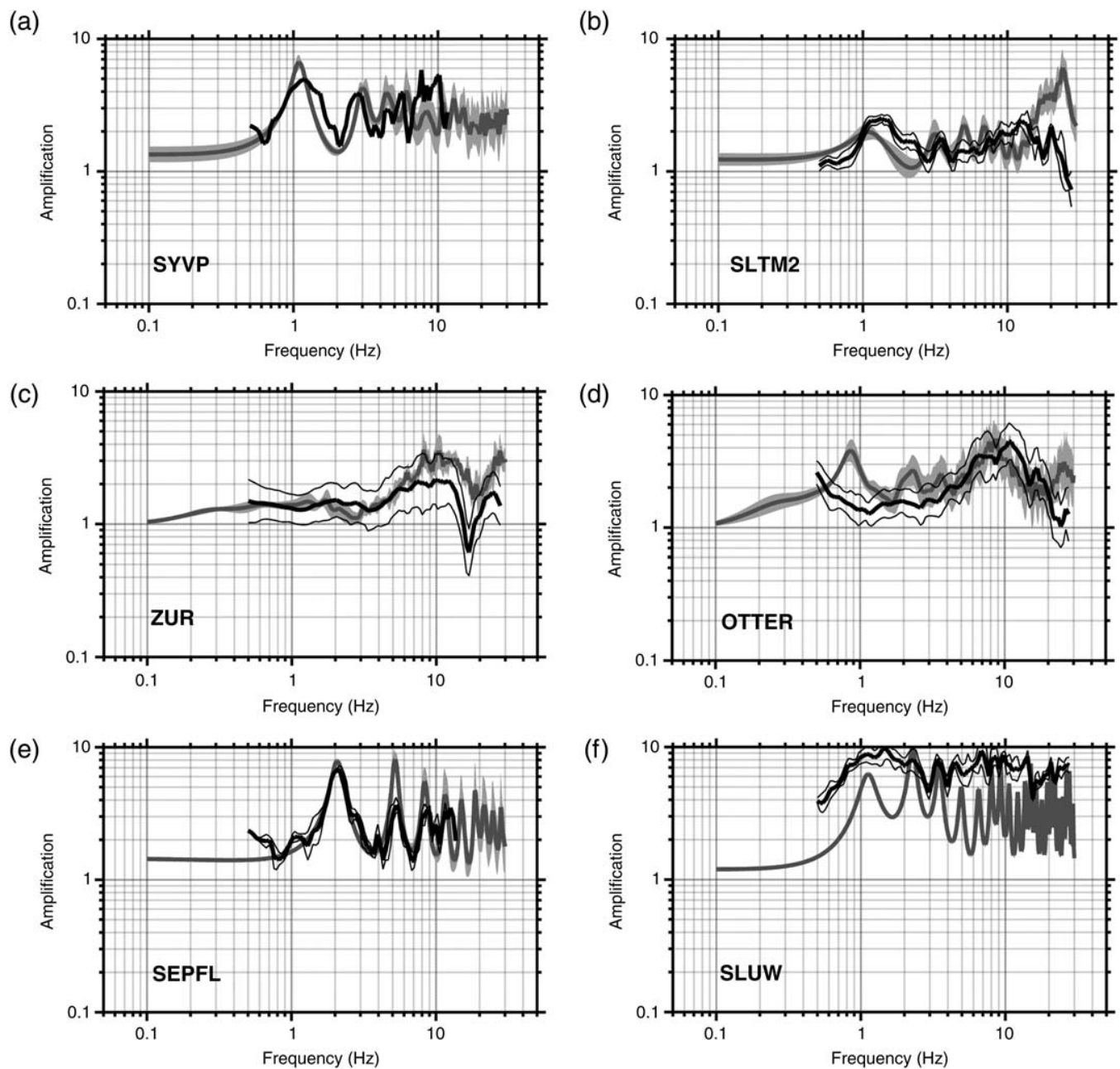
producing a much smoother result than that expected from full modeling.

The comparison between elastic ESM amplification functions from the spectral fitting approach and the corrected analytical elastic solution from SH-transfer function computation has been carried out for six stations of the SSMNet (SYVP, SLTM, ZUR, OTTER, SEPFL, and SLUW). These sites represent a selection of sites within the strong-motion network for which a reliable assessment of the velocity structure is available (Havenith *et al.*, 2007; Fäh *et al.*, 2009; Michel *et al.*, 2012). The selection was made to highlight the diversity of available sites in addition to the limitations of 1D site characterization. In addition to the stations previously described, station OTTER is located in Basel on top of a deep sedimentary basin of the Rhine Graben; ZUR is located on top of a molasse hill in the city of Zurich; station SYVP is located on the deep lacustrine basin of lake Neuchâtel in the city center of Yverdon-les-Bains; SLTM2 is located in the narrow but deeply-filled alpine valley of the Linth, and SEPFL is located on shallow lacustrine sediments on the shore of lake Geneva in the École Polytechnique Fédérale de Lausanne campus. The results of these comparisons are presented in Figure 5. Due to the correction of the SH-amplification functions using equation (7), all the examples refer to the Swiss rock reference.

The match between the two types of amplification functions is good. In some cases (SYVP and SEPFL) even fine-scale features, such as the resonance peaks, are well represented in addition to the overall smooth shape. This indicates that the dimensioning of the velocity interfaces along the velocity

model is consistent with the observed amplification. In other cases, the 1D SH-modeled resonance behavior mismatches with the amplification obtained using the spectral inversion approach at high frequencies (e.g., SLTM2). This may be because of the poor resolution of the velocity profile at shallow depths leading to an incorrect SHTF at high frequency. The same can be observed at low frequencies, if the input velocity profile is not sufficiently constrained at relatively large depth (e.g., OTTER). Nevertheless, some mismatch can also be ex-

pected independent of the reliability of the velocity profile. At the station ZUR, for instance, the high frequency part mismatches. This may be due to a residual presence of attenuation in the elastic ESM amplification function; attenuation might not be entirely removed or, as in this case, may be overcorrected for in the spectral modeling due to trade-off between inverted parameters. A special comment is necessary for the station SLUW, which exhibits amplification factors up to 10 in all approaches. In the comparison of SSR with ESM amplifications,



▲ **Figure 5.** Comparison of elastic ESM amplification functions from broadband spectral fitting (black line) and reference corrected elastic *SH*-wave transfer function modeling (in gray) at six test sites in Switzerland. Uncertainties are also shown, when available.

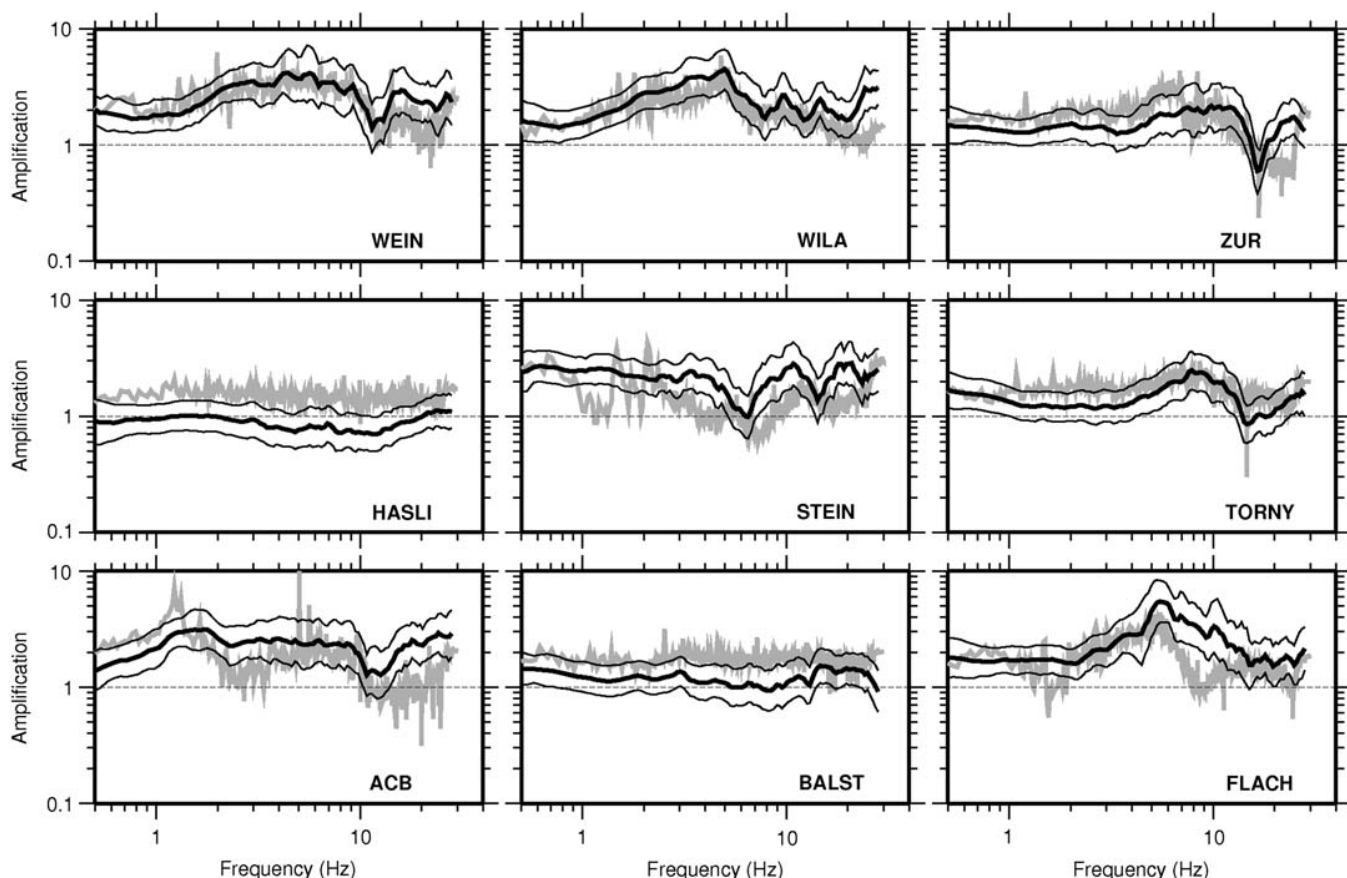
we observed an almost exact match, whereas in this case, a mismatch between ESM and SHTF amplification functions is induced by the presence of 2D/3D effects (e.g., [Thompson et al., 2009](#)), which cannot be accounted for with simple 1D modeling.

## COMPARISON OF EMPIRICAL SITE AMPLIFICATION WITH H/V RATIOS

The SDSNet is a broadband seismic network with installations typically on NEHERP rock or hard rock classes. Recordings of ambient noise from the continuous data stream were used to obtain single station H/V Fourier spectral ratios at all sites of the SDSNet. Recordings were taken over a duration of approximately one hour. Classical polarization analysis was then undertaken, following the approach detailed in [Fäh et al. \(2001\)](#). In order to avoid problems associated with the time variance of the noise field the ambient noise recordings are split into numerous 2048-sample (17-second) windows, each overlapping by 25%. With  $N$  as the number of windows, the geometrical average H/V, is then given by

$$\log\left[\frac{H}{V}(f)\right] = \frac{1}{N} \sum_{i=1}^N \log\left(\frac{\sqrt{H_{N,i}(f)H_{E,i}(f)}}}{V_i(f)}\right). \quad (8)$$

To compare with the H/V function, the elastic ESM amplification function is reconstructed from the product of  $a_j(f)$  and  $A_j$ , neglecting the attenuation term (Fig. 6). This is based on the assumption that the horizontal and vertical attenuation are comparable ([Bethmann et al., 2012](#)). The best match between the shape of the H/V curve and ESM amplification is found at sites WEIN and WILA. However, a constant offset between H/V and elastic ESM amplification is observed for most stations. The most important source for the differences in shape is that amplification is simply not adequately represented by H/V spectral ratios, most pronounced by the constant offset. Peaks and troughs in the curves are related to the fundamental frequency of resonance of the surface layers, best seen at sites WEIN, WILA, ZUR, TORNY, and FLACH. This is thought to represent a combination of  $S$ -wave resonance and Rayleigh wave ellipticity ([Poggi et al., 2012](#)), whereas in the case of the ESM, SSR, or SHTF, amplification is directly represented.



▲ **Figure 6.** H/V ratios for nine selected sites of the SDSNet compared with the elastic ESM amplification. The gray line shows the H/V derived from the ambient noise field using classical polarization analysis, the black line shows the elastic ESM amplification derived from earthquake recordings with corresponding standard deviation (thin black lines).

## CONCLUSIONS

We presented and tested a method to determine elastic site response and corresponding local attenuation, referenced to a regional velocity profile. The method has a wide possibility of application, as the size of the recorded earthquakes only limits the frequency bandwidth of the recovered site amplification; the method can therefore be applied even in regions of low seismicity such as Switzerland. However, the method is equally applicable in seismically active areas of the world, where small earthquakes are abundant, and can be used to estimate the linear amplification phenomena to be expected in the case of larger, damaging events. The recovered site amplification using this method reflects the observed site amplification in that it includes focusing effects, resonance phenomena, and topographical effects. No separation of these individual features was undertaken, however, comparison with 1D-SH modeling suggests that 2D and 3D effects may have a significant impact on local amplification, especially in Alpine valleys.

The proposed spectral fitting method was tested against standard methods for estimation of site response. The match with site-to-reference spectral ratios was excellent as long as we compared the ratio of amplifications in order to account for the fact that the SSR method may not have unitary reference amplification. Smoothing issues of the presented method at low frequencies were highlighted, however, and are due to the use of the multi-taper approach to compute the Fourier transform in addition to the duration-limited analysis signals. Unfortunately, there exists a trade-off between signal isolation and SNR maximization with the robustness of low-frequency estimation. In order to compare with a 1D modeling method, we corrected SH-transfer model amplifications to a common reference using the quarter-wavelength approximation. This is important because 1D SH-modeling typically has a local reference, usually the bedrock layer beneath the site. After correction, the two methods showed good agreement, in some cases even including fine-scale features such as resonance peaks.

Comparison of amplification from spectral fitting with estimations of the H/V ratio found an agreement in shape, although significant differences were present between amplitudes at most sites. The H/V analysis undertaken disagrees with the conclusions of Nakamura (1989), who suggested that the use of H/V ratios can approximate site response. While the approach does provide a reasonable first-order estimate of the shape of the amplification related to resonance behavior (i.e., the location of resonance peaks), the amplitudes obtained from H/V measurements are not representative of ground-motion amplification. One aspect to consider is that the H/V function rarely indicates deamplification, which is possible when amplification is considered with respect to a common reference. We conclude, therefore, that the H/V ratio should not be used to predict amplification.

Overall, the method presented here to determine elastic amplification functions for sites within a seismic network offers a useful tool for network operation and hazard assessment. The agreement with existing approaches showed the validity of

the method in specific cases for which detailed site information was available or a reference site with negligible amplification was nearby. The proposed method is extended without loss of generality to all sites in the network, regardless of whether velocity information or other site characterization information exists. In fact, the method can be useful in helping to characterize sites, for example, by providing information on resonance phenomena, indicating strong contrasts of impedance at depth or highlighting particularly strong or weak local attenuation. Application to the hazard analysis of specific sites such as sensitive facilities or unstable rock slopes (e.g., Burjanek *et al.*, 2012) can be considered through the installation of a strong-motion station for a limited period of time depending on the level of seismicity. ✉

## ACKNOWLEDGMENTS

This work was funded in part by the Swiss Federal Nuclear Safety Inspectorate (ENSI) and in part by the project for the Renewal of the Swiss Strong Motion Network (SSMNet), which is supported by the Federal Office for the Environment (FOEN), the Federal Roads Office (FEDRO), ENSI, Swiss Federal Railways (SBB), Schweizerischer Pool für Erdbebendeckung and ETH Zurich. The data used for this study are freely available online at [arlink.ethz.ch](http://arlink.ethz.ch). We thank Laurie Baise and Editor in Chief Jonathan Lees for their review of this manuscript.

## REFERENCES

- Abrahamson, N., and W. Silva (2008). Summary of the Abrahamson & Silva NGA ground-motion relations, *Earthq. Spectra* **24**, 67–97.
- Akkar, S., and J. J. Bommer (2010). Empirical equations for the prediction of PGA, PGV, and spectral accelerations in Europe, the Mediterranean region, and the Middle East, *Seismol. Res. Lett.* **81**, 195–206.
- Al Atik, L., N. Abrahamson, J. J. Bommer, F. Scherbaum, F. Cotton, and N. Kuehn (2010). The variability of ground-motion prediction models and its components, *Seismol. Res. Lett.* **81**, 794–801.
- Anderson, J. G., and S. E. Hough (1984). A model for the shape of the fourier amplitude spectrum of acceleration at high-frequencies, *Bull. Seismol. Soc. Am.* **74**, 1969–1993.
- Atkinson, G. M. (2006). Single-station sigma, *Bull. Seismol. Soc. Am.* **96**, 446–455.
- Atkinson, G. M., and D. M. Boore (2006). Earthquake ground-motion prediction equations for eastern North America, *Bull. Seismol. Soc. Am.* **96**, 2181–2205.
- Atkinson, G. M., and R. F. Mereu (1992). The shape of ground motion attenuation curves in southeastern Canada, *Bull. Seismol. Soc. Am.* **82**, 2014–2031.
- Bethmann, F., N. Deichmann, and P. M. Mai (2012). Seismic wave attenuation from borehole and surface records in the top 2.5 km beneath the city of Basel, Switzerland, *Geophys. J. Int.* **190**, 1257–1270.
- Bonnefoy-Claudet, S., C. Cornou, P. Y. Bard, F. Cotton, P. Moczo, J. Kristek, and D. Fah (2006). H/V ratio: A tool for site effects evaluation. Results from 1-D noise simulations, *Geophys. J. Int.* **167**, 827–837.
- Boore, D. M. (2004). Can site response be predicted? *J. Earthq. Eng.* **8**, 1–41.
- Borcherdt, R. D. (1970). Effects of local geology on ground motion near San Francisco Bay, *Bull. Seismol. Soc. Am.* **60**, 29–61.



- Brune, J. N. (1970). Tectonic stress and spectra of seismic shear waves from earthquakes, *J. Geophys. Res.* **75**, 4997–5009.
- Brune, J. N. (1971). Correction, *J. Geophys. Res.* **76**, 5002.
- Building Seismic Safety Council (BSSC) (2003). *The 2003 NEHRP Recommended Provisions for New Buildings and Other Structures (FEMA 450), Part 1: Provisions*, Federal Emergency Management Agency, Washington, D.C., 308 pp.
- Burjanek, J., J. R. Moore, F. X. Y. Molina, and D. Fäh (2012). Instrumental evidence of normal mode rock slope vibration, *Geophys. J. Int.* **188**, 559–569.
- Clinton, J., C. Cauzzi, D. Fäh, C. Michel, P. Zweifel, M. Olivieri, G. Cua, F. Haslinger, and D. Giardini (2011). The current state of strong motion monitoring in Switzerland, in *Earthquake Data in Engineering Seismology*, S. Akkar, P. Gülkan, and T. van Eck (Editors), Springer, Netherlands, 219–233, doi: [10.1007/978-94-007-0152-6\\_15](https://doi.org/10.1007/978-94-007-0152-6_15).
- Deichmann, N., J. Clinton, S. Husen, B. Edwards, F. Haslinger, D. Fäh, D. Giardini, P. Kästli, U. Kradolfer, and I. Marschall (2010). Earthquakes in Switzerland and surrounding regions during 2009, *Swiss J. Geosci.* **103**, 535–549.
- Edwards, B., and D. Fäh (2013). A stochastic ground-motion model for Switzerland, *Bull. Seismol. Soc. Am.* **103**, 78–98.
- Edwards, B., B. Allmann, D. Fäh, and J. Clinton (2010). Automatic computation of moment magnitudes for small earthquakes and the scaling of local to moment magnitude, *Geophys. J. Int.* **183**, 407–420.
- Edwards, B., D. Fäh, and D. Giardini (2011). Attenuation of seismic shear wave energy in Switzerland, *Geophys. J. Int.* **185**, 967–984.
- Edwards, B., A. Rietbrock, J. J. Bommer, and B. Baptie (2008). The acquisition of source, path, and site effects from microearthquake recordings using Q tomography: Application to the United Kingdom, *Bull. Seismol. Soc. Am.* **98**, 1915–1935.
- Fäh, D., S. Fritsche, V. Poggi, G. Gassner-Stamm, P. Kästli, J. Burjanek, P. Zweifel, S. Barman, J. Clinton, and L. Keller (2009). Determination of site information for seismic stations in Switzerland, *Swiss Seismological Service Tech. Rept.: SED/PRP/R/004/20090831 for the swiss-nuclear PEGASOS Refinement Project*.
- Fäh, D., F. Kind, and D. Giardini (2001). A theoretical investigation of average H/V ratios, *Geophys. J. Int.* **145**, 535–549.
- Fäh, D., F. Kind, and D. Giardini (2003). Inversion of local S-wave velocity structures from average H/V ratios, and their use for the estimation of site-effects, *J. Seismol.* **7**, 449–467.
- Fäh, D., J. R. Moore, J. Burjanek, I. Iosifescu, D. Dalguer, F. Dupray, C. Michel, J. Woessner, A. Villiger, and J. Laue (2012). Coupled seismogenic geohazards in alpine regions, *Bollettino Di Geofisica Teorica Ed Applicata* **53**, 485–508.
- Fäh, D., G. Stamm, and H. B. Havenith (2008). Analysis of three-component ambient vibration array measurements, *Geophys. J. Int.* **172**, 199–213.
- Field, E. H., and K. H. Jacob (1995). A comparison and test of various site-response estimation techniques, including three that are not reference-site dependent, *Bull. Seismol. Soc. Am.* **85**, 1127–1143.
- Havenith, H. B., D. Fäh, U. Polom, and A. Roulle (2007). S-wave velocity measurements applied to the seismic microzonation of Basel, Upper Rhine Graben, *Geophys. J. Int.* **170**, 346–358.
- Joyner, W. B., R. E. Warrick, and T. E. Fumal (1981). The effect of quaternary alluvium on strong ground motion in the Coyote Lake, California, earthquake of 1979, *Bull. Seismol. Soc. Am.* **71**, 1333–1349.
- Knopoff, L. (1964). A matrix method for elastic wave problems, *Bull. Seismol. Soc. Am.* **54**, 431–438.
- Konno, K., and T. Ohmachi (1998). Ground-motion characteristics estimated from spectral ratio between horizontal and vertical components of microtremor, *Bull. Seismol. Soc. Am.* **88**, 228–241.
- Michel, C., C. Cauzzi, D. Fäh, J. Clinton, P. Zweifel, and P. Kästli (2012). The Swiss strong-motion network: High-quality strong-motion monitoring in a region of low-to-moderate seismicity, in *Proc. 15th World Conference on Earthquake Engineering (15 WCEE)*, Lisbon, Portugal, 24–28 September 2012, paper no. 1470.
- Nakamura, Y. (1989). A method for dynamic characteristics estimation of subsurface using microtremor on the ground surface, *Railway Technical Research Institute, Quarterly Reports* **30**, 25–33.
- Poggi, V., and D. Fäh (2010). Estimating Rayleigh wave particle motion from three-component array analysis of ambient vibrations, *Geophys. J. Int.* **180**, 251–267.
- Poggi, V., B. Edwards, and D. Fäh (2011). Derivation of a reference shear-wave velocity model from empirical site amplification, *Bull. Seismol. Soc. Am.* **101**, 258–274.
- Poggi, V., D. Fäh, J. Burjanek, and D. Giardini (2012). The use of Rayleigh-wave ellipticity for site-specific hazard assessment and microzonation: Application to the city of Lucerne, Switzerland, *Geophys. J. Int.* **188**, 1154–1172.
- Roten, D., D. Fäh, C. Cornou, and D. Giardini (2006). Two-dimensional resonances in Alpine valleys identified from ambient vibration wavefields, *Geophys. J. Int.* **165**, 889–905.
- Roten, D., D. Fäh, K. B. Olsen, and D. Giardini (2008). A comparison of observed and simulated site response in the Rhone valley, *Geophys. J. Int.* **173**, 958–978.
- Scherbaum, F., K. G. Hinzen, M. Ohrnberger, and R. B. Herrmann (2003). Determination of shallow shear wave velocity profiles in the Cologne, Germany area using ambient vibrations, *Geophys. J. Int.* **152**, 597–612.
- Steidl, J. H., A. G. Tumarkin, and R. J. Archuleta (1996). What is a reference site? *Bull. Seismol. Soc. Am.* **86**, 1733–1748.
- Thompson, E. M., L. G. Baise, R. E. Kayen, and B. B. Guzina (2009). Impediments to predicting site response: Seismic property estimation and modeling simplifications, *Bull. Seismol. Soc. Am.* **99**, 2927–2949.
- Thompson, E. M., L. G. Baise, Y. Tanaka, and R. E. Kayen (2012). A taxonomy of site response complexity, *Soil Dynam. Earthq. Eng.* **41**, 32–43.

**Benjamin Edwards**  
**Clotaire Michel**  
**Valerio Poggi**  
**Donat Fäh**  
 Swiss Seismological Service  
 ETH Zürich, Sonneggstrasse, 5  
 8092 Zürich, Switzerland  
[edwards@sed.ethz.ch](mailto:edwards@sed.ethz.ch)

## 1.5 Extraire l'effet de la géologie locale des enregistrements de vibrations ambiantes (Michel *et al.*, 2014a)

Comme on l'a vu dans la partie 1.3, il est nécessaire de caractériser les propriétés physiques des sites afin de déterminer l'effet de la géologie locale sur le mouvement sismique. C'est d'autant plus important pour les sites d'implantation de stations permanentes qui livrent des données sismiques qu'il faut pouvoir interpréter. Si, dans la partie 1.4, on a vu qu'il était possible de séparer les effets de source, de propagation et de site pour les enregistrements sismiques, il est nécessaire de relier cette amplification aux conditions de site afin d'étendre la prédiction du mouvement du sol à des sites non instrumentés. Pour cela, on passe en général par des paramètres simples définissant le sol (voir partie 1.3) mais qui ne suffisent pas pour caractériser entièrement un site d'un point de vue sismique. Dans Michel *et al.* (2014a), nous proposons donc une procédure pour caractériser des sites d'implantation des stations permanentes du réseau suisse avec un bon compromis entre la qualité des informations et le coût des investigations. Elle est fondée sur des mesures systématiques des propriétés des ondes de surface sous vibrations ambiantes, complétées par d'autres types de mesures si nécessaire.

La nouveauté dans Michel *et al.* (2014a) est la comparaison systématique des résultats de la caractérisation sous vibrations ambiantes avec ceux de l'amplification sous séisme déterminée dans la partie 1.4. Elle permet, d'une part, d'éventuellement revoir les hypothèses de l'inversion des propriétés des ondes de surface et donc d'améliorer la caractérisation du site, et d'autre part, de détecter des phénomènes de génération d'ondes de surface locales (p. ex. en bord de bassin). La procédure présentée permet de réaliser une caractérisation 1D des sites mais aussi de détecter les effets 2D/3D, qu'il s'agisse de phénomènes de résonance (à partir de la polarisation du champ d'onde) ou de génération locale d'ondes de surface. Elle est appliquée à 30 nouvelles stations installées dans le cadre de la phase 1 du renouvellement du réseau accélérométrique suisse SSMNet.

## Assessment of Site Effects in Alpine Regions through Systematic Site Characterization of Seismic Stations

by Clotaire Michel, Benjamin Edwards, Valerio Poggi, Jan Burjánek, Daniel Roten, Carlo Cauzzi, and Donat Fäh

**Abstract** In the framework of the renewal project of the Swiss Strong Motion Network (SSMNet), a procedure for site characterization has been established. The aim of the procedure was to systematically derive realistic 1D velocity profiles at each station. It is mainly based on the analysis of surface waves, particularly from passive experiments, and includes cross checks of the derived amplification functions with those obtained through spectral modeling of recorded earthquakes. The systematic use of three component surface-wave analysis, allowing the derivation of both Rayleigh and Love dispersion curves, also contributes to the improvement of the quality of the retrieved profiles.

The procedure is applied to the 30 SSMNet stations installed on various site types within the project, covering different aspects of seismic risk. The characterization of these 30 sites gives an overview of the variety of possible effects of surface geology on ground motion in the Alpine area. Such effects ranged from deamplification at hard-rock sites to amplification up to a factor of 15 in lacustrine sediments with respect to the Swiss reference rock velocity model. The derived velocity profiles are shown to reproduce observed amplification functions from empirical spectral modeling. Although many sites are found to exhibit 1D behavior, the procedure allows the detection and qualification of 2D and 3D effects. The sites are therefore classified with respect to the occurrence of 2D/3D resonance and edge-generated surface waves. In addition to the large and deeply incised alpine valleys of the Rhône, the Rhine, and the Aar, smaller structures such as local alpine valleys and alluvial fans are shown to exhibit 2D/3D behavior.

### Introduction

Local site conditions have a significant impact on earthquake ground motions. This so-called site effect is dominantly controlled by variations in the shear-wave velocity of the subsurface. For instance, interfaces between high  $S$ -wave velocities in bedrock and low velocities in sediments can lead to the development of strong amplification and resonance phenomena. Urban areas around the world are often built on sedimentary basins to ease the access to water and avoid steep topography. Site effects therefore constitute a large part of the seismic hazard in urban areas (e.g., in Mexico City [Bard *et al.*, 1988], Caracas [Duval *et al.*, 2001], Los Angeles [Wald and Graves, 1998], Tokyo [Yamanaka *et al.*, 1989], or Bangkok [Poovarodom and Plalinyot, 2013]).

Assessment of amplification phenomena related to a site is often performed with an assumption of horizontally layered media (1D structure) using the theoretical  $SH$ -wave transfer function (Knopoff, 1964). However, non-1D effects related to sedimentary basins have been discussed since the 1970s and observed in strong-motion recordings (e.g., King

and Tucker, 1984). For instance, Thompson *et al.* (2009, 2012) evaluated and classified the limitations of the 1D assumption. The significant variability of observed amplification has also justified numerous numerical studies.

To fully consider the expected amplification at a site located in a narrow sedimentary basin, 3D effects should clearly be considered. However, although computing capabilities are improving dramatically, 3D numerical simulation of large areas still has a high computational cost. Furthermore, a good knowledge of the structure is required, which also defines the useful frequency band for modeling. Consequently, 3D models are typically developed at sites that have been previously well studied. In Switzerland, for instance, 2D effects in the Rhône valley have been quantified by extensive studies combining direct observations and modeling (Steimen *et al.*, 2003; Roten *et al.*, 2006, 2008; Ermert *et al.*, 2014). Before being able to model 2D/3D effects, however, local assessment of 1D velocity profiles is always needed, along with their lateral variation. Moreover, Burjánek *et al.* (2014) analyzed

25 sites with pronounced topography and showed that observed amplifications at such sites are tightly linked with the local subsurface structure rather than terrain geometry.

Explaining recorded ground motion through deconvolution of source, propagation, and site effects is a primary goal of engineering seismology. High quality characterization through independent geophysical investigation of each instrumented site is necessary to properly isolate and explain site effects and ultimately refine estimation of earthquake magnitude and seismic attenuation. The aim of this article is therefore to propose a procedure able to provide high quality but affordable site characterization for seismic stations including validation. The procedure quantifies site effects and qualitatively identifies 2D/3D effects.

The proposed method is implemented within the framework of the renewal project of the Swiss Strong Motion Network (SSMNet). The procedure for characterization of the sites of 30 newly installed stations is applied systematically. Geophysical site investigations are based on three-component (3C) surface-wave analysis, particularly of ambient vibration array recordings (Fäh *et al.*, 2008; Poggi and Fäh, 2010). A new procedure based on spectral modeling of earthquake ground motion at these stations (Edwards *et al.*, 2013) has been used to check the validity of the site characterization. Moreover, the whole process checks for 2D/3D effects, due to edge-generated surface waves (EGSW) and 2D/3D resonances. Sites are classified and compared with the classification proposed by Bard and Bouchon (1985) for 2D resonance in sedimentary basins.

### 2D/3D Phenomena

Bard and Bouchon (1980, 1985) identified two non-1D phenomena in sediment-filled valleys: (1) the inclined interfaces at the edge create laterally propagating surface waves that amplify the ground motion and (2) sufficiently slender valleys with large velocity contrasts exhibit 2D resonances or normal modes. Depending on the characteristics of the valley (velocity contrast and shape), one or both phenomena play a role in the transfer function (Bard and Bouchon, 1985). These authors also provide empirical limits of these characteristics for the occurrence of 2D resonance based on a numerical study.

Edge-generated surface waves were observed by Field (1996), Chavez-Garcia *et al.* (1999), Joyner (2000), Lebrun *et al.* (2001), Cornou and Bard (2003), and Roten *et al.* (2008). Moreover, numerical modeling has often been used in the literature to reproduce EGSW and wave-focusing effects (e.g., Paolucci and Morstabilini, 2006; Lenti *et al.*, 2009; Faccioli *et al.*, 2010). Kawase (1996) showed such effects were responsible for the large damage in Kobe 1995; the well-known “Kobe effect.” EGSW can generally be recognized on time traces of earthquake recordings in basins as long duration surface-wave trains. They typically occur on a broad frequency range starting from the fundamental frequency of the valley (e.g., Cornou and Bard, 2003; Cauzzi

*et al.*, 2011). The amplification function is then smooth and of large amplitude as found, for instance, by Lebrun *et al.* (2001) in Grenoble, France. Cornou and Bard (2003) proposed to compute the ratio of the observed amplification function to the 1D theoretical transfer function, termed the aggravation factor, to characterize these EGSW.

The 2D/3D normal modes are characterized by a constant resonance frequency on the entire valley, at which the motion is in phase and exhibits a shape characteristic of the considered mode (Roten *et al.*, 2006). 2D resonance was particularly observed in the Rhône valley in Switzerland (Steimen *et al.*, 2003; Roten *et al.*, 2006; Ermert *et al.*, 2014; Poggi *et al.*, 2014). Several authors underlined the shift of fundamental frequency peak compared with 1D assumption in 2D/3D cases (e.g., Guéguen *et al.*, 2007; Le Roux *et al.*, 2012), and a deviation of the dispersion curves from the 1D case that needs to be taken into account in the inversion (Roten and Fäh, 2007). However, without a good knowledge of the basin geometry, highlighting eventual shifts between 1D modeling and observed peaks is not possible. Steimen *et al.* (2003) and Roten *et al.* (2006) recommend the use of the reference station method to detect 2D modal shapes. Further, Ermert *et al.* (2014) and Poggi *et al.* (2014) proposed to apply modal analysis approaches from mechanical and civil engineering to determine the resonance frequencies and modal shapes of the basin. Alternatively, Fritsche *et al.* (2005) proposed to use the polarization of waves at the resonance frequency using azimuthal horizontal-to-vertical (H/V) spectral ratios. A strong polarization in the valley axis is an indication for the *SH*-mode shape and, therefore, the occurrence of 2D resonance. Ermert *et al.* (2014) followed the same approach but, instead of the azimuthal H/V, used the method developed by Burjánek *et al.* (2010) to characterize the polarization and showed the equivalence with the modal analysis approach.

### SSMNet Renewal Project

The SSMNet is currently undergoing major upgrades (Clinton *et al.*, 2011). In the framework of this renewal project, 30 state-of-the-art strong-motion stations in free-field conditions have been installed during a first phase (2009–2013), and an additional 70 stations are planned in a second phase (2013–2019). The current status of the SSMNet is displayed in Figure 1. The selection of instrumented sites, eventually replacing existing strong-motion dial-up stations, was made considering different aspects of seismic risk. This project achieved a better general spatial coverage over the country, while focusing on the instrumentation of areas with known historical earthquakes, on urban areas concentrating the largest risk exposure, and on areas with significant site amplification expected. As a result, the SSMNet stations widely sample typical sites of the alpine environment. Such sites are characterized by the presence of loose alluvium-filled valleys, alluvial fans, and steep slopes: often associated with significantly increased ground-motion amplitudes and therefore expected earthquake damage.





**Figure 2.** Alternative housing of the stations installed within the SSMNet renewal project. Left: small vault containing the sensor only and hut hosting the cabinet with the digitizer and communication instruments (station SYVP). Right: large vault containing the whole station (station SEPFL). The color version of this figure is available only in the electronic edition.

Depending on the objective, different levels of site characterization are available. These levels comprise diverse procedures with increasing complexity, which can be nevertheless categorized as follows:

1. simplified geological and geotechnical classification (e.g., design code approach);
2. geophysical characterization using a single parameter (e.g.,  $V_{S30}$ ,  $f_0$ );
3. 1D profiling of the linear elastic and eventually inelastic parameters; and
4. full microzonation using advanced 2D/3D models and nonlinear response analysis.

Given the different accuracy of these approaches in estimating the ground response, the level of characterization between different networks in the world and even within the same network can be very heterogeneous. For instance, in Italy, [Luzi et al. \(2010\)](#) compiled all the available information for each station, from the fundamental frequency of the site to the profiling of the geophysical properties obtained from borehole logging and seismic experiments. [Di Capua et al. \(2011\)](#) proposed a classification for sites with limited information. In Japan, velocity profiles from borehole logging are available for every KiK-net station ([Aoi et al., 2004](#)). In Taiwan, the sites of the whole network have been classified for a long time ([Lee et al., 2001](#)). In Iran ([Zaré et al., 1999](#)), Turkey ([Sandikkaya et al., 2009](#)), and Puerto Rico ([Odum et al., 2013](#)), 1D  $S$ -wave velocity profiles are provided at a number of sites using mostly active seismic techniques. In the United States, single parameter characterization is typically based on the average travel-time velocity over the first 30 m ( $V_{S30}$ ) obtained from measurements or inferred from surface geology ([Yong et al., 2013](#)).

Soil class and single parameter characterization represent the easiest approach and are generally recommended when

large areas have to be mapped. Different site classifications exist (e.g., EC8 design code [[Eurocode 8, 2004](#)], [Building Seismic Safety Council \[2004\]](#), etc.) and  $V_{S30}$  is nowadays the preferred parameter to define class boundaries. However, they do not provide good resolution and cannot explain the whole variety of local surface effects on the ground motion (even though important) such as the amplification induced by resonance. This gap therefore leads to strong limitations when using these data for scientific purposes. On the other hand, extended site-specific microzonation studies are generally too demanding where many sites are involved and useful only for detailed modeling of few selected sites.

For the renewal of the SSMNet, therefore, we tried to strike the right balance between invested resources and reliability of the site characterization results. This is achieved through the determination for each individual site of a set of 1D velocity profiles that are compatible with observed site response features.

To this aim, a standard methodology has been established ([Fig. 3](#)). Using different profiles allows us to map the uncertainty in the site response prediction. At some particular sites, information about nonlinear parameters is also provided, which is nevertheless not discussed in this article. Moreover, at some sites, insights about the complex 2D/3D geometry were derived by analyzing and mapping the variability of fundamental frequency of resonance over the neighboring area of the seismic station. Finally, a number of engineering parameters, such as  $V_{S30}$  and the quarter-wavelength velocity as a function of frequency or wavelength, can then be easily derived from the measured velocity profiles together with their uncertainties. Even though the engineering parameters will evolve with time due to new advances in research, the availability of 1D velocity profiles will give the possibility to progressively incorporate new information without reassessing the sites.

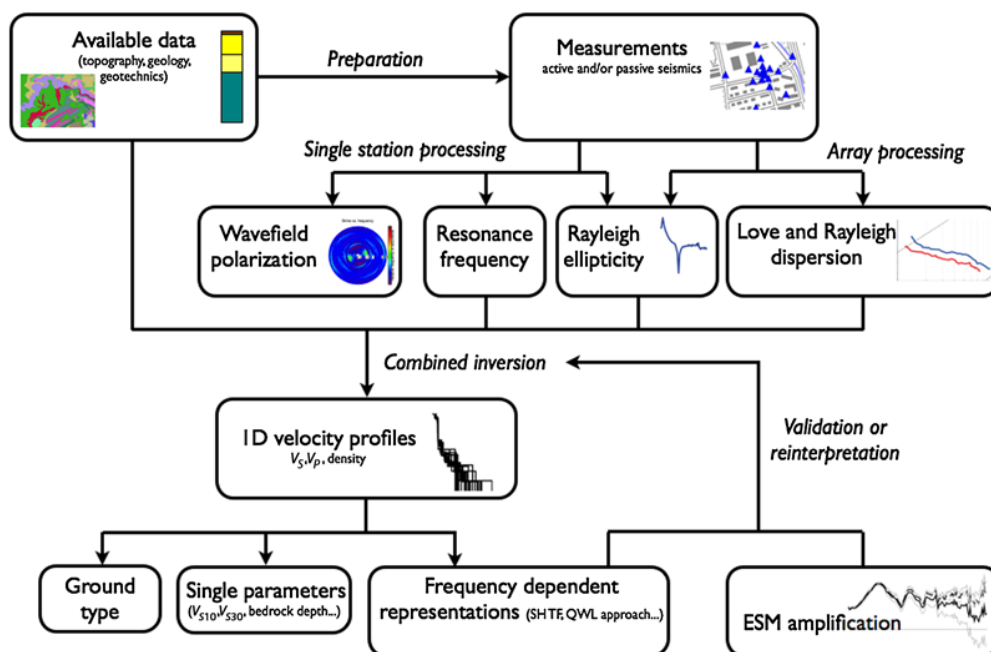


**Figure 3.** Site characterization procedure. The color version of this figure is available only in the electronic edition.

#### Retrieval of 1D Velocity Profiles

One-dimensional velocity profiles correspond to the sampling of the seismic velocities below the considered seismic station. Different methods exist to estimate 1D profiles. Borehole techniques such as sonic logging and downhole seismics are invasive but estimate the velocities with high resolution along the drilling line. Active and passive seismic surface-wave methods, on the other hand, are noninvasive but representative of finite volumes in the vicinity of the site. Small-scale heterogeneities within this volume are then averaged in a 1D profile, with resolution depending on the wavelengths involved in the method. This might lead to differences in the resulting 1D profiles with respect to direct borehole logging and between different methods.

The site characterization procedure adopted here is mainly based on surface-wave analysis of ambient vibration arrays. In some cases, it is complemented by surface-wave analysis of active seismic experiments (multichannel analysis of surface waves [MASW] technique). Passive techniques have been extensively applied and validated in the literature, especially in Europe (see Bard *et al.*, 2010, for a review). Combined passive and active surface-wave techniques have also been used to characterize strong-motion stations, for example, in Italy (Foti *et al.*, 2011) and Greece (Savvaidis *et al.*, 2006). Furthermore, part of the adopted procedure was already implemented to characterize 30 stations of the Swiss Seismic Networks (Havenith *et al.*, 2007; Fäh *et al.*, 2009).

A review of available geological, topographical, and geotechnical information is first performed to design geophysical experiments, to determine where the 1D assumption is valid, or at least to establish to which extent it can be valid.

Even if it could also provide information on the necessary array size, experience showed that the size of seismic deployments (arrays) in urban areas is generally limited by practical constraints such as main transportation lines or changes in the topography and surface geology. *A priori* information is also necessary to provide constraints on subsequent inversions in terms of realistic material properties and eventually depth of interfaces, especially the bedrock/sediment interface. For that purpose, geological and topographical maps and results from previous boreholes and geophysical experiments were collected. Table 1 lists all stations installed during this project along with the measurements performed (passive and active) at each site and the surface geology. Within the project, 27 array measurements with 60 to 480 m aperture and about 10 m minimum interdistance were performed. In addition, two existing passive measurements were reprocessed, and four MASW experiments were performed (typically 50 m long geophone linear arrays with 1–2 m interstation distance). The passive array measurements were typically made with 14 Lennartz 3C-5s seismometers data were acquired using Quanterra Q330 digitizers. An example of array setup for the site SBUH, with a large aperture, is shown in Figure 4. Two-hour recordings of 1–2 array layouts (rings of 3–5 stations with increasing radius around a central station) were made. In some cases, the recordings were made at night to minimize nearby noise sources. The MASW experiments were performed either using a sledgehammer or weight drop (120 kg) as active source, with data acquired on geophone strings and, in a few cases, seismological stations.

Following the acquisition of ambient vibration data, the following processing steps are applied to each dataset:

Table 1  
Overview of the 30 Stations Installed during the Project and Their Site Properties Sorted by  $V_{S30}$

Station Code	Name	Start Date (yyyy/mm/dd)	Meas.*	Site		Type	Resonance Frequency		Travel-Time Average S-Wave Velocity						EGSW†
				Surface Geology	Geology		EC8	$f_0$	Depth (m)	Interpretation	$V_{S10}$	$V_{S30}$	$V_{S50}$	$V_{S100}$	
SLUW	Luzern Werkhofstrasse	2010/12/23	P+A	Reclaimed land		C	1.15	200	Quaternary (unclear)	154	224	275	365	504	Yes
SEPL	Lausanne-EPFL	2011/10/26	A	High terrace (Pleistocene)		C	1.9	37	Quaternary (1D)	162	224				
SYVP	Yverdon-Philosophes	2011/09/07	P	Spit (Holocene)		C	1.15	80	Quaternary (1D)	194	257	279	353		Unclear
SINS	Interlaken	2012/09/17	P	Alluvia (Holocene)		C	0.51	380	Quaternary (2D)	202	266	313	371	455	Yes
SOLB	Solothurn Brühl	2011/11/22	P	Alluvial fan (Holocene)		C	0.6	180	Quaternary (unclear)	185	274	326	396	479	Yes
SLOP	Locarno Pompieri	2013/06/24	P	Alluvial fan (Holocene)		C	0.67	450	Quaternary (1D)	271	304	339	400	503	
SIOM	Sion-Mayennets	2011/01/06	P	Alluvial fan (Holocene)		C	0.46	150	Quaternary (2D)	351	365	432	504		Yes
SBERN	Bern Kleine Schanze	2013/06/07	P	Reclaimed land on moraine (Pleistocene)		C	2	40	Quaternary (1D)	254	366	433	567		
SBR5	Brig Spital	2012/09/03	P	Alluvial fan (Holocene)		C	1.4	200	Quaternary (unclear)	234	386	492	627	788	Unclear
SGEV	Genève-Vieux Billard	2011/12/13	P	Alluvia (Holocene)		B	4.2	24	Quaternary (1D)	286	415	562			
SBUH	Buchs-Hochschule	2012/10/22	P	Alluvia (Holocene)		B	0.6	250	Quaternary (1D)	301	420	360	380	465	Unclear
SOLZ	Solothurn Zeughaus	2012/01/18	P	Moraine (Pleistocene)		B	1.45	170	Quaternary + Tertiary (1D)	315	432	473	557		
STGK	St Gallen Klosterhof	2012/03/16	P	Moraine (Pleistocene)		B	4	40	Quaternary (1D)	241	440	577			
SBEG	Bettingen-Gewerbehau	2012/02/13	P	Alluvia (Holocene)		B	4	35	Quaternary (1D)	346	444	575			
SALTS	Altdorf Spital	2012/11/12	P	Alluvial fan (Holocene)		B	1.2	320	Quaternary (1D)	359	470	524	656	829	
SVAM	Vaz-Muldaun	2011/05/26	P	Flysch (Upper Cretaceous-Eocene)		B	4	45	Unstable slope (1D)	310	486	582			
SNIB	St Niklaus Bahnhofstrasse	2010/12/13	P	Alluvial fan (Holocene)		B	1.3	> 100	Quaternary (2D)	443	505	540	706		Unclear
SRER	Reinach-Rainenweg	2011/05/16	P	Low rubble terrace (Pleistocene)		B	0.45	> 570	Quaternary + part of Tertiary (1D)	474	514	557	613	788	Yes
SAIG	Aigle-rue de la Gare	2012/04/20	P	Alluvial fan (Holocene)		B	1.4	350	Quaternary (unclear)	420	535	587	777	1009	Unclear
SARK	Sarnen Kantonsschule	2012/05/30	P	Alluvia (Holocene)		E	2.3	160	Quaternary (1D)	307	541	709	939		
SMAO	Martigny Octodure	2012/11/12	P	Alluvia (Holocene)		B	0.85	250	Quaternary (unclear)	349	567	677	796	882	Unclear
SGRA	Grächen Ausblick	2010/12/13	P	Moraine		B	0.7	500	Unstable rock slope (1D)	398	576	694	878	1094	
SZUZ	Zürich Zeughausshof	2012/12/19	P	Gravels of the Sihl river (Pleistocene)		B	0.93	250	Quaternary + part of Tertiary (1D)	372	579	656	651	746	
SBUA2	Buchs-Altendorf	2011/08/17	P	Alluvial fan (Holocene)		B	3.6	90	Quaternary (2D)	405	618	771	1025		Unclear
SLIM2	Linthal-Matt2	2011/05/31	P	Slope waste (Holocene)		B	1.34	250	Quaternary (unclear)	468	620	723	876	994	
SCUG	Chur Gewerbeschulhaus	2011/18/11	P	Alluvial fan (Holocene)		B	0.46	700	Quaternary (2D)	516	714	825	960	1119	Unclear
SIEB	Sierre Ecole de Borzuat	2012/05/11	P	Slope loam (Holocene)		B	2.4	200	Quaternary (1D)	492	726	818	1015		
SCHS	Schaffhausen-Spital	2011/06/09	P	Moraine (Pleistocene)		A	12	15	Quaternary (1D)	646	960	1190			
SLUB	Luzern Bramberg	2011/12/02	P+A	Sandstone (Marine Molasse, Tertiary)		A			No resonance	711	1100	1426			
SBUB	Buchs-Buchserberg	2010/09/02	P+A	Limestone (Cretaceous)		A			No resonance	871	1563				

\*P, Passive array measurement; A, active seismics-MASW

†Edge-generated surface waves



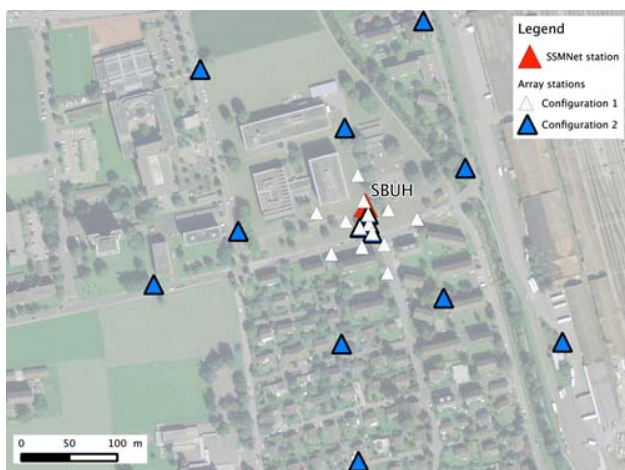


**Figure 4.** Array setup for site SBUH. The color version of this figure is available only in the electronic edition.

1. Single-station analysis through H/V spectral ratios and polarization analysis. The former are used to retrieve the fundamental frequency of resonance and—to some extent—the ellipticity of the fundamental mode of Rayleigh waves. The latter might indicate evidence of 2D resonance or unstable rock slopes.
2. Array analysis to retrieve the dispersion curves of Love and Rayleigh waves.
3. Combined inversion of dispersion, resonance, and ellipticity curves.

Each step is detailed hereafter and summarized in Figure 3.

Before any processing on the stations of the array, data quality is ensured in time and frequency domains to detect the presence of signal disturbances or vibrating structures. The orientation of the sensors is checked following the optimization procedure described in Poggi *et al.* (2012): the correlation of signals at low frequencies is used to detect the misorientation of sensors in the horizontal direction that can affect subsequent 3C processing. A correction is subsequently performed with respect to a reference station. Because a compass is used in the field to orient the instruments, errors up to  $10^\circ$  are commonly found, but larger errors might occur when sensors are placed close to disturbances of the magnetic field. H/V analysis of each recording of the array and other available recordings in the area is then performed using different approaches to ensure the quality of the results. In particular, methods based on time-frequency analysis are, at least theoretically, able to remove the Love-wave contribution on the horizontal components (Fäh *et al.*, 2009; Poggi *et al.*, 2012) and were therefore preferred to analyze Rayleigh-wave ellipticity functions. H/V spectral ratios are initially used to ensure the homogeneity of the measurement area (1D assumption) is fulfilled and, second, to estimate the fundamental mode of Rayleigh-wave ellipticity function and the fundamental frequency of resonance at the site. Maps of the fundamental frequencies ( $f_0$ ) were produced to under-

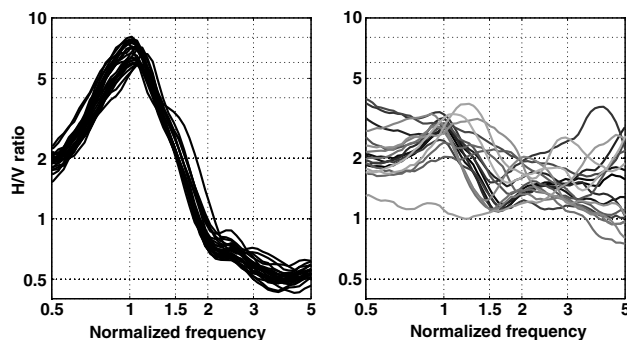


**Figure 5.** H/V analysis of array points of sites SBUH and SBUA2 using time–frequency analysis (Poggi *et al.*, 2012). The frequency axis has been normalized by the resonance frequency of the site.

stand the variability of the geology in the area of the seismic station. Figure 5 shows the example of a homogeneous site (SBUH, located on a large alluvial plain) and a site with strong lateral variability (SBUA2, located on an alluvial fan).

Following the computation of spectral ratios, single-station wavefield polarization analysis is performed using the approach of Burjánek *et al.* (2010). It provides, at each frequency, the azimuthal distribution of the energy of the ground motion and the parameters of the ground-motion ellipse. Pronounced ellipticity and focusing of ground motion in a particular azimuth are searched for throughout the array. Such effects may be interpreted as a 2D resonance of the structure if observed throughout the array. In case of identified 2D resonances, the ellipticity information is not used for the inversion of the 1D velocity profile because 1D theory of Rayleigh-wave propagation does not hold anymore around the frequencies of the 2D resonance. This is discussed in more detail in the last paragraph of this section.

For the array processing, high-resolution frequency–wavenumber (HRFK) analysis (Capon, 1969) on the vertical component is first performed using the software package Geopsy for ensuring quality (Wathelet *et al.*, 2008). Subsequently, 3C HRFK analysis following Fäh *et al.* (2008) and Poggi and Fäh (2010) is performed. Compared with the computation on vertical components only, 3C analysis makes optimal usage of the available channels to estimate, in addition, the dispersion of Rayleigh waves in the radial direction of propagation and of Love waves. Moreover, it allows the computation of the ellipticity function of Rayleigh waves. Figure 6 shows the 3C HRFK analysis performed to characterize the station SBUH.

For few difficult sites, such as those with very stiff soil and rock, active seismic experiments were also performed. The active source provides coherent energy at high frequency that in many cases is lacking in the ambient vibration wavefield. As a drawback, however, the maximum depth resolution is generally limited to about 30 m. MASW processing includes the standard  $f$ - $k$  technique (Park *et al.*, 1999) and the wavelet-based method of Poggi *et al.* (2013) to derive Rayleigh- and eventually Love-dispersion curves at high

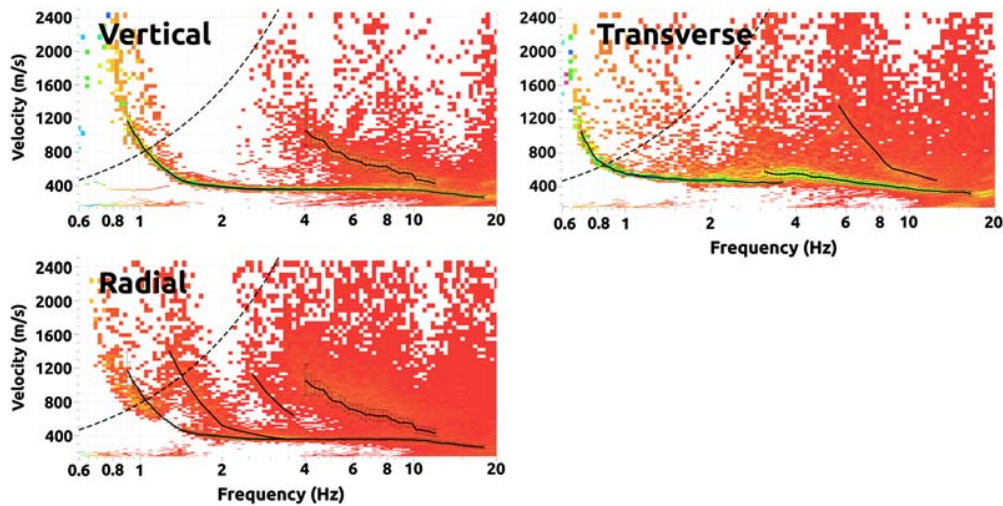


**Figure 6.** Three-component high-resolution frequency–wavenumber (3C HRFK) analysis (Poggi and Fäh, 2010) of an array around SBUH station. The dashed lines indicate the lower resolution limit of the array. The black lines indicate the selected dispersion curves with their uncertainty when available. The radial component highlights Rayleigh-wave higher modes that cannot be seen on the vertical component. The transverse component provides Love-wave modes. The color version of this figure is available only in the electronic edition.

frequencies, depending on the sensor availability (vertical or three component). The latter approach is particularly advantageous in use with continuous data from the seismological equipment of passive seismics. In some cases, other than just surface waves, head waves have been observed from  $f$ - $k$  analysis, which are useful to constrain the presence of shallow but large velocity contrasts.

Finally, all available information (Love and Rayleigh dispersion, ellipticity curves, and fundamental frequency of resonance) is inverted into a set of 1D velocity profiles using a direct search approach (global optimization) based on the modified neighborhood algorithm (Wathelet, 2008). A certain level of interpretation is needed for the input data before being inverted. As first, only the portions of the dispersion curves that lie within the array aliasing and resolution limits are considered (Wathelet *et al.*, 2008). From the ellipticity curve (H/V curve), only the right flank of the fundamental peak was generally used, because ellipticity can be identified best in this frequency range and contains information about the soil structure (Fäh *et al.*, 2001; Hobiger *et al.*, 2012). Extracted sections of dispersion curves are then compared and interpreted as fundamental or high-order modes (mode addressing). The interpretation can change during the procedure if new evidence arises, for example, in support of alternative modal patterns.

The resulting profiles are discrete representations of the elastic properties of the ground ( $V_P$ ,  $V_S$ , and density). Each profile is represented by a series of homogeneous horizontal layers. Given the highly nonlinear nature of the inversion problem to solve, additional *a priori* geological and geotechnical information are required to define the bounds of the search and consequently to restrict the size of the parameter space. This is useful to avoid unrealistic solutions due to overfitting (Wathelet, 2008) and trapping in local minima of

the misfit function. When available (in rare cases), borehole information was used to fix the depth of interfaces (e.g., at SEPFL site). Moreover, conditional constraints are often used, such as increasing velocity with depth (except if geology or particular characteristics in the dispersion curves suggest the presence of specific low-velocity layers) and realistic  $V_P/V_S$  ratios. For the latter, the Poisson's ratio is generally kept in the 0.2–0.4 range, although higher values were allowed just below the water table, where the  $V_P/V_S$  ratio can be rather large. Density values are fixed *a priori* based on the available local information (borehole data or literature); in practice, realistic changes in density have little impact in terms of amplification. Two different layer thickness schemes are used jointly, allowing fixed and free-layer interface depths. Using the fixed scheme has the advantage of reducing the nonuniqueness of the inversion problem but might lead to smooth velocity profiles. Conversely, a free-layer approach is very nonunique and might require considerable *a priori* information but lead to a better resolution of sharp velocity interfaces. An example of combined inversion of dispersion curves and ellipticity for station SBUH is presented in Figure 7.

A major issue related to the inversion of surface-wave data is the estimation of uncertainty in the results. Uncertainties are due to measuring errors such as the inaccurate picking of dispersion curves; and due to the forward modeling of surface-wave dispersion assuming a 1D velocity model with a limited number of layers. Because it is difficult to determine and represent the probability function in a space with many dimensions, the uncertainty was reflected by selecting a number of realistic profiles. This is done by performing the inversion on different parameterization schemes (free- and fixed-layer depths) and multiple inversion attempts using variable initial randomizations of the parameter space to be searched. Although this does not ensure the whole range of

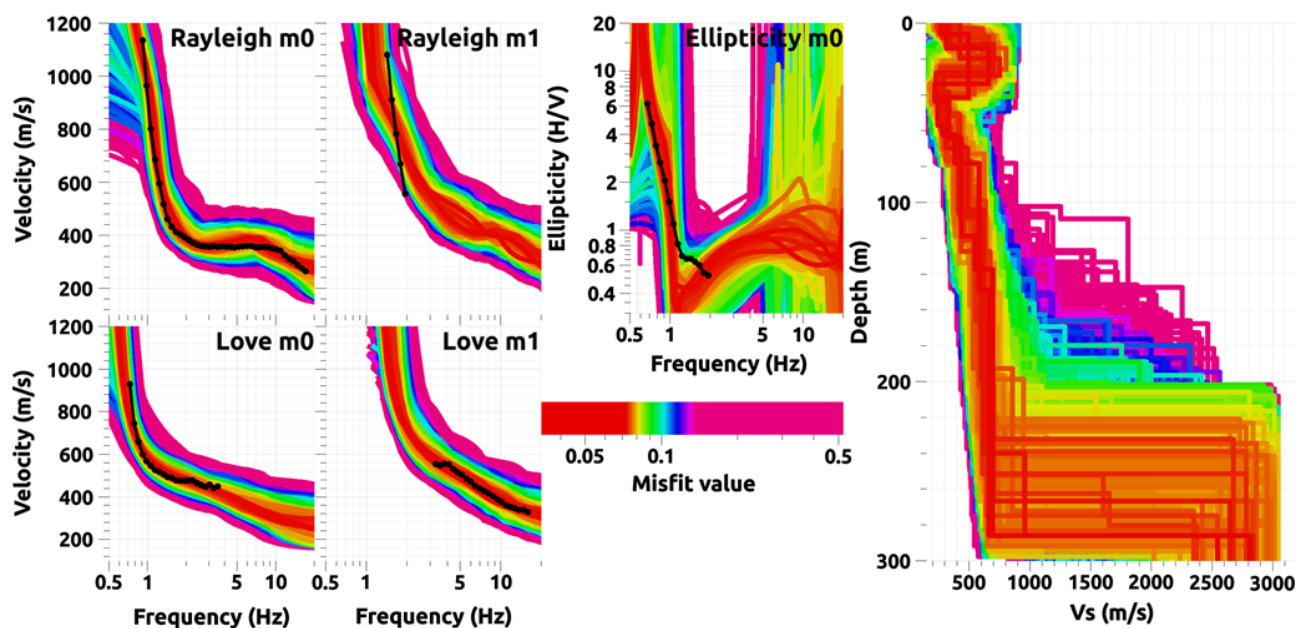


**Figure 7.** Combined inversion of dispersion curves (two modes of Rayleigh waves, two modes of Love waves) and right flank of the ellipticity of Rayleigh waves into velocity profiles (only  $V_S$  presented here). The black dotted lines indicate the observed properties, whereas the background lines indicate the inverted properties. The scale, denoting the misfit value, is consistent across the different plots. The color version of this figure is available only in the electronic edition.

uncertainties is covered, it nevertheless provides a homogeneous procedure to estimate the uncertainty to some extent.

From the selected 1D velocity profiles, several engineering parameters are derived along with their uncertainty. These parameters are the ground type, based on EC8 classification (Eurocode 8, 2004), travel-time average velocity at different depths (e.g., 5, 10, 20, 30, 50, 100 m) and frequency-dependent parameters: quarter-wavelength velocity (Joyner *et al.*, 1981), quarter-wavelength impedance contrast (Poggi, Edwards, and Fäh, 2012), and *SH*-wave transfer function for vertical incidence.

#### Comparison with Spectral Modeling

The site characterization undertaken for this project was based on well-established methods. However, to check the validity of the obtained velocity profiles, a comparison with amplification function from empirical spectral modeling (ESM) of earthquake ground motion at the permanent stations was performed. This technique has been described in detail by Edwards *et al.* (2008, 2013), with a similar approach shown by Thompson *et al.* (2012) to be able to distinguish non-1D effects. Each event detected by the seismological network is analyzed in near real time. The spectra of all recordings with sufficient signal-to-noise ratio are inverted to obtain the source parameters using a model for the path and known reference rock condition. The residuals at each station are interpreted as the site terms (Edwards *et al.*, 2008). Statistics over many small events allow convergence to a stable site amplification function, hereafter called ESM function, and its uncertainty. A region-dependent geometrical spread-

ing of Edwards and Fäh (2013) was implemented instead of the classical  $1/R$  decay. This allows us to avoid potential biases in the spectral estimation in particular in the near field. The ESM function describes the elastic amplification with respect to the Swiss reference rock velocity model (Poggi *et al.*, 2011). Therefore, it can be compared with 1D *SH* transfer function from site characterization after a correction from the reference rock, as shown by Edwards *et al.* (2013). This approach was systematically used here to check the validity of the 1D velocity profiles. The agreement between the two curves is checked relative to the presence of peaks, their frequency values, and the level of amplification. This comparison is performed keeping in mind that expected differences may occur; non-1D wave propagation phenomena such as EGSW or 2D/3D resonance cannot be reproduced by 1D transfer functions. Furthermore, there are potential trade-offs in the spectral inversion between elastic amplification and anelastic attenuation that may lead to incorrect amplification levels at high frequencies. The comparison between theoretical 1D-*SH* and ESM amplification led to a reinterpretation of the dispersion curves, and consequently to a new inversion for velocity profiles, in which significant differences were apparent.

An example of the *SH* versus ESM amplification comparison is presented in Figure 8 (station SBUH) in which the first inversion (without low-velocity zone) led to acceptable fit of the dispersion curves, but the empirical and theoretical amplification functions were not matching. Subsequently, allowing for a low-velocity zone close to the surface led to models that better reproduce the empirical amplification function. The low-velocity zone is due to the presence of fine uncompacted sediments below a gravel layer and was

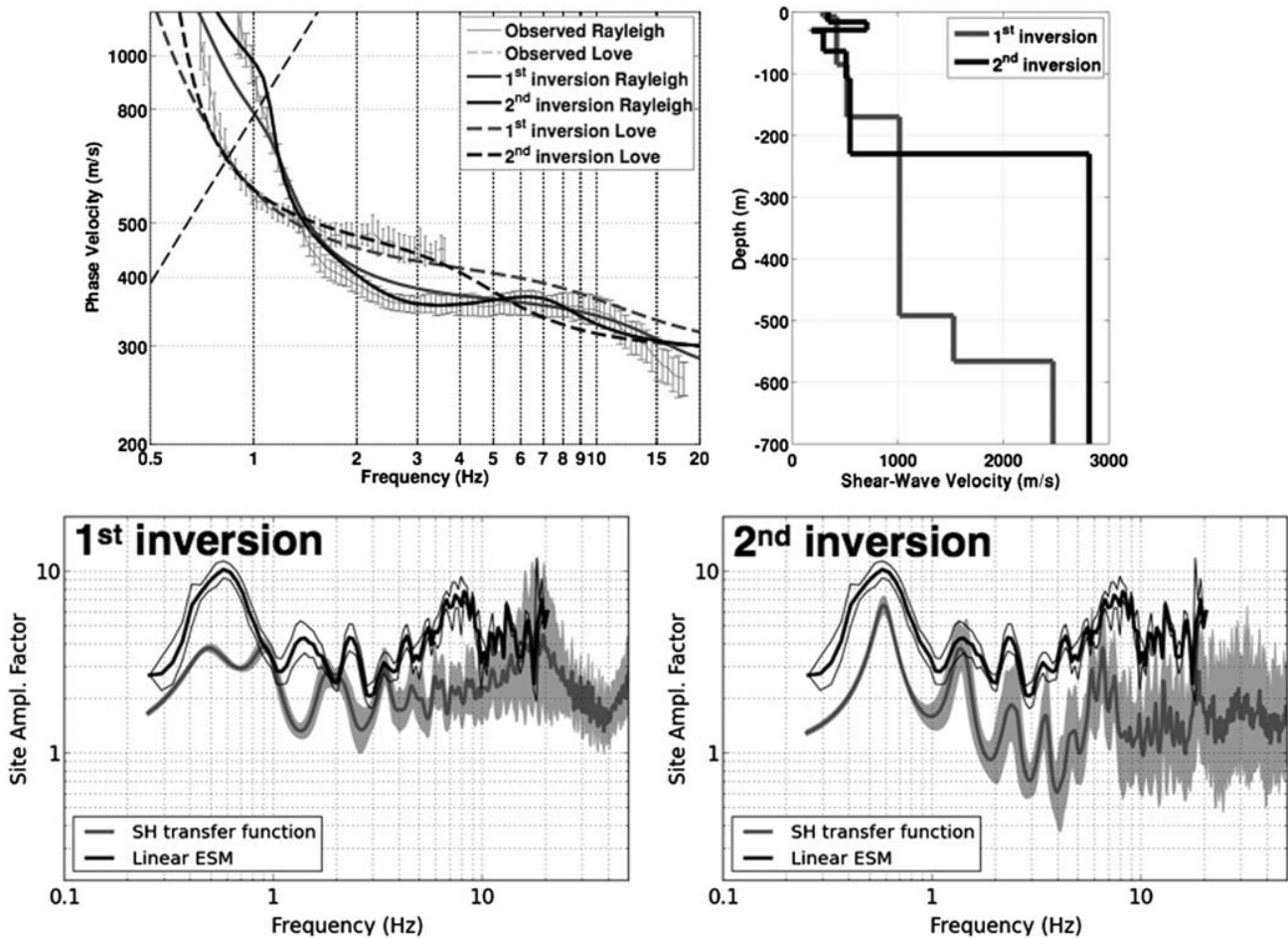


**Figure 8.** Comparison between the first inversion performed without velocity inversion and the second that allows a low-velocity zone. Top left: dispersion curves (fundamental Love and Rayleigh) of one selected model of each inversion and observations with error bars. Top right: selected models for each inversion. Bottom: comparison of ESM amplification and *SH* transfer function for each inversion.

confirmed by borehole analysis. Apart from the low-velocity zone close to the surface, the initial and adjusted velocity models are similar in the first 150 m. The bedrock depth, constrained only by the H/V peak, is also considerably different. This shows the difficulty to obtain reliable profiles beyond the depth constrained by the dispersion curves, even using the ellipticity. To estimate the depth where the profile is resolved, the quarter-wavelength approach can be used (Joyner *et al.*, 1981). For given velocity profiles, it can provide an estimate of the depth corresponding to the lowest frequency in the dispersion curves (0.85 Hz—corresponding to 120 m depth for the case in Fig. 8). However, this value is relatively rough and conservative.

#### Detection of 2D/3D Effects

To detect 2D resonance in our site characterization procedure, we used polarization analysis following the technique of Burjánek *et al.* (2010). This approach uses single-station processing of array data and assumes that a strong polarization in the valley axis is an indication for 2D resonance (Ermer *et al.*, 2014). Moreover, this procedure can

highlight 2D/3D effects in case of sites with pronounced topography (Burjánek *et al.*, 2012, 2014). The procedure outlined in this article aims to classify the sites of the stations (i.e., existence of 2D/3D effects). More investigations are necessary to better understand the 2D/3D behavior but are beyond the scope of this study.

The detection of EGSW is based on the comparison of the theoretical 1D-*SH* with the ESM amplification. The level of amplification of 1D models, and therefore of the aggravation factor (Cornou and Bard, 2003), is largely controlled by the bedrock velocity, which is generally uncertain. It may therefore be difficult to know whether deviations from observed amplification functions are due to unknown bedrock velocity at depth or 2D/3D effects. Nevertheless, by comparing the ESM amplification function, which integrates all geometrical (1D, 2D, 3D) effects, with the 1D-*SH* transfer function from the site characterization, we identified characteristic deviations in shape (peaky versus smooth functions) where EGSW were suspected. The classification of sites exhibiting EGSW was therefore objectively assessed based on the comparison of amplification shape rather than amplitude.

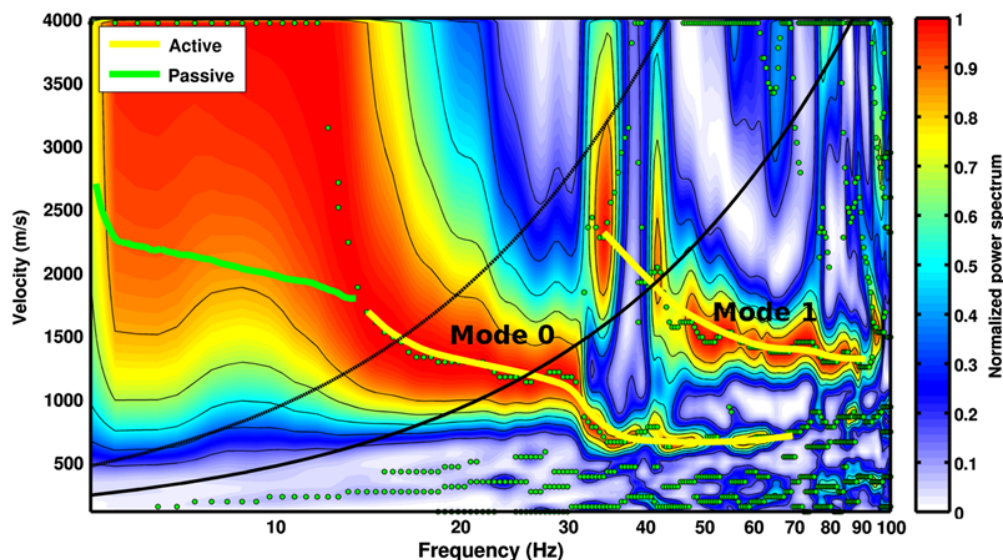


**Figure 9.** Multichannel analysis of surface wave (MASW) analysis at site SLUB (vertical component) with interpretation of Rayleigh-wave fundamental and first higher modes. The dispersion curve retrieved from the passive measurement is also displayed. The black bended line is the resolution limit of the MASW analysis. The color version of this figure is available only in the electronic edition.

### Results from 1D Site Characterization

Table 1 summarizes the results of the site characterization. The resonance frequencies across all sites range from 0.45 to 12 Hz. Using the combined inversion, the resonance frequencies are interpreted as the resonance of the soil column above an interface at a given depth (Table 1). The 30 sites range therefore from very deep sedimentary sites (down to 600 m depth) to shallow sediments (15 m depth) and rock sites (no resonance or at high frequency). Most of the time, particularly in the Alpine area, the fundamental frequency corresponds to the interface between sediments and the bedrock. At some sites, it has been clearly shown that the resonance frequency is related to 2D resonance of the whole basin (see [Classification of Sites with Respect to 2D/3D Response](#) section). In three cases (SOLZ, SRER, and SZUZ), all located in the Swiss foreland, the observed resonance corresponds to layers including Tertiary sediments. This fact was already recognized in previous studies concerning the region of Basel (station SRER, e.g., [Steimen et al., 2003](#)). In two other cases on alpine rock slopes, the resonance may be related to slope instability. This has been already shown for the Grächen case (SGRA) ([Fäh et al., 2012](#)) but needs more investigation for the site Obervaz (SVAM).

There is no doubt that the resulting velocity profiles benefit from the 3C array analysis technique because more information is retrieved: in particular the transverse component allows the retrieval of Love dispersion curves and the radial component sometimes better outlines the higher Rayleigh-wave modes than vertical-component analysis only. Misinterpretation of mode addressing can also be minimized leading to more robust and accurate inversions. This is illustrated in Figure 6: on the radial component, the first and second Rayleigh-wave higher modes appear, although they could not be seen on the vertical component. The third higher mode

may have been mistakenly interpreted as the first by looking at the vertical component only. At only two sites could no dispersion curves on the transverse component be observed: SLUW in the deep lacustrine basin of Lucerne ([Poggi et al., 2012](#)) and SIOM in the Rhône valley ([Roten et al., 2006](#)). This may be due to the absence of a velocity gradient in the basin, or at least one that is not very pronounced, because Love waves do not propagate at the surface of a homogeneous half-space.

Active seismics, particularly MASW, proved to be complementary to ambient vibration arrays ([Poggi et al., 2013](#)). Their combined use was helpful in the case of the rock site SLUB (Fig. 9). A 46 m string of 24 geophones was used together with a weight of 120 kg dropped from 1.1 m height. The upper 15 m were constrained by the active experiment, whereas the bottom part until 75 m depth was retrieved using a passive array of 160 m aperture. Unfortunately, none of these techniques provided good results on the hard-rock site SBUB, where it was necessary to employ refraction seismics.

According to the comparison with ESM, a revision of 13 out of 30 sites was performed. This large number is partly due to the low amount of previous knowledge of the sites. The main reasons that led to incorrect profiles, and therefore mismatch with the ESM amplification, were errors in mode assignment, overconfidence in the H/V function as proxy for the ellipticity, and unnoticed low-velocity layers at depth. Mode assignment has already been detected as an issue by [Cornou et al. \(2009\)](#) after an international blind test. The interpretation is especially difficult at osculation points, that is, where two modes are very close to each other. Moreover, even if some sections of H/V curve are in many cases a good proxy for the Rayleigh-wave ellipticity, many authors showed it may be biased by the Love-wave contribution and non-1D effects ([Fäh et al., 2001](#); [Bonnefoy-Claudet et al.,](#)

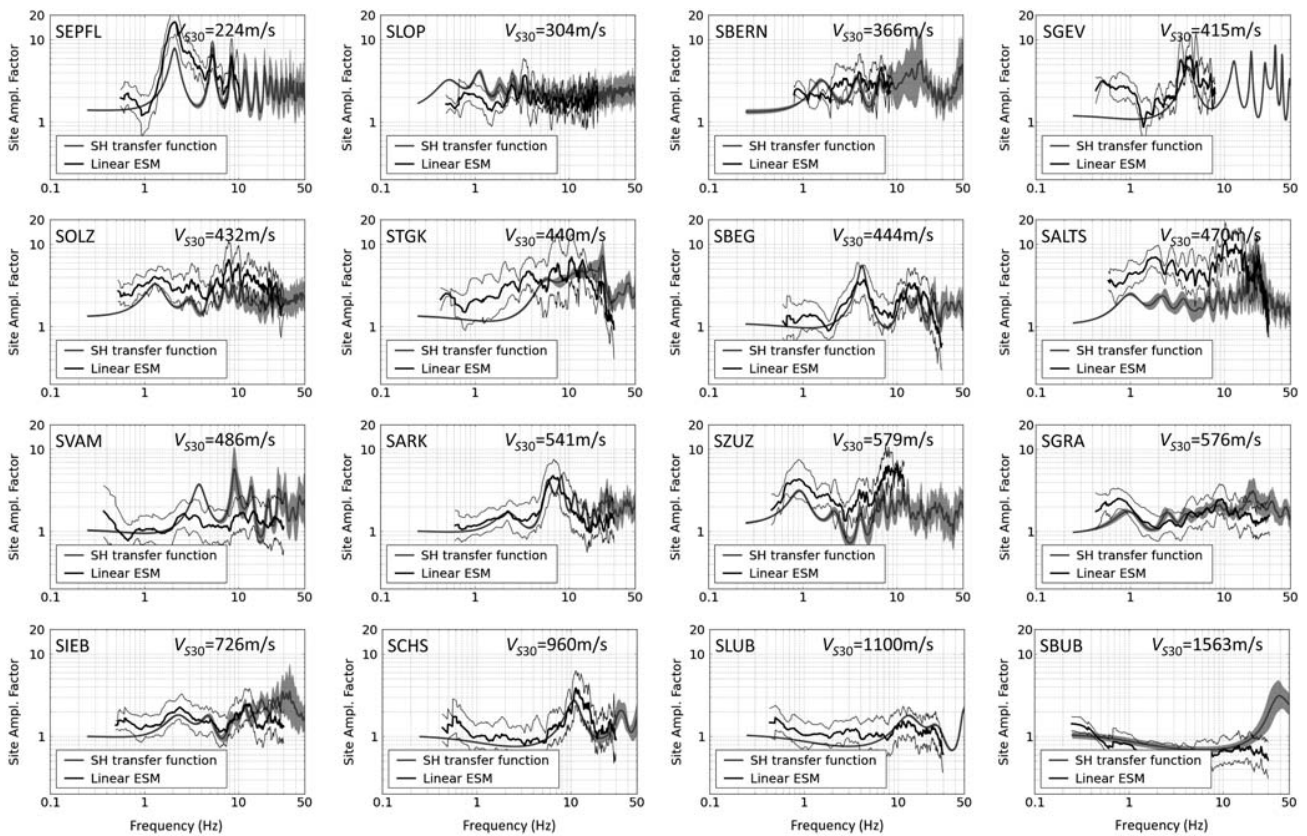


**Figure 10.** Comparison between *SH* transfer function from site characterization and ESM elastic amplification for 1D sites ordered by increasing  $V_{S30}$ .

2006). In our procedure, Love-wave contribution to the H/V ratio was minimized using time–frequency analysis (Poggi *et al.*, 2011) and 3C array analysis (Poggi and Fäh, 2010). Finally, as explained in the previous section, low-velocity zones were considered only if no model with increasing velocity with depth could be found that explains the observations. Surface-wave analysis alone in general is not robust enough to reliably resolve low-velocity zones. A comparison with ESM amplification and complementary data (borehole information, when available) should therefore be used.

It should be underlined that the comparison process does not ensure that profiles are unbiased, even in 1D cases. There are trade-offs between different parameters in the inversions that cannot be tested through this comparison. For instance, the inversion of bedrock depth and velocity at depth, where no dispersion curve is available, is generally nonunique and relies on the H/V curve that may not always represent the ellipticity of the fundamental-mode Rayleigh wave. However, the comparison with empirical amplification helps reduce the bias on the estimated velocity profiles.

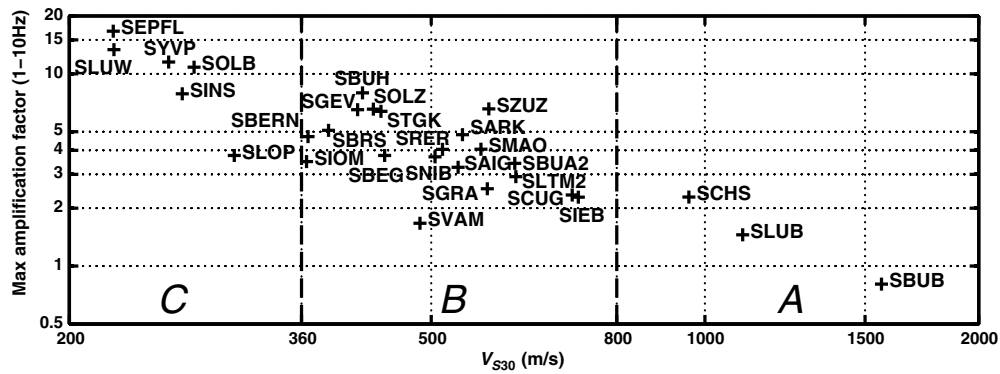
The comparison of the retrieved velocity profiles for 1D sites is presented in Figure 10. The 1D profiles are particularly good at representing the elastic amplification at each site. Other sites are treated in the next section.

Figure 11 presents the  $V_{S30}$  of all sites with respect to the maximum amplification value in the ESM function in the fre-

quency band 1–10 Hz. It shows the clear correlation between  $V_{S30}$  and amplification but is particularly useful to show the range of these two parameters. This figure shows the majority of sites are categorized as ground type B (stiff sediments). This is due to the fluvial-glacial nature of a large part of the alpine sediments. They cause amplification with respect to the Swiss reference of a factor 1.7–8. Glacial-lacustrine sediments are also present (six sites) and correspond to ground type C with  $V_{S30}$  values from 220 to 300 m/s. Their maximal amplification is between 4 and 17. No site belongs to ground type D ( $V_{S30} < 180$  m/s). Three rock sites have been instrumented with very different characteristics such as a hard-rock site in the Alps (SBUB), a site on molasse rock in the Foreland (SLUB), and a hard-rock site in the Jura zone overlain by a thin consolidated moraine layer (SCHS). SLUB is comparable to the Swiss reference velocity model, whereas SBUB shows deamplification and SCHS amplification up to 30%. Only one site (SARK) falls in the EC8 definition of ground type E (thin layer of C or D ground type on rock).

#### Classification of Sites with Respect to 2D/3D Response

Figure 12 classifies the different sites with respect to the presence of EGSW and 2D/3D resonance (see also



**Figure 11.** Distribution of the station sites with respect to  $V_{S30}$  and maximum amplification in the ESM function in the 1–10 Hz frequency band. Definition of A, B, and C ground types of EC8 (Eurocode 8, 2004), based on  $V_{S30}$ , are also displayed.

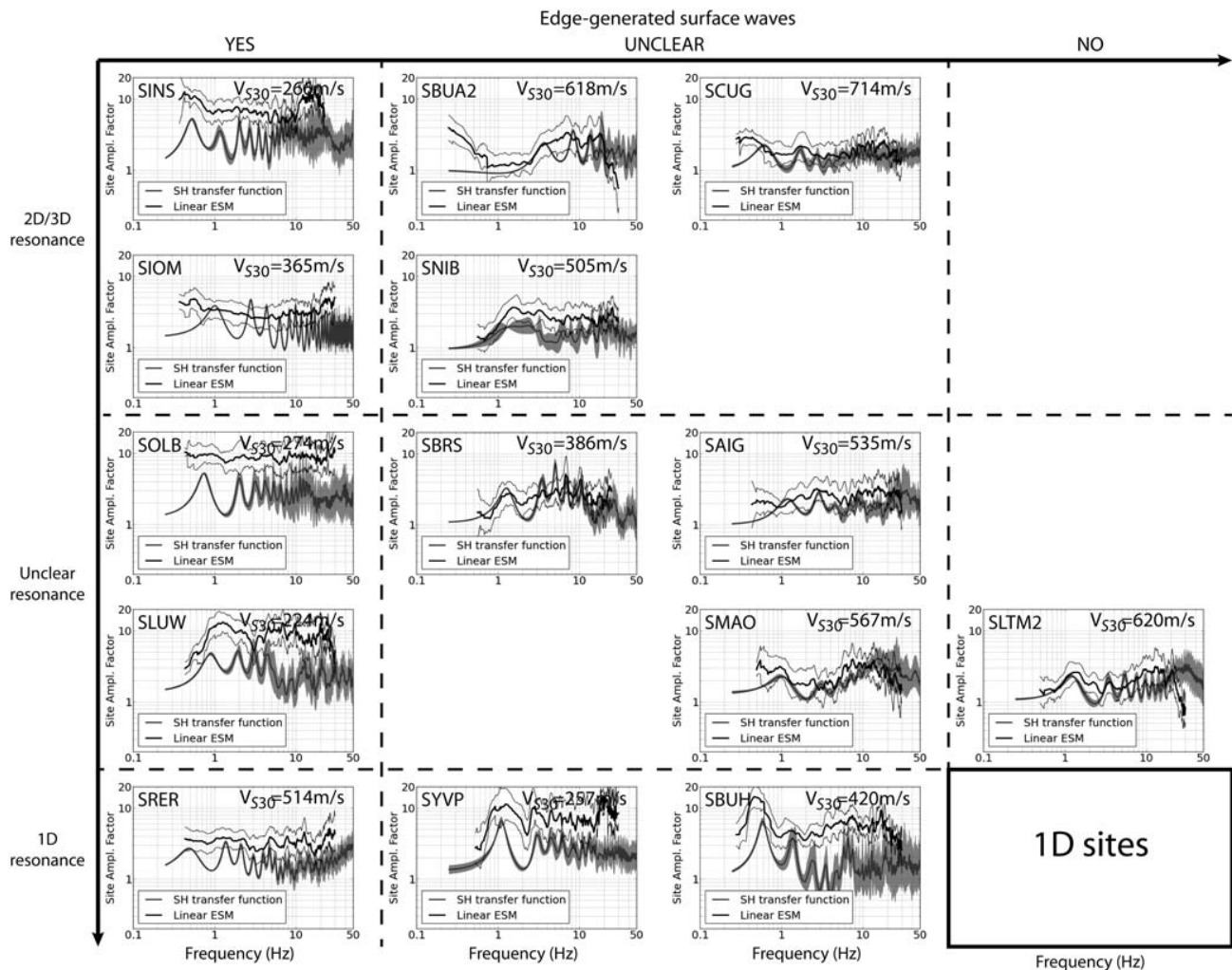


**Figure 12.** Comparison between *SH* transfer function from site characterization and ESM elastic amplification for sites with clear or possible 2D/3D effects. Horizontal axis: classification of edge-generated surface waves (EGSW) using the level of agreement of the ESM with the theoretical 1D response (from left to right: presence of EGSW, unclear case, and no EGSW); Vertical axis: classification of 2D/3D resonance using the polarization analysis comparison (from top to bottom: 2D/3D resonance, unclear case, and 1D resonance).

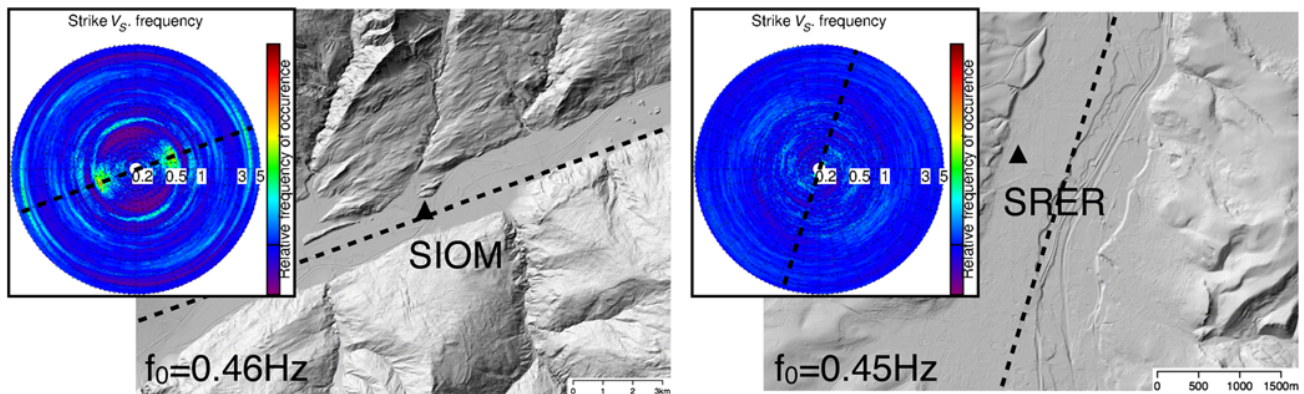


**Figure 13.** Polarization analysis of sites SIOM (2D/3D resonance with EGSW) and SRER (1D with EGSW) and topographic map of the sites. Dashed black lines are showing the valley axis of each site and are reproduced on the polar plot. The polar plots represent the azimuthal distribution of the energy for frequencies between 0.2 and 5 Hz. The color version of this figure is available only in the electronic edition.

Table 1). Clear 1D sites are excluded from this figure and are presented in Figure 10. EGSW can be observed at sites SIOM, SINS, SOLB, SLUW, and SRER. Even if the velocity contrasts are not so large, the difference due to EGSW at site SRER is clear. Their presence at some other sites cannot be excluded. These sites are therefore classified as unclear. For instance, at SCUG, the velocity contrasts are low so that the smooth shape of the amplification function cannot be clearly attributed to these low contrasts or EGSW. At station SBUA2, the smooth part between the first and second peak in the ESM function is likely to be related to EGSW. A more detailed characterization of this effect requires a 2D parameterization of the sites and numerical modeling (Paolucci and Morstabilini, 2006) that will be performed in future studies.

Five sites show a clear polarization of the wavefield at the resonance frequency in the expected direction of a 2D resonance. Sharp peaks in the spectra, related to industrial activities and polarized in the direction of the source, were excluded from the analysis. SIOM, SINS, and SCUG are located in the deeply filled valleys of the Rhône, Aare, and Rhine rivers, in the Alpine area, respectively. At their fundamental frequency of resonance, the wavefield is polarized along the valley axis, corresponding therefore to the fundamental  $SH$  mode (e.g., Fig. 13 for SIOM station). More refined studies should be applied to array recordings along cross section to detect the other resonance modes (e.g., Roten *et al.*, 2006; Ermert *et al.*, 2014). SBUA2 and SNIB are located in much smaller structures, namely an alluvial fan on the side of the Rhine valley and the small alpine valley of the river Matternvispa (Fritsche *et al.*, 2005). Both sites clearly show a polarization in the axis of these structures at the resonance frequency. For several other sites, polarization could be detected but was either weak (e.g., SOLB) and/or in a direction not corresponding to the main valley axis. For stations SLTM2 and SAIG, the polarization at the resonance frequency is perpendicular to the valley axis. They are both

located on alluvial fans that may influence the wavefield, but their small sizes compared with the whole valley may indicate that the fundamental  $P$ - $SV$  mode is observed. These sites are nevertheless categorized as unclear in Figure 12. Moreover, at some sites like SRER, no particular polarization of the wavefield could be noticed (Fig. 13), and these sites are therefore classified as exhibiting 1D resonance.

A further indication of 2D/3D resonance is given by the shape ratio and velocity contrast of the considered 2D structure, as shown by Bard and Bouchon (1985). The shape ratio is defined for sine-shaped valleys as the ratio of maximum sediment thickness  $h$  to the valley half-width  $l$ . Bard and Bouchon (1985) also defined an equivalent shape ratio for any other valley type as  $h/2w$ , with  $2w$  the total width over which the sediment thickness is greater than half its maximum value. The velocity contrast is computed as the ratio of the bedrock  $S$ -wave velocity to the travel-time average  $S$ -wave velocity of the sediments layers. The bedrock velocity and shape ratio are sparsely known in our project because we were focused on 1D and not 2D geometry. However, at many sites, these values could be estimated, sometimes with a large interval of uncertainty, and are displayed in Figure 14. These results are in agreement with the conditions defined by Bard and Bouchon (1985) for the critical curve, because sites on the right part of this curve were already identified as exhibiting 2D/3D behavior, taking the uncertainties into account. Unclear sites are mostly located close to the critical curve. SOLB and SLUW, based on this figure could eventually be reclassified as 1D resonance sites with EGSW. Sites recognized without 2D/3D resonance are located on the left part of the plot as predicted by Bard and Bouchon (1985). These authors also clearly state that the transition is smooth from 1D to 2D behavior and that the critical curve is in reality more blurred, which is also consistent with the results found here. Unclear sites may therefore be renamed as “transition” sites but may never be classified exclusively in 1D or 2D/3D resonance categories.



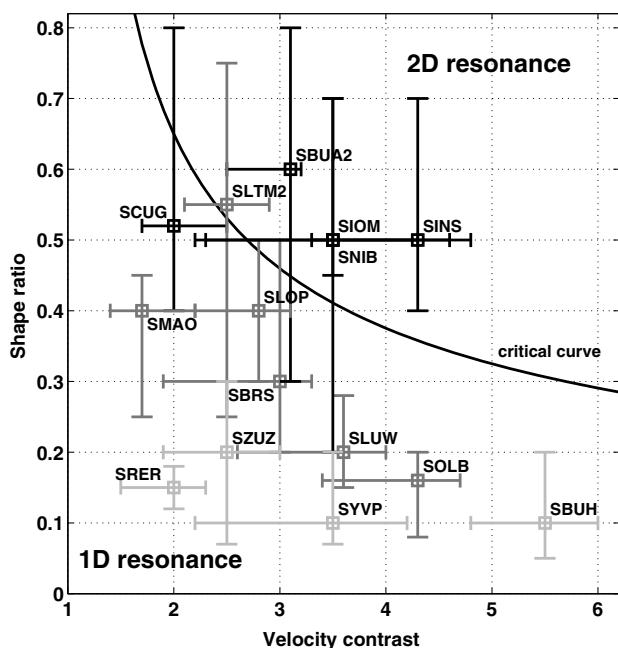


**Figure 14.** Shape ratio as a function of velocity contrast for a selection of studied sites (squares with uncertainty intervals) and proposed critical curve (black line) from Bard and Bouchon (1985). Site classification with respect to resonance from Figure 12: 2D (black), unclear (dark gray), and 1D (light gray).

Finally, 2D/3D effects are most significant at sites SIOM and SINS with clear 2D resonance and EGSW. At eight other sites, resonance and/or EGSW are considered as unclear, but 2D/3D effects are present. EGSW are sensitive to geometry and velocity contrasts at the basin edges (locally), whereas 2D/3D resonance is a global phenomenon and therefore depends on average parameters (geometry and elastic properties) of the whole geological structure. For instance, at site SRER in the Rhine graben, steep normal faults at the basin edge generate EGSW, but the basin is too flat to generate 2D resonance (Steimen *et al.*, 2003). However, in the case of alpine valleys such as the upper Rhône, Rhine, and Aar valleys, more regular, EGSW and 2D resonance are more likely to occur together.

## Conclusions

In the framework of the SSMNet renewal project phase 1, we proposed and systematically applied a site characterization procedure based on surface-wave analysis, particularly using ambient vibrations. A method based on spectral modeling was used to check the validity of the retrieved 1D velocity profiles. Despite the relevance of the collected data and their analysis, this comparison procedure led to numerous reinterpretations, strongly contributing to an increase in the quality of the results. Such a comparison procedure can therefore be recommended for future projects.

The whole procedure allowed the detection of non-1D effects, namely 2D/3D resonance using polarization analysis and EGSW using the comparison between 1D transfer function and ESM amplification. It has been found that a 1D assumption was valid and sufficient to represent the ground response to seismic motion in many of the studied cases. However, field measurements are absolutely necessary to extract 1D profiles representative of the seismic response. Because of the variable nature of the ground properties, other proxies such as geology are not sufficient to relevantly assess the ground amplification.

2D/3D effects are also critical to be recognized because they may greatly increase the local hazard. However, these effects are present only at particular sites that need to be recognized. In Switzerland, these sites are parts of the deep sediment valleys of the Rhône, Rhine, and Aar rivers as well as smaller structures like small alpine valleys, alluvial fans, and pronounced lateral changes in the velocity structure. The previously studied case of the Rhône Valley (e.g., Roten *et al.*, 2006) is a particular case with strong 2D effects. The highlighted cases will now be studied in more detail with 2D/3D characterization. Indeed, except for some well-studied cases, little is known of the geometry and the elastic properties of sedimentary valleys. This study also again confirmed the relevancy of the study by Bard and Bouchon (1985). The critical shape ratio and velocity contrasts they propose are in accordance with the observations presented here.

The use of ESM amplification directly within the combined inversion procedure of 1D cases is planned for future work. The case of structures with 2D/3D effects can be identified with the comparison, but a different approach needs to be developed to invert for the 2D structure (Roten and Fäh, 2007). Within the spectral modeling process, the anelastic attenuation term is also obtained in terms of site-specific kappa (Edwards *et al.*, 2011) and could be used to derive the quality factors of the sediments. Relating the inverted anelastic term of kappa from spectral modeling to attenuation models is therefore a topic for future work.

Besides site effects, numerous sites presented in this study cover aspects of different scientific and societal interest. It is the basis for future work on earthquake hazard and risk, including source effects, nonlinear site response and liquefaction, and earthquake-triggered landslides.

## Data and Resources

Data from the SED permanent network used in this article can be obtained from the Arclink server of SED ([arclink.ethz.ch](http://arclink.ethz.ch); last accessed June 2014) or alternatively from the European Integrated waveform Data Archive (EIDA) node of ETH Zurich ([eida.ethz.ch](http://eida.ethz.ch); last accessed June 2014). Geographical data from the Swiss Federal Office for Topography (Swisstopo) are used in this article. The data were partly processed using the Geopsy software suite ([www.geopsy.org](http://www.geopsy.org); last accessed December 2012) including geopsy and dinver. Some figures were made using the Quantum Geographic

Information System (QGIS) (<http://qgis.osgeo.org/>; last accessed September 2013).

## Acknowledgments

The Renewal project of the Swiss Strong Motion Network (SSMNet) is supported by the Federal Office for the Environment (FOEN), the Federal Roads Office (FEDRO), Swiss Federal Nuclear Safety Inspectorate (ENSI), the Swiss Federal Railways (SBB), the Schweizerischer Pool für Erdbebendeckung, and ETH Zurich. The authors also thank Sabine Wöhlbier-Röthlisberger who produced Figure 1. They are also grateful to Associate Editor Stefano Parolai, Roberto Paolucci, and an anonymous reviewer for their help in the improvement of the article.

## References

- Aoi, S., T. Kunugi, and H. Fujiwara (2004). Strong-motion seismograph network operated by NIED: K-NET and KiK-net, *J. Jpn. Assoc. Earthq. Eng.* **4**, no. 3, 65–74, doi: [10.5610/jaee.4.3\\_65](https://doi.org/10.5610/jaee.4.3_65).
- Bard, P.-Y., and M. Bouchon (1980). The seismic response of sediment-filled valleys. Part 2. The case of incident *P* and *SV* waves, *Bull. Seismol. Soc. Am.* **70**, no. 5, 1921–1941.
- Bard, P.-Y., and M. Bouchon (1985). The two-dimensional resonance of sediment-filled valleys, *Bull. Seismol. Soc. Am.* **75**, no. 2, 519–541.
- Bard, P.-Y., H. Cadet, B. Endrun, M. Hobiger, F. Renalier, N. Theodulidis, M. Ohrnberger, D. Fäh, F. Sabetta, P. Teves-Costa, *et al.* (2010). From non-invasive site characterization to site amplification: Recent advances in the use of ambient vibration measurements, in *Earthquake Engineering in Europe*, M. Garevski and A. Ansal (Editors), Vol. 17, Springer, Dordrecht, The Netherlands, 105–123, doi: [10.1007/978-90-481-9544-2](https://doi.org/10.1007/978-90-481-9544-2).
- Bard, P.-Y., M. Campillo, F. J. Chavez-Garcia, and F. Sanchez-Sesma (1988). The Mexico earthquake of September 19, 1985—A theoretical investigation of large- and small-scale amplification effects in the Mexico City Valley, *Earthq. Spectra* **4**, no. 3, 609–633, doi: [10.1193/1.1585493](https://doi.org/10.1193/1.1585493).
- Bonnefoy-Claudet, S., F. Cotton, and P.-Y. Bard (2006). The nature of noise wavefield and its applications for site effects studies, *Earth-Science Rev.* **79**, nos. 3/4, 205–227, doi: [10.1016/j.earscirev.2006.07.004](https://doi.org/10.1016/j.earscirev.2006.07.004).
- Building Seismic Safety Council (2004). *NEHRP Recommended Provisions for Seismic Regulations for New Buildings, and Other Structures (FEMA 450): Provisions*, National Institute of Building Sciences.
- Burjánek, J., B. Edwards, and D. Fäh (2014). Empirical evidence of local seismic effects at sites with pronounced topography: A systematic approach, *Geophys. J. Int.* **197**, 608–619, doi: [10.1093/gji/ggu014](https://doi.org/10.1093/gji/ggu014).
- Burjánek, J., G. Gassner-Stamm, V. Poggi, J. R. Moore, and D. Fäh (2010). Ambient vibration analysis of an unstable mountain slope, *Geophys. J. Int.* **180**, no. 2, 820–828, doi: [10.1111/j.1365-246X.2009.04451.x](https://doi.org/10.1111/j.1365-246X.2009.04451.x).
- Burjánek, J., J. R. Moore, F. X. Yugsi Molina, and D. Fäh (2012). Instrumental evidence of normal mode rock slope vibration, *Geophys. J. Int.* **188**, no. 2, 559–569, doi: [10.1111/j.1365-246X.2011.05272.x](https://doi.org/10.1111/j.1365-246X.2011.05272.x).
- Capon, J. (1969). High-resolution frequency-wavenumber spectrum analysis, *Proc. IEEE* **57**, no. 8, 1408–1418, doi: [10.1109/PROC.1969.7278](https://doi.org/10.1109/PROC.1969.7278).
- Cauzzi, C., and J. Clinton (2013). A high- and low-noise model for high-quality strong-motion accelerometer stations, *Earthq. Spectra* **29**, no. 1, 85–102, doi: [10.1193/1.4000107](https://doi.org/10.1193/1.4000107).
- Cauzzi, C., E. Faccioli, and G. Costa (2011). 1D and 2D site amplification effects at Tarcento (Friuli, NE Italy), 30 years later, *J. Seismol.* **15**, no. 1, 1–17, doi: [10.1007/s10950-010-9202-y](https://doi.org/10.1007/s10950-010-9202-y).
- Chavez-Garcia, F. J., W. R. Stephenson, and M. Rodríguez (1999). Lateral propagation effects observed at Parkway, New Zealand. A case history to compare 1D versus 2D site effects, *Bull. Seismol. Soc. Am.* **89**, no. 3, 718–732.
- Clinton, J., C. Cauzzi, D. Fäh, C. Michel, P. Zweifel, M. Olivieri, G. Cua, F. Haslinger, and D. Giardini (2011). The current state of strong motion monitoring in Switzerland, in *Earthquake Data in Engineering Seismology*, S. Akkar, P. Gülkan, and T. van Eck (Editors), Vol. 14, Springer, Dordrecht, The Netherlands, 219–233, doi: [10.1007/978-94-007-0152-6](https://doi.org/10.1007/978-94-007-0152-6).
- Cornou, C., and P.-Y. Bard (2003). Site-to-bedrock over 1D transfer function ratio: An indicator of the proportion of edge-generated surface waves? *Geophys. Res. Lett.* **30**, no. 9, 1453, doi: [10.1029/2002GL016593](https://doi.org/10.1029/2002GL016593).
- Cornou, C., M. Ohrnberger, D. M. Boore, K. Kudo, and P.-Y. Bard (2009). Derivation of structural models from ambient vibration array recordings: Results from an international blind test, in *Third International Symposium on the Effects of Surface Geology on Seismic Motion*, Grenoble, France, 30 August–1 September 2006, 1127–1219.
- Di Capua, G., G. Lanzo, V. Pessina, S. Peppoloni, and G. Scasserra (2011). The recording stations of the Italian strong motion network: Geological information and site classification, *Bull. Earthq. Eng.* **9**, no. 6, 1779–1796, doi: [10.1007/s10518-011-9326-7](https://doi.org/10.1007/s10518-011-9326-7).
- Ditommaso, R., M. Mucciarelli, M. R. Gallipoli, and F. Ponzio (2010). Effect of a single vibrating building on free-field ground motion: Numerical and experimental evidences, *Bull. Earthq. Eng.* **8**, no. 3, 693–703, doi: [10.1007/s10518-009-9134-5](https://doi.org/10.1007/s10518-009-9134-5).
- Duval, A.-M., S. Vidal, J.-P. Méneroud, A. Singer, F. De Santis, C. Ramos, G. Romero, R. Rodriguez, A. Pernia, N. Reyes, *et al.* (2001). Caracas, Venezuela, site effect determination with microtremors, *Pure Appl. Geophys.* **158**, no. 12, 2513–2523, doi: [10.1007/PL00001183](https://doi.org/10.1007/PL00001183).
- Edwards, B., and D. Fäh (2013). A stochastic ground-motion model for Switzerland, *Bull. Seismol. Soc. Am.* **103**, no. 1, 78–98, doi: [10.1785/0120110331](https://doi.org/10.1785/0120110331).
- Edwards, B., D. Fäh, and D. Giardini (2011). Attenuation of seismic shear wave energy in Switzerland, *Geophys. J. Int.* **185**, no. 2, 967–984, doi: [10.1111/j.1365-246X.2011.04987.x](https://doi.org/10.1111/j.1365-246X.2011.04987.x).
- Edwards, B., C. Michel, V. Poggi, and D. Fäh (2013). Determination of site amplification from regional seismicity: Application to the Swiss National Seismic Networks, *Seismol. Res. Lett.* **84**, no. 4, 611–621, doi: [10.1785/0220120176](https://doi.org/10.1785/0220120176).
- Edwards, B., A. Rietbrock, J. J. Bommer, and B. Baptie (2008). The acquisition of source, path, and site effects from microearthquake recordings using Q tomography: Application to the United Kingdom, *Bull. Seismol. Soc. Am.* **98**, no. 4, 1915–1935, doi: [10.1785/0120070127](https://doi.org/10.1785/0120070127).
- Ermert, L., V. Poggi, J. Burjánek, and D. Fäh (2014). Fundamental and higher 2-D resonance modes of an Alpine valley, *Geophys. J. Int.* **198**, no. 2, 795–811, doi: [10.1093/gji/ggu072](https://doi.org/10.1093/gji/ggu072).
- Eurocode 8 (2004). Design of structures for earthquake resistance—Part 1: General rules, seismic actions and rules for buildings, EN 1998-1, European Committee for Standardization (CEN), Brussels, 1–229.
- Faccioli, E., M. Villani, M. Vanini, and C. Cauzzi (2010). Mapping seismic hazard for the needs of displacement-based design, in *The Case of Italy, in Geotechnical, Geological and Earthquake Engineering—Advances in Performance-Based Earthquake Engineering*, M. N. Fardis (Editor), Vol. 13, Springer, Dordrecht, The Netherlands, 3–14, doi: [10.1007/978-90-481-8746-1\\_1](https://doi.org/10.1007/978-90-481-8746-1_1).
- Fäh, D., S. Fritsche, V. Poggi, G. Gassner-Stamm, P. Kästli, J. Burjánek, P. Zweifel, S. Barman, J. Clinton, L. Keller, P. Renault, and S. Heuberger (2009). *Determination of Site Information for Seismic Stations in Switzerland*, SED report SED/PRP/R/004/20090831, Zurich, Switzerland.
- Fäh, D., F. Kind, and D. Giardini (2001). A theoretical investigation of average H/V ratios, *Geophys. J. Int.* **145**, 535–549.
- Fäh, D., J. R. Moore, J. Burjánek, I. Iosifescu, L. A. Dalguer, F. Dupray, C. Michel, J. Woessner, A. Villiger, J. Laue, *et al.* (2012). Coupled seismogenic geohazards in Alpine region, *Bollettino Di Geofisica Teorica Ed Applicata* **53**, 485–508, doi: [10.4430/bgta0048](https://doi.org/10.4430/bgta0048).
- Fäh, D., G. Stamm, and H.-B. Havenith (2008). Analysis of three-component ambient vibration array measurements, *Geophys. J. Int.* **172**, no. 1, 199–213, doi: [10.1111/j.1365-246X.2007.03625.x](https://doi.org/10.1111/j.1365-246X.2007.03625.x).
- Field, E. H. (1996). Spectral amplification in a sediment-filled valley exhibiting clear basin-edge-induced waves, *Bull. Seismol. Soc. Am.* **86**, no. 4, 991–1005.

- Foti, S., S. Parolai, P. Bergamo, G. Di Giulio, M. Maraschini, G. Milana, M. Picozzi, and R. Puglia (2011). Surface wave surveys for seismic site characterization of accelerometric stations in ITACA, *Bull. Earthq. Eng.* **9**, no. 6, 1797–1820, doi: [10.1007/s10518-011-9306-y](https://doi.org/10.1007/s10518-011-9306-y).
- Fritsche, S., D. Fäh, and D. Giardini (2005). Damage fields and site-effects. Investigations on the 1855 earthquake in Switzerland, in *250th Anniversary of the 1755 Lisbon Earthquake International Conference*, Lisbon, Portugal, 1–4 November 2005.
- Gorini, A., M. Nicoletti, P. Marsan, R. Bianconi, R. Nardis, L. Filippi, S. Marcucci, F. Palmo, and E. Zambonelli (2010). The Italian strong motion network, *Bull. Earthq. Eng.* **8**, no. 5, 1075–1090, doi: [10.1007/s10518-009-9141-6](https://doi.org/10.1007/s10518-009-9141-6).
- Guéguen, P., C. Cornou, S. Garambois, and J. Banton (2007). On the limitation of the H/V spectral ratio using seismic noise as an exploration tool: Application to the Grenoble Valley (France), a small apex ratio basin, *Pure Appl. Geophys.* **164**, no. 1, 115–134, doi: [10.1007/s00024-006-0151-x](https://doi.org/10.1007/s00024-006-0151-x).
- Havenith, H.-B., D. Fäh, U. Polom, and A. Roullé (2007). S-wave velocity measurements applied to the seismic microzonation of Basel, Upper Rhine Graben, *Geophys. J. Int.* **170**, no. 1, 346–358, doi: [10.1111/j.1365-246X.2007.03422.x](https://doi.org/10.1111/j.1365-246X.2007.03422.x).
- Hobiger, M., C. Cornou, M. Wathelet, G. Di Giulio, B. Knapmeyer-Endrun, F. Renalier, P.-Y. Bard, A. Savvaidis, S. Hailemichael, B. N. Le, M. Ohrmberger, and N. Theodoulidis (2012). Ground structure imaging by inversions of Rayleigh wave ellipticity: Sensitivity analysis and application to European strong-motion sites, *Geophys. J. Int.* **192**, no. 1, 207–229, doi: [10.1093/gji/ggs005](https://doi.org/10.1093/gji/ggs005).
- Joyner, W. B. (2000). Strong motion from surface waves in deep sedimentary basins, *Bull. Seismol. Soc. Am.* **90**, no. 6B, S95–S112.
- Joyner, W. B., R. E. Warrick, and T. E. Fumal (1981). The effect of Quaternary alluvium on strong ground motion in the Coyote Lake, California, earthquake of 1979, *Bull. Seismol. Soc. Am.* **71**, no. 4, 1333–1349.
- Kawase, H. (1996). The cause of the damage belt in Kobe: “The Basin-Edge Effect,” Constructive interference of the direct S-wave with the basin-induced diffracted/Rayleigh waves, *Seismol. Res. Lett.* **67**, no. 5, 25–34, doi: [10.1785/gssrl.67.5.25](https://doi.org/10.1785/gssrl.67.5.25).
- King, J. L., and B. E. Tucker (1984). Observed variations of earthquake motion across a sediment-filled valley, *Bull. Seismol. Soc. Am.* **74**, no. 1, 137–151.
- Knopoff, L. (1964). A matrix method for elastic wave problems, *Bull. Seismol. Soc. Am.* **54**, no. 1, 431–438.
- Le Roux, O., C. Cornou, D. Jongmans, and S. Schwartz (2012). 1-D and 2-D resonances in an Alpine valley identified from ambient noise measurements and 3-D modelling, *Geophys. J. Int.* **191**, no. 2, 579–590, doi: [10.1111/j.1365-246X.2012.05635.x](https://doi.org/10.1111/j.1365-246X.2012.05635.x).
- Lebrun, B., D. Hatzfeld, and P.-Y. Bard (2001). Site effect study in urban area: Experimental results in Grenoble (France), *Pure Appl. Geophys.* **158**, no. 12, 2543–2557, doi: [10.1007/PL00001185](https://doi.org/10.1007/PL00001185).
- Lee, C., C. Cheng, C. Liao, and Y. Tsai (2001). Site classification of Taiwan free-field strong-motion stations, *Bull. Seismol. Soc. Am.* **91**, no. 5, 1283–1297.
- Lenti, L., S. Martino, A. Paciello, and G. Scarascia Mugnozza (2009). Evidence of two-dimensional amplification effects in an Alluvial Valley (Valnerina, Italy) from velocimetric records and numerical models, *Bull. Seismol. Soc. Am.* **99**, no. 3, 1612–1635, doi: [10.1785/0120080219](https://doi.org/10.1785/0120080219).
- Luzi, L., S. Lovati, E. D’Alema, S. Marzorati, D. Giacomo, S. Hailemichael, E. Cardarelli, M. Cercato, G. Di Filippo, G. Milana, *et al.* (2010). Italian accelerometric archive: Geological, geophysical and geotechnical investigations at strong-motion stations, *Bull. Earthq. Eng.* **8**, no. 5, 1189–1207, doi: [10.1007/s10518-009-9153-2](https://doi.org/10.1007/s10518-009-9153-2).
- McNamara, D. E., and R. P. Buland (2004). Ambient noise levels in the Continental United States, *Bull. Seismol. Soc. Am.* **94**, no. 4, 1517–1527, doi: [10.1785/012003001](https://doi.org/10.1785/012003001).
- McNamara, D. E., C. R. Hutt, L. S. Gee, H. M. Benz, and R. P. Buland (2009). A method to establish seismic noise baselines for automated station assessment, *Seismol. Res. Lett.* **80**, no. 4, 628–637.
- Odum, J. K., W. R. Stephenson, R. A. Williams, and C. von Hillebrandt-Andrade (2013).  $V_{s30}$  and spectral response from collocated shallow, active-, and passive-source  $V_s$  data at 27 sites in Puerto Rico, *Bull. Seismol. Soc. Am.* **103**, no. 5, 2709–2728, doi: [10.1785/0120120349](https://doi.org/10.1785/0120120349).
- Paolucci, R., and L. Morstabilini (2006). Non-dimensional site amplification functions for basin edge effects on seismic ground motion, in *Third International Symposium on the Effects of Surface Geology on Seismic Motion*, Grenoble, France, 30 August–1 September 2006, 823–831.
- Park, C. B., R. D. Miller, and J. Xia (1999). Multichannel analysis of surface waves, *Geophysics* **64**, no. 3, 800–808, doi: [10.1190/1.1444590](https://doi.org/10.1190/1.1444590).
- Poggi, V., and D. Fäh (2010). Estimating Rayleigh wave particle motion from three-component array analysis of ambient vibrations, *Geophys. J. Int.* **180**, no. 1, 251–267, doi: [10.1111/j.1365-246X.2009.04402.x](https://doi.org/10.1111/j.1365-246X.2009.04402.x).
- Poggi, V., B. Edwards, and D. Fäh (2011). Derivation of a reference shear-wave velocity model from empirical site amplification, *Bull. Seismol. Soc. Am.* **101**, no. 1, 258–274, doi: [10.1785/0120100060](https://doi.org/10.1785/0120100060).
- Poggi, V., B. Edwards, and D. Fäh (2012). Characterizing the vertical to horizontal ratio of ground-motion at soft sediment sites, *Bull. Seismol. Soc. Am.* **102**, no. 6, 2741–2756.
- Poggi, V., L. Ermert, J. Burjánek, C. Michel, and D. Fäh (2014). Modal analysis of 2-D sedimentary basin from frequency domain decomposition of ambient vibration array recordings, *Geophys. J. Int.* (in press).
- Poggi, V., D. Fäh, J. Burjánek, and D. Giardini (2012). The use of Rayleigh-wave ellipticity for site-specific hazard assessment and microzonation: Application to the city of Lucerne, Switzerland, *Geophys. J. Int.* **188**, no. 3, 1154–1172, doi: [10.1111/j.1365-246X.2011.05305.x](https://doi.org/10.1111/j.1365-246X.2011.05305.x).
- Poggi, V., D. Fäh, and D. Giardini (2013). Time–frequency–wavenumber analysis of surface waves using the continuous wavelet transform, *Pure Appl. Geophys.* **170**, no. 3, 319–335, doi: [10.1007/s00024-012-0505-5](https://doi.org/10.1007/s00024-012-0505-5).
- Poovarodom, N., and N. Plalinyot (2013). Site characterization in the Greater Bangkok area by microtremor observations, *J. Earthq. Eng.* **17**, no. 2, 209–226, doi: [10.1080/13632469.2012.707346](https://doi.org/10.1080/13632469.2012.707346).
- Roten, D., and D. Fäh (2007). A combined inversion of Rayleigh wave dispersion and 2-D resonance frequencies, *Geophys. J. Int.* **168**, no. 3, 1261–1275, doi: [10.1111/j.1365-246X.2006.03260.x](https://doi.org/10.1111/j.1365-246X.2006.03260.x).
- Roten, D., D. Fäh, C. Cornou, and D. Giardini (2006). Two-dimensional resonances in Alpine valleys identified from ambient vibration wavefields, *Geophys. J. Int.* **165**, no. 3, 889–905, doi: [10.1111/j.1365-246X.2006.02935.x](https://doi.org/10.1111/j.1365-246X.2006.02935.x).
- Roten, D., D. Fäh, K. B. Olsen, and D. Giardini (2008). A comparison of observed and simulated site response in the Rhône valley, *Geophys. J. Int.* **173**, no. 3, 958–978, doi: [10.1111/j.1365-246X.2008.03774.x](https://doi.org/10.1111/j.1365-246X.2008.03774.x).
- Sandikkaya, M. A., M. T. Yilmaz, B. S. Bakır, and Ö. Yilmaz (2009). Site classification of Turkish national strong-motion stations, *J. Seismol.* **14**, no. 3, 543–563, doi: [10.1007/s10950-009-9182-y](https://doi.org/10.1007/s10950-009-9182-y).
- Savvaidis, A., H. Cadet, P. Guéguen, A. Panou, C. Michel, N. Theodoulidis, and I. Kalogeras (2006). Accelerograph stations site characterization using ambient noise: Selected stations in Greece, in *Third International Symposium on the Effects of Surface Geology on Seismic Motion*, Grenoble, France, 30 August–1 September 2006, 791–800.
- Steimen, S., D. Fäh, F. Kind, C. Schmid, and D. Giardini (2003). Identifying 2D resonance in microtremor wave fields, *Bull. Seismol. Soc. Am.* **93**, no. 2, 583–599.
- Thompson, E. M., L. G. Baise, R. E. Kayen, and B. B. Guzina (2009). Impediments to predicting site response: Seismic property estimation and modeling simplifications, *Bull. Seismol. Soc. Am.* **99**, no. 5, 2927–2949, doi: [10.1785/0120080224](https://doi.org/10.1785/0120080224).
- Thompson, E. M., L. G. Baise, Y. Tanaka, and R. E. Kayen (2012). A taxonomy of site response complexity, *Soil Dyn. Earthq. Eng.* **41**, 32–43, doi: [10.1016/j.soildyn.2012.04.005](https://doi.org/10.1016/j.soildyn.2012.04.005).
- Wald, D. J., and R. W. Graves (1998). The seismic response of the Los Angeles basin, California, *Bull. Seismol. Soc. Am.* **88**, no. 2, 337–356.
- Wathelet, M. (2008). An improved neighborhood algorithm: Parameter conditions and dynamic scaling, *Geophys. Res. Lett.* **35**, no. 9, 1–5, doi: [10.1029/2008GL033256](https://doi.org/10.1029/2008GL033256).

- Wathelet, M., D. Jongmans, M. Ohrnberger, and S. Bonnefoy-Claudet (2008). Array performances for ambient vibrations on a shallow structure and consequences over  $V_S$  inversion, *J. Seismol.* **12**, no. 1, 1–19, doi: [10.1007/s10950-007-9067-x](https://doi.org/10.1007/s10950-007-9067-x).
- Yamanaka, H., K. Seo, and T. Samano (1989). Effects of sedimentary layers on surface-wave propagation, *Bull. Seismol. Soc. Am.* **79**, no. 3, 631–644.
- Yong, A., A. Martin, K. Stokoe, and J. Diehl (2013). ARRA-funded VS30 measurements using multi-technique approach at strong-motion stations in California and Central-Eastern United States. Reston, Virginia, *U.S. Geol. Surv. Open-File Rept. 2013-1102*, 59.
- Zaré, M., P.-Y. Bard, and M. Ghafory-Ashtiany (1999). Site characterizations for the Iranian strong motion network, *Soil Dyn. Earthq. Eng.* **18**, 101–123.

ETHZ-SED  
Sonneggstrasse 5  
CH-8092 Zurich, Switzerland  
(C.M., B.E., V.P., J.B., C.C., D.F.)

University of California, San Diego  
San Diego Supercomputer Center  
MC 0505, 9500 Gilman Drive  
La Jolla, California 92093-0505  
(D.R.)

Manuscript received 7 April 2014;  
Published Online 11 November 2014

## 1.6 Combiner la caractérisation géophysique des sites aux observations sous séisme pour cartographier l'amplification (Michel *et al.*, 2016)

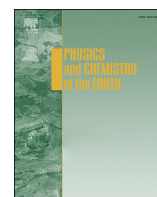
Les travaux présentés dans les parties précédentes, dont le point fort est la combinaison des données sous vibrations ambiantes et séismes, ouvrent de nombreuses perspectives. Nous sommes allés au bout de la démarche dans Michel *et al.* (2016) où nous proposons une carte détaillée de l'amplification du spectre de réponse à chaque période pour la région de Bâle (Suisse). Cette carte trouvera des applications pratiques dans le logiciel ShakeMap et pour la réalisation de scénarios de perte ainsi que des analyses de risque (Michel *et al.*, 2017b). L'article développe le calcul des fonctions ESM pour le spectre de réponse et le valide. La région de Bâle a été largement étudiée durant les 20 dernières années avec de nombreuses mesures géophysiques. Nous avons cependant modifié deux interprétations faites par de précédents auteurs : le rocher géophysique, responsable de la fréquence fondamentale de résonance dans le bassin a été déplacé au niveau des calcaires mésozoïques et non des marnes du Sannoisien (Tertiaire) et nous avons montré que le second pic dans le H/V n'était pas dû à la résonance des couches du Quaternaire.

Pour le calcul de la carte d'amplification, nous avons combiné les données ESM et géophysiques : dans le bassin, l'amplification variant de manière régulière, une simple interpolation des nombreuses fonctions ESM a été réalisée ; hors du bassin, l'amplification est en général due à une couche de sédiments meubles sur le rocher et a été calculée en modulant les fonctions ESM aux quelques stations disponibles par la fréquence de résonance obtenue à l'aide de nombreuses mesures géophysiques. Le résultat est comparable à la carte obtenue en 2006 lors du microzonage, réalisé à l'aide de modélisations 1D, 2D et 3D. Il montre de plus fortes variations spatiales en dehors du bassin et de moins fortes dans le bassin que celles obtenues par le microzonage. Ce travail permet en outre de valider le microzonage et de montrer quelles améliorations pourraient être apportées. Il est ainsi fortement conseillé d'installer des stations permanentes lors de la réalisation d'un microzonage afin de le valider et de le mettre à jour par la suite.



Contents lists available at ScienceDirect

## Physics and Chemistry of the Earth

journal homepage: [www.elsevier.com/locate/pce](http://www.elsevier.com/locate/pce)

## Site amplification at the city scale in Basel (Switzerland) from geophysical site characterization and spectral modelling of recorded earthquakes

Clotaire Michel<sup>a, \*</sup>, Donat Fäh<sup>a</sup>, Benjamin Edwards<sup>b</sup>, Carlo Cauzzi<sup>a</sup>

<sup>a</sup> Swiss Seismological Service (SED), Swiss Federal Institute of Technology of Zurich (ETHZ), Switzerland

<sup>b</sup> Department of Earth, Ocean and Ecological Sciences, University of Liverpool, UK

## ARTICLE INFO

## Article history:

Received 29 February 2016

Received in revised form

13 July 2016

Accepted 29 July 2016

Available online xxx

## Keywords:

Site effects

Ground motion amplification

Strong motion

Seismic network

ShakeMap

## ABSTRACT

Hazard assessment at the city scale requires a detailed characterization of the effect of surface geology on ground motion (site effects). Though this analysis is commonly achieved using geophysical site characterization and site response modelling, we propose here a complementary analysis based on amplification functions retrieved from Empirical Spectral Modelling (ESM) of earthquake recordings. We applied this method to the city of Basel (Switzerland) that benefits from a detailed microzonation and a dense Strong Motion Network with 21 modern free-field stations. We first verified the accuracy of ESM amplification functions for this region and used them to determine the bedrock interface at a site with a detailed velocity profile. While the interface between Upper and Lower Tertiary was, until now, considered responsible for the fundamental frequency of resonance in the Rhine Graben, we found that the bedrock interface in fact lies at the Mesozoic limestone. We also investigated the second peak of the H/V ratios that is clustered in a particular area of the basin where amplification is found to be different. We successfully used the ESM amplification functions to verify the microzonation of 2006 and would strongly advise the installation of strong motion stations where such studies are performed in the future. Outside the Rhine Graben, where shallow sediments are found, we propose an amplification functional form based on ESM and the fundamental frequency of resonance. Finally, we combined all our findings and generated amplification maps of the response spectrum at any period of interest for earthquake engineering. This map is proposed for a high resolution real-time implementation in ShakeMap and will be used for seismic loss assessment.

© 2016 Elsevier Ltd. All rights reserved.

### 1. Introduction

The city of Basel is located at the south-eastern edge of the Upper Rhine Graben, at the border between France, Germany and Switzerland. Seismic hazard in the city of Basel is moderate, with uniform hazard spectra from the 2015 Swiss national seismic hazard maps of the Swiss Seismological Service (SED) indicating peak ground acceleration (PGA) at a rock horizon ( $V_{s,30} = 1105$  m/s) of 0.1 g at a return period of 475 years, and 0.5 g at 10,000 years (SED, 2015a). It was struck in 1356 by the largest earthquake known to have occurred North of the Alps, with  $M_w \sim 6.6$  according to recent studies (Fäh et al., 2009). The earthquake destroyed the city

and caused damage in many villages nearby. The number of fatalities was probably limited, most likely due to the numerous foreshocks that made the inhabitants leave their houses. Two fatalities have been certified, although the real number is unknown (Fäh et al., 2009). Other historical events of magnitude 5 and above occurred in 1650 and 1721, causing slight damage to the city (Schwarz-Zanetti and Fäh, 2011; Gisler and Fäh, 2011). More recently, the 2006  $M_w = 3.2$  event induced by petrothermal activities caused widespread minor non-structural damage that led to about 9 M\$ damage claims (Giardini, 2009). This is in stark contrast to a similar geothermal event that occurred in St. Gallen, Switzerland in 2013, which caused insignificant damage, as would be expected for this size of event (Edwards et al., 2015a). A key question therefore is whether amplification phenomena in Basel lead to high ground-motions.

The first qualitative microzonation study for the city was carried

\* Corresponding author. SED-ETHZ, Sonneggstrasse 5, 8092 Zürich, Switzerland.  
E-mail address: [clotaire.michel@sed.ethz.ch](mailto:clotaire.michel@sed.ethz.ch) (C. Michel).

out by Fähr et al. (1997). It was followed in 2006 by a quantitative microzonation project (Fähr and Huggenberger, 2006) that was eventually implemented in the local building code (Fähr and Wenk, 2009). Apparent from the microzonation studies is significant amplification of earthquake ground motions, which varies according to the mechanical properties of the deposits: in the Rhine Graben, deep sedimentary layers with various degrees of consolidation have been deposited since the Tertiary, whereas outside the Graben, alluvial valleys are filled with unconsolidated Quaternary sediments. This geological complexity and the resulting site response motivated the development of site characterization techniques based on ambient vibrations (e.g. Kind et al., 2005; Havenith et al., 2007) and site response analyses based on numerical modelling (e.g. Oprsal et al., 2005).

We propose here an alternative, data-driven approach to assess the amplification of earthquake ground motions that should complement classical geophysical site characterization. Our study is motivated by the “Basel Risk Mitigation” project promoted by the Canton Basel-City between 2013 and 2015 with the goal of assessing the consequences of significant earthquakes on local school buildings, and as a pilot study for real-time loss assessment for the whole city (Michel and Fähr, 2016). Our approach is based on collecting observations of site amplification at permanent seismic stations with respect to a known reference rock profile, as detailed by Poggi et al. (2011) and Edwards et al. (2013). The main source of our data is the Swiss Strong Motion Network (SSMNet; Clinton et al., 2011; Michel et al., 2014) that was densified in the region throughout the development of this study.

In this paper, we present and discuss the amplification maps developed for the studied area. Our goal is to define the amplification of the 5% damped response spectrum in the range of the vibration frequencies of typical Swiss buildings, i.e., between 1 and 10 Hz. The amplification maps derived herein can be used as input to loss assessment studies through high-resolution earthquake scenarios and ShakeMaps (Wald et al., 1999; Worden et al., 2010; Cauzzi et al., 2015) for the Basel area.

In this paper, the Basel context is first presented including the geology, the existing microzonation studies and the SSMNet with its recent modernization and extension, completed by the installation of temporary stations within this project. We recall how the spectral modelling technique of Edwards et al. (2013) is implemented on the whole Swiss Network to retrieve information on the Fourier site amplification from recorded events. We validate this approach in Basel and propose a method to compute the site amplification for the response spectrum. Two results concerning the interpretation of the observed site amplification are presented: the interpretation of the bedrock depth and the secondary peaks in the Rhine Graben. Further, a verification of the 2006 microzonation is presented. Finally, we propose a method to combine the available data with the site characterization information to derive an amplification map for a prototype implementation in a high-resolution ShakeMap.

## 2. The Basel area

### 2.1. Geology

The area of Basel (Fig. 1) comprises two major distinct geological domains, namely the Rhine Graben and the Jura mountains. The Rhine Graben opened during the Oligocene and Miocene ages (starting 35 Myrs ago) and has been filled with thick marine and freshwater sediments since that time (Fig. 2). East of the master fault of the Graben, the Tabular Jura is made of Mesozoic rock, carved by the Rhine and smaller rivers, generally overlaid by Quaternary sediments of variable (but generally limited to 35 m in

most areas) thickness. In the South, the Graben extends to the folded Jura with a gradually decreasing thickness. Defining the Eastern and Southern boundaries between these two geologic features is not straightforward. They can be defined based on tectonic considerations (e.g. the location of the main Eastern fault – although this is not well defined), sedimentary considerations (e.g., presence of Tertiary sediments deposited during the extension of the Graben), or engineering seismology considerations (e.g., a jump in the resonance frequency as used in Fähr et al., 2006). In this project, we used a simplified representation of the main geological units based on the available geological maps and the 2006 microzonation map, as shown in Fig. 1.

Outside the Rhine Graben, the Quaternary sediments exceed 35 m thickness only for small areas of the Rhine valley (e.g. at station SMZW) and of the Ergolz valley (GeORG project team, 2013). According to Fähr et al. (2006), three main types of sediments can be found in this area: Pleistocene sediments are mostly made of alluvial terraces of the main rivers and are in general compact; Loess sediments, which are very soft, can be found on top of hills and were formed by wind transport; Holocene sediments are in general unconsolidated alluvial sediments (gravel and sand).

In the Rhine Graben, the Quaternary sediments are also rarely thicker than 35 m (GeORG project team, 2013). Loess hills in the South-West were distinguished from the rest of the Rhine Graben as explained in section 4.2. The Tertiary deposits (Fig. 2) are mostly marls of lacustrine origin with various degrees of consolidation filling the basin with a thickness of 50–1000 m in Basel (GeORG project team, 2013). They are particularly deep in the “Mulde von St-Jakob-Tüllingen” (Fig. 2), along the Eastern limit of the Graben until Reinach in the South as well as West of the Allschwil fault.

The upper Tertiary (Oligocene age) is made of various sediment types with freshwater origin superimposing seawater sediments mostly made of mudstone, both poorly consolidated (GeORG project team, 2013). The lower Tertiary is mostly constituted by a thick consolidated marl layer (formerly called Sannoisian marl).

The upper Mesozoic layers in the graben are made of massive limestone of Oxfordian age. The Lower Tertiary has been considered as the geophysical bedrock since the first studies on Basel (Fähr et al., 1997). However, we show in section 4.1 that the geophysical bedrock could be located at the top of the Mesozoic units.

### 2.2. Microzonation studies

Fähr et al. (1997) first proposed a qualitative microzonation of the city of Basel. They collected geological and geotechnical data, used SPT (Standard Penetration Test) to estimate the shear-wave velocity ( $V_s$ ) and used the Horizontal-to-Vertical (H/V) Spectral Ratios at about 20 measurements points in the city to compute the dominant frequencies of the site response. They interpreted the fundamental frequency as the resonance of the Upper Tertiary and Quaternary layers, based on the transition between soft sediments and harder rock observed in deep boreholes. They proposed a qualitative microzonation, mostly relying on the Quaternary geology (14 criteria out of 20). This microzonation strategy was implemented in the whole city and related to amplification of earthquake ground motions in terms of EMS-98 (Grünthal, 1998) macroseismic intensity in Fähr et al. (2001). Kind (2002) further developed the use of single station measurements (255 measurement points) and introduced ambient vibration array measurements to estimate the  $V_s$  profiles at 5 sites (Kind et al., 2005). Further 2D numerical modelling was performed, and the Rhine Graben was split into five zones of assumed similar amplification. Steimen et al. (2003) studied 2D resonance in the Rhine Graben using observation and modelling and concluded that no 2D resonance was occurring in Basel but that 2D geometry was playing a

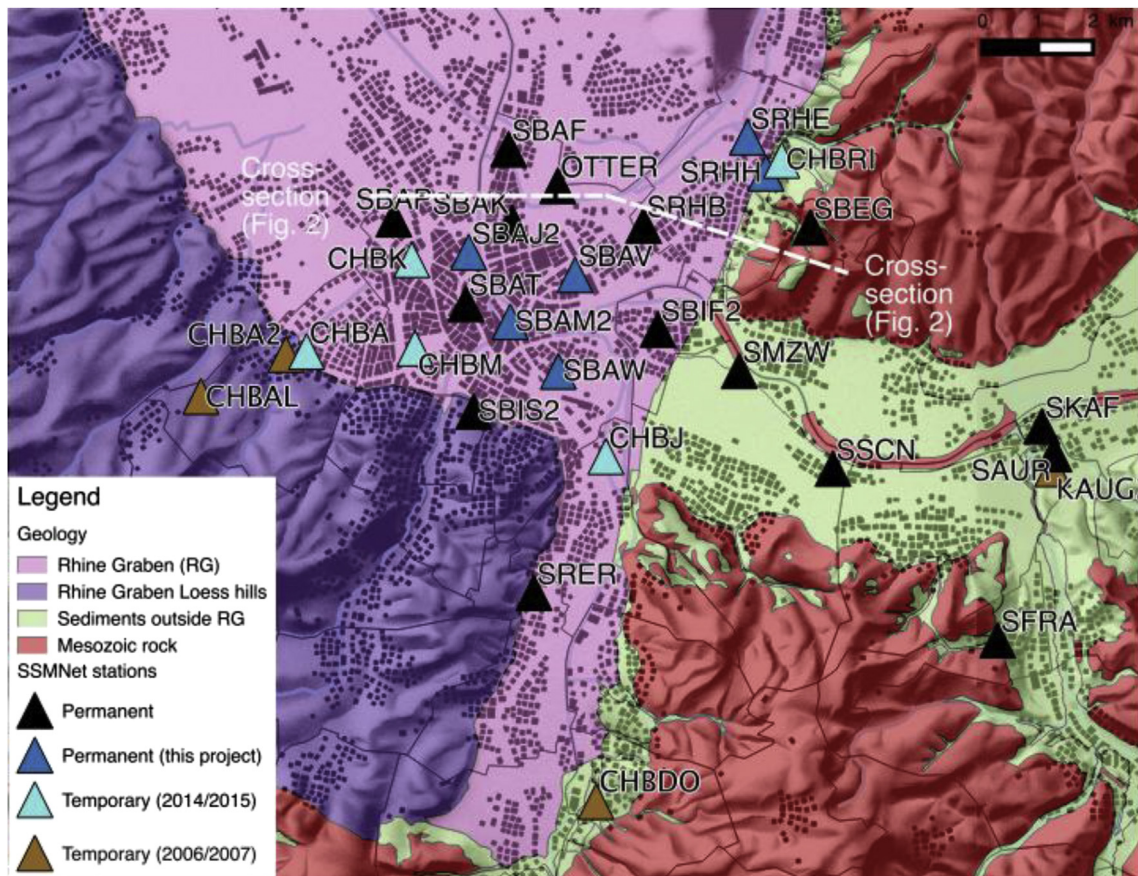


**Fig. 1.** Swiss Strong Motion Network (SSMNet) and simplified surface geology of the Basel area. The seismic stations are shown as coloured triangles. The cloud of light grey rectangles in the background is a simplified plan view of the Basel building stock. The elevation in the area ranges between 245 and 665 m asl. (245–391 m in the Graben).

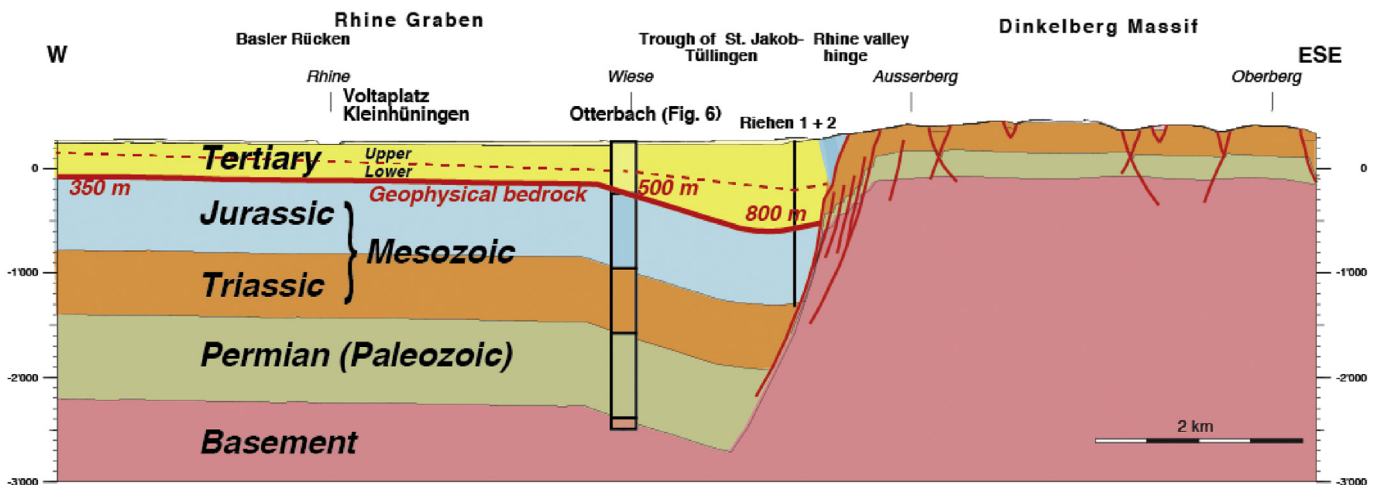


**Fig. 2.** E–W geological cross-section of the Basel area through site Otterbach (OTTER), see Fig. 1. The geophysical bedrock and its depth are displayed in red. Modified from Häring (2006). (For interpretation of the references to colour in this figure legend, the reader is referred to the web version of this article.)

role in the response of the basin. Based on the velocity model of Kind (2002), Oprsal et al. (2005) proposed the first 3D model to simulate earthquake ground motion in Basel with an extended source using the finite difference method.

Fäh and Huggenberger (2006) proposed a quantitative microzonation for Basel that was then implemented in the local building code (Fäh and Wenk, 2009). 700 single-station measurements and

30 new array measurements were used, together with active seismic, to improve the velocity model (Havenith et al., 2007) for the city area. 1D, 2D and 3D numerical modelling was performed. For the microzonation, the city and adjacent areas was split into 14 zones (and more subzones), each of them with an amplification function in terms of pseudo spectral acceleration (PSA) and a corresponding design spectrum (Fäh and Havenith, 2006; Fäh and



Wenk, 2009). The PSA amplification functions were derived as the envelope of the average modelled responses in 1D, 2D and 3D in each zone. These functions are discussed and validated in section 5.

The SED site characterization database (SED, 2015b, Fig. 3) therefore contains a large amount of data collected in the Basel area from passive single station and/or array measurements as well as from active geophysical measurements from the different projects carried out in Basel, as first presented by Havenith et al. (2007). Since then, new data have been gathered after the 2006 geothermal events (Ripperger et al., 2009) and within the framework of the current project.

### 2.3. SSMNet and temporary seismic networks in Basel

With an average interstation distance smaller than 2 km, the Swiss Strong Motion Network (SSMNet) in the Basel area is remarkably dense (Fig. 1). It currently comprises 21 permanent free-field stations, continuously recording and transmitting data to the Swiss Seismological Service (SED). The development of the SSMnet in Basel started in the early 1990s, with 9 low-gain accelerometer stations with dial-up communication installed between 1990 and 1998. In the framework of the aforementioned 2006 microzonation project, 8 modern broadband accelerometer stations with continuous telemetry were installed in 2005/2006. Another 2 modern stations were installed in 2007/2008. Since 2010, 5 supplementary stations have been modernized or newly installed in the framework of the national renewal project (Michel et al., 2014) (SBEG, SRER, SBAK, SBIF2, SSCN). Between 2013 and 2015, 6 additional high-quality (Cauzzi and Clinton, 2013) free-field strong-motion stations (SBAM2, SBAJ2, SBAV, SBAW, SRHE, SRHH) were installed through the Basel risk mitigation project. Five of these new stations are located close to school buildings. 1D velocity

profiles were determined for all the newly installed permanent stations based on array measurements of ambient vibrations as proposed by Michel et al. (2014). The information related to the SSMNet stations in Basel, and especially their site characterization, is stored in the SED (Swiss Seismological Service, 2015a,b) station database, and is available through a web interface at [stations.seismo.ethz.ch](http://stations.seismo.ethz.ch).

In addition to the permanent network, five temporary stations (CHBA, CHBJ, CHBK, CHBM, CHBRI) were installed and were operational from August 2014 to September 2015 (Fig. 1). They were fully integrated in any routine operations of the national monitoring network including real-time and rapid delivery of earthquake locations, magnitudes and associated products. During one year of operation, the temporary stations recorded 2 to 13 events with a sufficient signal to noise ratio across the distance and frequency range defined by Edwards et al. (2013). Station CHBK was located in the noisiest area of the city and therefore recorded only 2 events, while stations located in quiet suburbs recorded about 10 events. The seismicity was low during the recording period. The network clearly recorded all events with  $M_L > 3$  within Switzerland and surrounding regions (see Diehl et al., 2015). In 2006/2007 a temporary network was also installed to monitor the seismicity induced by the Deep Heat Mining Project (Ripperger et al., 2009).

## 3. Site amplification from earthquake spectral modelling (ESM)

### 3.1. Empirical spectral modelling and validation

Following Edwards et al. (2013), the Fourier amplitude spectra of recorded earthquakes at each station of the network are modelled in near real-time (i.e., within minutes of real-time earthquake

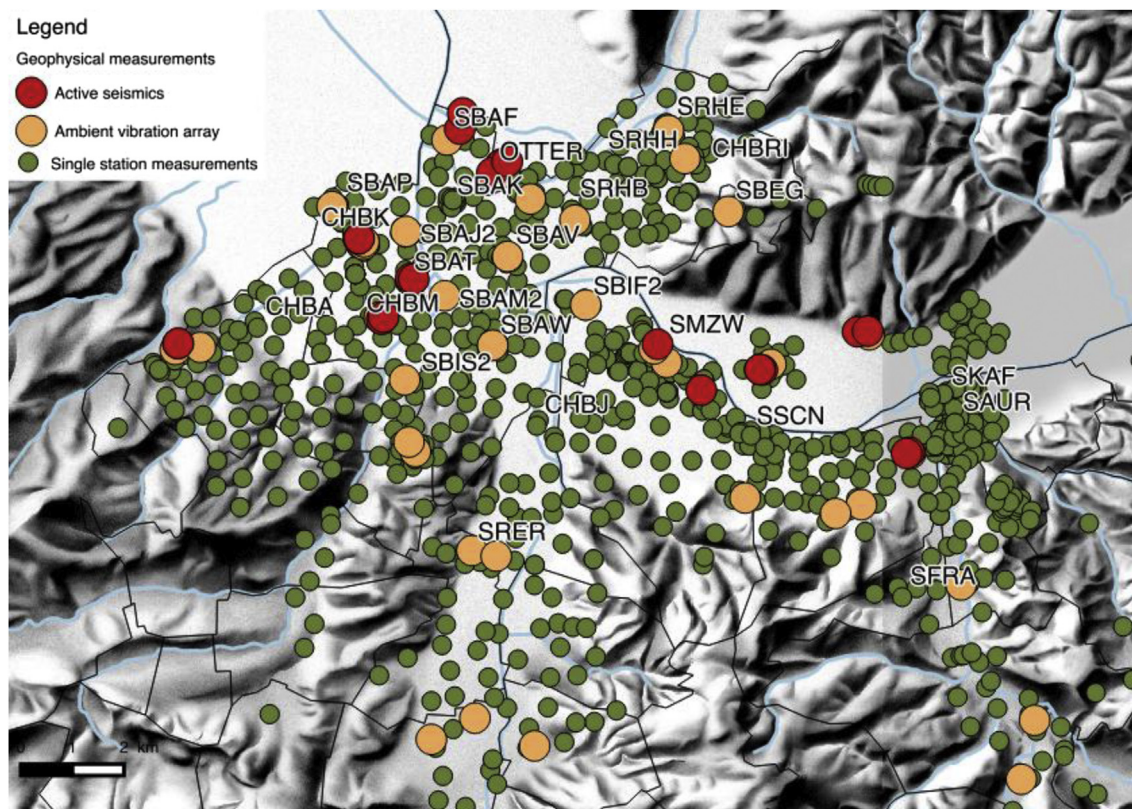


Fig. 3. Digital elevation model of the area of Basel and distribution of the measurements available in the SED site characterization database (SED, 2015b).

detection and location). All signals with sufficient signal-to-noise ratio ( $\text{SNR} > 3$ ) are used to retrieve information about the source (moment magnitude  $M_W$  and stress parameter), the path (geometrical spreading and anelastic attenuation) and the average amplification  $A_j$  at each site  $j$ . The residuals at each frequency of the modelling with respect to the observations are assumed to be the frequency-dependent site amplification function  $a_j(f)$  at each site. The elastic ESM amplification function is retrieved by statistical analysis over a large number of recorded events of  $A_j \times a_j(f)$ . The anelastic ESM amplification function, relative to the reference rock model  $A_j \times a_j(f) \times e^{-\pi f \Delta \kappa_j}$  is also computed, with  $\Delta \kappa_j$  defining the difference in attenuation between site  $j$  and the theoretical reference rock site. However, the large uncertainty in  $\Delta \kappa_j$  imposes a large standard deviation to the anelastic ESM function at high frequencies (e.g. Fig. 4; Edwards et al., 2015b). The reference of these amplification functions is the Swiss reference rock model of Poggi et al. (2011).

Although Edwards et al. (2013) showed that the ESM functions are usually reliable, the ESM results may be biased until stations have several recordings. The shape of the amplification function  $a_j(f)$  is already reasonably constrained by few events, but the average amplification  $A_j$  may be uncertain if the recorded events are not adequately spatially distributed. Many events recorded in Basel were induced by the geothermal Deep Heat Mining Project and recorded at less than 5 km from the rupture (Deichmann and Giardini, 2009). Events pertaining to induced sequences occur at about the same location with similar source mechanisms and radiation of energy for a given station. This breaks the assumption of the computation of the ESM amplification, which does not include radiation pattern, instead assuming a homogeneous distribution of events to ensure no bias due to source effects. The ESM function retrieved at some temporary stations installed during the geothermal sequence were considered unreliable for this reason and therefore not used in this study.

Moreover, in our computations the average amplification ( $A_j$ ) values of Basel stations SBAP, OTTER, SBAT, SRHB and SMZW are

assumed to be known *a priori* along with those of 22 other regional stations that were used to define the Swiss reference rock model of Poggi et al. (2011). Note that  $A_j$  values for the other stations are inverted for each event. We studied the *a posteriori* average amplification  $A_j$  computed for each event and aforementioned station as the average observed spectrum divided by the modelled spectrum without site term. Our goal is to track possible biases in these amplification function due to the geothermal events (Deichmann and Giardini, 2009). As a result, we found that the only station with non-normally distributed  $\ln(A_j)$  is OTTER, located at the epicentre of the geothermal events, showing that the radiation patterns of the induced events have an impact on the average amplification value fixed for this station. Therefore, only the natural events are used in the following. The correction factors computed for the amplification function at the fixed stations are therefore defined as the mean correction of all natural events without outliers (correction factors greater than 2.5). The obtained correction factors are summarized in Table 1. The only large correction (36%) is for station OTTER. Station SBAP shows a correction of 12%, which is not a large value when considering the uncertainties of the amplification function. The others are 7% or less indicating that the  $A_j$  values retrieved in Poggi et al. (2011) were accurate.

Moreover, during the estimation procedure, a trade-off between site amplification terms  $A_j$  and  $\Delta \kappa_j$  may also result in deviations in parts of the amplification function. In the following, we verify that this issue is not affecting the amplification functions by comparing the ratios of the ESM functions with the Fourier standard spectral

**Table 1**

$A_j$  correction factors with respect to  $A_{j, \text{fixed}}$  (Poggi et al., 2011) ( $A_j/A_{j, \text{fixed}}$ ) of ESM for the stations in Basel with available  $A_{j, \text{fixed}}$

Station	$A_j$ correction factor ( $A_j/A_{j, \text{fixed}}$ )
SBAP	0.88
OTTER	1.36
SBAT	1.04
SRHB	1.07
SMZW	1.02

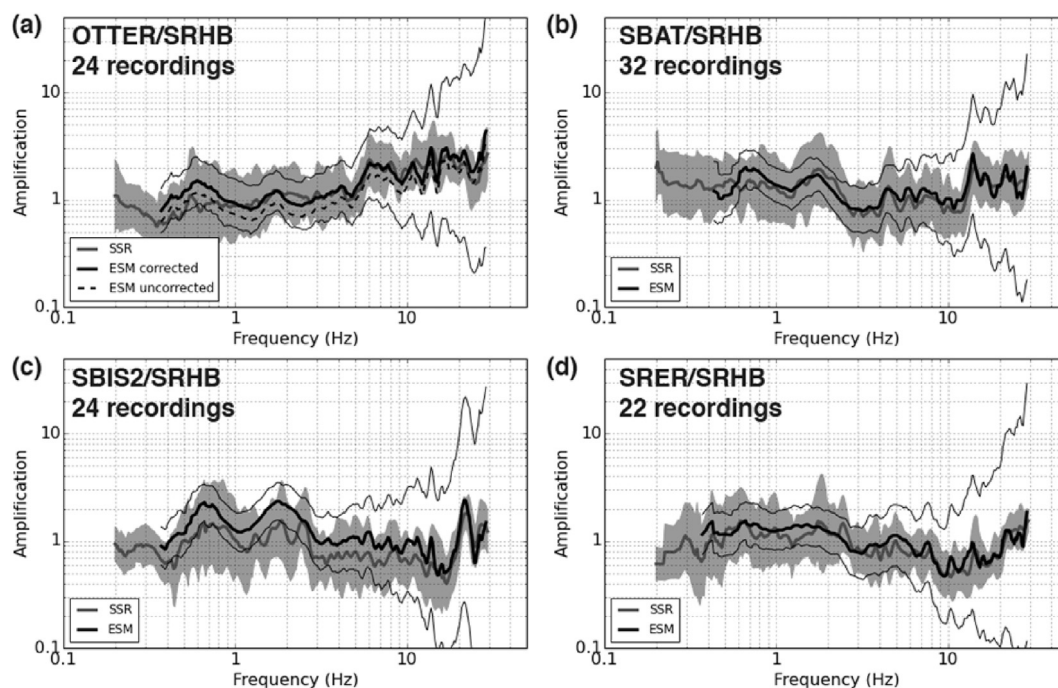


**Fig. 4.** Comparison of standard spectral ratios (SSRs, grey lines and grey shading) and ratios of anelastic ESM functions (black lines), with their respective standard deviations, for stations in the Rhine Graben with respect to SRHB. For OTTER station, the ESM ratios without correction (dashed line) are displayed as well.

ratios (SSRs; Borchardt, 1970) of the recordings of natural events with respect to station SRHB, located in the Rhine Graben (Fig. 4), and station SKAF, located outside (Fig. 5). While not a rock station, SRHB, located in the centre of the basin, was chosen for its relatively flat amplification function. SKAF is a rock station, however it is located relatively far from the rest of the network (Fig. 1). The numbers of recordings given in Figs. 4 and 5 correspond to those of the SSR curves and are modulated at low and high frequencies by the signal-to-noise ratio. Note also that fewer event recordings are available for the pairs of stations used to compute the SSRs than for the ESM at single stations, so that reliable SSRs could not be computed for all station pairs. Even so, the match is good for most of the stations. The  $A_j$  correction proposed above improves the results, especially for OTTER station (Fig. 4a). The trade-off with  $\Delta k_j$  may be the reason for the slight mismatch at station SBIS2 (Fig. 4c).

As a conclusion, the ESM functions, even though sometimes based on few earthquakes only, are reliably depicting the amplification at each SSMNet station. Biases due to the distribution of events can however still be present in both ESM and SSR and will be removed once more recordings will become available. Amplification analysis through ESM overcomes the drawbacks of the Standard Spectral Ratio technique as use for instance by Ullah et al. (2013) for the same purpose. SSR requires a reference station on rock and assumes that the effects of propagation between the stations is negligible. As previously mentioned, ESM also allows the use of more recordings.

### 3.2. ESM amplification in the response spectral domain

Whilst widely used in seismology, Fourier spectra are not as commonly used in earthquake engineering, where the seismic demand is traditionally specified in terms of damped response spectra, especially pseudo spectral acceleration (PSA). We therefore also computed the ESM amplification functions in terms of PSA using Random Vibration Theory (RVT) (Cartwright and Longuet-Higgins, 1956; Liu and Pezeshk, 1999). RVT provides a theoretical

framework for passing from the Fourier domain to the response spectral domain; effectively a short-cut to producing complete time-domain stochastic-phase accelerograms (Boore, 2003) when only peak values of oscillation are required (e.g., Bora et al., 2015). This approach is often used in engineering seismology for the adjustment of ground motion prediction equations (e.g., Campbell, 2003; Edwards et al., 2016). Simulations for a given scenario of magnitude 5 at 50 km were generated using the Swiss Stochastic Model (Edwards and Fäh, 2013) with (a) anelastic (i.e., including  $\kappa_0$ ) Fourier amplification at the reference rock model of Poggi et al. (2011), and (b) site-specific anelastic Fourier amplification (Figs. 4 and 5). The resulting response spectra from (a) and (b) were then used to compute the amplification function between the site and the Swiss Reference in the response spectral domain. We found out that this PSA amplification was insensitive to the scenario (magnitude, distance) used for the range of interest to engineering design ( $M \geq 5$ ;  $R < 100$  km). Future improvements should however include an assessment of the uncertainties on these functions. At long periods ( $T > 0.2$  s) the response and Fourier amplification are similar, however, at short periods ( $T < 0.1$  s) the Fourier and response spectral amplification differ significantly (Bora et al., 2016). While the Fourier ESM amplification functions are used to better understand the nature of site effects in sections 4, PSA ESM amplification functions are used in sections 5 and 6 to quantify the amplification for engineering applications.

### 4. Re-interpretation of site characterization data

In this study, two new key findings concerning the site characterization in Basel are presented and discussed: the interpretation of the bedrock depth and the distribution of the second peak in the H/V data.

#### 4.1. Bedrock depth

At Otterbach (station OTTER), a sonic logging of  $V_p$  data from

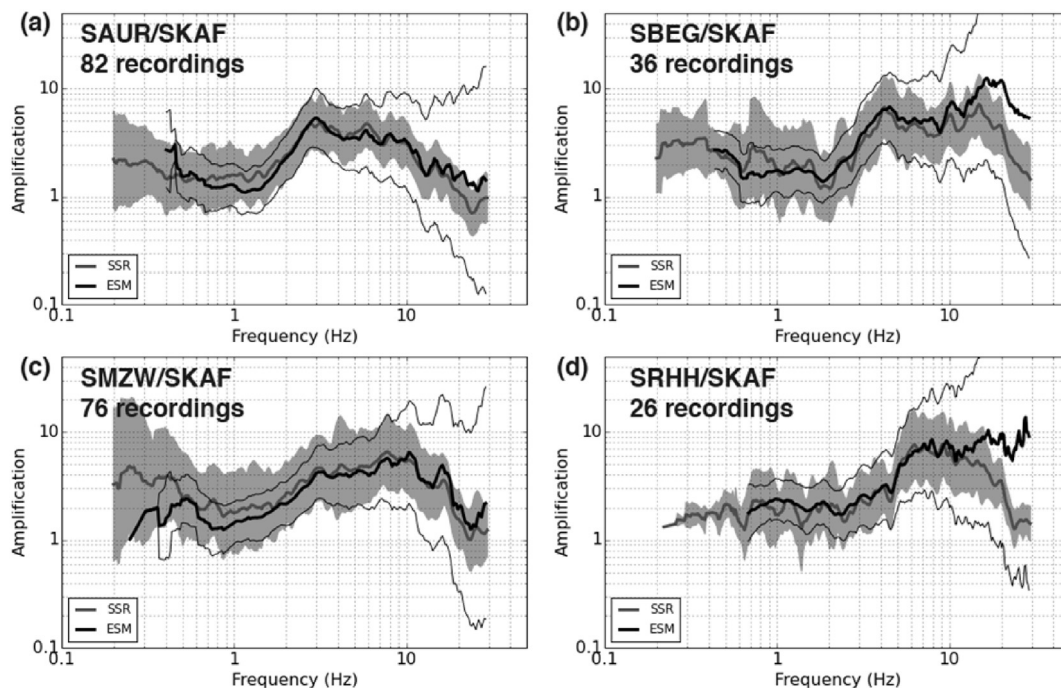


Fig. 5. Comparison of standard spectral ratios (SSRs, grey lines and grey shading) and ratios of anelastic ESM functions (black lines), with their respective standard deviations, for stations outside the Rhine Graben with respect to SKAF.

30 m to 2500 m depth was made available by the DHM project (Häring, 2006). Data from a second borehole of the same project (BS-1) between 450 m and 5000 m depth and located at about 1 km to the NNW allow the extension of the data ( $V_p$  and  $V_s$ ) to greater depths. The two logs are shifted in depth by 102 m due to the shape of the basin. The Otterbach sonic logging provides the P-wave velocity in the borehole at 5 cm intervals. We interpreted these data using homogeneous layers based on the observed velocity variations and geology logs (Häring, 2006). Density was also obtained from the borehole logging. We estimated the S-wave velocity (Fig. 6) based on a constant  $V_p/V_s$  ratio of 1.9 (Poisson ratio of 0.31) in the sedimentary layers and 1.75 (Poisson ratio of 0.25) in the crystalline basement. These values were obtained from data of the second borehole but could be larger at the surface. Other geophysical measurements confirmed this model except for the first 70 m, where the shear-wave velocity decreases rapidly, and therefore the Poisson ratio increases. At this site OTTER, the Quaternary sediments are 18 m thick (velocity not measured). The Upper Tertiary layers extend to 273 m depth and have a shear wave velocity of about 1000 m/s. The Lower Tertiary unit has a velocity of about 1600 m/s and the Mesozoic, at 500 m depth, a velocity of about 2400 m/s. The shear wave velocity in the crystalline basement, starting at 2650 m depth, is 3400 m/s.

Following Edwards et al. (2013), we used the simplified  $V_s$  model of Fig. 6 to compute the elastic SH transfer function. We corrected it to the Swiss reference rock of Poggi et al. (2011) by computing the impedance contrast between the velocity of the lowermost layer and the Swiss reference (Eq. (7) of Edwards et al., 2013). We compared the corrected SH transfer function to the ESM amplification function derived at OTTER (Fig. 7) and observed a good agreement between the empirical and the numerical approach as to both the frequency and amplitude of the fundamental peak. Discrepancies at higher frequencies are due to the lack of data within the first 70 m of the soil column. By removing the rock layers one after the other at the bottom of the simplified  $V_s$  profile, we identified that the interface between the Lower Tertiary unit and the Mesozoic layers at 500 m depth controls the fundamental frequency of the site response, between 0.4 Hz and 1 Hz.

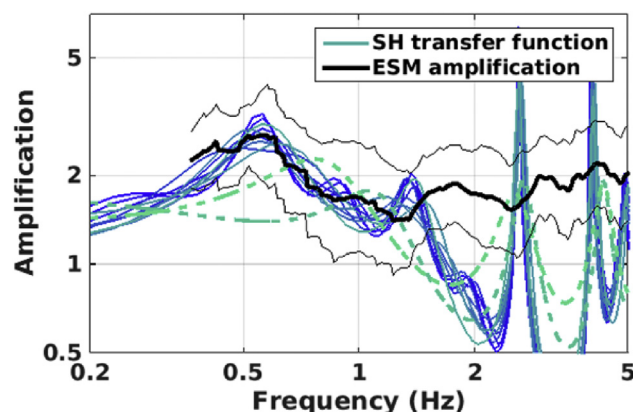


Fig. 7. Comparison between the observed ESM function at OTTER station (black curves) and the SH transfer function from the 1D velocity model from the sonic logging (blue curves), gradually reducing the number of layers at the bottom of the profile. The results are similar until the Mesozoic layer is removed (dashed lines). (For interpretation of the references to colour in this figure legend, the reader is referred to the web version of this article.)

The geophysical bedrock is therefore the Mesozoic limestone at this site. As a result, future numerical models of the site should account for this interface.

#### 4.2. Second peak in the H/V ratios

Nearly all the single-stations recordings available in Basel were homogeneously reprocessed using the H/V method (2200 points). The recording quality of this dataset is heterogeneous since the measurements were performed between 1997 and 2014. All points in the city-centre were re-picked including second peaks, when existing. While the fundamental peak is related to the interface with the bedrock, secondary peaks may relate to intermediate layering and may also play an important role in the amplification. For instance, at the permanent station SBIS2 (Fig. 4c) a peak at 2 Hz

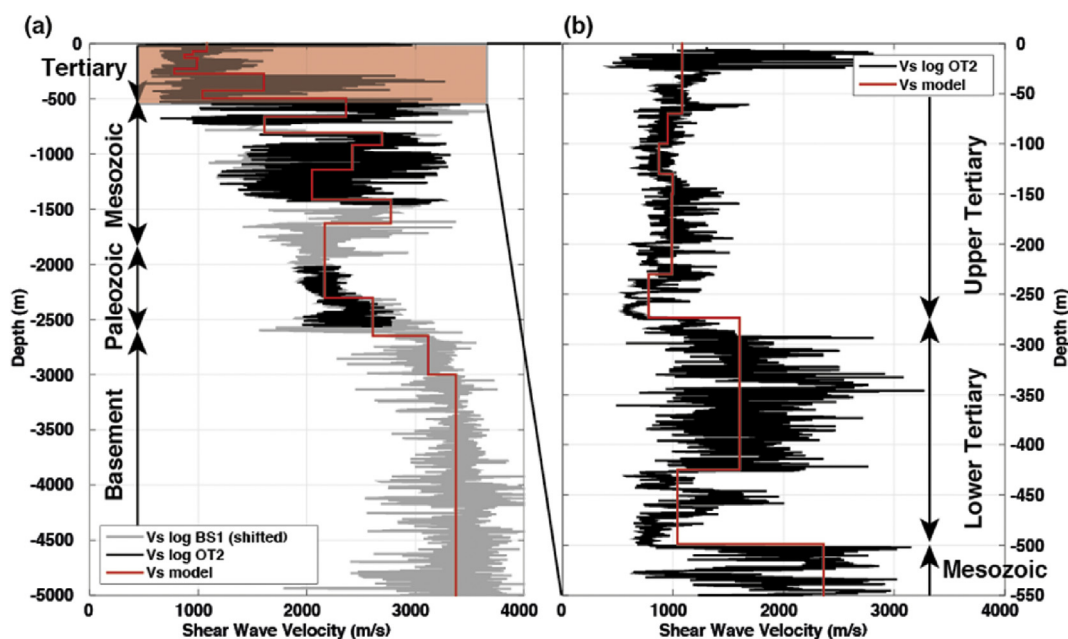


Fig. 6.  $V_s$  profile at site Otterbach (OT2) from borehole logging over the whole available depth (a) and zoom over the 550 first meters (b). Velocity data from borehole BS 1 are vertically shifted 102 m to reflect the observed differences in the layer depths.

in the amplification function can be related to a peak at the same frequency in the H/V curve. It is observed that this peak is stable with time in the H/V ratios of SBIS2. Fig. 8a shows the map of these second peaks. Some high-frequency values (above 10 Hz, white to blue) can be recognized at various places in the basin, with a high variability. These sites are characterised by shallow low-velocity layers, in some cases anthropogenic infill. Second peaks at lower frequencies (below 10 Hz, white to red) are found only in the Loess hills in the South of Basel (yellow area), which justified segregating the Rhine Graben into 2 zones. The lowermost frequency of the second peaks is about 2 Hz but it is difficult to map it precisely because the peak has a small amplitude and is not apparent everywhere. Its frequency value is not correlated with the thickness of the Quaternary layer (Fig. 8b). Moreover, the array analyses available in Basel do not show any noticeable velocity contrast between Tertiary and Quaternary layers. The second peak is partly reproduced in the microzonation of 2006 by the 2D model (Fäh and Havenith, 2006) but not by the 1D SH transfer function. At site CHBAL, it is also not reproduced by 1D site characterization (site Allschwil 1 in Havenith et al., 2007). A topographic origin for this second peak cannot be excluded but is unlikely (Burjanek et al., 2014). However, additional work, including simulation with a reliable 3D model capable of taking into account the local generation of surface waves and focusing and defocusing effects, is necessary to provide a final interpretation.

## 5. Validation of the microzonation of 2006

In order to validate the PSA amplification functions derived from the microzonation, we first changed the reference of each of them to the generic Swiss rock (Poggi et al., 2011) by computing the correction from the impedance contrast between the reference of Fäh and Havenith (2006) and the Swiss reference velocity profiles expressed as the ratio of their quarter-wavelength velocities. We did not account for differences in the anelastic attenuation. These curves are compared to the PSA ESM amplification functions of stations located in each zone, if any.

The zone “Basel Nord” includes the city centre and hosts a large number of SSMNet stations (Fig. 9a). Its amplification function

shows a peak around 1 Hz. Although the amplitudes match with the observations, a large variability among the observed ESM functions is observed. Some stations in the North-East (SBAF, OTTER) show lower amplifications. The sub-zones Holocene and Pleistocene show a difference above 2 Hz that does not correspond to any feature in the ESM function. The eastern part of the Rhine Graben (zone “Rheingraben Ost”) shows an amplification function in the microzonation with amplitudes decreasing from 3 to 2 at 10 Hz (Fig. 9b). Most of the stations in the zone show similar amplification, with little variability.

The Loess hills are represented by the zone “Basel West” located western from the Allschwil fault and the zone “Rheingraben West” that have a comparable amplification function with an average amplitude of 3 (Fig. 9c). Stations CHBAL and CHBA2 show similar amplitudes though the second peak in the H/V ratios around 4 Hz induces a peak that is not covered by the amplification function proposed for the microzonation. The ESM function of station SBIS2 matches well with the amplification of the microzonation, including the second peak at 2 Hz.

Outside the Rhine Graben, the zones of microzonation aggregate areas with properties strongly varying over short distances. They show a ramp function increasing from unity to about 3 (Fig. 10). The resonance frequency at the stations’ sites strongly influences the amplification function so that the comparison between microzonation and stations is difficult. However, amplification up to 2 Hz matches in general while at higher frequencies, the peak amplification of the ESM functions may exceed notably the values from the microzonation. The rocky subzone “Basel Ost HF” (Fig. 10) overestimates the amplification between 1 and 10 Hz observed at station SKAF. This station shows deamplification with respect to the reference rock and has therefore higher Vs values than the reference model ( $V_{S30} = 1100$  m/s). It corresponds to recently eroded rock by the Rhine river.

As a conclusion, the microzonation and the observed ESM amplifications match well overall, particularly in the Rhine Graben (Fig. 9) where they are relatively homogeneous. Some high-frequency amplifications, for instance in the Loess hills in the South of Basel, are however not reproduced. Outside the Rhine Graben (Fig. 10), a larger variability is expected and observed, so

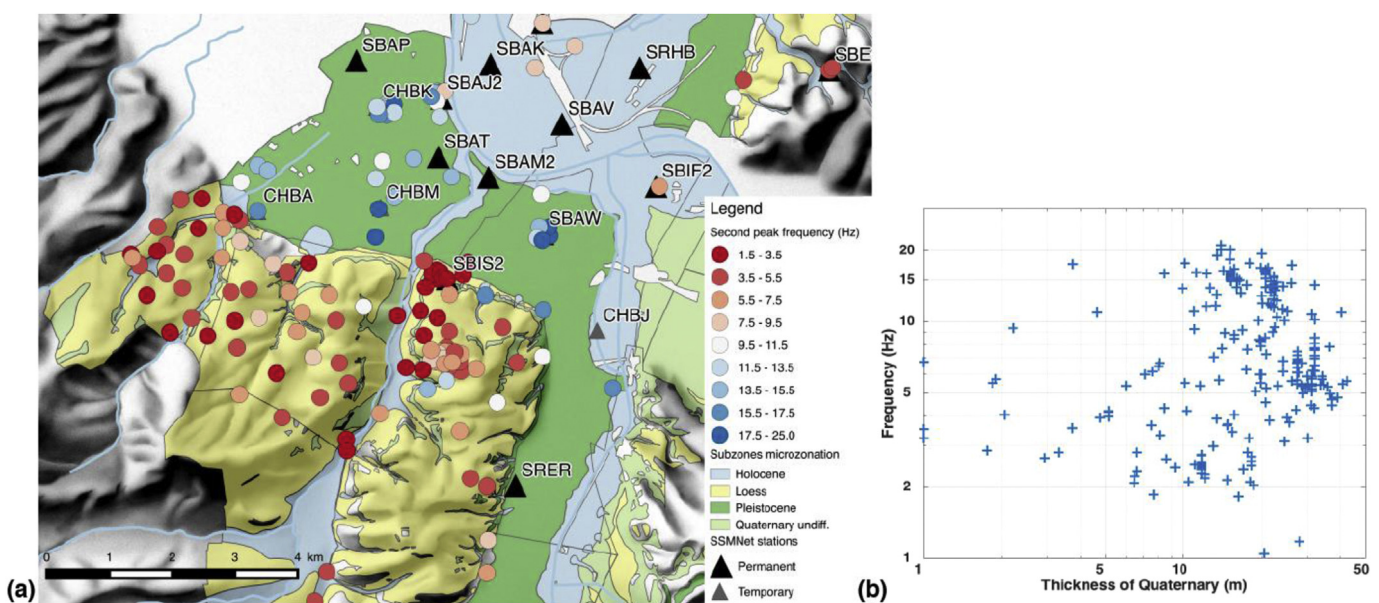
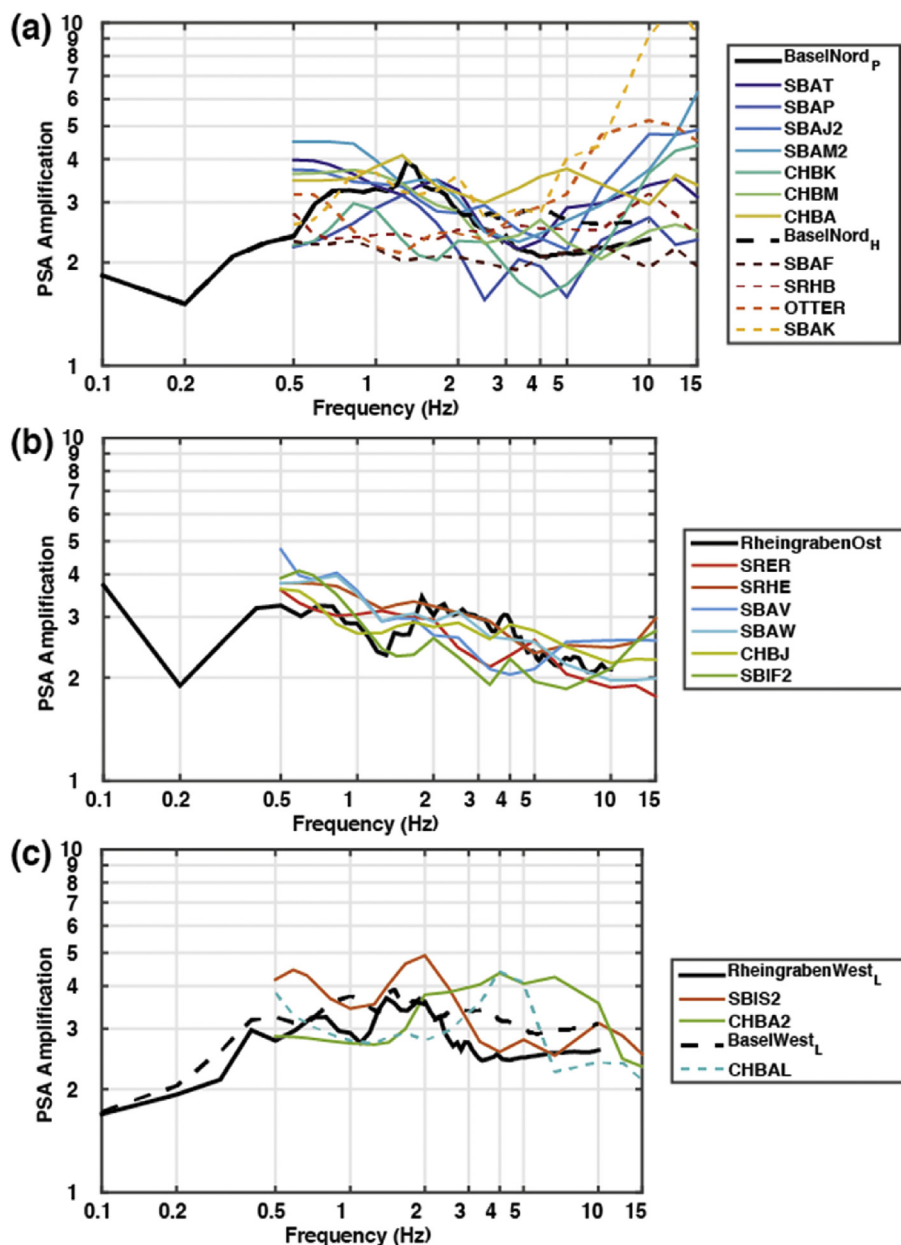


Fig. 8. Second peak in the H/V ratios in the Rhine Graben in Basel. a) Map of the frequency distribution related to surface sediments as mapped by the 2006 microzonation; b) Frequency values with respect to the thickness of the Quaternary sediments (GeORG project team, 2013).



**Fig. 9.** Comparison of the PSA amplification in different zones of the 2006 microzonation inside the Rhine Graben (black curves) and PSA ESM functions of stations located in the corresponding zones (coloured curves). a) Zone "Basel Nord"; b) Zone "Rheingraben Ost"; c) Zones "Rheingraben West" and "Basel West" (Loess hills). Subscripts P (Pleistocene), H (Holocene) and L (Loess) denote the subzones.

that the microzonation hardly models the amplification. In the area outside of the Rhine Graben, for a high resolution amplification mapping, a single amplification function per zone is not enough due to the variability of the fundamental frequency of resonance.

## 6. High-resolution amplification maps and application

As shown in section 5, the amplification maps derived within the framework of previous microzonation studies can be considered as suitable, though they could be improved using newly available data. Therefore, we propose here a new method to derive amplification maps based on observed ESM functions in PSA. According to the results in section 5, the inner and outer portions of the Rhine Graben are treated separately in the following.

### 6.1. Amplification in the Rhine Graben

The amplification in the Rhine Graben is mostly controlled by the deep sediments and varies smoothly as shown by the ESM functions (Fig. 9). Michel et al. (2014) showed that this could indicate 2D or 3D site effects. However, no 2D resonance is expected, but only generation of surface waves at the edge of the basin (Steimen et al., 2003; Michel et al., 2014). The depth of the sediments, increasing towards the east (trough of St-Jakob Tüllingen), controls the fundamental frequency, between 0.4 and 1 Hz, that is not prominent in the ESM amplification functions. It should be noticed that the ESM function is not available below 0.6 Hz due to a lack of recordings of large earthquakes.

As shown previously, a noticeable exception is observed at site Bruderholz (SBIS2) that shows large amplifications with a second

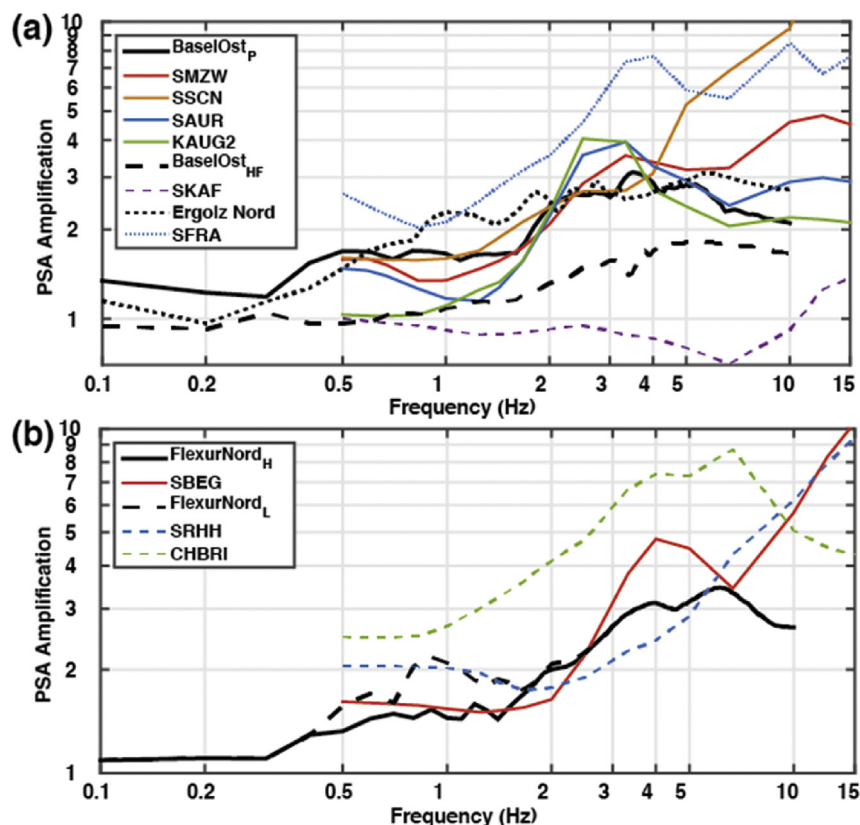


**Fig. 10.** Comparison of the PSA amplification in different zones of the 2006 microzonation outside the Rhine Graben (black curves) and PSA ESM functions of stations located in the corresponding zones (coloured curves). a) Zone "Basel Ost"; b) Zone "Flexur Nord". Subscripts P (Pleistocene), H (Holocene) and L (Loess) identify the subzones.

peak at 2 Hz and to a lesser extent at sites CHBAL and CHBA2, also located on the Loess hills in the South of Basel. This peak is discussed in section 4.2 although no final interpretation could be found. We have therefore to rely on the empirical observation, based on homogeneous H/V curves and ESM amplification, that the amplification is larger in the Loess hills. The site response in this area remains poorly understood compared to the rest of the Graben.

## 6.2. Amplification outside the Rhine Graben

Outside the Rhine Graben, the depth of the Quaternary sediments is generally limited though the resonance frequency can be as low as 1 Hz in some areas. The assumption of a single layer over the bedrock can be made there as 1D site characterization is generally capturing the amplification at the sites (Michel et al., 2014). Site-response is then controlled by the thickness of the sediments and their S-wave velocity. The fundamental frequency of resonance  $f_0$  has the property to integrate these two parameters. Although it cannot explain the whole amplification, it is expected to capture its main features. Therefore, we studied the amplification functions normalized by the fundamental frequency of the site  $f_0$ , obtained through H/V ratios.

Cadet et al. (2012) proposed a generic model called SAPE for amplification functions based on  $f_0$ ,  $V_{S2}$  (travel time average S-wave velocity over the  $z$  first meters) or any combination of these parameters, based on Japanese sites. We compared their model using  $f_0$  only to our observations from ESM, normalized by  $f_0$  (Fig. 11). Moreover, we compared them to the amplification curves from the microzonation for zones outside the Rhine Graben. The first peak in the amplification function was considered as the fundamental frequency  $f_0$ . The shapes of the obtained functions are comparable.

The peak amplitude of the ESM functions is variable but it is not clearly correlated with parameters such as the peak amplitude in the H/V ratios,  $f_0$  or the sediment type. It indicates variations in the quality of the surface sediments that cannot be represented with available proxies. The microzonation and the SAPE function show lower amplitudes than the ESM curves and a smoother function. The SAPE model is based on the average over a large amount of different sites that do not fully reflect the situation in Basel. Moreover, the SAPE model depends on  $f_0$  with decreasing amplitude at the peak with increasing  $f_0$ , while we observed the opposite.

The amplitudes after the peak are generally lower for the microzonation than for the ESM functions. In the ESM function, the amplification after the peak is controlled by the site-specific anelastic attenuation  $\Delta\kappa_j = \kappa_{0j} - \kappa_{0,Ref}$ . The observed  $\Delta\kappa_j$  values using ESM are negative indicating a lower attenuation compared to the Swiss Reference rock, which corresponds to amplification as expected in shallow sediments over a stiff bedrock. Conversely,  $\Delta\kappa_j$  values in the Rhine Graben are generally positive and correspond to stronger attenuation with respect to the reference. However, the uncertainty has the same order of magnitude as the mean (Edwards et al., 2015b) so that the observed variability in the ESM function after the peak cannot be completely trusted.

An amplification functional form is therefore proposed as the average of the available ESM amplification functions outside the Rhine Graben (Fig. 11). It is extended at low frequency using the curve from the microzonation. This function can be used in combination with the fundamental frequency of the site to predict the amplification at any frequency (see next section).

## 6.3. Computation of amplification maps

We showed in the previous sections that the average

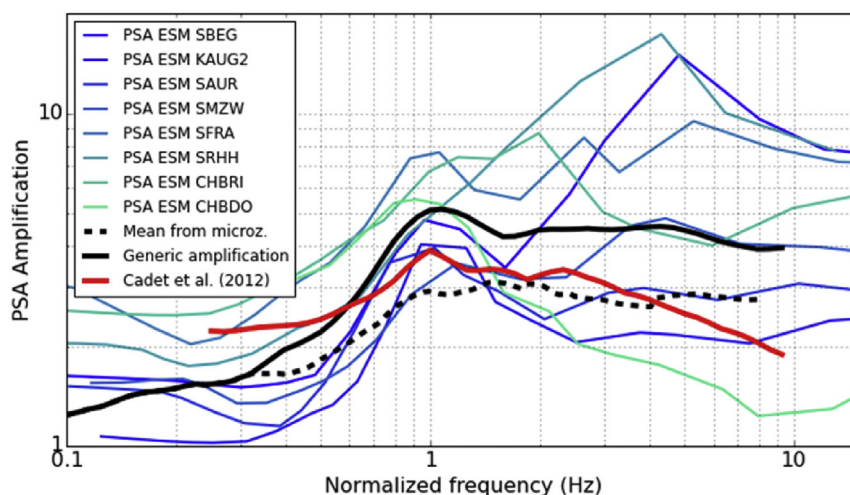


**Fig. 11.** Amplification function normalized by the fundamental resonance frequency of the site  $f_0$  (purple to green curves: ESM functions; solid black line: selected functional form; dashed black line: mean of the microzonation amplification functions; red line: SAPE function of Cadet et al., 2012). (For interpretation of the references to colour in this figure legend, the reader is referred to the web version of this article.)

amplification does not vary significantly in the Rhine Graben where many stations are available. Therefore, we performed a spatial interpolation of the station ESM amplification in the Rhine Graben. For that purpose, we used the robust nearest neighbour method that separates the space into Voronoi cells around the known points and assigns one value per cell (Cressie, 1993).

We also showed that the Loess hills in the South and the West of Basel were exhibiting different behaviour (secondary peaks, higher amplification) so that data in this area is interpolated separately from the rest of the basin. Only 3 stations with very different amplification functions are available in this area so our interpolation using the nearest neighbour method remains uncertain.

Outside the Graben, we used the amplification functional form developed in the previous section (solid black line in Fig. 11) to compute the amplification at each available  $f_0$  values. The results are interpolated over the whole area except in zones considered as rock (in red in Fig. 1) using the inverse distance weighting (IDW) algorithm (Cressie, 1993). IDW allows a simple and smooth interpolation based on the values at a given number of neighbours weighted by their distance. However, depending on the weighting function and the distribution of available data, it may create unrealistic artefacts. The power  $p$  used to weight with respect to distance can be modulated. A large value (16) simulates the nearest neighbour method. A value of 2 is used here as a trade-off.

The final amplification maps, which quantify the site effects, are displayed in Fig. 12 and compared to the amplification of the 2006 microzonation at period of 0.3 and 1 s (frequencies of 3.3 and 1 Hz, respectively). Rock areas are set to the default unit value for each method. One can notice that the change in the rock reference for the microzonation affects this value at 0.3 s, leading to an insignificant de-amplification. A grid size of 40 m has been selected for the computation as a good trade-off regarding the density of available data. It should be noticed that the microzonation is available in a limited area, for instance not outside the Swiss border, where a default value of 1 is displayed. The amplification maps resulting from this study show similar orders of magnitude compared to the 2006 microzonation. However, the Rhine valley outside the Rhine Graben shows larger values than the microzonation at 0.3 s but lower at 1 s. The interpolated map extends also to the right riverside of the Rhine (Germany) where data is also available. Towards west (France), however, the results are extrapolated.

#### 6.4. Towards a high-resolution implementation in ShakeMap

ShakeMap is a worldwide-known scientific and technical framework that delivers near real-time earthquake shaking maps based on recorded and predicted ground-motions, spectral amplitudes and macroseismic intensity levels, including amplification due to local site effects. ShakeMap was first developed for significant earthquakes in California (Wald et al., 1999) and is nowadays routinely used in many other regions in the United States and worldwide (Worden et al., 2010) in order to optimize emergency response capabilities and information dissemination following relevant earthquakes. The latest nation-wide implementation for Switzerland is documented by Cauzzi et al. (2015). Consistent with engineering seismology studies in Switzerland, it uses the Swiss stochastic model of Edwards and Fäh (2013) and a strategy to site amplification based on expected macroseismic intensity increments with respect to median intensity predictions for the country (Fäh et al., 2011). The high-resolution (40 m) amplification maps derived in the previous section can be used in the future for a local ShakeMap implementation as selectively described in the following.

In Swiss ShakeMaps (Cauzzi et al., 2015), macroseismic intensity  $I$  is converted from peak ground velocity (PGV) based on Faenza and Michelini (2010). For conversion of PSA levels, one can rely on Faenza and Michelini (2011) for vibration periods equal to 0.3, 1 and 2 s. The low-energy events characterising the seismicity of Switzerland and the typical vibration frequencies of the Swiss building stock led us to choose 0.3 s as a good candidate for this exercise. The conversion equation of Faenza and Michelini (2011) is given by:

$$I = 1.24 + 2.47 \log_{10} [PSA(0.3s)] \quad (1)$$

The relationship between the intensity increments  $\Delta I$  and the amplification of the spectral acceleration at 0.3 s ( $A^{0.3s}$ ) is then:

$$\Delta I = 2.47 \log_{10} \left[ \frac{PSA(0.3s)}{PSA_{ref}(0.3s)} \right] = 2.47 \log_{10} [A^{0.3s}] \quad (2)$$

where  $PSA_{ref}$  denotes the PSA at the Swiss reference rock model.

Fig. 13 shows the amplification yielded by Eq. (2) and the previously described spatial interpolation schemes compared to the



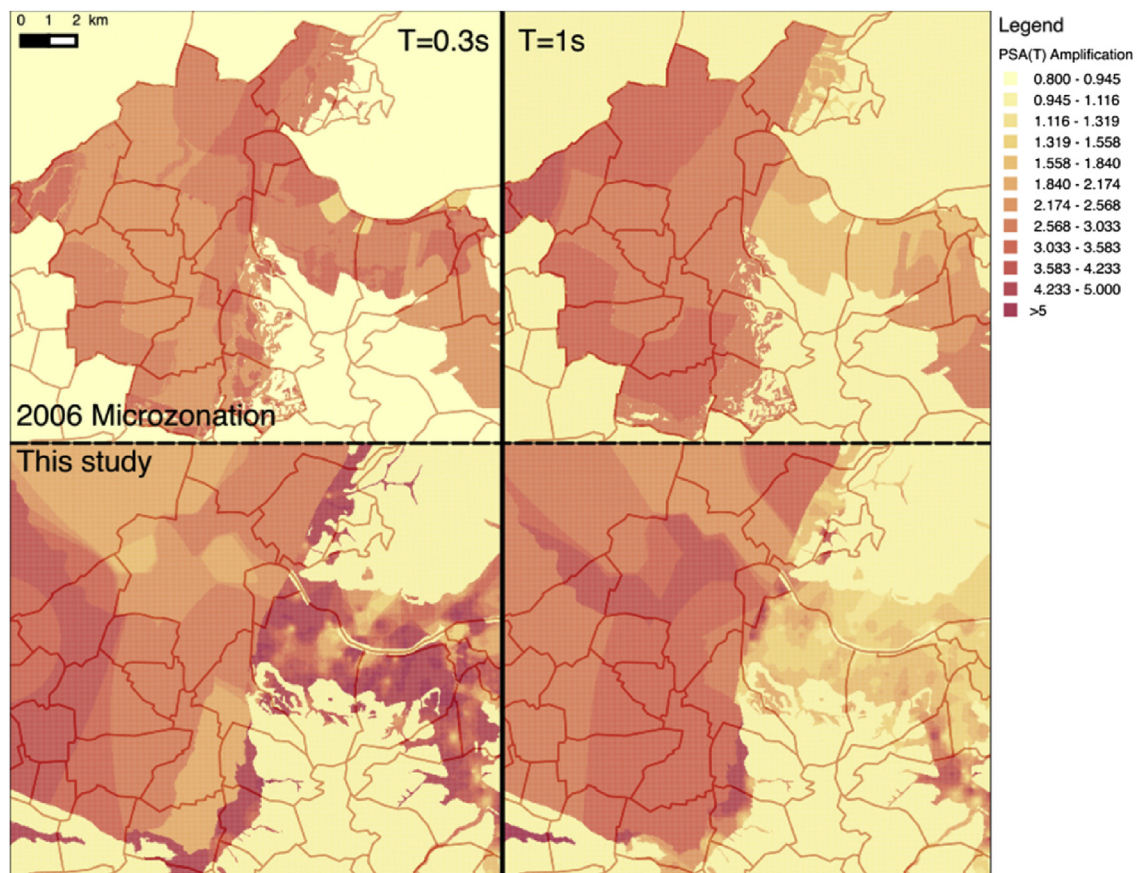


Fig. 12. Amplification maps in Basel in terms of spectral acceleration at 0.3 s and 1 s based on the 2006 microzonation and the new interpolation.

amplification data used for the national ShakeMaps, based on macroseismic data and surface geology (Cauzzi et al., 2015). As apparent from the figure, the use of new, high-resolution data results into a significantly reduced amplification on rock-like ground and more homogeneous amplification levels in the Rhine Graben. A shaking scenario of the possible repetition of the 1356  $M_w$  6.6 event is shown in Fig. 14. This purely predictive ShakeMap uses the amplification data of Fig. 13a and the source geometry of Ferry et al. (2005) and Cauzzi et al. (2015). Predicted intensity reaches degree IX as reported in the ECOS-09 catalogue (Fäh et al., 2011).

## 7. Discussion and conclusions

The recent recordings of high-quality permanent and temporary accelerometer stations have significantly improved our understanding and representation of earthquake ground-motion amplification in the municipal area of Basel. We estimated the amplification at each station using empirical spectral modelling of records from the whole permanent network. This method is complementary to site characterization and overcomes limitations of SSRs, particularly the absence of rock reference station. It accounts for 2D/3D effects naturally included in the used earthquake records

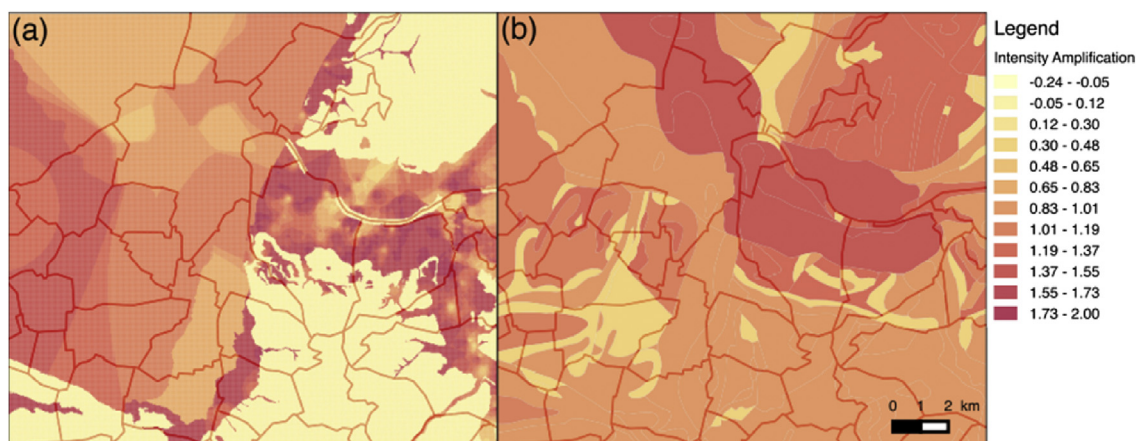
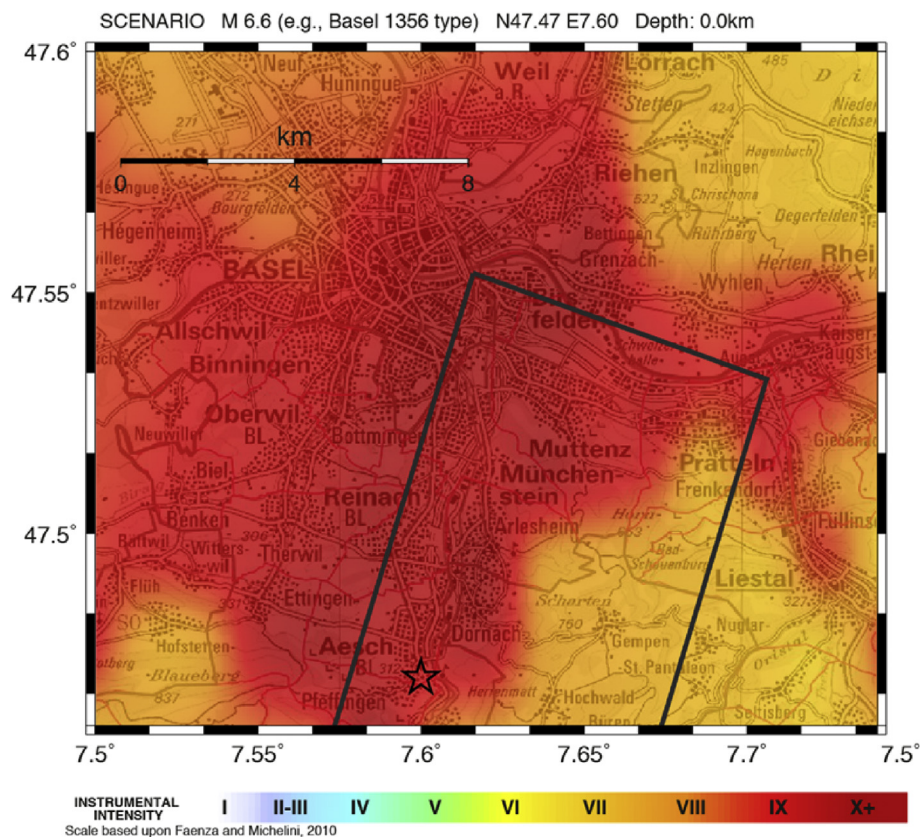


Fig. 13. Amplification map in Basel in terms of macroseismic intensity increments. a) this study; b) nation-wide amplification map (Fäh et al., 2011).



**Fig. 14.** ShakeMap of the possible repetition of the 1356  $M_w$  6.6 event, computed as explained in the text. The star is the ECOS-09 epicentre, while the solid grey lines show the surface projection of the ruptured fault in the city area.

but the resolution is too low to map these rapidly changing effects at the edge of the basin and close to faults (Panzer et al., 2016). Moreover, it is only based on the recording of weak motions and cannot account for non-linear behaviour of the sediments as detailed numerical site response analysis could.

We identified the most important features that play a role in the site amplification. In the Rhine Graben, the interface with the Mesozoic bedrock and 2D/3D effects; outside the Rhine Graben, the depth of the Quaternary sediments and their material properties. This should be used to improve the 3D numerical models in the future. However, questions are remaining regarding the interpretation of the bedrock since our assessment is based on a single borehole. For instance, the interface between the upper and the lower Tertiary, also showing a strong velocity contrast, could also produce a resonance frequency at other locations in the basin. More research using the large available H/V dataset and 3D modelling should be performed to achieve a complete understanding of site effects in this area. This shows again the complementarity of ESM technique and geophysical site characterization.

We could verify the amplification functions derived in 2006 microzonation and propose improvements. We placed emphasis on the importance of using monitoring stations to verify microzonation studies. We proposed a new method to derive amplification maps from the individual amplification functions. In the Rhine Graben, where amplification varies only little in space, we interpolated the amplification functions obtained at each station of the network; outside the Rhine Graben, we used an amplification functional form obtained from the individual functions at the accelerometric sites coupled with fundamental frequencies mapped through single station measurements and H/V analysis.

Compared to the 2006 microzonation, a larger spatial variability of the amplification and more extreme values have been identified. Although derived under low-strain seismic excitation, the amplification maps resulting from this study can be tentatively used as input to shaking scenarios for loss assessment, eventually produced in real-time. The high-resolution (40 m) of the amplification maps presented in this manuscript is optimally tailored at earthquake risk assessment at the building level.

#### Acknowledgements

This work has been funded by the Crisis Organization of the Canton Basel-Stadt. The authors thank Geo-Energie Suisse AG who provided the sonic logging data and the GeORG project team who provided geological data (<http://www.geopotenziale.eu/>). The authors are grateful to the two anonymous reviewers who helped improve the paper.

#### References

- Bora, S.S., Scherbaum, F., Kuehn, N., Stafford, P., 2016. On the relationship between Fourier and response spectra: implications for the adjustment of empirical ground-motion prediction equations (GMPEs). *Bull. Seismol. Soc. Am.* 106 (3), 1235–1253.
- Bora, S.S., Scherbaum, F., Kuehn, N., Stafford, P., Edwards, B., 2015. Development of a response spectral ground-motion prediction equation (gmpe) for seismic-hazard analysis from empirical Fourier spectral and duration models. *Bull. Seismol. Soc. Am.* 105, 2192–2218.
- Boore, D.M., 2003. Simulation of ground motion using the stochastic method. *Pure Appl. Geophys.* 160, 635–676.
- Borcherdt, R.D., 1970. Effects of local geology on ground motion near San Francisco Bay. *Bull. Seismol. Soc. Am.* 60, 29–61.
- Burjánek, J., Edwards, B., Fäh, D., 2014. Empirical evidence of local seismic effects at

- sites with pronounced topography: a systematic approach. *Geophys. J. Int.* 197, 608–619.
- Cadet, H., Bard, P., Duval, A.-M., Bertrand, E., 2012. Site effect assessment using KiK-net data: Part 2-site amplification prediction equation based on  $f_0$  and  $V_{sz}$ . *Bull. Earthq. Eng.* 10 (2), 451–489. <http://dx.doi.org/10.1007/s10518-011-9298-7>.
- Campbell, K.W., 2003. Prediction of strong ground motion using the hybrid empirical method and its use in the development of ground-motion (attenuation) relations in Eastern North America. *Bull. Seismol. Soc. Am.* 93, 1012–1033.
- Cartwright, D.E., Longuet-Higgins, M.S., 1956. The statistical distribution of the maxima of a random function. *Proc. R. Soc. Lon Ser-A* 237, 212–232.
- Cauzzi, C., Edwards, B., Fäh, D., Clinton, J., Wiemer, S., Kästli, P., Cua, G., Giardini, D., 2015. New predictive equations and site amplification estimates for the next-generation Swiss ShakeMaps. *Geophys. J. Int.* 200, 421–438. <http://dx.doi.org/10.1093/gji/ggu404>.
- Cauzzi, C., Clinton, J., 2013. A high- and low-noise model for high-quality strong-motion accelerometers stations. *Earthq. Spectra* 29, 85–102. <http://dx.doi.org/10.1193/1.4000107>.
- Clinton, J., Cauzzi, C., Fäh, D., Michel, C., Zweifel, P., Olivieri, M., Cua, G., Haslinger, F., Giardini, D., 2011. The current state of strong motion monitoring in Switzerland. In: Akkar, S., Gülkan, P., van Eck, T. (Eds.), *Earthquake Data in Engineering Seismology, Geotechnical, Geological, and Earthquake Engineering*. Springer Netherlands, Dordrecht, pp. 219–233. <http://dx.doi.org/10.1007/978-94-007-0152-6>.
- Cressie, N., 1993. *Statistics for Spatial data*. John Wiley Sons, New York, p. 900.
- Deichmann, N., Giardini, D., 2009. Earthquakes induced by the stimulation of an enhanced geothermal system below Basel (Switzerland). *Seismol. Res. Lett.* 80, 784–798. <http://dx.doi.org/10.1785/gssrl.80.5.784>.
- Diehl, T., Deichmann, N., Clinton, J., Kästli, P., Cauzzi, C., Kraft, T., Behr, Y., Edwards, B., Guilhem, A., Korger, E., Hobiger, M., Haslinger, F., Fäh, D., Wiemer, S., 2015. Earthquakes in Switzerland and surrounding regions during 2014. *Swiss J. Geosci.* 108, 425–443. <http://dx.doi.org/10.1007/s00015-015-0204-1>.
- Edwards, B., Cauzzi, C., Danciu, L., Fäh, D., 2016. Region-specific assessment, adjustment, and weighting of ground-motion prediction models: application to the 2015 Swiss Seismic-Hazard Maps. *Bull. Seismol. Soc. Am.* 106 (4), 1840–1857. <http://dx.doi.org/10.1785/0120150367>.
- Edwards, B., Kraft, T., Cauzzi, C., Kästli, P., Wiemer, S., 2015a. Seismic monitoring and analysis of deep geothermal projects in St Gallen and Basel, Switzerland. *Geophys. J. Int.* 201, 1020–1037. <http://dx.doi.org/10.1093/gji/ggv059>.
- Edwards, B., Ktenidou, O.-J., Cotton, F., Abrahamson, N., Van Houtte, C., Fäh, D., 2015b. Epistemic uncertainty and limitations of the  $\kappa_0$  model for near-surface attenuation at hard rock sites. *Geophys. J. Int.* 202 (3), 1627–1645. <http://dx.doi.org/10.1093/gji/ggv222>.
- Edwards, B., Michel, C., Poggi, V., Fäh, D., 2013. Determination of site amplification from regional seismicity: application to the Swiss national seismic networks. *Seismol. Res. Lett.* 84 (4), 611–621. <http://dx.doi.org/10.1785/0220120176>.
- Edwards, B., Fäh, D., 2013. A stochastic ground-motion model for Switzerland. *Bull. Seismol. Soc. Am.* 103 (1), 78–98. <http://dx.doi.org/10.1785/0120110331>.
- Faenza, L., Michelini, A., 2011. Regression analysis of MCS intensity and ground motion spectral accelerations (SAs) in Italy. *Geophys. J. Int.* 186, 1415–1430. <http://dx.doi.org/10.1111/j.1365-246X.2011.05125.x>.
- Faenza, L., Michelini, A., 2010. Regression analysis of MCS intensity and ground motion parameters in Italy and its application in ShakeMap. *Geophys. J. Int.* 180, 1138–1152. <http://dx.doi.org/10.1111/j.1365-246X.2009.04467.x>.
- Fäh, D., Giardini, D., Kästli, P., Deichmann, N., Gisler, M., Schwarz-Zanetti, G., Alvarez-Rubio, S., Sellami, S., Edwards, B., Allmann, B., Bethmann, F., Wössner, J., Gassner-Stamm, G., Fritsche, S., Eberhard, D., 2011. *ECOS-09 Earthquake Catalogue of Switzerland Release 2011. Report and Database*. Public catalogue, 17.4.2011. Swiss Seismological Service ETH Zürich, Report SED/RISK/R/001/20110417.
- Fäh, D., Gisler, M., Jaggi, B., Kästli, P., Lutz, T., Masciadri, V., Matt, C., Mayer-Rosa, D., Rippmann, D., Schwarz-Zanetti, G., Tauber, J., Wenk, T., 2009. The 1356 Basel earthquake: an interdisciplinary revision. *Geophys. J. Int.* 178 (1), 351–374. <http://dx.doi.org/10.1111/j.1365-246X.2009.04130.x>.
- Fäh, D., Wenk, T., 2009. Mikrozonierung für die Kantone Basel Stadt und Basel Landschaft : Optimierung der Form der Antwortspektren und der Anzahl der Mikrozononen : Abschlussbericht: Teilbericht B. WTH Zurich.
- Fäh, D., Steiner, B., Havenith, H.-B., Steimen, S., Huggenberger, P., Fäh, E., 2006. INTERREG III Projekt: Erdbebenmikrozonierung Am Südlichen Oberrhein. Teilbericht 1: Zoneneinteilung. <http://dx.doi.org/10.3929/ethz-a-006411876>.
- Fäh, D., Havenith, H., 2006. INTERREG III Projekt: Erdbebenmikrozonierung am südlichen Oberrhein. Teilbericht 5: Bestimmung der zonenspezifischen Antwortspektren. <http://dx.doi.org/10.3929/ethz-a-006412190>.
- Fäh, D., Huggenberger, P., 2006. INTERREG III Projekt: Erdbebenmikrozonierung Am Südlichen Oberrhein: Zusammenfassung. <http://dx.doi.org/10.3929/ethz-a-006412199>.
- Fäh, D., Kind, F., Lang, K., Giardini, D., 2001. Earthquake scenarios for the city of Basel. *Soil Dyn. Earthq. Eng.* 21, 405–413.
- Fäh, D., Rüttener, E., Noack, T., Kruspan, P., 1997. Microzonation of the city of Basel. *J. Seismol.* 1, 87–102.
- Ferry, M., Meghraoui, M., Delouis, B., Giardini, D., 2005. Evidence for Holocene palaeoseismicity along the Basel-Reinach active normal fault (Switzerland): a Seismic source for the 1356 earthquake in the Upper Rhine graben. *Geophys. J. Int.* 160, 554–572.
- GeORG project team, 2013. *Geopotenziale des tieferen Untergrundes im Oberreingraben, Fachlich-Technischer Abschlussbericht des INTERREG-Projekts GeORG, Teile 1–4*. – Internet. <http://www.geopotenziale.eu>.
- Giardini, D., 2009. Geothermal quake risks must be faced. *Nature* 462, 848–849.
- Gisler, M., Fäh, D., 2011. Grundlagen des Makroseismischen Erdbebenkatalogs der Schweiz Band 2: 1681–1878. Schweizerischer Erdbebendienst. <http://dx.doi.org/10.3218/3407-3>.
- Grünthal, G., Musson, R.M.W., Schwartz, J., Stucchi, M., 1998. *European Macroseismic Scale 1998, vol. 15. Cahiers du Centre Européen de Géodynamique et de Séismologie*, Luxembourg.
- Häring, 2006. *Geothermie-sondierbohrung Otterbach 2. Technical report, Geothermal Explorers Ltd, Basel*.
- Havenith, H.-B., Fäh, D., Polom, U., Roullé, A., 2007. S-wave velocity measurements applied to the seismic microzonation of Basel, Upper Rhine Graben. *Geophys. J. Int.* 170 (1), 346–358. <http://dx.doi.org/10.1111/j.1365-246X.2007.03422.x>.
- Kind, F., Fäh, D., Giardini, D., 2005. Array measurements of S-wave velocities from ambient vibrations. *Geophys. J. Int.* 160 (1), 114–126. <http://dx.doi.org/10.1111/j.1365-246X.2005.02331.x>.
- Kind, F., 2002. *Development of Microzonation Methods: application to Basle, Switzerland*. PhD Thesis Nr. 14548, ETH Zuerich.
- Liu, L., Pezeshk, S., 1999. An improvement on the estimation of pseudoresponse spectral velocity using RVT method. *B Seismol. Soc. Am.* 89, 1384–1389.
- Michel, C., Fäh, D., 2016. *Basel Earthquake Risk Mitigation – Computation of Scenarios for School Buildings*. Technical Report. ETHZ-SED, Zürich, Switzerland, p. 69. <http://dx.doi.org/10.3929/ethz-a-010646514>.
- Michel, C., Edwards, B., Poggi, V., Burjānek, J., Roten, D., Cauzzi, C., Fäh, D., 2014. Assessment of site effects in alpine regions through systematic site characterization of seismic stations. *Bull. Seismol. Soc. Am.* 104 (6), 2809–2826. <http://dx.doi.org/10.1785/0120140097>.
- Opršal, I., Fäh, D., Mai, P.M., Giardini, D., 2005. Deterministic earthquake scenario for the Basel area: simulating strong motions and site effects for Basel, Switzerland. *J. Geophys. Res.* 110 (B4), 1–19. <http://dx.doi.org/10.1029/2004JB003188>.
- Panzera, F., Lombardo, G., Monaco, C., 2016. New evidence of wavefield polarization on fault zone in the lower NE slope of Mt. Etna. *Italian J. Geoscience* 135 (2), 250–260. <http://dx.doi.org/10.3301/IJG.2015.22>.
- Poggi, V., Edwards, B., Fäh, D., 2011. Derivation of a reference shear-wave velocity model from empirical site amplification. *Bull. Seismol. Soc. Am.* 101 (1), 258–274. <http://dx.doi.org/10.1785/0120100060>.
- Ripperger, J., Kästli, P., Fäh, D., Giardini, D., 2009. Ground motion and macroseismic intensities of a seismic event related to geothermal reservoir stimulation below the city of Basel - observations and modelling. *Geophys. J. Int.* 179 (3), 1757–1771. <http://dx.doi.org/10.1111/j.1365-246X.2009.04374.x>.
- Schwarz-Zanetti, G., Fäh, D., 2011. Grundlagen des Makroseismischen Erdbebenkatalogs der Schweiz Band 1: 1000–1680. Schweizerischer Erdbebendienst. <http://dx.doi.org/10.3218/3407-3>.
- Steimen, S., Fäh, D., Kind, F., Schmid, C., Giardini, D., 2003. Identifying 2D resonance in microtremor wave fields. *Bull. Seismol. Soc. Am.* 93 (2), 583–599.
- Swiss Seismological Service (SED) at ETH Zurich, 2015a. *Swiss National Probabilistic Seismic Hazard Assessment 2015*. Federal Institute of Technology, Zurich retrieved on 23/05/2016 from: [http://www.seismo.ethz.ch/prod/Erdbebengefaehrungsmodell\\_2015/index\\_EN](http://www.seismo.ethz.ch/prod/Erdbebengefaehrungsmodell_2015/index_EN).
- Swiss Seismological Service (SED) at ETH Zurich, 2015b. *The Site Characterization Database for Seismic Stations in Switzerland*. Federal Institute of Technology, Zurich. <http://dx.doi.org/10.12686/sed-stationcharacterizationdb> retrieved on 04/02/2016 from: <http://stations.seismo.ethz.ch>.
- Ullah, S., Bindi, D., Pittore, M., Pilz, M., Orunbaev, S., Moldobekov, B., Parolai, S., 2013. Improving the spatial resolution of ground motion variability using earthquake and seismic noise data: the example of Bishkek (Kyrgyzstan). *Bull. Earthq. Eng.* 11, 385–399. <http://dx.doi.org/10.1007/s10518-012-9401-8>.
- Wald, D.J., Quitoriano, V., Heaton, T.H., Kanamori, H., Scrivner, C.W., Worden, C.B., 1999. TriNet "ShakeMaps": rapid generation of peak ground motion and intensity maps for earthquakes in Southern California. *Earthq. Spectra* 15 (3), 537–555.
- Worden, C.B., Wald, D.J., Allen, T.I., Lin, K., Garcia, D., Cua, G., 2010. A revised ground-motion and intensity interpolation scheme for ShakeMap. *Bull. Seism. Soc. Am.* 100 (6), 3083–3096.

## 1.7 Perspectives

Nous avons montré que les fonctions d'amplification ESM obtenues à partir des enregistrements de séismes était un formidable outil pour comprendre les effets de site et mieux interpréter les données géophysiques. Celles-ci restent néanmoins capitales compte tenu du fait qu'on ne peut installer qu'un nombre limité de stations permanentes alors qu'une technique comme le H/V peut-être utilisée sur une maille très serrée. Il existe un énorme potentiel pour l'analyse des effets de site à l'aide de réseaux très denses développés par l'industrie pétrolière et désormais utilisés pour la recherche (Bowden *et al.*, 2015). Plus généralement, la décomposition du champ d'ondes en différents types d'ondes de surface et de volume, la détermination de leurs propriétés et de la part d'énergie de chacune doit permettre de mieux interpréter les enregistrements. Les méthodes telles que WaveDec (Maranò *et al.*, 2012) et MUSIQUE (Hobiger *et al.*, 2016) permettent cette décomposition et doivent être mises en œuvre. La détermination et la prédiction de l'atténuation anélastique des sites reste également à développer et pourrait bénéficier de ces méthodes.

L'inversion des propriétés des ondes de surface a besoin de développements car elle nécessite une grande part d'interprétation (et donc d'expérience) de la part de l'utilisateur. Dans la résolution du problème direct, les paramètres peuvent se compenser pour donner les mêmes propriétés des ondes de surface (non-unicité de la solution). Les incertitudes lors de cette inversion sont liées, d'une part, aux incertitudes sur les propriétés des ondes de surface, mais aussi et surtout aux choix de la paramétrisation du problème. L'incertitude sur les courbes de dispersion est facile à caractériser. En revanche, l'utilisation de la courbe des rapports spectraux H/V pour représenter l'ellipticité des ondes de Rayleigh est souvent source d'incertitudes difficiles à quantifier. Enfin, contrairement à ce qui est affirmé dans Garofalo *et al.* (2016b), la façon de paramétrer les couches supérieures et inférieures, au-delà des limites de résolution classiques, a un effet sur les résultats de l'inversion. Ces couches doivent être prises en compte même si le résultat de l'inversion montre que leurs propriétés sont peu ou pas contraintes. Une quantification objective des incertitudes devra donc pouvoir être proposée dans le futur.

Si la modélisation numérique se développe rapidement, elle souffre toujours de deux limitations majeures : 1) son coût si l'on veut modéliser de grandes structures géologiques avec une maille suffisamment fine pour atteindre des fréquences qui intéressent la sismologie de l'ingénieur (1-10 Hz) ; 2) le besoin en données d'entrée pour ces grands domaines d'étude, la variation en profondeur tout comme leur variabilité latérale. Dans Michel *et al.* (2014a), nous avons montré que de nombreux sites avaient un comportement 1D pour lequel de tels simulations complexes sont inutiles. Nos travaux permettent de détecter les structures qui mériteraient d'être étudiées à l'aide de modèles 2D/3D. A part la vallée du Rhône qui offre l'exemple le plus clair de résonance 2D en Suisse et qui a fait l'objet de nombreuses études (p. ex. Roten *et al.*, 2008), ces phénomènes ont été observés dans la vallée du Rhin en amont du lac de Constance, la vallée de l'Aar et dans quelques structures de plus petite taille comme des vallées alpines (vallée de la Vispa à St-Nicolas VS) ou des cônes alluviaux (Buchs-Altendorf SG). Des études plus avancées sont envisagées sur ces sites.

Parmi les méthodes d'analyse de la résonance 2D/3D, nous avons proposé d'utiliser les techniques d'analyse modale employées en général pour les structures de génie civil (voir partie 2.3) pour les bassins sédimentaires dans Poggi *et al.* (2015). La technique employée permet de déterminer de manière précise les fréquences de résonance du bassin, les déformées modales associées, ainsi que l'amortissement. Les déformées permettent d'une part de relier les fréquences de résonance aux modes de propagations des ondes dans les bassins mais elles sont aussi le reflet de la géométrie et des propriétés de la structure. Une inversion de ces propriétés peut donc être envisagée. Enfin, l'amortissement pourrait être utilisé afin de remonter à un modèle d'atténuation anélastique dans la structure.

Enfin, le comportement non-linéaire des sols, pas abordé dans ce document, est critique dans certaines conditions de site. La collecte des paramètres nécessaires à sa modélisation reste à développer, tant en quantité de mesures que dans les types de paramètres mesurés. C'est en outre un aspect déterminant dans le calcul probabiliste du risque sismique : nous avons montré dans Michel *et al.* (2010c) et dans le projet « Risque sismique du bâti existant » de l'Office Fédéral de l'Environnement que le risque pour les bâtiments les plus résistants dépendait très largement de l'aléa aux longues périodes de retour pour lesquelles la non-linéarité du sol peut avoir un effet déterminant. Se pose également la question du mouvement du sol maximal possible. Cette problématique a été récemment confirmée par Silva *et al.* (2016) qui intègrent le risque jusqu'à un PGA de  $3.5 \text{ m/s}^2$ , ce qui est plus fort que la valeur maximale enregistrée dans le monde. Dans le cadre du renouvellement du réseau accélérométrique, cet aspect est donc également étudié.

J'ai constitué en Suisse avec mes collègues du groupe de sismologie de l'ingénieur, une base de données regroupant toutes les données sur les sites collectées depuis une vingtaine d'années. Une partie est accessible publiquement sur le site <http://stations.seismo.ethz.ch>. Elle sera à la base de toutes les études à venir en Suisse sur les mouvements forts, l'aléa, le risque et les effets induits.

# Chapitre 2

## Avancées dans la compréhension de la réponse des structures de génie civil aux séismes

### 2.1 Enregistrer les vibrations des structures

Milne (1888) fut le premier à mettre à profit les instruments sismologiques qu'il avait lui-même développés à l'Université de Tokyo afin d'enregistrer des séismes dans des bâtiments. Il note les caractéristiques du bâtiment et du sol de fondation, les amplitudes et les directions et en déduit des généralités en fonction du type de bâtiment et de l'étage d'enregistrement. Omori (1900) poursuit ses travaux en ajoutant la période des ondes enregistrées et indique que les murs « se comportent comme des pendules inversés » et plus tard que les bâtiments sont des « ressorts élastiques » (Omori, 1905). Dès 1894, il enregistre les vibrations du bâtiment du Département de Génie Civil de l'Université de Tokyo (Omori, 1900) puis du Musée d'Histoire Naturelle (Omori, 1903a) et de la banque Mitsubishi (Omori, 1905). Par ailleurs, il détermine les fréquences de résonance de cheminées (Omori, 1903b, 1918) et de ponts (Omori, 1902, 1903c, 1907b,a, 1910) excités par le vent et le passage des trains.

Hall (1912) développe à son tour à l'Université de Berkeley (Californie) un sismographe capable d'enregistrer ce que l'on peut désormais appeler les vibrations ambiantes des bâtiments. Il est persuadé que des mesures dans de nombreux bâtiments sont nécessaires pour déterminer leurs périodes de vibrations et présente lui-même cinq cas, principalement des bâtiments en briques. Derleth (1921) utilise son instrument pour enregistrer les vibrations d'une tour en construction entre 1914 et 1917 et échange avec Omori à ce sujet en 1918. Après cet échange, Omori semble montrer un regain d'intérêt pour les vibrations des bâtiments et il étudie à son tour l'évolution de la fréquence durant la construction d'une tour-relais (Omori, 1921b), les vibrations d'une tour en brique (Omori, 1921c) et d'une stupa bouddhiste (Omori, 1921a). Il est le premier à enregistrer les vibrations ambiantes d'un bâtiment avant et après un séisme et à en étudier les variations de fréquence (Omori, 1922). Aux Etats-Unis, les enregistrements dans 16 bâtiments de San Francisco sont réalisés avec l'instrument de Hall (Byerly *et al.*, 1931).

En Suisse, de Quervain (1922) fait la démonstration de son sismographe transportable en enregistrant les vibrations de l'église en béton armé de Fluntern (Zurich, Suisse) alors que les cloches sonnent, mais ne semble pas prêter d'intérêt aux vibrations des structures. Les « Mesures des mouvements d'un bâtiment dans des conditions tranquilles » par Ishimoto et Takahasi (1929) montrent l'étendue des connaissances de l'époque (en français!). Les auteurs insistent sur la connaissance des propriétés élastiques des bâtiments pour l'analyse sismique. Ils privilégient les enregistrements avec plusieurs capteurs afin de mieux comprendre le comportement des structures, comme le fait leur contemporain Saida. En 1930, Suyehiro et ses collaborateurs enregistrent (pour la première fois d'après Trifunac, 2009) un fort séisme à la base et sur le toit de trois bâtiments de Tokyo.

Carder (1936a,c) mène entre 1934 et 1936 une campagne de mesures pour l'U.S. Coast and Geodetic Survey dans 336 bâtiments de Californie et 7 du Montana. Dans ce dernier état, il s'agit de structures ayant subi le séisme d'Helena de 1935 afin de mieux comprendre les dommages (Carder, 1936a). Dans le même programme, Carder (1936b) enregistre les vibrations de châteaux d'eau en acier et Carder (1937) celles de ponts. La première relation entre la période des bâtiments et leur hauteur est publiée (Sparks, 1935). Enfin, toujours dans le cadre du programme de l'U.S. Coast and Geodetic Survey, Blume (1935) met au point un excitateur pour forcer les vibrations des bâtiments.

Après la seconde guerre mondiale, les vibrations dans les structures sont à nouveau étudiées au Japon, notamment par Kanai (Kanai *et al.*, 1949; Kanai et Tanaka, 1951; Kanai et Yoshizawa, 1952) et aux États-Unis par Housner (Hudson *et al.*, 1952; Alford et Housner, 1953; Hudson, 1962; Housner et Brady, 1963). Ce dernier privilégie l'utilisation d'excitateurs. Pour plus de détails, le lecteur peut se reporter à Michel (2007).

Si le Japon a déployé tardivement son réseau accélérométrique permanent (section 1.1), il inclut dès l'origine en 1952 des instruments en structures. En 1965, on compte 33 bâtiments instrumentés (ERI, 1965). Aujourd'hui, le Building Research Institute (BRI) japonais exploite 74 réseaux de stations dans des bâtiments. En 1965, la ville de Los Angeles vote une loi obligeant tous les bâtiments de plus de 10 étages à être équipés d'au moins 3 accélérographes. Ainsi, 50 bâtiments instrumentés permettent l'enregistrement du séisme de San Fernando en 1971. En 1972 est lancé le California Strong Motion Instrumentation Program (CSMIP) dont le but est d'obtenir des enregistrements accélérométriques de séismes, notamment dans les structures. 200 stations sont installées dans des bâtiments, 27 dans des barrages et 66 sur des ponts en Californie. En parallèle, au niveau fédéral, l'USGS exploite aujourd'hui 94 réseaux en structure, 69 dans des barrages et 14 sur des ponts à travers le programme NSMP (<http://earthquake.usgs.gov/monitoring/nsmp/structures/>).

Depuis 1992, Taïwan possède également son programme d'enregistrement de mouvements forts en structures (CWB TSMIP) qui comporte aujourd'hui 58 réseaux en bâtiments. En Suisse, si l'on exclue les centrales nucléaires dont l'instrumentation a commencé en 1970 à Beznau, les premiers accélérographes ont été placés sur le barrage d'Emosson en 1975, avant même les installations en champ libre. Dans les années 1990, 5 barrages-voûtes ont été densément instrumentés (Emosson, Mauvoisin, Grande Dixence, Mattmark et Punt dal Gall), permettant des études internationales (p. ex. Darbre *et al.*, 2000; Chopra et Wang, 2010) mais n'ont pas bénéficié de renouvellement depuis lors. L'Italie a lancé son propre programme au début des années 2000 et compte aujourd'hui 127 bâtiments, 7 ponts et 1 barrage instrumentés (Dolce *et al.*, 2017). En France, le programme NBAP du RAP-RESIF, lancé en 2004, comporte 5 bâtiments instrumentés : l'Hôtel de Ville de Grenoble (Michel *et al.*, 2010a), la Tour Ophite de Lourdes, la tour de la préfecture de Nice, le Centre de Découverte des Sciences de la Terre en Martinique (Guéguen, 2012) et le collège de Basse-Pointe en Martinique. En Nouvelle-Zélande, le programme BIP du réseau GeoNet a instrumenté 11 bâtiments et 3 ponts depuis 2007. D'autres pays possèdent des stations accélérométriques permanentes en bâtiments comme le Chili, le Mexique, la

Grèce, la Turquie, la Roumanie, la Moldavie, la Macédoine ou encore la Chine et la Corée du Sud.

En outre, il est de plus en plus aisé de réaliser des instrumentations temporaires de structures afin d'analyser leur vibrations ambiantes : capteurs de plus en plus petits, synchronisation sans fils, etc. Par ailleurs, d'autres techniques voient le jour comme la vibrométrie LASER à longue distance qui pourrait permettre d'acquérir les vibrations de nombreux bâtiments en limitant les déplacements et sans devoir pénétrer dans les structures (Guéguen *et al.*, 2010; Valla *et al.*, 2015).

## 2.2 Prédire le mouvement des structures sous séisme : Problématique

Les enregistrements en structures ont permis de comprendre les paramètres essentiels menant aux dommages dans les bâtiments lors de tremblements de terre. Ils ont permis de proposer des modèles reproduisant le comportement des structures et leurs dommages.

Reprenons l'équation du mouvement pour le déplacement relatif d'un système à un degré de liberté  $x$  avec une masse  $M$ , soumis à une accélération du sol  $\ddot{x}_g(t)$  :

$$M\ddot{x} + R(x, x_g) + F_s(x) = -M\ddot{x}_g$$

avec  $M\ddot{x}$  la force d'inertie,  $R$  la force d'amortissement,  $F_s$  la force de rappel et  $M\ddot{x}_g$  la sollicitation. La réponse de la structure dépend de sa géométrie et des conditions aux limites, des pertes d'énergie du système ( $R$ ) et de la relation entre la force de rappel ( $F_s$ ) et le déplacement (donc de la rigidité si l'on se place dans un contexte linéaire). Tous ces éléments peuvent présenter des difficultés lors de leur estimation : les conditions aux limites peuvent être complexes (interaction sol-structure, appuis élastomères pour des ponts, appuis des barrages-voûtes sur les rives), la géométrie du bâti existant peut être incertaine, la rigidité de certains matériaux peut être inconnue *a priori* (p. ex. la maçonnerie), la non-linéarité de la relation force-déformation peut être complexe (p. ex. pour le béton armé), les pertes d'énergie sont généralement inconnues et prises en compte de manière empirique. La Fig. 2.1 montre la prédiction à l'aveugle des déplacements et des accélérations d'un élément de structure (géométrie simple et connue, matériaux connus) testé sur une table vibrante par le *Pacific Earthquake Engineering Research Center* (PEER) et le *Network for Earthquake Engineering Simulation* (NEES). Même pour les plus faibles séismes, la variabilité des prédictions est d'environ un ordre de grandeur ce qui montre qu'il existe une marge de progression dans la modélisation et les enregistrements de vibrations ont un rôle à jouer dans ce processus. En effet, ils constituent des mesures *in situ* qui permettent, en théorie, de réduire les incertitudes de la modélisation.

L'enjeu des enregistrements est donc d'améliorer ces modèles de prédiction du comportement sous séisme, de leur fournir des paramètres physiques d'entrée, voire de les suppléer quand la physique ne permet pas d'expliquer les observations (modèles empiriques). A ces objectifs de prédiction s'ajoute le suivi de l'état des structures dans le temps (*Structural Health Monitoring*) qui doit permettre de déterminer leur sécurité à tout instant et de planifier leur entretien. Les parties qui suivent présentent les avancées réalisées pour comprendre et prédire le comportement linéaire puis le comportement non-linéaire des structures.



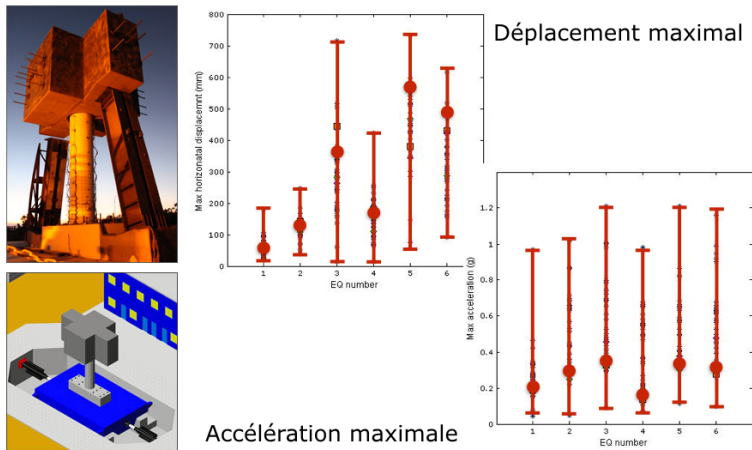


**Figure 2.1** – Résultats d’une prédiction à l’aveugle NEES/PEER en 2010 (41 participants). À gauche : structure modélisée et testée en taille réelle ; à droite : prédiction des participants (barres d’erreurs en rouge) et valeurs mesurées (points rouges) pour les 6 séismes testés, en déplacement (en haut) et en accélération (en bas). D’après PEER (2010).

## 2.3 Comprendre le comportement linéaire des structures

### 2.3.1 Comportement des bâtiments et point de départ linéaire pour l’analyse de vulnérabilité sismique

L’objectif de ma thèse de doctorat était de mieux comprendre le comportement linéaire des structures de génie civil, notamment des bâtiments, pour aider à l’estimation de leur vulnérabilité sismique à l’aide d’enregistrements de leurs vibrations (Michel, 2007). La grande quantité de données collectées dans des bâtiments de la ville de Grenoble ont notamment permis d’exposer les caractéristiques du bâti typique, en béton et en maçonnerie (Michel *et al.*, 2010b, 2012). Nous avons proposé un modèle de comportement sous séisme fondé sur les enregistrements de vibrations ambiantes (Michel *et al.*, 2008). L’Hôtel de Ville de Grenoble, le premier bâtiment instrumenté en France par le RAP-RESIF a permis de valider ce modèle, grâce à une étude sous vibrations ambiantes et séismes, en collaboration avec des chercheurs en dynamique des structures qui ont proposé un modèle dynamique non-linéaire de la structure reproduisant en grande partie les observations (Michel *et al.*, 2010a). À partir de ce modèle, une nouvelle méthode permettant de prédire les dommages sismiques légers, donc de caractériser la vulnérabilité sismique, a été proposée et mise en œuvre pour la ville de Grenoble (Michel *et al.*, 2012). Un scénario réaliste d’un séisme de magnitude 5.5 à 15 km a été simulé par fonctions de Green empiriques et la probabilité de dommage au moins léger a été estimée pour toute la ville. La répartition des dégâts est plus homogène qu’attendue (probabilité de dommages de 40% en moyenne) à cause des effets de site qui ont tendance à augmenter la demande sismique pour les bâtiments en béton armé pourtant moins vulnérables. Nous avons également suivi cette méthode pour analyser des bâtiments en béton armé (coffrage tunnel, sans contreventement longitudinal) en Guadeloupe (Michel et Guéguen, 2008). Nous avons estimé la probabilité de dommage au moins léger pour les séismes enregistrés à Pointe-à-Pitre dans les années précédentes (pas de dommage, comme observé). Nous avons aussi prédit la probabilité de dommage au moins léger pour des sollicitations correspondant à une période de retour de 475 ans : la direction longitudinale de ces structures a le plus souvent près de 50% de chance de subir des dommages, alors qu’il est peu probable que la direction transversale soit touchée.

L’étude des vibrations ambiantes et du comportement sous séisme permet également de mieux comprendre la torsion dans les structures. La torsion autour de l’axe vertical est le troisième degré de liberté évident pour les bâtiments, après la flexion dans les directions horizontales. Le mode fondamental de torsion apparaît dans les bâtiments suffisamment réguliers à une fréquence légèrement supérieure aux modes de flexion (Michel *et al.*, 2010a). Son amplitude relative est souvent notable, ce qui montre

qu'il est bien activé par les vibrations ambiantes. En revanche, si la structure est régulière, il disparaît sous séisme car la sollicitation de la fondation est homogène (Michel et Guéguen, 2010). Les structures irrégulières affichent, en revanche, des modes couplés flexion/torsion sous vibrations ambiantes : l'étude séparée des directions principales de la structure n'est alors plus possible. Un exemple extrême que nous avons étudié est le bâtiment du Burgerheim à Berne (Suisse, Fig. 2.2) (Oropeza *et al.*, 2010). Ce bâtiment de 15 étages en maçonnerie non renforcée (!) est très irrégulier en plan et les trois premières fréquences de résonance montrent un comportement intimement couplé.

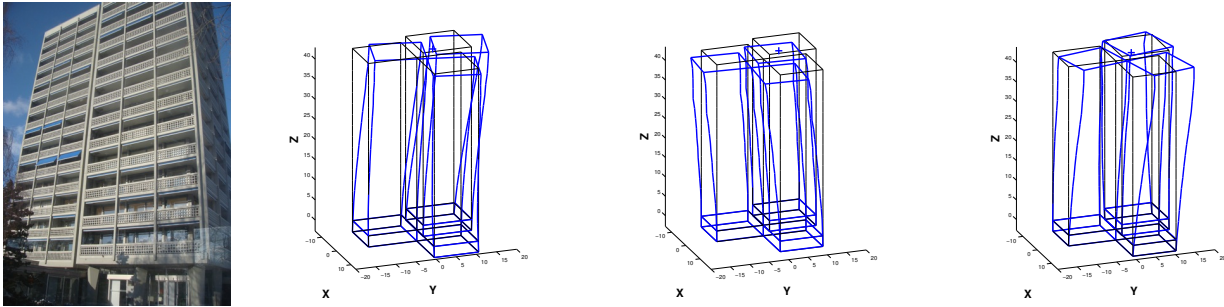


**Figure 2.2** – Analyse modale du Burgerheim à Berne (Suisse). Déformées modales des trois premiers modes de résonance à 1.22 (torsion et flexion couplées), 2.73 (flexion diagonale) et 2.21 Hz (torsion et flexion couplées). Voir aussi Oropeza *et al.* (2010).

### 2.3.2 Comportement des ponts et identification structurale sous vibrations ambiantes

Dans le cadre du doctorat de J.A. Goulet à l'EPFL, nous avons étudié la capacité des caractéristiques modales obtenues sous vibrations ambiantes à déterminer les propriétés physiques des ponts (identification structurale). Alors que les méthodes classiques dites de *Model Updating* tendent à minorer les incertitudes et en particulier les biais de modélisation, nous nous sommes concentrés sur cet aspect afin d'améliorer la robustesse de l'identification. Nous avons pour cela utilisé une recherche systématique dans l'espace des paramètres et combiné toutes les incertitudes (et leurs corrélations) liées à la modélisation afin de voir si l'observation des modes de vibrations permettait d'écarter certaines hypothèses de modélisation à l'aide d'un test statistique (Goulet *et al.*, 2013). Dans le cas du pont du Langensand à Lucerne (Suisse), nous avons montré que les modèles n'incluant pas de restriction partielle dans le fonctionnement des appuis du pont ne permettaient pas de reproduire les observations. Cette restriction partielle est due à la faible amplitude des vibrations ambiantes (pas de trafic) qui ne permet pas aux appuis élastomères de se déplacer librement, alors que des observations très différentes ont été réalisées sous trafic. C'est ce paramètre qui influence en premier lieu la fréquence du mode fondamental du pont. Alors que le second mode permet de rejeter certaines combinaisons de paramètres physiques du pont, les modes supérieurs n'apportent pas d'information supplémentaire sur les paramètres étudiés. Il faut noter que seules les fréquences de résonance ont été prises en compte. A cause des incertitudes du modèle, il n'est donc pas possible de déterminer plus précisément qu'un expert la rigidité des matériaux constitutifs du pont. En revanche, l'analyse a permis d'écarter des hypothèses de modélisation des conditions aux limites (appuis) et de mieux comprendre les mesures effectuées sous vibrations ambiantes. Une interprétation simpliste de ce cas aurait conduit à surestimer la rigidité de la structure de près de 20%.

Un autre résultat de cette étude est qu'il existe un manque de connaissance sur les incertitudes

épistémiques (liées aux hypothèses de modélisation) dans les modèles de génie civil. C'est pourquoi dans Goulet *et al.* (2014), nous avons étudié l'effet de ces hypothèses sur la modélisation d'un pont et quantifié ces incertitudes épistémiques. Nous avons montré que ces incertitudes induisaient souvent des biais systématiques pour certains paramètres précis et non une variabilité. Pour éviter ces biais, il est plus approprié de comparer des paramètres « globaux » de la structure (p. ex. les fréquences de résonance) que des paramètres locaux comme la déformation en un point. Nous avons appliqué la méthode développée dans l'article précédent à un pont situé entre les villes de Grand-Mère et St-Georges au Québec (Canada). Dans ce cas, une plus grande influence des propriétés mécaniques a été notée, certains modes précis ayant une influence plus forte sur un paramètre particulier comme le module d'Young du béton par exemple.

## 2.4 Comprendre le comportement non-linéaire des structures

Si déterminer le comportement linéaire des structures est un préalable à l'analyse sismique, leur étude sous mouvement fort nécessite de s'intéresser à leur comportement non-linéaire : alors que, en théorie, sous mouvement faible, forces et déformations sont proportionnelles, c'est-à-dire la rigidité est constante (loi de Hooke), les oscillations plus fortes conduisent à faire baisser la rigidité apparente (en particulier à cause de la fissuration) et à modifier la relation force/déformation. Au delà de la limite élastique, c'est la déformation (le déplacement) qui devient le paramètre déterminant pour l'état de la structure et donc son endommagement. Par le passé, de nombreux essais en laboratoire ont permis de mieux comprendre cette relation force/déformation et proposer des modèles de comportement pour les différents matériaux (p. ex. Schwab et Lestuzzi, 2007). Tous ces modèles présentent une première partie linéaire jusqu'à la limite élastique de la structure et dont la pente est proportionnelle au carré de la période fondamentale de résonance. Dans ces modèles, la rigidité, et donc la fréquence de résonance, ne peut que diminuer.

Dans Michel et Guéguen (2010), nous avons proposé une méthode d'analyse temps-fréquence permettant de suivre la variation de la fréquence de résonance sous séisme. Elle a notamment permis d'observer finement la chute de fréquence de la Millikan Library à Pasadena (Californie, Fig. 2.3) lors du séisme de San Fernando en 1971 au cours duquel elle a été modérément endommagée. Les enregistrements de l'hôtel de ville de Grenoble ont montré que la plus grande partie des variations observées ainsi n'étaient qu'apparentes et ne reflétaient pas l'état de la structure. En revanche, dans Michel *et al.* (2010a) à l'aide d'un modèle de signal auto-régressif, nous avons pu observer les faibles variations transitoires de sa fréquence de résonance à des niveaux de déformation bien inférieurs à la limite élastique des matériaux constituant la structure (2% de variation à un niveau de déformation 10 fois plus faible que la limite élastique en traction du béton). L'explication la plus probable pour ces variations à faible déformation est l'effet de l'interaction sol-structure, bien que dans ce cas précis elle n'ait pas encore été prouvée (voir la partie 2.4.1).

Les enregistrements sous vibrations ambiantes permettent de mesurer la rigidité « réelle » des structures, y compris celle de leur fondation et des éléments non-structuraux. Ces derniers ont soit une influence négligeable (cloisons légères etc.), soit doivent être pris en compte dans l'analyse sismique car ils modifient le comportement de la structure (p. ex. remplissages en maçonnerie ou éléments de façade, Hans *et al.*, 2005). S'ils s'endommagent plus rapidement que la structure porteuse, ils ne peuvent néanmoins pas être ignorés même à des niveaux de dommages avancés (p. ex. Hashemi et Mosalam,

2006).

Quoi qu'il en soit, la transition entre comportement linéaire et non-linéaire n'est pas abrupte comme dans la plupart des modèles de comportement et nécessite d'être quantifiée par les observations. En effet, la demande en déformation sous séisme dépend du carré de la période fondamentale, ses variations doivent donc être quantifiées pour déterminer les déformations que doit subir la structure et donc prédire son endommagement. C'est sur ces points que j'ai réalisé les avancées les plus significatives, détaillées dans les parties suivantes.



**Figure 2.3** – *Bâtiment de la Millikan Library sur le campus de Caltech, Pasadena, Californie. Ce bâtiment instrumenté depuis 1968 et équipé d'un excitateur à balourd à son dernier étage est la structure la plus étudiée dans la communauté (p. ex. Clinton et al., 2006) sans que toutes les observations ne puissent aujourd'hui encore être expliquées (problématique de l'interaction sol-structure). Il a subi des dommages lors du séisme de San Fernando en 1971.*

### 2.4.1 Chute de fréquence sous séisme (Michel *et al.*, 2011b)

Pour observer les variations des fréquences de résonance des bâtiments, on peut s'intéresser aux données des structures instrumentées de manière permanente (p. ex. Michel *et al.*, 2010a; Michel et Guéguen, 2010) ou aux données d'essais en laboratoire. C'est cette deuxième voie que nous avons explorée dans Michel *et al.* (2011b). Elle permet d'observer des niveaux de dommages jusqu'ici jamais atteints par des structures instrumentées existantes. Nous nous sommes plus particulièrement intéressés aux bâtiments en maçonnerie non renforcée, plus vulnérables que les structures en voiles en béton armé, qui constituent une grande partie du bâti en Suisse. Les essais étudiés ici ont été réalisés par l'EU-Centre à Ispra (Italie) dans le cadre du projet ESECMaSE qui s'intéressait à la vulnérabilité sismique du bâti en maçonnerie non renforcée, avec pour objectif de savoir si l'on pouvait toujours construire en maçonnerie non renforcée en zone sismique. Le manque de données sur le bâti en maçonnerie ne permettant pas de répondre à cette question, ce matériau est, en effet, le plus souvent délaissé quand des normes parasismiques sont mises en place. Cet essai a été réalisé en mode « pseudo-dynamique » à l'aide d'un mur de réaction. Les fréquences de résonance et les amortissements ont été estimés en fonction du temps au cours de plusieurs tests d'amplitude croissante.

Le résultat principal de cette étude est que la baisse de fréquence ne dépend pas de l'état d'endommagement initial : au cours des essais consécutifs, la structure s'endommage, la fréquence fondamentale sous vibrations ambiantes diminue, mais la baisse relative de fréquence lors de l'essai suivant reste la même et ne dépend que de la déformation. Cette baisse n'est cependant pas la même pour les deux spécimens testés, construits avec des matériaux différents. Nous avons donc pu quantifier la baisse relative de fréquence jusqu'à la limite élastique de la structure, définie ici par une déformation de 1 mm/m. Cette

chute de fréquence entre les vibrations ambiantes et la limite élastique est de  $2/3$  pour les matériaux testés. Si ce chiffre doit être déterminé également pour le béton armé, son ordre de grandeur ne devrait pas être différent. Comme nous l'avons discuté dans Michel *et al.* (2010b), les ingénieurs structures ne considèrent souvent pas les fréquences déterminées sous vibrations ambiantes car elles sont plus grandes que la fréquence élastique qui est constatée sous séisme. Grâce à notre estimation, il est possible de réconcilier enregistrements sous vibrations ambiantes et fréquences utiles pour l'ingénieur.

Dans Michel *et al.* (2011b), nous étudions aussi un essai en grandeur réelle : une villa en maçonnerie non renforcée située à Monthey (Suisse). Vouée à la démolition, cette structure a été testée à l'aide d'un vibreur de grandes dimensions par l'EMPA (Institut interdisciplinaire de recherche pour les sciences des matériaux et le développement de technologies, Dübendorf, Suisse) et les vibrations enregistrées par un réseau d'accéléromètres. Là encore, une baisse de fréquence directement liée à l'amplitude des vibrations a été mesurée. Cependant, cette baisse a lieu pour des déformations beaucoup plus faibles que dans l'essai précédent. Si nous soupçonnions dans cette étude un effet de l'interaction sol-structure, nous avons démontré cet effet dans Michel *et al.* (2011a). En utilisant la vitesse de propagation des ondes dans la structure, nous avons montré que la totalité de la baisse observée était due à l'interaction sol-structure (bascule de la fondation) alors que la structure elle-même ne changeait pas de propriétés dynamiques. En effet, l'EMPA a montré qu'elle n'avait subi aucun dommage.

Enfin, nous avons étudié les variations de l'amortissement qui ne se laissent pas bien expliquer par l'amplitude comme c'était le cas pour la fréquence. Ces résultats mériteraient cependant d'être approfondis.

## Quantification of fundamental frequency drop for unreinforced masonry buildings from dynamic tests

C. Michel<sup>1,4,\*</sup>, B. Zapico<sup>2,5</sup>, P. Lestuzzi<sup>1</sup>, F. J. Molina<sup>2</sup> and F. Weber<sup>3</sup>

<sup>1</sup>*Ecole Polytechnique Fédérale de Lausanne (EPFL), Applied Computing and Mechanics Laboratory (ENAC-IIC IMAC), Switzerland*

<sup>2</sup>*European Commission, Joint Research Center, IPSC, European Laboratory for Structural Assessment (ELSA), Italy*

<sup>3</sup>*Swiss Federal Laboratories for Materials Science and Technology, Structural Engineering Research Laboratory, Switzerland*

<sup>4</sup>*ETH Zürich, Swiss Seismological Service, Switzerland*

<sup>5</sup>*ARUP VB, Bridges Department, The Netherlands*

### SUMMARY

The knowledge of fundamental frequency and damping ratio of structures is of uppermost importance in earthquake engineering, especially to estimate the seismic demand. However, elastic and plastic frequency drops and damping variations make their estimation complex. This study quantifies and models the relative frequency drop affecting low-rise modern masonry buildings and discusses the damping variations based on two experimental data sets: Pseudo-dynamic tests at ELSA laboratory in the frame of the ESECMaSE project and *in situ* forced vibration tests by EMPA and EPFL. The relative structural frequency drop is shown to depend mainly on shaking amplitude, whereas the damping ratio variations could not be explained by the shaking amplitude only. Therefore, the absolute frequency value depends mostly on the frequency at low amplitude level, the amplitude of shaking and the construction material. The decrease in shape does not vary significantly with increasing damage. Hence, this study makes a link between structural dynamic properties, either under ambient vibrations or under strong motions, for low-rise modern masonry buildings. A value of 2/3 of the ambient vibration frequency is found to be relevant for the earthquake engineering assessment for this building type. However, the effect of soil–structure interaction that is shown to also affect these parameters has to be taken into account. Therefore, an analytical methodology is proposed to derive first the fixed-base frequency before using these results. Copyright © 2010 John Wiley & Sons, Ltd.

Received 17 September 2009; Revised 19 October 2010; Accepted 23 October 2010

**KEY WORDS:** unreinforced masonry; fundamental frequency; damping ratio; seismic demand; pseudo-dynamic tests; forced vibrations; ambient vibrations

### 1. INTRODUCTION

The dynamic behaviour of buildings suffers variations when the shaking amplitude increases. Their modal properties, i.e. resonance frequencies, damping ratios and modal shapes, are modified first in the elastic range and then in the plastic domain with increasing damage. The knowledge of these variations is a key issue in order to estimate the seismic demand and then the seismic performance of structures.

\*Correspondence to: C. Michel, ETHZ-SED, Sonneggstrasse 5, 8092 Zürich, Switzerland.

†E-mail: clotaire.michel@sed.ethz.ch

Many authors show a decrease in the fundamental frequency in reinforced concrete (RC) buildings [1–7] both in the elastic and plastic domains. The opening of cracks in the construction material produces a temporary or permanent decrease in stiffness and therefore a decrease in the fundamental frequency and possibly an increase in the damping ratio. The observed frequency may also be affected by other phenomena such as variation of the frequency content of the input motion [7], of temperatures [5] or of the soil–structure interaction (SSI) effects [8, 9]. SSI, i.e. differential motions (horizontal and rocking) between the building basement and the surrounding soil, affects the observed frequencies since it adds to the studied system an additional oscillating layer at the base. The observed frequencies are therefore lower than those of the fixed-base structure [10–12]. Isolating the fixed-base frequency from vibration recordings is however not straightforward. Therefore, approximate analytical results are used here to derive the fixed-base frequency following Wolf [10].

Contrary to RC buildings, the dynamic behaviour of masonry structures remains only partially known. Authors showed how their in-plane physical behaviour was difficult to predict [13–17]. The physical parameters of masonry walls are very variable depending on the brick material, the mortar and the construction techniques so that conventional force-based earthquake engineering methods hardly apply.

Moreover, ambient vibration recordings in such structures (e.g. [18]) help in understanding their dynamic behaviour at low excitation level. The experimental modal approach avoids the estimation of physical parameters such as stiffness [19, 20]. It gives directly the fundamental frequency that is the most important parameter to estimate the seismic demand, as stated by Housner and Brady [21]: ‘The natural period of vibration is the single most informative fact about the internal structure of buildings’. The objective of this paper is to contribute to filling the gap between modal properties at low level of excitation and modal properties at damaging states, relevant for earthquake engineering, for masonry buildings.

For that purpose, the variations of modal frequencies and damping ratio are studied as a function of motion amplitude for two experimental data sets on low-rise brick masonry buildings: two pseudo-dynamic (PsD) test series conducted in the ELSA laboratory (Italy) in the frame of the ESECMaSE project and three *in situ* forced vibration recording sequences performed by EMPA and EPFL in Monthey (Switzerland).

## 2. TESTS DATA

### 2.1. ELSA tests data

Within the activities of ESECMaSE project, two masonry house models were tested at the ELSA laboratory using PsD setups [22]. The project was concerned with the assessment of the seismic behaviour of modern unreinforced masonry (URM) structures.

The specimen was a model of a 2-storey terraced house with a rigid base and two RC floor slabs at scale 1:1 (Figures 1 and 2). Because of the presence of wide openings in the lateral walls, its response was basically unidirectional and it was adequately described by two degrees-of-freedom (DoFs) corresponding to the two floors. The specimen, with global dimensions of 5.30 m × 4.75 m and a height of 5.40 m, represented one symmetric half of a house with a width of 2 times 5.30 m. One of the models was made of calcium silicate bricks while the other used clay bricks. For the PsD tests, one horizontal actuator was attached at each side of each floor slab. Within the hypothesis of unidirectional response and in-plane infinitely rigid slabs, both actuators at each floor were controlled with the same displacement reference so that no torsion was allowed for the seismic tests. Each actuator was fed back with an optical encoder displacement transducer installed between the floor slab and an unloaded reference frame. They also gave the floor displacement recordings. At each step, once the computed displacement in each transducer is reached, the force in each actuator is measured by its load cell. Additional devices (relative displacement transducers and inclinometers) were installed on the elements likely to exhibit the most significant behaviour.



Figure 1. Picture of the ELSA test specimens.

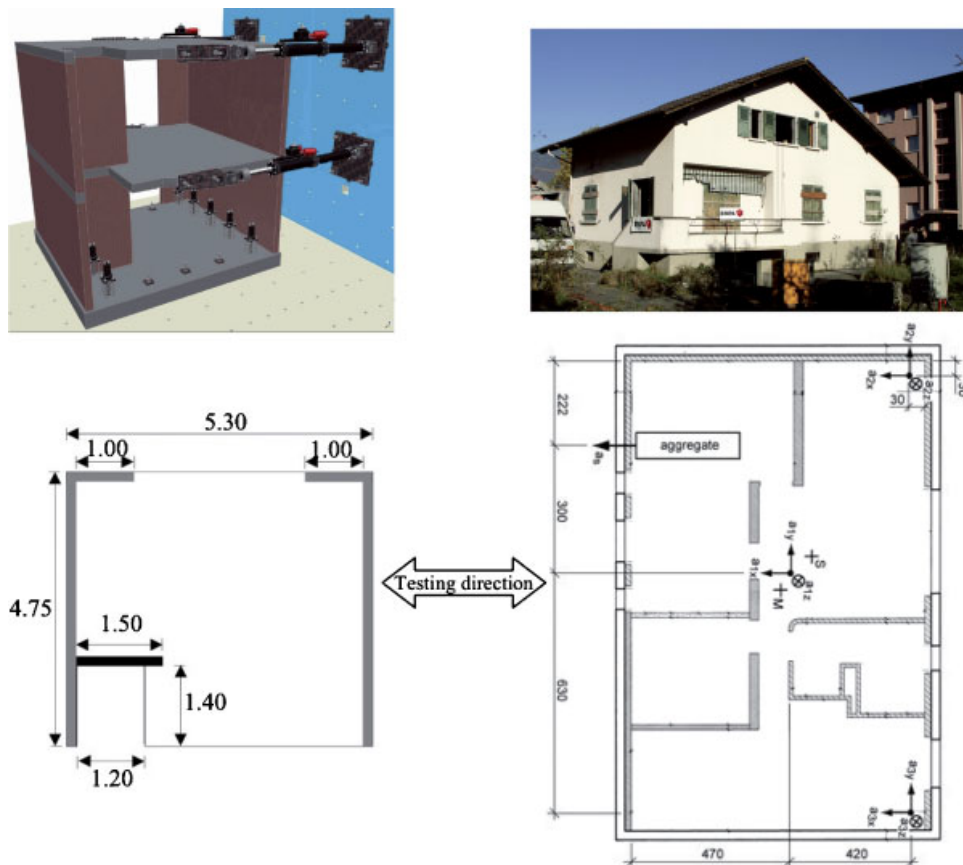


Figure 2. Structure subjected to PsD tests in the ELSA laboratory (left) and Monthey house, Switzerland, subjected to forced vibration tests by EMPA and EPFL (right). Adapted from [22, 23].

The specimens were subjected to an artificial accelerogram for increasing intensities ( $2\%g$ ,  $4\%g$ , ...), and the testing program was stopped just before the failure ( $20\%g$  for the calcium silicate specimen and  $22\%g$  for the clay one). The serviceability limit state, i.e. the occurrence of the first large crack, was reached after the fifth test ( $10\%g$ ) in both prototypes. They remained under the ultimate limit state, i.e. near collapse, until a load intensity of  $16\%g$ . Tests with a higher intensity should not reflect completely the actual behaviour of the structure.



## 2.2. EMPA-EPFL tests

The study building is a single-family detached house built in the 1970s in Monthey (Valais, Switzerland) (Figure 2). The load-bearing system is made of concrete block masonry walls. A rigid diaphragm is ensured by RC beam floors. The building is founded with an RC shallow slab on the soft Rhone sediments. Contrary to the first experiment, SSI is likely to happen in such a structure, especially foundation rocking.

As the building had to be demolished, the Ecole Polytechnique Fédérale de Lausanne (EPFL) and the Swiss Federal Laboratories for Materials Testing and Research (EMPA) launched an ambient and forced vibration test program to monitor the increasing damage induced by a servo-hydraulic shaker. This study has similarities with the one presented by De Sortis *et al.* [24]. The shaker of 32 kN maximum force was placed on the first floor in order to force the building into vibration in the transverse direction (Figure 2) [23]. The recording setup was made of a uni-axial accelerometer for the input motion (acceleration of the shaker mass) and tri-axial accelerometers for the output motion placed at 5 points of the building: 3 on the first floor, one on the ground floor and 1 on the basement. A preliminary ambient vibration recording (AV5), followed by 2 sequences of tests (T2 and T3) with increasing shaker amplitude (5, 10, 15, 20, 30, 70 and 100%) with a flat spectrum between 2 and 12 Hz (white noise) and a final ambient vibration recording (AV6) have been analyzed here, whereas other tests exist [23]. Only the transverse fundamental frequency is studied here.

## 3. OBSERVATIONS AND ANALYSIS METHODS OF THE EXPERIMENTAL DATA

### 3.1. ELSA tests

During the first tests, at a low intensity, the main shear wall of both prototypes, parallel to the testing direction, showed a rocking behaviour. This gave rise to slight damage of the shear wall itself and to a higher demand on the adjacent wall. The inter-storey drift (I-S drift) remained under 0.2%.

The prototypes started step-wise cracking during the sixth test (12%g, I-S drift <0.5%). These cracks were stable, as they did not extend further through the bricks, but just along the joints. During the last experiments, 20 and 22%g (I-S drift <2.2%), the buildings were seriously damaged, mostly on the second floor. They evidenced diagonal step-wise cracking on the main shear walls and horizontal openings on the long walls.

The frequency and damping ratio in the PsD test were obtained by identifying a spatial model from the resulting values of forces and displacements [25]. This technique is based on the identification of a linear model in terms of stiffness and damping matrices of the structure using a short time window of the experimental response. Within this model, it is assumed that the measured restoring forces and the corresponding displacements and velocities are linked, for every discrete time  $n$  of the original accelerogram record, of the form

$$\mathbf{r}(n) = \mathbf{K}\mathbf{d}(n) + \mathbf{C}\mathbf{v}(n) + \mathbf{o} \quad (1)$$

where  $\mathbf{r}(n)$ ,  $\mathbf{d}(n)$  and  $\mathbf{v}(n)$  are the results of the test,  $\mathbf{K}$  and  $\mathbf{C}$  are unknown matrices of stiffness and damping and  $\mathbf{o}$  is an unknown vector of offset (residual) forces. For identification purposes, the model can be rewritten in the form

$$[\mathbf{d}^T(n) \ \mathbf{v}^T(n) \ 1] \begin{bmatrix} \mathbf{K}^T \\ \mathbf{C}^T \\ \mathbf{o}^T \end{bmatrix} = \mathbf{r}^T(n) \quad (2)$$

Once  $\mathbf{K}$ ,  $\mathbf{C}$  and  $\mathbf{o}$  have been estimated by a least-squares solution, the complex eigenfrequencies and mode shapes can be obtained by solving the generalized eigenvalue problem

$$\begin{bmatrix} \mathbf{C} & \mathbf{M} \\ \mathbf{M} & \mathbf{0} \end{bmatrix} \boldsymbol{\varphi} + \begin{bmatrix} \mathbf{K} & \mathbf{0} \\ \mathbf{0} & -\mathbf{M} \end{bmatrix} \boldsymbol{\varphi} = \mathbf{0} \quad (3)$$

where  $\mathbf{M}$  is the theoretical mass matrix. The complex conjugate eigenvalues can be expressed in the form

$$s_n, s_n^* = \omega_n(-\zeta_n \pm j\sqrt{1-\zeta_n^2}) \quad (4)$$

where  $\omega_n$  is the natural frequency and  $\zeta_n$  the damping ratio. The corresponding mode shape is also given by the first  $n_{\text{DOF}}$  rows of the associated eigenvector  $\boldsymbol{\varphi}_n$ .

Since this model assumes an invariant system, at any selected time instant, an identification has to be done based on a data time window. The duration of this window must be roughly equal to the period of the first mode, and it has to be centred around the considered time instant. The adopted time window has to be narrow enough so that the system does not change too much inside it, but, at the same time, it has to contain enough data to allow for the compensation of different existing data noises and nonlinearities. The selection of the most appropriate window length is done by trial and error.

For each window, the frequency value is associated with the maximum I-S drift of the preceding oscillation period. To compute the I-S drift, the initial displacements were first removed.

### 3.2. EMPA-EPFL tests

In the EMPA-EPFL tests, the I-S drifts were calculated by double integration of the accelerometric noise recordings. A Butterworth filter between 4.5 and 30 Hz was applied before the integration since the noise level of the accelerometers at low frequency was high. Between AV5 and AV6, they reached  $6.3 \times 10^{-5}$  (during sinus tests not detailed here), which stays below the concrete limit tensile strain (approximately  $10^{-4}$ ) and therefore induced *a priori* no damage. These tests are therefore useful to study the elastic frequency drop but not the plastic one.

As the input loading was available and theoretically white noise, input–output as well as output-only modal analysis method can be performed. Among the numerous available methods, the Frequency Domain Decomposition method (FDD, [26]) and particularly its Enhanced version (EFDD, [27]) and the Matrix Pencil Method (MPM, [28]) have been used to obtain the experimental modal parameters (frequencies, modal shapes and damping). FDD method consists of a singular value decomposition of the power spectral density matrices, i.e. the Fourier transform of the cross-correlation between all recordings. The system resonance frequencies are found in the peaks of the first and possibly the following singular values and the modal shapes on the corresponding singular vectors. In the EFDD method, the parts of the singular values corresponding to the identified modes are extracted by comparing the singular vector of each point with the one at the peak. These density functions are zero-padded and turned into the time domain to derive the impulse response function. The damping ratio and a more precise frequency value are then found using the classical logarithmic decrement method. The forward–backward MPM method is a high-resolution method to estimate spectra and therefore resonance frequencies. It performs better than the Fourier transform in noisy signals [28]. Only part of the results is displayed in this paper, for more details, see [23].

## 4. DEPENDENCY OF FREQUENCY ON AMPLITUDE

As shown by other authors in RC structures [1–6], it is found that the resonance frequencies decrease with increasing amplitudes in both forced-vibration and laboratory tests. For the first ELSA tests as well as for the EMPA-EPFL tests, this decrease remains elastic because the frequency at the end of the test is the initial frequency. This nonlinear elastic behaviour is due to the opening

of preexisting cracks in the load-bearing system that temporarily decreases the apparent stiffness of the building. The non-structural elements that are rigidly connected to the structure in the case of the EMPA-EPFL tests also contribute to the stiffness but since they are not damaged, it seems that they cannot explain the observed non-linearity. However, from the 8%g ELSA test, the frequency decreases permanently because of the increasing damage. The EMPA-EPFL house does not reach this level but for this real case, the damage of the predicted non-structural elements may imply a more rapid frequency decrease. Nevertheless, the amplitude of this effect is not known and may be negligible compared to the structural stiffness loss.

The objective of this study is to relate the frequency with the shaking amplitude in order to quantify the relative drop due to elastic and also plastic phenomena. The parameter chosen to represent this amplitude is the maximum I-S drift. For ELSA data, the frequency is available at many time steps, whereas only one frequency value for each EMPA-EPFL test has been calculated. In ELSA tests each frequency value is associated with the maximum I-S drift of the preceding oscillation period, which varies much during the test, whereas, in the EMPA-EPFL tests, the value is associated with the maximum I-S drift of the whole test. It does not take the steady state of the process into account.

In order to study the relative frequency drop, all frequencies have been normalized by the low vibration level frequency of each test  $f_0$ , or the ambient vibration frequency when it was available (EMPA-EPFL data). The parameter in ordinate is therefore the relative or normalized frequency and gives directly the relative frequency drop during each test. All the tests are therefore considered as different buildings with different initial frequencies (initial damage).

#### 4.1. ELSA tests

The shape of relative frequency as a function of I-S drift appears to be similar from one test to another. At very low amplitudes, until an I-S drift value  $D_0$ , the relative frequency is 1, i.e. the frequency remains constant equal to  $f_0$ , then it starts to decrease slowly with a slope  $a_1$  and finally, a second decrease with a greater slope  $a_2$  occurs. A linear tendency in three distinct parts appears in logarithmic scale following the model:

$$\begin{aligned} D \leq D_0, & \quad \frac{f}{f_0} = 1 \\ D_0 < D \leq D_1, & \quad \frac{f}{f_0} = 1 - a_1 \log\left(\frac{D}{D_0}\right) \\ D_1 < D, & \quad \frac{f}{f_0} = \left(1 - a_1 \log\left(\frac{D_1}{D_0}\right)\right) \left(1 - a_2 \log\left(\frac{D}{D_1}\right)\right) \end{aligned} \quad (5)$$

with  $D$  being the I-S drift and  $f$  the frequency. The  $f_0$  value is uncertain for ELSA data because for the larger tests only a few data points are available at low drifts. The estimated value for each test can be found in Table I.

It is of particular importance to remark that the shape of the frequency drop does not depend much on the initial damage state, which justified the normalization. The frequency decrease is exponential and therefore very fast. The logarithmic scale should not be misinterpreted: the scatter exists from one test to another and within every single test, but the general shape remains surprisingly the same. In other words, the I-S drift explains well the variance of the frequency, even though some unexplained variance remains. This residual variance may be due to plastic phenomena and identification errors. It should be emphasized that the parts of signals where cracks are created are

Table I. Initial frequency value  $f_0$  for each ELSA test estimated from the identification results.

Tests (%g)	0.02	0.04	0.06	0.08	0.10	0.12	0.14	0.16	0.18	0.20	0.22
Clay (Hz)	6.1	5.9	5.7	5.5	5.2	5.0	4.45	4.1	4.0	3.6	3.1
Calcium silicate (Hz)	6.3	6.2	6.25	6.0	5.8	5.6	4.3	4.45	4.15	3.4	—

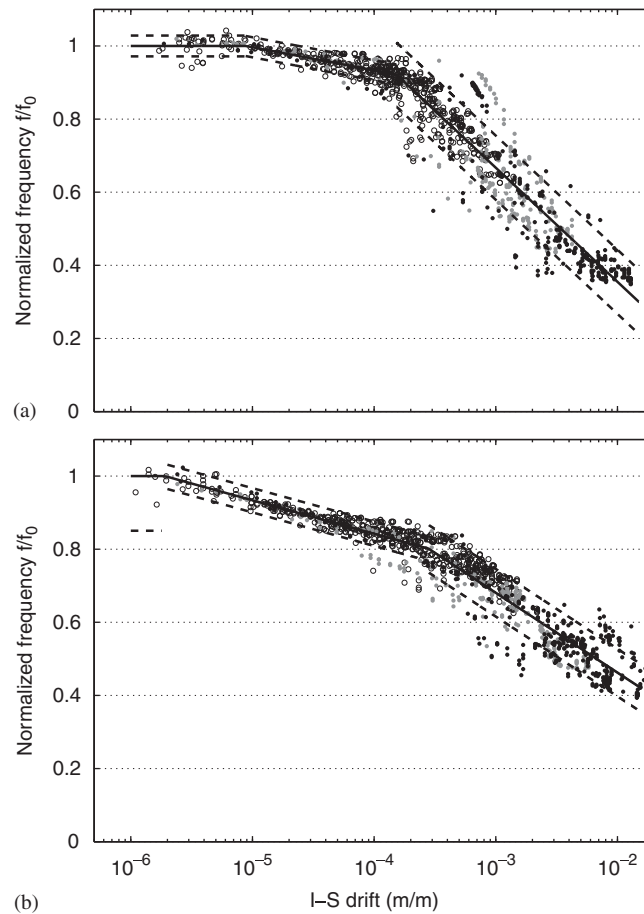


Figure 3. Frequency versus amplitude normalized by the initial frequency from ELSA tests on calcium silicate (a) and clay (b) masonry structures. White dots: tests 2–10%g, grey dots: tests 12–14%g and black dots: tests after 16%g. Tri-linear fit of this data set (solid line) with 80% confidence interval (dashed lines).

considered together with parts where existing cracks are opening or closing. Attempts to separate these parts did not lead to a significant reduction of variance.

The best  $D_0$ ,  $D_1$ ,  $a_1$  and  $a_2$  for all ELSA tests merged together (Figure 3) were fitted using a least-square objective function and the PGSL algorithm [29]. The results of the regression as well as the 80% confidence intervals are displayed in Figure 3. The parameter values of this model do not change much from one test to another. Looking more in detail, the first slope  $a_1$  increases slightly with damage but the uncertainties due to the low number of points and the unexplained variance remain larger for the other parameters.

During the first part (I-S drift lower than  $D_0$  equal to  $8.7 \times 10^{-6}$  or  $1.8 \times 10^{-6}$ , for calcium silicate and clay, respectively, but poorly constrained), the frequency remains constant. We can consider this part as the ambient vibration range, but it is not well described by this data set because of the low number of samples in that range. After this point  $D_0$ , the frequency starts to decrease slowly, without apparent damage. The slope  $a_1$  varies from  $-0.027$  for calcium silicate to  $-0.040$  for clay. Dunand *et al.* [4] described this elastic decrease for RC buildings, with a maximum frequency drop of 25%. Here, the maximum elastic decrease is 8 (calcium silicate) to 20% (clay).

The major kink in the curve, at  $D_1$  equal to 0.015% (calcium silicate) and 0.028% (clay) occurs before the apparition of the major crack in the building during the 12%g test (Figure 3). This first damage drift is close to the concrete tensile strength (0.01%). It could be related to EMS

damage grade 1 [30], which is generally not considered because it does not imply retrofitting. Therefore,  $D_0$  can be seen as the I-S drift limit between the linear and the non-linear behaviour in the elastic range and  $D_1$  the I-S drift limit between the elastic and the plastic ranges. During the 12%g test, the serviceability limit, i.e. damage grade 3 EMS, is reached. It occurs therefore between 0.15 and 0.3% I-S drift for calcium silicate and between 0.2 and 0.5% I-S drift for clay, which is in accordance with the value 0.3% given by Calvi [31]. Contrary to the initial damage state, the construction material seems to influence much the ulterior frequency drop: the calcium silicate masonry with its corresponding mortar remains very linear until this first damage state, whereas the clay masonry has a more pronounced non-linear behaviour in its elastic range.

After this first damage state  $D_1$ , the frequency decreases more rapidly indicating the development of cracking in the masonry. The uncertainty increases as well, showing that the amplitude does not explain all the phenomena (hysteretic behaviour). This decrease does not show singular points that could indicate other damage steps: the damage process is continuous. The observations indicate that the ultimate drift (damage grade 4–5) occurs during the 16%g test, therefore 0.5% I-S drift which is the value given by Calvi [31]. The slope  $a_2$  becomes  $-0.135$  for calcium silicate and  $-0.095$  for clay. One can note that this shape should be simpler than for RC structures because of the absence of ductility provided by steel rebars [32]. However, the first part of the relationship may be somehow similar with not much different values for the elastic decrease and the first damage drift.

According to Figure 3, the ‘ultimate state’ at 0.5% I-S drift corresponds approximately to 50% relative frequency drop. However, the total frequency drop is approximately 80% at this stage and it is not clear whether this decrease could have been reached at one time, i.e. from the undamaged building to the collapse. This topic should be investigated in more in detail, but the authors are not fully convinced that the key issue of ultimate drift can be solved in the manner adopted in this paper since no plastic phenomena are modelled. Moreover, it should be emphasized that the suggested relationship is not able to predict the permanent stiffness loss because it cannot estimate the stiffness recovery, also depending on the hysteretic behaviour. The objective of this frequency decrease model is only to better estimate the seismic demand, and it allows determining whether the first damage grades are reached by analyzing earthquake recordings in structures.

#### 4.2. EMPA-EPFL forced vibration tests

The tests at the ELSA laboratory focussed on the structural aspect but it is also interesting to study a whole existing soil–structure system as tested by the EMPA-EPFL in Monthey (Figure 4). The results derived from *in situ* measurements are related to the whole soil–structure system. However, in the case of stiff structures like masonry structures on soft sediments such as in Monthey, SSI is likely to modify these results [10]. The effects of SSI on the dynamic properties of a linear system can be estimated analytically [10]. However, the non-linear effects are still challenging for the community.

As the I-S drift reached  $8.4 \times 10^{-6}$ , these tests, which remained elastic, can only be compared to the first two parts of the tri-linear relationship proposed above (Figure 3(a)). In order to obtain comparable results, the frequencies are normalized by the ambient vibration frequency AV5. Moreover, the building initial frequency did not change significantly between AV5 and AV6 tests ( $10.0 \pm 0.1$  Hz) according to the EFDD analysis, i.e. the building was not damaged by the two sequences of forced tests T2 and T3, as supposed, considering the low I-S drifts. The different tests and modal analysis methods give consistent results, however with some discrepancies due to estimation errors and other phenomena such as temperature variations. Figure 4 shows a similar decrease in shape compared to the bi-linear clay model proposed above, with the same derivative  $a_1$  values, around  $-0.037 \pm 0.008$ . The elastic decrease seems to start early for a drift  $D_0$  around  $0.5 \times 10^{-6}$  but the decrease is significant only after  $1 \times 10^{-6}$  (Figure 4), which is lower than the ELSA data for clay bricks and therefore the absolute values remain lower. One reason for these lower values is that the torsion mode is prominent in the noise forced test so that the maximum I-S drift in the structure occurs at the extremities of the building and not at the centre where it is estimated. The displacements at the extremities show, therefore, maximum values 40–60% greater

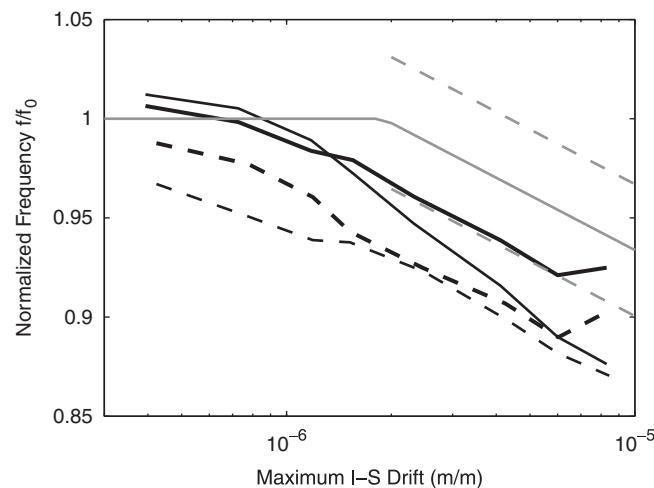


Figure 4. Normalized system frequency versus amplitude of EMPA-EPFL-forced vibration tests T2 (solid black lines) and T3 (dashed black lines) analysed using MPM (thick black lines) and EFDD (thin black lines) methods compared with the multi-linear relationship found in Figure 3(a) (grey solid and dashed lines).

than at the building centre. Moreover, the double integration of accelerometric recordings may not give very accurate results considering the quality of the sensors and may also be lower than these values. The influence of the SSI is not included in the ELSA tests (fixed-base) and therefore in the proposed frequency–amplitude relationship.

Thus, the discrepancy could also result from SSI occurring in the *in situ* tests. The non-linear evolution of SSI is however unknown and should be further investigated by experimental means. For example, Todorovska [33] proposed to use the wave travel time in structures obtained by deconvolving top and base signals to derive the fixed-base frequency. The applicability of this method to squat masonry structures should be further investigated.

## 5. ‘ELASTIC’ FUNDAMENTAL FREQUENCY

Earthquake engineering simplifies the computations needed to evaluate the ‘elastic fundamental frequency’ of structures. Ambient vibration recordings and analysis provide the real linear elastic fundamental frequency of structures but this value cannot be used for simplified computations because of the non-linear effects showed in the previous sections. Indeed, as the pure elasto-plastic model is often used, the engineers ‘elastic fundamental frequency’ corresponds to the frequency at the yield of the structure (Figure 5). Figure 5 shows a classical elasto-plastic model that represents roughly the elastic and plastic behaviour of structures and a curve  $A = \omega^2(D) * D$  with  $A$  the acceleration,  $D$  the displacement and  $\omega(D)$  the angular frequency depending on the displacement as proposed in Equation (5). This curve is closer to the real behaviour of the building in the elastic part but does not take plastic effects into account. By definition, these curves cross close to yield point in the elasto-plastic model. According to Calvi [31], this point occurs at around 0.1% I-S drift for masonry buildings. The frequency value at yield in Equation (5) gives therefore the frequency value needed for engineering computations as a function of the ambient vibration frequency. In the case of low-rise brick masonry buildings, at 0.1% I-S drift, a rate of  $67 \pm 9\%$  (calcium silicate) and  $68 \pm 6\%$  (clay) of the initial frequency is found. A straightforward value of  $2/3$  of the ambient vibration frequency may therefore be used as ‘elastic’ frequency for earthquake engineering computations for brick masonry structures. It corresponds to a stiffness reduction of approximately 50%, which is coherent with the effective stiffness generally used for this type of building. However, this value does not account for SSI effects.

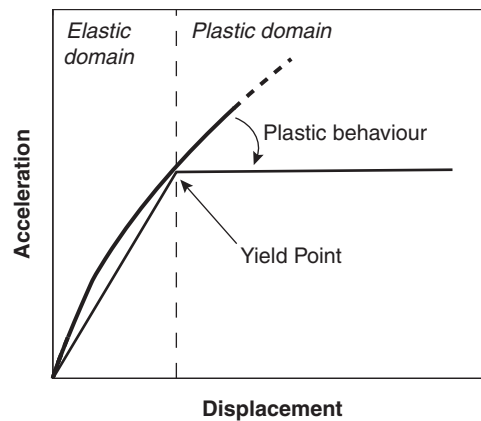


Figure 5. Acceleration–displacement diagram with a classical elasto-plastic model (thin line) and comparison with the proposed frequency–displacement relationship (thick line).

In order to practically use this value, one should therefore first evaluate the fixed-base frequency, i.e. without SSI. For that purpose, it is proposed to use Wolf [10] results about a single DoF system based on a circular foundation. In this simple formulation, the soil is modelled as a half space and no embedment of the foundation is accounted for. The ratio between the fixed-base frequency  $f_0$  and the frequency of the whole soil–structure system  $f_{\text{sys}}$  is computed as [10]:

$$\frac{f_{\text{sys}}}{f_0} = \sqrt{\frac{1}{1 + \frac{\bar{m}\bar{s}^2}{8} \left[ \frac{2-\nu}{\bar{h}^2} + 3(1-\nu) \right]}} \quad (6)$$

with  $\bar{s} = 2\pi f_0 h / V_s$ , the stiffness ratio,  $\bar{m} = m / \rho a^3$  the mass ratio,  $\bar{h} = h / a$  the slenderness ratio,  $f_0$  the fixed-base frequency,  $h$  the height of the structure,  $V_s$  the shear-wave velocity,  $m$  the equivalent mass of the structure,  $\rho$  the density of the ground and  $a$  the characteristic length of the foundation. The equivalent mass  $m$  for the single DoF system can be computed following [16] as  $m = \sum m_i \phi_i$  with  $m_i$  the mass of each floor and  $\phi_i$  the amplitude of the floor in the first modal shape, obtained using ambient vibration modal analysis or assuming a simple shape (e.g. triangular). Knowing the soil–structure system frequency  $f_{\text{sys}}$ , the equation becomes:

$$f_0 = f_{\text{sys}} \sqrt{\frac{1}{1 - \frac{\bar{m}}{8} \frac{4\pi^2 f_{\text{sys}}^2 h^2}{V_s^2} \left[ \frac{2-\nu}{\bar{h}^2} + 3(1-\nu) \right]}} \quad (7)$$

In the case of Monthey (EMPA-EPFL tests), a microzonation was performed in 2004 [34]. The uppermost layers of the site were considered to be torrential alluvial deposits made of loamy sandy gravels with an uncertain  $V_s$  evaluated in a range from 200 to 400 m/s [34]. This was confirmed after the destruction of the building, shortly after the tests [35]. Moreover, concerning the characteristics of these layers,  $\rho$  was 2.1 tons/m<sup>3</sup> and  $\nu = 0.25$ . Concerning the building properties,  $h$  is 5.02 m,  $a$  as 3.95 m (transverse direction) and  $f_{\text{sys}}$  under ambient vibration is 10 Hz. The equivalent mass  $m$ , obtained using the experimental modal shape that is very close to a triangular shape, with a storey mass of 107 tons, is 159 tons.

The fixed-base frequency under ambient vibrations ranges, therefore, between 12.1 Hz for a shear wave velocity of 400 m/s and goes to infinity for  $V_s$  close to 225 m/s. Lower velocity values are not possible according to this model. This divergence to infinity occurs when the pure rigid body motion is dominating the observed frequency. This case can be observed in the experimental modal shapes with at least two sensors at the ground floor and one at the top. In such a situation, it is not possible to infer the fixed-base frequency from the measurements.

In the present case, without a better knowledge of the soil properties, it is therefore only possible to give a lower bound of the fixed-base frequency. The frequency value that can be used to estimate the seismic demand is therefore two thirds of the resulting value, i.e. greater than or equal to 8 Hz.

This fixed-base frequency, inferred from the measured system frequency should not be considered as precise as a measurement, and is not relevant in case of very high SSI interaction effects, but it gives easily a value to be compared to numerical or analytical computations in order to validate or not modelling assumptions.

## 6. DEPENDENCY OF DAMPING RATIO ON AMPLITUDE

Even though the damping ratio is not so critical as the frequency is in the demand estimation, its influence is not negligible. However, as its origin has never been clearly stated, it is very difficult to model. Identified viscous equivalent damping ratio is plotted here with respect to the maximum I-S drift in the same way as frequency in the preceding paragraph (Figure 6). As many other studies [1, 36, 37], the ELSA data show a large scatter in damping ratio values either due to structural reasons or estimation errors (including negative values). It seems that the damping ratio remains constant for low to intermediate amplitude values (until 0.01% for calcium silicate and 0.04% for clay). For larger amplitudes, i.e. when the building is damaged, the average damping value seems to increase dramatically but the scatter also increases much. This is particularly true for the calcium silicate bricks for which the average value is approximately multiplied by 3 between 0.01 and 0.5% I-S drifts (from 2 to 6%). There is not enough data at low amplitudes to determine whether damping increases with drift. Contrary to what happens with the frequency, it is clear that the maximum I-S drift does not explain well the damping variations.

The EMPA-EPFL Monthey data indicate a slight continuous increase from approximately 5 to 6% with increasing amplitude (around 15% increase between  $10^{-6}$  and  $2 \times 10^{-5}$  drifts) (Figure 7). It should however be remarked that outliers due to estimation errors had to be removed showing that analysis methods are not always reliable. This damping increase may be either due to structural reasons or due to SSI.

## 7. CONCLUSIONS

The analysis of dynamic and PSDs on low-rise brick masonry buildings showed that the frequency evolution was an important phenomenon in their elastic and inelastic behaviour. This study shows that the initial frequency value and the vibration amplitude mainly explain the frequency variations and that the initial damage state did not significantly influence the shape of the frequency decrease. For the fixed-base PSD tests, the elastic frequency drop, i.e. without damage, shows a maximum value of 20%. The first damage (DG 1 EMS) occurs for an I-S drift between 0.015 and 0.028%, inducing a faster frequency decrease that is continuous until collapse. The comparison with a real structure tested *in situ* showed equivalent decrease in shape with some differences that may be due to SSI. Moreover, its effect may be more important at larger drifts.

The amplitude–frequency decay relationship is found to vary with the construction material, but not with the initial damage state. The proposed relationship, based on data from low-rise brick masonry may extend to all brick masonry structures but other relationships should be built for other construction materials, especially for reinforced concrete. The shape of an RC amplitude–frequency relationship is believed to be more complicated because of RC ductility but the first part should be somehow similar.

The major practical application of this work could be a way of converting ambient vibration frequencies into ‘elastic’ fundamental frequency needed for earthquake engineering by taking the frequency value at yield in the proposed amplitude–frequency relationship, i.e. two third of the ambient vibration frequency value for low-rise modern masonry structures on stiff soils. For structures on soft soils, a method based on Wolf [10] is proposed to first estimate the fixed-base frequency from the frequency values obtained under ambient vibrations before taking the two-third



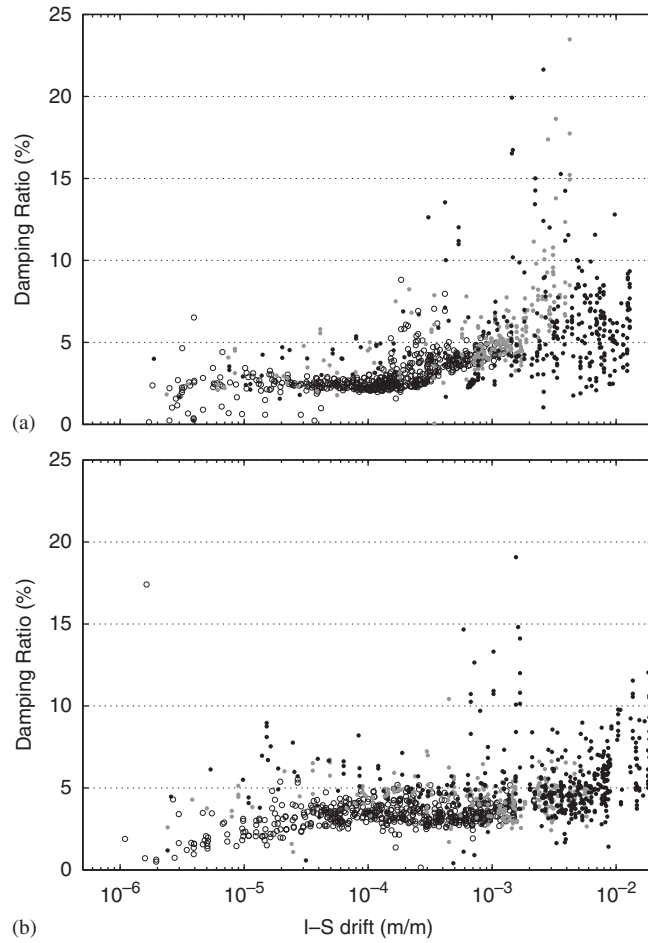


Figure 6. Damping ratio versus amplitude (dots) from all tests on ELSA clay (a) and calcium silicate (b) masonry structures. White dots: tests 2–10%g, grey dots: tests 12–14%g and black dots: tests after 16%g.

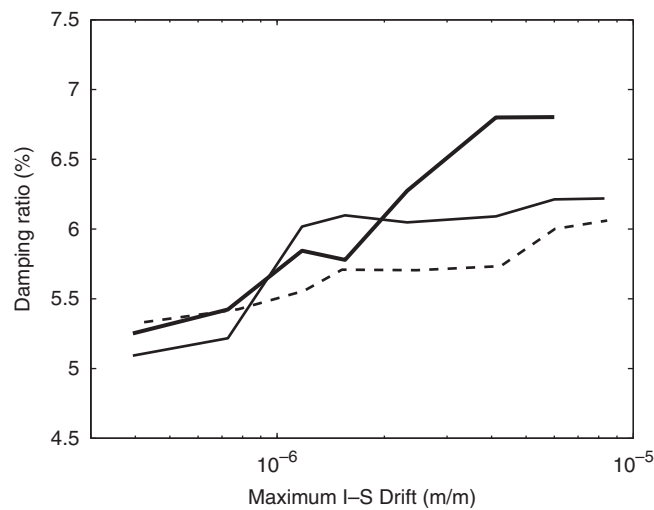


Figure 7. Damping ratio versus amplitude of EMPA-EPFL forced vibration tests T2 (solid black lines) and T3 (dashed black lines) analysed using MPM (thick black lines) and EFDD (thin black lines) methods. Outliers were removed.

value. In the real *in situ* study-case, SSI was found to have a significant impact on frequency values (at least 20% but with large uncertainties on the soil properties). In case of high SSI, when the structure is behaving as a rigid body, it is no more possible to infer the fixed-base frequency from the measurement. This case can be detected by using the experimental modal shapes.

Todorovska [33] proposed a method based on the travel times of waves in structures to estimate directly the fixed-base frequency from the recordings. This method may be used in future works to better estimate the influence of SSI on the proposed relationships using recordings.

The damping ratio suffers much scatter, often due to estimation errors. However, it seems to increase slightly until moderate damage occurs and dramatically after this damage grade. The SSI is believed to play a major role in the damping value variation and should be investigated in further studies.

#### ACKNOWLEDGEMENTS

The work presented in this paper was partially funded by the European Commission through the ESEC-MaSE project (n. COLL-CT-2003-500291), by the Foundation for Structural Dynamics and Earthquake Engineering (EMPA-EPFL tests) and by the Foundation of Swiss Cantonal Insurances (VKF). The authors also thank R. Peruzzi, Civil Engineer in Monthey, for his help in the design of EMPA-EPFL test. The authors thank the two reviewers for their major contribution in the improvement of the paper.

#### REFERENCES

1. Molina FJ, Gonzalez MP, Pegon P, Varum H, Pinto A. Frequency and damping evolution during experimental seismic response of civil engineering structures. *COST F3 Conference on System Identification and Structural Health Monitoring*, 2000.
2. Zembaty Z, Kowalski M, Pospisil S. Dynamic identification of a reinforced concrete frame in progressive states of damage. *Engineering Structures* 2006; **28**:668–681.
3. Calvi GM, Pinho R, Crowley H. State-of-the-knowledge on the period elongation of RC buildings during strong ground shaking. *The 1st European Conference of Earthquake Engineering and Seismology*, Geneva, Switzerland, vol. 1535, 2006.
4. Dunand F, Guéguen P, Bard PY, Rodgers J, Celebi M. Comparison of the dynamic parameters extracted from weak, moderate and strong building motion. *The 1st European Conference of Earthquake Engineering and Seismology*, Geneva, Switzerland, vol. 1021, 2006.
5. Clinton JF, Bradford SC, Heaton TH, Favela J. The observed wander of the natural frequencies in a structure. *Bulletin of the Seismological Society of America* 2006; **96**(1):237–257.
6. Lestuzzi P, Bachmann H. Displacement ductility and energy assessment from shaking table tests on RC structural walls. *Engineering Structures* 2007; **29**:1708–1721.
7. Michel C, Guéguen P. Time–frequency analysis of small frequency variations in civil engineering structures under weak and strong motions using a reassignment method. *Structural Health Monitoring* 2010; **9**(2):159–171.
8. Todorovska M, Al Rjoub Y. Effects of rainfall on soil–structure system frequency: examples based on poroelasticity and a comparison with full-scale measurements. *Soil Dynamics and Earthquake Engineering* 2006; **26**:708–717.
9. Todorovska M. Soil–structure system identification of Millikan library north–south response during four earthquakes (1970–2002): what caused the observed wandering of the system frequencies? *Bulletin of the Seismological Society of America* 2009; **99**(2A):626–635.
10. Wolf JP. *Dynamic Soil–Structure Interaction*. Prentice-Hall: Englewood Cliffs, NJ, 1985.
11. Todorovska M, Trifunac M. Impulse response analysis of the van nuys 7-storey hotel during 11 earthquakes and earthquake damage detection. *Structural Control and Health Monitoring* 2008; **15**:90–116.
12. Todorovska M, Trifunac M. Earthquake damage detection in the imperial county services building III: analysis of wave travel times via impulse response functions. *Soil Dynamics and Earthquake Engineering* 2008; **28**(1):387–404.
13. Magenes G, Calvi GM. In-plane seismic response of brick masonry walls. *Earthquake Engineering and Structural Dynamics* 1997; **26**:1091–1112.
14. Benedetti D, Carydis P, Pezzoli P. Shaking table tests on 24 masonry buildings. *Earthquake Engineering and Structural Dynamics* 1998; **26**:67–90.
15. Tomažević M. *Earthquake Resistant Design of Masonry Buildings*. Imperial College Press: London, 1999.
16. Lang K, Bachmann H. On the seismic vulnerability of existing buildings: a case study of the city of basel. *Earthquake Spectra* 2004; **20**(1):43–66.
17. Magenes G. Masonry building design in seismic areas: recent experiences and prospects from a European standpoints. *The 1st European Conference of Earthquake Engineering and Seismology*, Geneva, Switzerland, vol. K9, 2006.

18. Turek M, Thibert K, Ventura C, Kuan S. Ambient vibration testing of three unreinforced brick masonry buildings in Vancouver, Canada. *The 24th International Modal Analysis Conference (IMAC)*, St Louis, MO, 2006.
19. Michel C, Guéguen P, Bard PY. Dynamic parameters of structures extracted from ambient vibration measurements: an aid for the seismic vulnerability assessment of existing buildings in moderate seismic hazard regions. *Soil Dynamics and Earthquake Engineering* 2008; **28**(8):593–604.
20. Michel C, Guéguen P, El Arem S, Mazars J, Kotronis P. Full-scale dynamic response of an RC building under weak seismic motions using earthquake recordings, ambient vibrations and modelling. *Earthquake Engineering and Structural Dynamics* 2010; **39**(4):419–441.
21. Housner G, Brady AG. Natural periods of vibration of buildings. *Journal of Engineering Mechanics* 1963; **89**:31–65.
22. Anthoine A. Definition and design of the test specimen. Deliverable D 8.1 of enhanced safety and efficient construction of masonry structures in Europe (ESECMASE), Ispra, Italy, 2007.
23. Weber F, Huth O, Gsell D, Feltrin F, Lestuzzi P, Peruzzi P, Motavalli M. Forced Vibration Measurements of a One-Family House in Monthey, Switzerland. *The 1st European Conference of Earthquake Engineering and Seismology*, Geneva, Switzerland, vol. 60, 2006.
24. De Sortis A, Antonacci E, Vestroni F. Dynamic identification of a masonry building using forced vibration tests. *Engineering Structures* 2005; **27**:155–165.
25. Molina FJ, Magonette G, Pegon P, Zapico B. Monitoring damping in pseudo-dynamic tests. *Journal of Earthquake Engineering*, in press.
26. Brincker R, Zhang L, Andersen P. Modal identification of output only systems using frequency domain decomposition. *Smart Materials and Structures* 2001; **10**:441–445.
27. Brincker R, Ventura C, Andersen P. Damping estimation by frequency domain decomposition. *The 19th International Modal Analysis Conference (IMAC)*, Kissimmee, FL, 2001; 698–703.
28. Fernandez del Rio JE, Sarkar TK. Comparison between the matrix pencil method and the fourier transformation technique for high-resolution spectral estimation. *Journal of Digital Signal Processing* 1996; **6**:108–125.
29. Raphael B, Smith IFC. A direct stochastic algorithm for global search. *Journal of Applied Mathematics and Computation* 2003; **146**(2–3):729–758.
30. Grünthal G, Musson R, Schwartz J, Stucchi M. European Macroseismic Scale 1998. Cahiers du Centre Européen de Géodynamique et de Séismologie 1998; **15**, Luxembourg.
31. Calvi GM. A displacement-based approach for vulnerability evaluation of classes of buildings. *Journal of Earthquake Engineering* 1999; **3**(3):411–438.
32. Brun M, Reynouard J, Jezequel L. A simple shear wall model taking into account stiffness degradation. *Engineering Structures* 2003; **25**:1–9.
33. Todorovska M. Seismic interferometry of a soil–structure interaction model with coupled horizontal and rocking response. *Bulletin of the Seismological Society of America* 2009; **99**(2A):611–625.
34. Lacave C, Tissières P. Microzonage sismique spectral de la région de Monthey. Rapport 220.03, Résonance Ingénieurs-Conseils SA et Tissières SA pour le DTEE, Géologue cantonal du Valais, 2004, in French.
35. Peruzzi R. *Personal Communication*.
36. Celebi M. Comparison of damping in buildings under low amplitude and strong motions. *Journal of Wind Engineering and Industrial Aerodynamics* 1996; **59**:309–323.
37. Satake H, Yokota N. Evaluation of vibration properties of high-rise steel buildings using data of vibration tests and earthquake observations. *Journal of Wind Engineering and Industrial Aerodynamics* 1996; **59**:265–282.

### 2.4.2 Déplacement maximal sous séisme (Michel *et al.*, 2014b)

On a vu précédemment que les dégâts sismiques aux bâtiments sont directement liés à leur déformation. Le déplacement maximal du toit des bâtiments est donc un paramètre crucial pour les modèles d'analyse sismique, utilisés pour le dimensionnement de structures neuves et l'analyse de vulnérabilité du bâti existant, et donc pour le risque. Lorsqu'une structure s'endommage, et même avant comme on l'a vu dans la partie précédente, ses propriétés modales sont affectées et sa réponse diffère de la réponse d'un modèle gardant ses propriétés élastiques. Cependant, Veletsos et Newmark (1960) ont montré que le déplacement maximal de ces structures restait le même que celui du modèle élastique, à la condition que la structure élastique initiale soit suffisamment souple (fréquence de résonance inférieure à une certaine valeur, dépendant en particulier du spectre du séisme considéré). Cette règle, non intuitive, s'appelle la *règle des déplacements égaux*. Elle permet des calculs simples de la demande en analyse sismique.

De nombreux modèles ont été proposés pour les structures plus rigides (bâtiments de 3 étages ou moins d'après l'Eurocode 8, 6 étages ou moins d'après Michel *et al.*, 2010b, 2011b) en tentant de chercher un lien avec la réponse du modèle élastique, ceci afin d'éviter de mettre en œuvre un calcul dynamique, coûteux et difficile à réaliser. Ces méthodes sont donc statiques non-linéaires. Le paramètre explicatif utilisé le plus souvent est le facteur de réduction  $R$  qui est une mesure du « niveau de non-linéarité » atteint. On l'obtient par le rapport entre la réponse du modèle élastique (accélération ou déplacement) et la limite d'élasticité.

Ces méthodes dites « de linéarisation » sont passées en revue dans l'article suivant (Michel *et al.*, 2014b). Nous y montrons que les méthodes actuelles, en particulier celle utilisée dans l'Eurocode 8 pour le dimensionnement de structures neuves, peuvent sous-estimer fortement la réponse en déplacement pour les forts niveaux de non-linéarité. Nous invalidons également, comme d'autres auteurs avant nous, la règle dite des « énergies égales », bien qu'elle soit toujours utilisée dans certaines publications. Nous proposons une nouvelle méthode pour l'analyse sismique, avec une utilisation graphique possible. En revanche, cette méthode est conservatrice et ne peut donc pas être utilisée pour l'analyse du risque.

Afin d'évaluer ces différentes méthodes, nous avons comparé leurs résultats avec la réponse dynamique non-linéaire de modèles hystérétiques classiques. Ces modèles ont été soumis à des accélérogrammes synthétiques ajustés aux spectres de réponse des normes. Si ces signaux diffèrent des enregistrements réels, ils permettent en revanche de mieux comprendre le comportement des modèles étudiés.

En présentant les résultats dans le plan déplacement/période, notre étude montre l'importance critique de la valeur de la fréquence fondamentale élastique : les erreurs sur ce paramètre se payent au carré sur le calcul du déplacement maximal. Comme indiqué dans les parties précédentes, la fréquence fondamentale élastique des structures est donc un paramètre capital en analyse sismique, même lorsque l'on entre dans le domaine plastique.

## Simplified non-linear seismic displacement demand prediction for low period structures

Clotaire Michel · Pierino Lestuzzi ·  
Corinne Lacave

Received: 13 March 2013 / Accepted: 4 January 2014 / Published online: 28 January 2014  
© Springer Science+Business Media Dordrecht 2014

**Abstract** The prediction of non-linear seismic demand using linear elastic behavior for the determination of peak non-linear response is widely used for seismic design as well as for vulnerability assessment. Existing methods use either linear response based on initial period and damping ratio, eventually corrected with factors, or linear response based on increased equivalent period and damping ratio. Improvements to the original EC8 procedure for displacement demand prediction are proposed in this study. Both propositions may be graphically approximated, which is a significant advantage for practical application. A comparison with several other methods (equal displacement rule, EC8 procedure, secant stiffness and empirical equivalent period methods) is performed. The study is based on non-linear SDOF systems subjected to recorded earthquakes, modified to match design response spectra of different ground types, and focuses on the low frequency range that is of interest for most European buildings. All results are represented in the spectral displacement/fundamental period plane that highlights the predominant effect of the fundamental period on the displacement demand. This study shows that linearized methods perform well at low strength reduction factors but may strongly underestimate the displacement demand at strength reduction factors greater than 2. This underestimation is an important issue, especially for assessment of existing buildings, which are often related with low lateral strength. In such cases, the corresponding strength reduction factors are therefore much larger than 2. The new proposals significantly improve the reliability of displacement demand prediction for values of strength reduction factors greater than 2 compared to the original EC8 procedure. As a consequence, for the

---

C. Michel · P. Lestuzzi  
Applied Computing and Mechanics Laboratory (IMAC), Ecole Polytechnique  
Fédérale de Lausanne (EPFL), Lausanne, Switzerland

C. Michel (✉)  
Swiss Seismological Service (SED), Swiss Federal Institute of Technology  
of Zurich (ETHZ), Sonneggstrasse 5, 8092 Zurich, Switzerland  
e-mail: clotaire.michel@sed.ethz.ch

P. Lestuzzi · C. Lacave  
Résonance Ingénieurs-Conseils, Carouge, Switzerland

seismic assessment of existing structures, such as unreinforced masonry low-rise buildings, the current procedure of EC8 should be modified in order to provide accurate predictions of the displacement demand in the domain of the response spectrum plateau.

**Keywords** Displacement-based methods · Vulnerability assessment · Equal displacement rule · Secant stiffness · Hysteretic models · Seismic behavior · Recorded earthquakes · Displacement demand prediction · Non-linear displacement demand

## 1 Introduction

It is well established that structures do not remain elastic under extreme ground motion. Non-linear behavior therefore constitutes the key issue in seismic design and assessment of structures. However, to avoid the use of more elaborate analysis, structural engineering approaches are usually based on simplified static methods to determine seismic action. In these simplified methods, compared to linear behavior, seismic action is reduced according to the deformation capacity and the energy dissipation capacity of the structure as it undergoes large inelastic deformations. The majority of the building codes around the world are based on this design philosophy.

Seismic assessment using any method but non-linear time history analysis therefore requires a reliable estimation of the seismic displacement demand. Since [Veletsos and Newmark \(1960\)](#), it has been widely accepted that the displacements of elastic and inelastic systems are approximately the same (*Equal displacement principle*). This empirical principle was confirmed by numerous numerical and experimental investigations (e.g. [Lestuzzi and Badoux 2003](#)), except for low period structures, for which inelastic displacements are rather higher than elastic displacements. Since then, many authors tried to model inelastic displacements using linear approaches in order to allow earthquake engineers to easily perform these computations (e.g. [Fajfar 1999](#)). It should be emphasized that, until non-linear time history analysis becomes a standard procedure, there is a need for such simplified methods to estimate inelastic seismic demand.

The plateau range of the design spectra is of particular significance for seismic design and assessment. For instance, most of the buildings in Europe are lower than 5-story structures, and therefore have a natural period lower than 1 s. As a consequence, the natural period of a large part of these structures is located on the plateau of the design spectra, i.e. out of the assumed standard range of application of the equal displacement rule.

Moreover, contrary to design procedures, assessment procedures may lead to account for high strength reduction factors, due to several reasons. First, the shear strength of existing structures, especially unreinforced masonry structures, may be very low despite a creditable displacement capacity; these two parameters being not necessary linearly related. This has been shown in laboratory tests (e.g. [ElGawady et al. 2005](#); [Tomazevic and Weiss 2010](#)). Second, some codes allow relatively high strength reduction factors, e.g. 3–4 in Germany for unreinforced masonry structures. In Switzerland, the minimum permitted compliance factor (ratio of the capacity of the structure over the demand in the current codes) is 0.25. Weak buildings therefore have to be assessed to high demands compared to their capacity, thus leading to computing the demand for high strength reduction factors (up to 8) nevertheless resulting in compliant values. Even if these computations are theoretical, they are of practical need for the engineers.

Current linearization methods can be grouped into one of two categories: (1) methods based on  $R - \mu - T$  relationships and (2) equivalent damping approaches

(Lin and Miranda 2009). While the latter were developed and included in the design code in the US (Kowalsky 1994; ATC 2005), the former has been more inspiring in Europe (Fajfar 1999; CEN 2004). However, it has been shown that the simplification of the N2 method (Fajfar 1999) in EC8 led to an underestimation of the demand in some cases (Norda and Butenweg 2011). Therefore, there is a need for a simple method of estimation of the demand that should be at least conservative for structures on the plateau of the design spectra.

In this paper, different linearization methods are evaluated with respect to an inelastic model and compared to a new simple  $R - \mu - T$  relationship based on graphical assumptions.

## 2 Approaches for predicting the non-linear displacement

### 2.1 Current available approaches

#### 2.1.1 $R - \mu - T$ relationships

Veletsos and Newmark (1960) first found out that for large to medium periods, the displacements of elastic and inelastic systems were approximately the same. This empirical statement known as equal displacement principle or equal displacement rule (EDR) is nowadays widely used for seismic design purposes, e.g. in Eurocode 8 (CEN 2004). The basic assumption of the EDR is to model an inelastic system using the equivalent elastic system with the same period and damping coefficient. As illustrated in Fig. 1a, the equal displacement rule states that inelastic peak displacements ( $y_p$ ) are approximately equal to elastic peak displacements ( $y_{el}$ ) whatever the selected yield strength ( $F_y = F_{el}/R$  or yield displacement  $y_y = y_{el}/R$ ) of the structure. Note that when assuming that the stiffness is independent of strength, the equal displacement rule leads to a strength reduction factor ( $R$ ) equal to the global displacement ductility.

Numerous studies of the so-called  $R - \mu - T$  relationships propose adjustments to this approximate prediction by giving the strength reduction factor  $R$  as a function of displacement

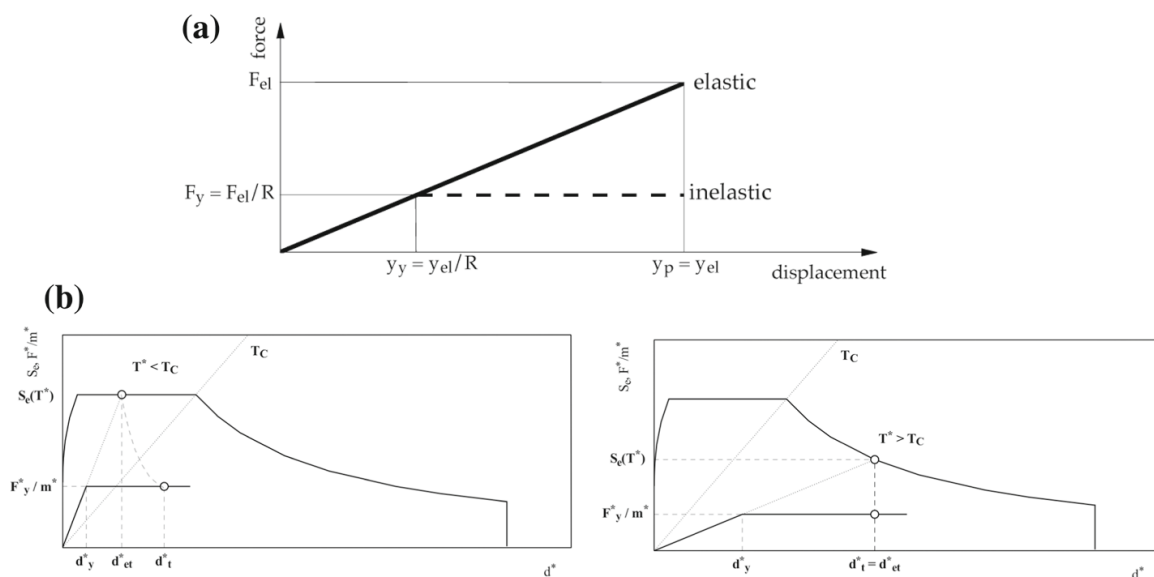


**Fig. 1** a Schematic description of the equal displacement rule. b ADRS representation of the non-linear displacement demand according to EC8 (adapted from CEN 2004)

ductility  $\mu$  and possibly period  $T$ , as reviewed by [Miranda and Bertero \(1994\)](#), [Miranda and Ruiz-Garcia \(2002\)](#) or [Chopra and Chintanapakdee \(2004\)](#).

On the plateau period range of the design spectra, [Riddell et al. \(1989\)](#) and later [Vidic et al. \(1994\)](#) first proposed the linear variation of the strength reduction factor as a function of the period for a constant displacement ductility demand, later used in EC8:

$$R = 1 + (\mu - 1) \frac{T_0}{T} \quad (1)$$

In this assumption, the strength reduction factor varies between 1 for a zero period and the value of the displacement ductility demand for the period  $T_0$  being close to the end of the plateau  $T_C$  (0.25–0.4 s for moderate to high hazard countries). Based on Eq. 1, the peak response  $y_{N2}$ , implemented in a more general seismic analysis method, the N2 method ([Fajfar 1999](#)) is computed as follows:

$$\begin{cases} T_0 = 0.65 \times \mu^{0.3} \times T_c \leq T_c \\ \forall T < T_0 & y_{N2} = y_{el} \\ \forall T \geq T_0 & y_{N2} = \frac{y_{el}}{R} \left( 1 + (R - 1) \frac{T_0}{T} \right) \end{cases} \quad (2)$$

In EC8 ([CEN 2004](#)), a simplified version of the N2 method is proposed for seismic assessment using pushover analysis (Fig. 1b). The determination of the displacement demand (target displacement) is performed according to the equal displacement rule for medium and long period structures and according to the N2 method for short period structures. While assuming that  $T_0 = T_c$  for the sake of simplification as proposed by [Fajfar \(1999\)](#). In this paper, both versions (i.e. original and EC8) of the procedure are investigated.

[Miranda \(2001\)](#) showed using statistical analysis that the strength reduction factors were approximately equal to the displacement ductility (equal displacement rule) from approximately 0.2 s for a ductility of 1.5 and 1.2 s for a ductility of 6. All methods based on the  $R - \mu - T$  relationships tend to use the equal displacement rule for periods greater than 0.25–0.5 s. For lower period values, some researchers suggested using the so-called equal energy approximation (EEA). [Miranda \(2006\)](#) considers this “rule” as a “myth”, showing there is no statistical correlation between its results and non-linear displacement values. [Ye and Otani \(1999\)](#) further developed the equal energy concept and conclude that it cannot be applied to short period systems. However, it is still used by some researchers and engineers especially to interpret experimental tests in terms of ductility (e.g. [Lu and Kasa 2008](#)). This modification of the strength reduction factor using the equal energy rule leads to a response  $y_{EEA}$  that can be calculated using:

$$y_{EEA} = \frac{R^2 + 1}{2R} y_{EDR} \quad (3)$$

Even if the equal displacement rule has been shown to be accurate on average through statistical analysis in the intermediate to long period range, the resultant displacement values may not be necessary conservative due to the associated variability, as stated by [Miranda and Bertero \(1994\)](#). However, corrections on the displacement demand using the strength reduction factors can only change the average value, i.e. the bias, but do not change the variability, inherent in the inelastic behavior. The only way to handle this issue with  $R - \mu - T$  relationships is to adopt conservative values for design purposes.



### 2.1.2 Equivalent period and damping ratios

In the second category, in order to consider inelastic systems as equivalent linear systems, as first proposed by [Jacobsen \(1930\)](#), [Rosenblueth and Herrera \(1964\)](#) suggested using the secant stiffness instead of the linear or initial one. [Iwan and Gates \(1979\)](#); [Miranda and Ruiz-Garcia \(2002\)](#); [Sullivan et al. \(2004\)](#); [Priestley \(2006\)](#); [Miranda \(2006\)](#) or [Lin and Miranda \(2009\)](#) already extensively reviewed these methods. The period  $T_e$  corresponding to the secant stiffness assuming a hardening  $r$ , defined as the ratio between initial and post-yield stiffness, is given by the equation:

$$T_e = T \sqrt{\frac{\mu}{1 - r + r\mu}} \quad (4)$$

Or more simply, assuming  $r=0$  which corresponds to the pure elasto-plastic model:

$$T_e = T \sqrt{\mu} \quad (5)$$

These researchers assume that the best elastic system to represent an inelastic one has a larger period and a higher damping ratio than is obtained using formulae based on the energy dissipated during cycles. Several researchers (e.g. [Gülkan and Sozen 1964](#); [Iwan and Gates 1979](#)) argued that the equivalent damping ratio  $\xi_e$  given by [Rosenblueth and Herrera \(1964\)](#), based on the harmonic response, was overestimated ([Miranda and Ruiz-Garcia 2002](#)) and suggested several modifications based on theoretical considerations ([Chopra and Goel 1999](#); [Calvi 1999](#); [Levy et al. 2006](#)) or by fitting the displacement obtained by inelastic SDOF models loaded by recorded strong motions ([Dwairi et al. 2007](#)). [Dwairi et al. \(2007\)](#), which gives very close damping values to the formulation of [Calvi \(1999\)](#), is one of the most recent. They propose several relationships for the equivalent damping ratio depending on parameters of the hysteretic model. The equation related to the Small Takeda model ( $r=0$ ,  $\alpha = 0.5$ ,  $\beta = 0$ ) has been selected for this study:

$$\xi_e = \xi + C \frac{\mu - 1}{\pi \mu}$$

$$\text{with } \begin{cases} \forall T_e > 1 & C = 0.5 \\ \forall T_e \leq 1 & C = 0.5 + 0.4 \cdot (1 - T_e) \end{cases} \quad (6)$$

Recently, this method has been used by [Colombi et al. \(2008\)](#) to assess the vulnerability of Italian buildings, following the work of [Borzi et al. \(2008\)](#). They chose this model for masonry buildings and the Large Takeda model ( $r=0$ ,  $\alpha = 0$ ,  $\beta = 1$ ) for RC buildings.

These linearization methods are now widely used for design purposes ([ATC 2005](#)) as well as for large-scale seismic vulnerability assessment ([FEMA 1999](#); [Calvi 1999](#); [Borzi et al. 2008](#); [Colombi et al. 2008](#)). This approach, slightly more complicated than the initial stiffness methods, is aimed at better describing the physics of structural damage, even if its theoretical basis remains arbitrary ([Miranda 2006](#)).

Finally, other authors suggest intermediate values of equivalent periods and damping ratios using empirical relationships. [Iwan \(1980\)](#) computed fully empirical relations for both equivalent periods and damping ratios using few recorded signals and found relationships that outperform the previous described techniques. [Lin and Miranda \(2008\)](#) followed the same approach but used more extensive data and computed these parameters as a function of the strength reduction factor  $R$  in order to avoid iterations. Their results are the following:

$$T_e = T \cdot \left( 1 + \frac{0.026}{T^{0.87}} \cdot (R^{1.8} - 1) \right) \quad (7)$$

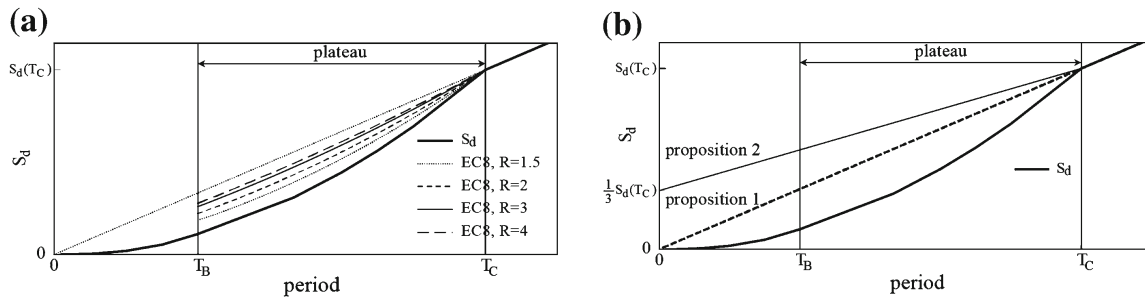


**Fig. 2** **a** Spectral displacement representation for increasing strength reduction factors ( $R$ ) of the non-linear displacement demand according to EC8. **b** The two propositions for the non-linear displacement demand in the period range for the plateau

$$\xi_e = \xi + \frac{0.016}{T^{0.84}} \cdot (R - 1) \tag{8}$$

Bringing more knowledge into the models (more parameters, more degrees of freedom in the regression equation), these more complicated linearization methods therefore aim to decrease the errors in the computation of the maximum displacement, especially at low periods where the equal displacement rule is not relevant anymore. They are successful in this task as shown by [Lin and Miranda \(2009\)](#).

### 2.2 New proposed $R$ - $\mu$ - $T$ simplified relationships

It is obvious that linear methods will never be able to reproduce the complexity of non-linear computations. Moreover, the objective of these linearization methods for the engineer is to be able to practically estimate the displacement demand that the studied structure may experience for a given hazard level. In most of the cases, the engineer prefers having (slightly) conservative values in order to be on the safe side. For more advanced applications, non-linear computations would nowadays be employed. Therefore, simple, slightly conservative and graphically obvious ways of estimating the non-linear displacement demand for low period buildings on the plateau of the design spectra are proposed here. They should only depend on the natural frequency of the structure and therefore be independent of the strength reduction factor.

Observing the non-linear displacement demand according to EC8 (Fig. 2a), in the period range for the plateau of the corresponding design spectrum (between  $T_B$  and  $T_C$ ), the displacement demand tends quickly to a linear variation for increasing strength reduction factors ( $R$ ). This linear variation is the prolongation of the Equal Displacement Rule that is valid for the period range after the plateau and constitutes Proposition 1 (Fig. 2b). Proposition 2 keeps the linear variation but with an initial value of one third of the spectral displacement at the end of the plateau.

**Proposition 1** Proposition 1 is the linear extension of the  $[T_C \ T_D]$  interval of the design spectra, i.e. the constant pseudo-velocity interval. This corresponds to the EC8 formula with an infinite strength reduction factor (Eq. 2). With  $S_{ap}$  the spectral acceleration value of the plateau, the proposed spectral inelastic displacement  $S_{d,inel}^{prop1}$  in this period range corresponds to the following equation:

$$\forall T \in [T_B, T_C], S_{d,inel}^{prop1}(T) = S_{ap} \left( \frac{T_C}{2\pi} \right)^2 \frac{T}{T_C} \tag{9}$$

Since in this period range (the plateau), the elastic displacement response spectra is:  $\forall T \in [T_B, T_C], S_{d,el}^{code}(T) = S_{ap} \left(\frac{T}{2\pi}\right)^2$ , the corresponding ductility demand can be simply written:

$$\forall T \in [T_B, T_C], \mu = \frac{S_{d,inel}^{prop1}(T)}{S_{d,el}^{code}(T)} = \frac{T_C}{T} \tag{10}$$

With the ductility tending to 1 (equal displacement rule) when T approaches the corner of the plateau.

**Proposition 2** In case the conservative Proposition 1 is not conservative enough for moderate to large non-linearity levels, a further linear extension of the spectrum is proposed (Proposition 2) with an ordinate at the origin being a fraction  $\alpha$  of the displacement demand in  $T_C$ . In this case, the displacement demand is written as follows:

$$\forall T \in [T_B, T_C], S_{d,inel}^{prop2}(T) = S_{ap} \left(\frac{T_C}{2\pi}\right)^2 \left(\frac{T}{T_C}(1 - \alpha) + \alpha\right) \tag{11}$$

and the corresponding ductility demand is as follows:

$$\forall T \in [T_B, T_C], \mu = \frac{S_{d,inel}^{prop2}(T)}{S_{d,el}^{code}(T)} = \left(\frac{T_C}{T}\right)^2 \left(\frac{T}{T_C}(1 - \alpha) + \alpha\right) = \frac{T_C}{T}(1 - \alpha) + \left(\frac{T_C}{T}\right)^2 \alpha \tag{12}$$

In the following,  $\alpha$  is chosen as  $\alpha = 1/3$  for graphical reasons explained hereafter.

### 2.2.1 Graphical estimation of displacement demand prediction

The proposed simplified displacement demand predictions can be easily graphically approximated. This constitutes a significant advantage for practical applications. Starting from the spectral displacement related to the natural frequency of the structures and corresponding to the EDR, the increase of the displacement demand predictions may be approximated by a portion of the spectral displacement difference between the natural frequency of the structure and the plateau corner period ( $T_C$ ) of the design response spectrum. As illustrated in Fig. 3, in the standard ADRS format, proposition 1 corresponds to an additional one third of the spectral displacement difference and proposition 2 corresponds to an additional one half.

Such a graphical estimation allows the displacement demand prediction to be performed with less than 5 % error compared to the exact values of the propositions.

Note that since proposition 1 constitutes the upper bound of the original EC8 displacement demand prediction, the corresponding graphical estimation (an additional one third of the spectral displacement difference) may be used for a quick check of computed displacement demand in a practical case using the current EC8 method.

## 3 Methodology

Figure 4 illustrates the methodology used in this study. It consists in the computation of the non-linear responses of SDOF systems subjected to earthquake records and of the assessment of the difference between the obtained peak displacement demands and those predicted by selected approaches. For the non-linear time-history analyses, structural behavior is described

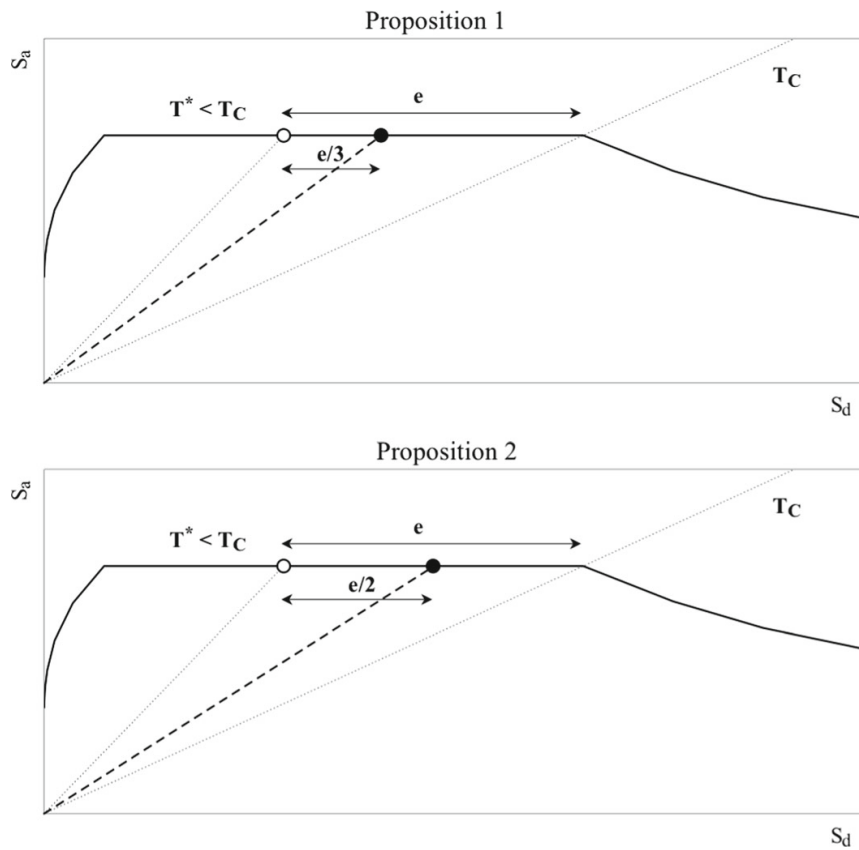


**Fig. 3** Graphical estimation of the two proposed displacement prediction in the ADRS format

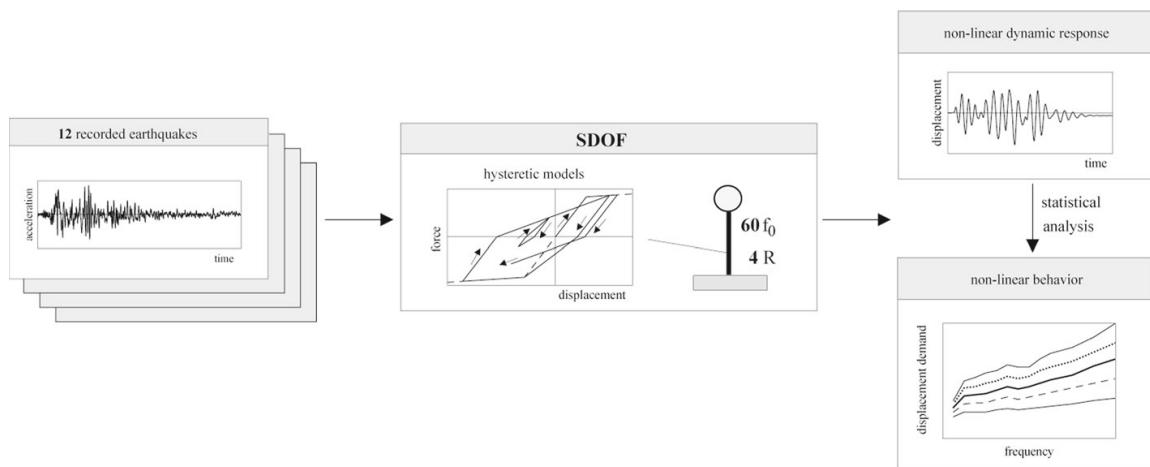


**Fig. 4** Schematic description of the methodology used

by several widely used hysteretic models such as Takeda or Gamma models (Lestuzzi and Badoux 2003). Four sets of 12 records selected from the European Strong Motion Database (Ambraseys et al. 2002), slightly modified to match design response spectra for different ground types, are developed to evaluate the different methods.

### 3.1 Ground motions

As the objective is to propose a practical but relevant method to estimate inelastic displacements, and not a physical theory aiming at explaining the phenomena, the validation is made using ground motions matching design spectra. Though these ground motions do not

represent a realistic hazard, they facilitate the understanding of key parameters influencing the results.

### 3.1.1 ESMD database of recorded ground motions

Non-linear time-history analysis may be carried out using both recorded earthquakes or artificially generated earthquakes (e.g. Schwab and Lestuzzi 2007). In the past, artificial ground motions were preferred for earthquake engineering purposes since they could be easily generated to match an elastic design spectrum and therefore be used in the frame of design codes. This approach is criticized in the literature because generated ground motions may not be realistic and do not cover the variability of actual ground motions (e.g. Lestuzzi et al. 2004). Nowadays, the amount of records of strong earthquake is exponentially increasing so that real accelerograms with given characteristics, such as their similarity with design spectra, can be selected (e.g. Iervolino et al. 2011).

Schwab and Lestuzzi (2007) selected 164 recorded ground acceleration time histories from the European Strong Motion Database (Ambraseys et al. 2002). The selection of the records in this initial database is based on structural engineering considerations rather than seismological ones. As a consequence, earthquakes with different focal mechanisms are incorporated into the dataset. The main objective is to perform a statistical study of the non-linear response of structures undergoing any earthquake record.

In order to consider earthquakes that may produce significant non-linearities in structural behavior, only records with a magnitude larger than 5 were considered for this selection. The magnitudes range from 5.0 to 7.6, the epicentral distances range from 2 to 195 km and the peak ground accelerations (PGA) range from 0.61 to 7.85 m/s<sup>2</sup>.

This selection was already used in other research projects in the field of seismic non-linear behavior (Lestuzzi et al. 2004 and 2007).

### 3.1.2 Selection of sets of 12 records

Out of this preliminary selection, sets of 12 records best matching different design response spectra were extracted. For the selection of these sets, four design response spectra from EC8 are considered. These EC8 spectra are of type 1, for the usual viscous damping ratio of 5% and for ground types A, B, C and D. They are scaled for a peak ground acceleration of 1 m/s<sup>2</sup> corresponding to the design response spectra of the Swiss seismic zone 2 (SIA 2003).

The selection is performed for the best match to the considered response spectrum (target spectrum) through ranking the 164 records of the initial database by the difference between their response spectrum and the target spectrum. The best twelve records form the set related to the considered target response spectrum. As an example, the response spectrum of the twelve records selected for the best fit to the design spectrum of ground type C are plotted separately in Fig. 5. Finally, a total of 33 records are selected for the four sets of 12 records each; with several records belonging to two or more sets. The main characteristics of the 33 selected records and their corresponding sets are listed in the Table 1.

### 3.1.3 Modification of records for matching target spectra

After selection into the initial database, the 33 records are modified with the non-stationary spectral matching technique of Abrahamson (1992) in order to match individually the related design spectrum. Spectral matching for a given design spectrum is not always regarded

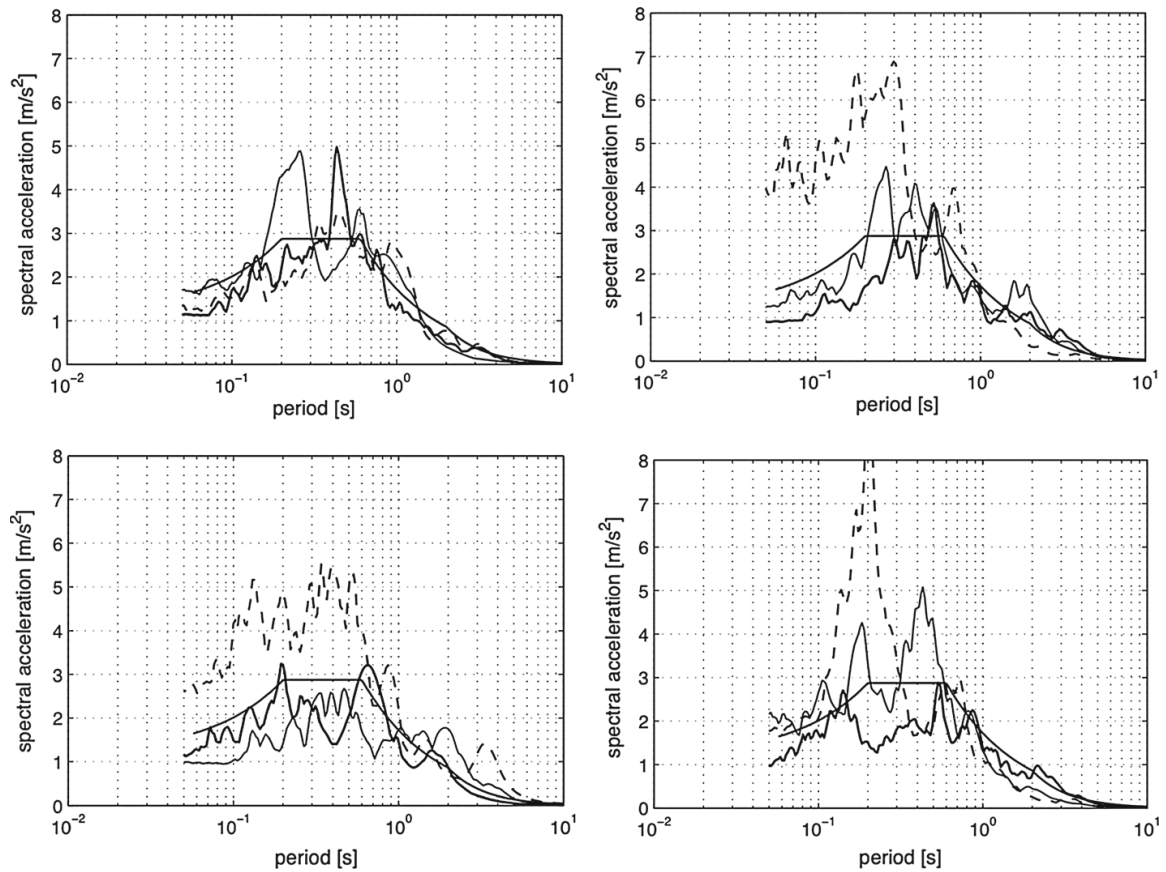


**Fig. 5** Response spectrum of the twelve records selected for the best fit to the design spectrum of ground type C

**Table 1** Main characteristics of the 33 selected records and their distribution in the four different sets of twelve records each (as=aftershock)

Earthquake	Date	Magnitude	Distance [km]	PGA [ $\text{m/s}^2$ ]	Soil A	Soil B	Soil C	Soil D
Friuli (as)	11.09.1976	5.3 Mw	8	1.931	X			
Friuli (as)	16.09.1977	5.4 Mw	14	0.910	X			
Volvi	04.07.1978	5.12 Ms	16	1.125	X			
El Asnam (as)	08.11.1980	5.2 Mw	18	0.946	X			
Friuli (as)	15.09.1976	6 Mw	11	1.069		X	X	
Basso Tirreno	15.04.1978	6 Mw	18	1.585			X	X
Volvi	20.06.1978	6.2 Mw	29	1.430		X	X	
Montenegro (as)	24.05.1979	6.2 Mw	30	0.754	X			
Montenegro (as)	24.05.1979	6.2 Mw	17	2.703		X		
Alkion	25.02.1981	6.3 Mw	25	1.176		X	X	X
Aigion	15.06.1995	6.5 Mw	43	0.911			X	
Montenegro	15.04.1979	6.9 Mw	65	2.509			X	X
Campano Lucano	23.11.1980	6.9 Mw	23	1.776				X
Campano Lucano	23.11.1980	6.9 Mw	26	0.903			X	
Campano Lucano	23.11.1980	6.9 Mw	16	1.725				X
Campano Lucano	23.11.1980	6.9 Mw	33	0.975	X	X		
Spitak	07.12.1988	6.7 Mw	36	1.796				X

**Table 1** continued

Earthquake	Date	Magnitude	Distance [km]	PGA [m/s <sup>2</sup> ]	Soil A	Soil B	Soil C	Soil D
Strofades	18.11.1997	6.6 Mw	144	0.907	X			
Strofades	18.11.1997	6.6 Mw	32	1.289		X		
Tabas	16.09.1978	7.4 Mw	55	1.003	X	X		
Tabas	16.09.1978	7.4 Mw	100	1.002	X			
Manjil	20.06.1990	7.4 Mw	81	0.951	X	X		
Manjil	20.06.1990	7.4 Mw	131	1.341				X
Gulf of Akaba	22.11.1995	7.1 Mw	93	0.894	X	X		
Izmit	17.08.1999	7.6 Mw	172	0.974	X			
Izmit	17.08.1999	7.6 Mw	110	1.698			X	
Izmit	17.08.1999	7.6 Mw	48	2.334			X	X
Izmit	17.08.1999	7.6 Mw	78	1.040		X	X	X
Izmit	17.08.1999	7.6 Mw	96	1.120		X	X	
Izmit	17.08.1999	7.6 Mw	10	2.192				X
Izmit	17.08.1999	7.6 Mw	39	1.266				X
Izmit	17.08.1999	7.6 Mw	34	3.542				X
Izmit	17.08.1999	7.6 Mw	103	0.871		X	X	

as relevant, since design spectra are envelopes of possible earthquake spectra. The reason to perform a selection and matching of the records to the design spectra is to show the consequences of the choice of a linearization method in terms of spectra, i.e. for engineering purposes. In addition, it allows the removal of the variability due to ground motion in order to evaluate that due to the estimation of the response only. Moreover, the corner period  $T_c$  is often used as a parameter to compute the reduction factors (e.g. Vidic et al. 1994). Spectral matching is therefore a way to have sets of ground motion time histories with a well-defined  $T_c$ .

The matching process is performed for the period range from the beginning of the plateau of the considered target spectrum and for a maximum of ten iterations. Statistical characteristics of the response spectra for the sets of the twelve records before and after modification for matching target spectrum show the efficiency of the technique of Abrahamson. As an example, response spectrum average and mean values plus and minus one standard deviation are plotted in Fig. 6 for ground type C. The figure clearly shows that the selection performed on the twelve records for each set already leads to a good match with respect to mean values. The modification using the technique of Abrahamson then always produces an improvement of the match and is associated to a significant reduction of the variability.

### 3.2 Hysteretic models

The non-linear SDOF system is defined by its initial natural frequency or period  $T$ , its strength reduction factor  $R$  and the hysteretic model according to which the structure behaves in the non-linear range. Several hysteretic models were used to compute the non-linear responses: the modified Takeda-model, the Q-model (Saïdi and Sozen 1981) and the Gamma model (Lestuzzi and Badoux 2003). However, as already reported in other studies (e.g. Lestuzzi et al. 2007) the results are similar and lead to the same conclusions. Therefore, only the results

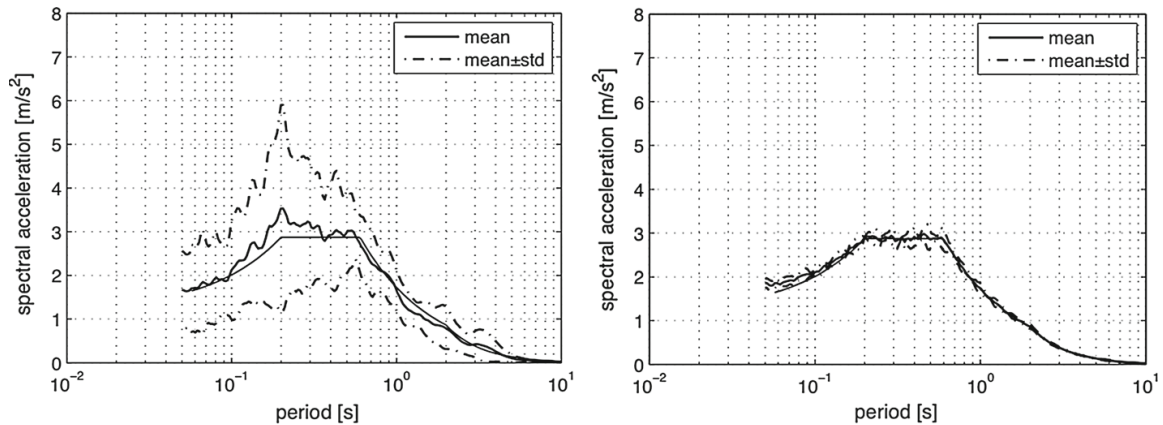
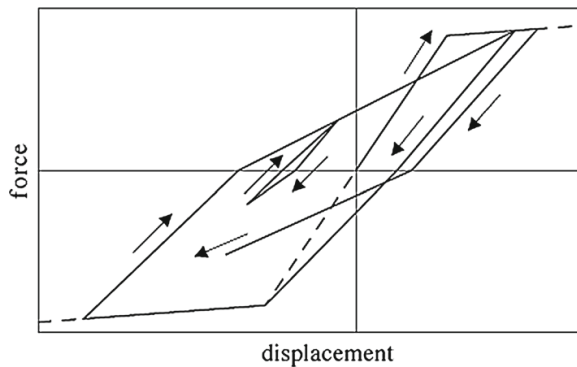


**Fig. 6** Statistical characteristics of the response spectra for the set of the twelve records selected for the best fit to the design spectrum of soils class C before (*left*) and after (*right*) modification for matching target spectrum

**Fig. 7** Force-displacement relationship defining the modified Takeda hysteretic model



related to the modified Takeda-model are presented in the following. The Takeda-model was initially proposed in an original version by [Takeda et al. \(1970\)](#). The modified Takeda-model was developed independently by [Otani \(1974\)](#) and [Litton \(1975\)](#). It was later adapted by many researchers. The version used here is the one of [Allahabadi and Powell \(1988\)](#). The related force-displacement relationship is plotted in [Fig. 7](#). The modified Takeda-model provides a much better simulation of the behavior of materials such as reinforced concrete than the classical elasto-plastic model.

The force-displacement relationship of the modified Takeda-model is specified through five parameters: the initial stiffness, the yield displacement, the post-yield stiffness, a parameter relating the stiffness degradation ( $\alpha$ ) and a parameter ( $\beta$ ) specifying the target for the reloading curve. Standard values of the parameters corresponding to the widely used “small Takeda model” ( $\alpha = 0.4$  and  $\beta = 0.0$ ) are used in all analyses ([Lestuzzi et al. 2007](#)). Note that a low  $\alpha$  value improves the rate of convergence of computations. Values of 0, 5 and 10 % have been tested for the hardening coefficient  $r$  (post-yield stiffness).

### 3.3 Processing

For each target response spectrum, the following computations are made for each strength reduction factor  $R$ , each hardening coefficient  $r$  and each selected ground motion:

- The elastic peak displacement  $y_{el}$  is obtained calculating the linear response of a SDOF of period  $T$  and damping ratio  $\xi$ . It corresponds to the inelastic displacement according to the equal displacement rule.



- The yield displacement associated with each computation, calculated as follows:

$$y_y = \frac{y_{el}}{R} \quad (13)$$

- The corresponding non-linear maximum displacement value  $y_{nl}$  using the hysteretic model.
- The displacement ductility is then computed based on the inelastic model, for a given strength reduction factor  $R$ :

$$\mu = R \frac{y_{nl}}{y_{el}} \quad (14)$$

- The displacement demand predictions according to the N2 method (Vidic et al. 1994), the version implemented in the EC8 (CEN 2004) and equal energy approximation are obtained following Eq. 2 and 3. It can be noticed that  $\mu$  is needed for the original Vidic et al. (1994) computation and  $T_c$  is known since the response spectra is assumed.
- The estimation of the linearized response as proposed by Dwairi et al. (2007) by computing the response of the SDOF for an equivalent period and damping using Eqs. 5 and 6 and the ductility.
- Finally, the linearized response following Lin and Miranda (2008), which is estimated by computing the linear response of the SDOF for an equivalent period and damping following Eqs. 7 and 8.
- Finally, the proposed estimates are computed using Eqs. 9 and 11.

The chosen representation of these results is the period-peak displacement plane, commonly used for displacement response spectra. Compared to the representation of the standard error with respect to a reference inelastic peak displacement, this representation shows better if the trend of the different linearized methods is correct and if their variability is coherent with the non-linear computations. For engineering purposes, the accuracy of the method is not critical but it is important not to underestimate the displacement demand that can be observed in this representation.

Moreover, this representation recalls that the spectral displacement in the plateau region is a function of the square of the period, such that a small uncertainty in the period estimation leads to large errors in the displacement demand estimate. Michel et al. (2010), computed the standard deviation of period height-relationships for RC shear wall buildings in France from ambient vibration measurements and found 0.08 s, i.e. up to 50 % of the period value on the plateau. Even numerical models, based on simplified assumptions, cannot predict the period with an excellent accuracy.

The displacement demand predicted by the different approaches is compared to the statistical characteristics of the peak displacements computed according to hysteretic model for various periods and strength reduction factors. This study is focused on displacement demand prediction in the short period range corresponding to the plateau of the related design response spectrum. Therefore, the methodology detailed above has been applied for periods  $T$  between 0.1 and 1 s and strength reduction factors  $R$  of 1.5, 2, 4 and 6. The initial damping ratio  $\xi$  was set to 5 %. A constant value for strength reduction factor  $R$  is used instead of a constant displacement ductility  $\mu$  to ensure the same non-linearity level for each ground motion. The goal of the study is to determine in which cases the different methods avoid an underestimation of the peak displacement demand.

## 4 Results

### 4.1 Performance of the classical methods

First the simplest methods are evaluated with respect to the “true” inelastic response. Fig. 8 (left part) compares this inelastic response with the linear response (equal displacement rule), the equal energy approximation and the N2 method as implemented in the EC8 (CEN 2004) for ground type B. The variability of the non-linear response is well demonstrated by the black area in Fig. 8. The simple linearization methods such as that used in EC8, on the contrary, just propagate the residual uncertainty from the spectral matching method. These methods cannot reproduce this variability so they have to choose between representing the inelastic response on average (best-estimate), for instance for risk assessment, or in a conservative way, for engineering purposes.

For low strength reduction factors ( $R \leq 2$ ), these methods provide reasonable displacements on average in the investigated period range for all ground types, even the equal displacement rule. The non-linear phenomena are limited so that the variability of the non-linear response is not critical. EC8 is slightly conservative, especially for ground type D (not displayed). The equal energy approximation gives relevant values only below 0.5 s. For intermediate strength reduction factors ( $R=4$ ), the inelastic response deviates significantly from the elastic response. At low periods (below 0.4 s), the increased inelastic displacement can be clearly seen. The equal energy approximation provides relevant values on a narrow period range only. The EC8 approach underestimates the increase in displacement at low periods, which leads to non-conservative values of inelastic displacement for periods lower than 0.3 s,

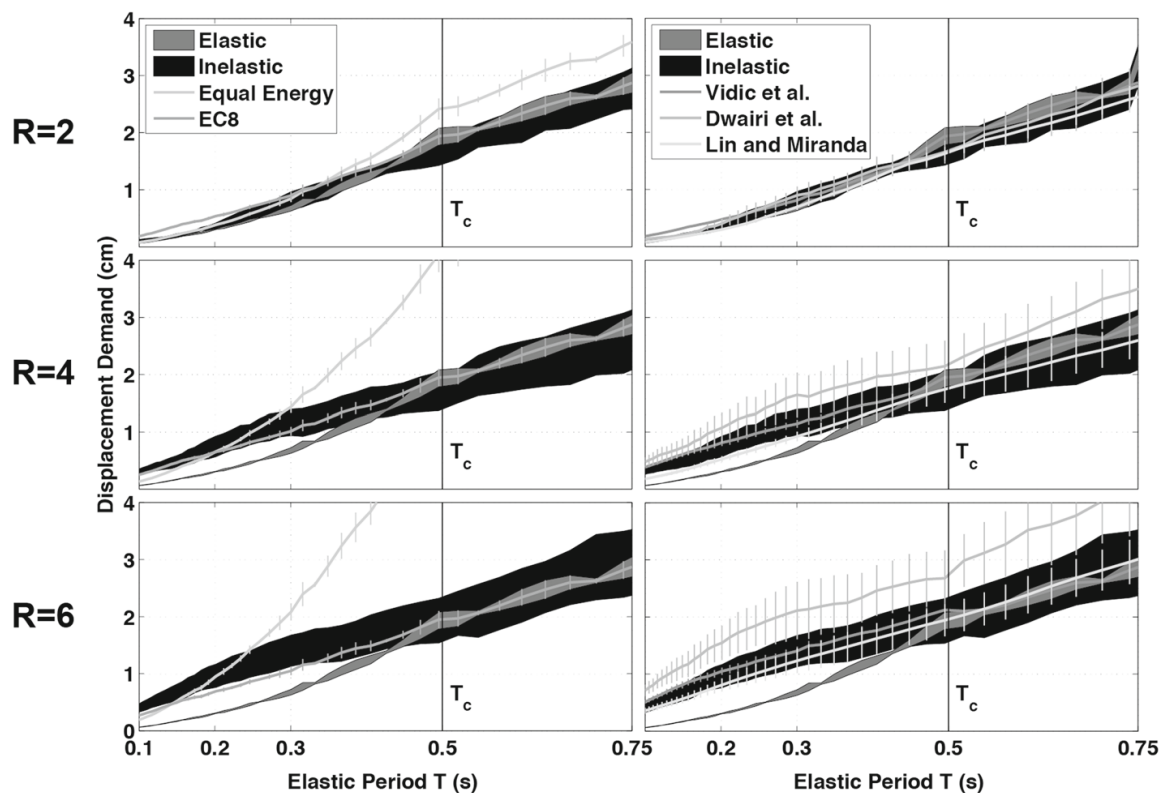


**Fig. 8** Displacement demand for increasing reduction factor  $R$  (ground type B, hardening coefficient  $r=5\%$ ). Comparison between elastic demand, inelastic demand (Takeda hysteretic model) and on the *left*: equal energy “rule” and EC8 prediction; on the *right*: Vidic et al. (1994); Dwairi et al. (2007) and Lin and Miranda (2008) predictions

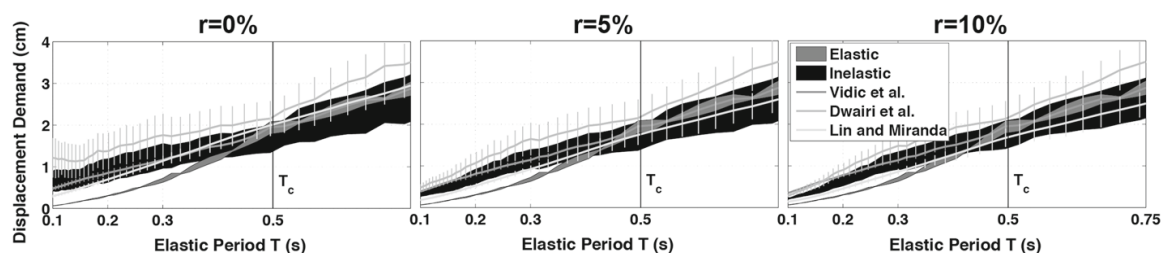


**Fig. 9** Displacement demand for increasing hardening coefficient  $r$  (ground type B and reduction factor  $R=4$ ). Comparison between elastic demand, inelastic demand (Takeda hysteretic model), Vidic et al. (1994); Dwairi et al. (2007) and Lin and Miranda (2008) predictions

i.e. for RC shear wall buildings lower than 3-stories high according to the EC8 (CEN 2004) frequency/height relationship. The inelastic displacement even exceeds the upper bound of the EC8 (infinite  $R$  – linear trend) even for  $R=4$  for several soil classes. It is therefore already obvious that proposition 1 is not conservative enough for moderate to large non-linearity levels. Finally, at large strength reduction factors ( $R=6$ ), these phenomena are amplified, with the equal energy approximation being simply irrelevant and EC8 strongly underestimating the displacement at low periods.

The more advanced methods of Vidic et al. (1994); Dwairi et al. (2007) and Lin and Miranda (2008), representative respectively of methods using the initial stiffness, the secant stiffness and the intermediate stiffness are compared in Fig. 8 (right part). These methods perform particularly well on average at low strength reduction factors, even reproducing partly the variability of the response. This is not valid anymore looking at higher reduction factors. The Dwairi et al. (2007) values, in particular, strongly overestimate the response at low periods, whereas the Lin and Miranda (2008) relationship may underestimate the response in some cases for very low periods. Figure 9 investigates the effect of the hardening coefficient  $r$ . No hardening (pure plastic behavior) is not realistic and leads to large displacements at low periods that are not reproduced by the different methods. More realistic values of hardening lead to a better match with the different models. This means that comparisons with zero hardening (e.g. pure elasto-plastic models) should be avoided. Otherwise, the impact of this parameter on the results is limited.

The results are slightly affected by the used hysteretic model but same trends are obtained. It can be noticed, however, that only ductile behavior is considered here. Non-ductile behavior may change the conclusions. An important conclusion here is that reproducing the non-linear response of structures using linear SDOF systems is not an easy task, even by adding more and more parameters to the relationships. Moreover, extending the study to MDOF systems would introduce even more variability (e.g. Erduran and Kunnath 2010).

The approach of choosing intermediate periods between the initial and secant stiffness (Lin and Miranda 2008) is doubtless the most relevant from a physical point of view, but these results show that the improvements it provides are not critical. Considering the fast development of non-linear modeling, linearized models have only a future for first order design and assessment purposes. Therefore, instead of looking for more complex – but still linear - models, we propose simplified, conservative estimates for design code purposes.

#### 4.2 Performance of the proposed method

Figure 10 shows the comparison of the peak displacement predicted by the original EC8 procedure, both propositions, and the inelastic response related to the Takeda hysteretic model for various periods, strength reduction factors and for ground types A, B and C.

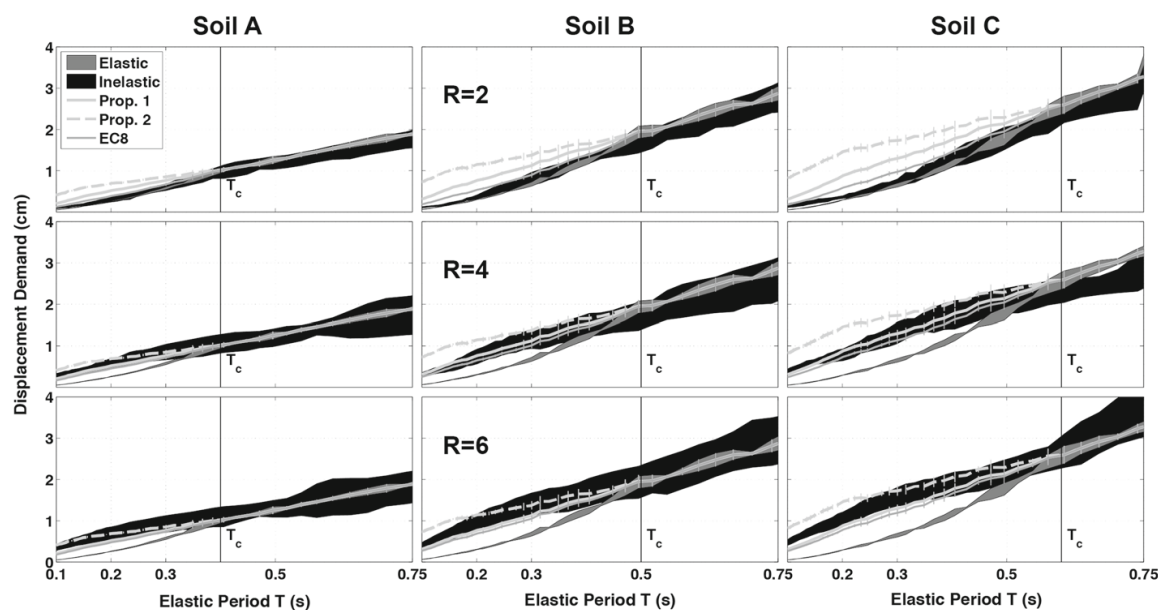


**Fig. 10** Displacement demand for increasing reduction factor  $R$  and the ground types  $A$ ,  $B$  and  $C$ . Comparison between elastic demand, inelastic demand (Takeda hysteretic model), the two propositions in this study and EC8 prediction

Compared to EC8 displacement demands that are not on the safe side, proposition 1 leads to better results, in the engineering sense, for moderate strength reduction factors up to  $R=4$ . Proposition 2 may be applied for higher strength reduction factors. However, for strength reduction factors higher than  $R=6$ , displacement demand increases significantly and the equal displacement rule is no longer valid, even for intermediate and large periods.

The same trends are related to the different ground types. However, the displacement demand predictions corresponding to ground type  $A$  are less accurate than for the other ground types. The results show that for this type of design spectra, with short corner periods of the plateau, even the displacement demand predictions according to proposition 2 underestimate the results for high strength reduction factors.

## 5 Summary and conclusions

The comparison of several methods (equal displacement rule – EDR –, equal energy approximation, a secant stiffness method and two empirical equivalent period and damping methods) was performed in order to evaluate their efficiency, more specifically in the period range of the plateau of the design spectra. The study focused on the reliability of the methods' seismic displacement demand prediction with respect to their complexity when compared to the statistical characteristics of the response of the modified Takeda hysteretic model. In order to load this non-linear model, recorded ground motions were selected and slightly modified to match design spectra of different ground types in order to study the effect of the structural response, irrespective of the ground motion variability.

As shown by previous similar studies, knowledge invested in a more complex – but still linear – method can improve the accuracy of the predictions, especially for intermediate to large periods. However, this investment may not be justified for all applications such as preliminary structural design or assessment. The results show that detailed computations lead to an incorrect understanding of accuracy, since other uncertainties, such as that of the fundamental period, limit the precision of the demand estimation in any case. For low periods,

none of the examined methods perform satisfactorily in all cases. Particularly, the original procedure proposed in EC8 systematically underestimates the demand in this period range. The equal energy “rule”, still often proposed for this period range, diverges dramatically. Consequently, the linear approximation seems not to be justified for the lowest periods, corresponding to low-rise buildings.

Therefore, following the “principle of consistent crudeness” (Elms 1985) two new simple, but conservative, displacement demand estimation methods are proposed. The peak displacement predicted by the original EC8 procedure and both propositions were compared the inelastic response of to the modified Takeda hysteretic model for various periods and strength reduction factors. Both propositions may be graphically approximated which is a significant advantage for practical application. The results show that, except for low strength reduction factors up to  $R=2$ , the propositions prevent the underestimation of the displacement demand that was observed with original EC8 procedure. The propositions may be further improved for a better prediction of displacement demand. However, such an improvement would be related with a more sophisticated expression, which may not be justified for practical applications. The reported investigations are focused on SDOF and on hysteretic models featuring ductile structural seismic behavior. These options are related to the objectives of the study. Even if some slight differences arise with MDOF (e.g. Schwab and Lestuzzi 2007), the crucial characteristics of the seismic response are captured with SDOF. Compared to ductile structural behavior, limited hysteretic energy dissipation behavior still increases the non-linear demand (Lestuzzi et al. 2007) and further investigations would be necessary in order to propose adequate displacement demand predictions for such cases.

The significance of the obtained results should be distinguished between new and existing structures. The impact is relatively limited for the design of new structures. For conventional design, current procedures are reliable because only relatively small values of the strength reduction factor are allowed. The usual construction codes practice of considering the equal displacement rule for the whole period range is even validated by the results. For ductile design, such as capacity design, restricted modifications may be involved for the low period range only. By contrast, for the seismic assessment of existing structures, such as unreinforced masonry low-rise buildings, the current procedure of EC8 should be modified in order to provide accurate predictions of the displacement demand in the domain of the response spectrum plateau. Current procedure is reliable only for small values of the strength reduction factors ( $R \leq 2$ ). For higher values of strength reduction factors, the two propositions developed in this study lead to significantly more relevant displacement demand prediction. Consequently, it is suggested to replace the current EC8 procedure by the proposition 1 for strength reduction factors between 2 and 4 and by proposition 2 for higher strength reduction factors.

## References

- Abrahamson NA (1992) Non-stationary spectral matching. *Seismol res lett* 63(1):30
- Allahabadi R, Powell GH (1988) Drain-2DX user guide. Report No. UCB/EERC-88/06. College of Engineering, University of California, Berkeley
- Ambraseys N, Smit P, Sigbjornsson R, Suhadolc P, Margaris B (2002) Internet site for European strong-motion data. European Commission, Research Directorate General, Environment and Climate Program
- Applied Technology Council (ATC) (2005) Improvement of nonlinear static seismic analysis procedures, FEMA-440, ATC, California, USA

- Borzi B, Pinho R, Crowley H (2008) Simplified pushover-based vulnerability analysis for large scale assessment of RC buildings. *Eng Struct* 30(3):804–820
- Calvi G (1999) A displacement-based approach for vulnerability evaluation of classes of buildings. *J Earthq Eng* 3(3):411–438
- CEN (Comité Européen de Normalisation) (2004) Eurocode8: design provisions for earthquake resistance of structures: part 1: general rules, seismic actions and rules for buildings. EN 1998–1:2004
- Chopra AK, Chintanapakdee C (2004) Inelastic deformation ratios for design and evaluation of structures: single degree-of-freedom bilinear systems. *J Struct Eng* 130:1309–1319
- Chopra AK, Goel RK (1999) Capacity-demand-diagram methods for estimating seismic deformation of inelastic structures: Sdf systems., Technical Report 2, Pacific Earthquake Engineering Research Center (PEER) University of California, Berkeley
- Colombi M, Borzi B, Crowley H, Onida M, Pinho R (2008) Deriving vulnerability curves using italian earthquake damage data. *Bull Earthq Eng* 6:485–504
- Dwairi H, Kowalsky M, Nau J (2007) Equivalent damping in support of direct displacement-based design. *J Earthq Eng* 11:512–530
- ElGawady MA, Badoux M, Lestuzzi P (2005) In plane seismic response of URM walls upgraded with composites. *ASCE J Compos Construct* 9(6):524–535
- Elms DG (1985) Principle of Consistent Crudeness. Workshop on Civil Engineering Applications of Fuzzy Sets. Purdue University, West Lafayette, Indiana, USA
- Erduran E, Kunnath, SK (2010) Enhanced displacement coefficient method for degrading multi-degree of-freedom systems. *Earthq Spectr* 26(2):311–326. doi:[10.1193/1.3381157](https://doi.org/10.1193/1.3381157)
- Fajfar P (1999) Capacity spectrum method based on inelastic demand spectra. *Earthq Eng Struct Dyn* 28: 979–993
- FEMA (1999) HAZUS Earthquake loss estimation methodology. Federal Emergency Management Agency, Washington, DC
- Gülkan P, Sozen M (1964) Inelastic response of reinforced concrete structures to earthquake motions. *J Eng Mech Div* 90(37–48)
- Iervolino I, Galasso C, Paolucci R, Pacor F (2011) Engineering ground motion record selection in the Italian accelerometric archive. *Bull Earthq Eng* 9(6):1761–1778
- Iwan W, Gates NC (1979) Estimating earthquake response of simple hysteretic structures. *J Eng Mech Div* pp. 391–405
- Iwan W (1980) Estimating inelastic response spectra from elastic spectra. *Earthq Eng Struct Dyn* 8:375–388
- Jacobsen LS (1930) Steady forced vibrations as influenced by damping. *Trans ASME* 52:169–181
- Jennings PC (1968) Equivalent damping for yielding structures. *J Eng Mech Div* 94:103–116
- Kowalsky, M. J. (1994). Displacement-based design—a methodology for seismic design applied to RC bridge columns. Master's thesis, University of California, San Diego, La Jolla, California
- Kramer S (1996) Geotechnical earthquake engineering. Prentice Hall, NJ
- Lestuzzi P (2002) Effective Stiffness of RC Walls in Dynamic Tests. Proceedings of the 12th European Conference on Earthquake Engineering. Paper no 861. London
- Lestuzzi P, Bachmann H (2007) Displacement ductility and energy assessment from shaking table tests on RC structural walls. *Eng Struct* 29(8):1708–1721
- Lestuzzi P, Badoux M (2003) An experimental confirmation of the equal displacement rule for RC structural walls. In: Proceedings of the fib-Symposium: concrete structures in seismic regions. Paper no 127. Athens, Greece
- Lestuzzi P, Badoux M (2003) The gamma model: a simple hysteretic model for RC walls. Proceedings of the fib-Symposium: Concrete Structures in Seismic Regions. Paper no 126. Athens, Greece
- Lestuzzi P, Belmouden Y, Trueb M (2007) Non-linear seismic behavior of structures with limited hysteretic energy dissipation capacity. *Bull Earthq Eng* 5:549–569
- Lestuzzi P, Schwab P, Koller M, Lacave C (2004) How to choose earthquake recordings for non-linear seismic analysis of structures. In 13th World Conference of Earthquake Engineering (WCEE). Vancouver, BC, Canada
- Levy R, Rutenberg A, Qadi K (2006) Equivalent linearization applied to earthquake excitations and the  $r$ - $\mu$ - $t$  relationships. *Eng Struct* 28:216–228
- Litton RW (1975) A contribution to the analysis of concrete structures under cyclic loading. Ph.D. Thesis, Civil Engineering Dept., University of California, Berkeley
- Lin Y-Y, Miranda E (2009) Evaluation of equivalent linear methods for estimating target displacements of existing structures. *Eng Struct* 31(12):3080–3089. doi:[10.1016/j.engstruct.2009.08.009](https://doi.org/10.1016/j.engstruct.2009.08.009)
- Lin Y, Miranda E (2008) Noniterative equivalent linear method for evaluation of existing structures. *J Struct Eng* 134(11):1685–1695. doi:[10.1061/\(ASCE\)0733-9445\(2008\)134:11\(1685\)](https://doi.org/10.1061/(ASCE)0733-9445(2008)134:11(1685))

- Lu S, Kasa M (2008) Seismic test program of special designed clay blocks due to earthquake resistance by Wienerberger consisting real-scale shaking table-, cyclic shear-, diagonal tension- and compression tests. In: Proceedings of the 14th World Conference on Earthquake Engineering, Beijing, China
- Michel C, Guéguen P, Lestuzzi P, Bard P (2010) Comparison between seismic vulnerability models and experimental dynamic properties of existing buildings in France. *Bull Earthq Eng* 8(6):1295–1307. doi:10.1007/s10518-010-9185-7
- Miranda E (1993) Site-dependent strength-reduction factors. *J Struct Eng* 119(12):3503–3519
- Miranda E, Bertero VV (1994) Evaluation of strength reduction factors for earthquake-resistant design. *Earthq Spectr* 10(2):357–379
- Miranda E (2001) Estimation of inelastic deformation demand of sdf systems. *J Struct Eng* 127:1005–1012
- Miranda E, Ruiz-Garcia J (2002) Evaluation of approximate methods to estimate maximum inelastic displacement demands. *Earthq Eng Struct Dyn* 31:539–560
- Miranda E (2006) Reflections on the use of elastic or secant stiffness for seismic evaluation and design of structures. In 1st European Conference of Earthquake Engineering and Seismology, number 1476, Geneva, Switzerland
- Norda H, Butenweg C (2011) Möglichkeiten und Grenzen der Anwendbarkeit statisch nichtlinearer Verfahren nach DIN EN 1998–1. D-A-CH-Mitteilungsblatt. *Bauingenieur* 86:S13–S21
- Otani S (1974) Inelastic analysis of R/C frame structures. *J Struct Div* 100(7):1433–1449
- Priestley N (2006) Initial stiffness or secant stiffness for seismic design—which is more appropriate? In: 1st European Conference of Earthquake Engineering and Seismology, number 469, Geneva, Switzerland,
- Riddell R, Hidalgo P, Cruz E (1989) Response modification factors for earthquake-resistant design of short period structures. *Earthq Spectra* 5(3):571–590
- Rosenblueth E, Herrera I (1964) On a kind of hysteretic damping. *J Eng Mech Div* 90:37–48
- Saiidi M, Sozen MA (1981) Simple nonlinear seismic analysis of R/C structures. *Journal of the Structural Division*. In: Proceedings of the American Society of Civil Engineers (ASCE) 107(ST5):937–952
- Santa-Ana PR, Miranda E (2000) Strength reduction factors for multi-degree of freedom systems. In: 12th World Conference of Earthquake Engineering (WCEE), number 1446, Auckland, Australia
- Schwab P, Lestuzzi P (2007) Assessment of the seismic non-linear behavior of ductile wall structures due to synthetic earthquakes. *Bull Earthq Eng* 5(1):67–84
- SIA (2003) SIA 261 Actions on structures. Zurich, Swiss society of engineers and architects
- Sullivan TJ, Calvi GM, Priestley N (2004) Initial stiffness versus secant stiffness in displacement-based design. In: 13th World Conference of Earthquake Engineering (WCEE), number 2888, Vancouver, BC, Canada
- Takeda T, Sozen MA, Nielsen NN (1970) Resinforced concrete response to simulated earthquakes. *J Struct Div ASCE*, 2557–2573
- Tomazevic M, Weiss P (2010) Displacement capacity of masonry buildings as a basis for the assessment of behavior factor: an experimental study. *Bull Earthq Eng* 8:1267–1294
- Veletsos A, Newmark N (1960) Effect of inelastic behavior on the response of simple systems to earthquake motion. In: 2nd World Conference on Earthquake Engineering, vol 2. pp. 895–915, Tokyo, Japan
- Vidic T, Fajfar P, Fischinger M (1994) Consistent inelastic design spectra: strength and displacement. *Earthq Eng Struct Dyn* 23:507–521
- Ye L, Otani S (1999) Maximum seismic displacement of inelastic systems based on energy concept. *Earthq Eng Struct Dyn* 28:1483–1499

## 2.5 Perspectives

La problématique de la réponse des structures aux séismes, et, par extension, leur vulnérabilité sismique, ne peut être résolue par la modélisation seule : les enregistrements de vibrations ambiantes et de séismes en structures permettent de développer et de valider les modèles, de leur fournir des paramètres d'entrée, voire de les suppléer (modèles empiriques). Cela impose une compréhension mutuelle et une collaboration renforcée entre sismologues et ingénieurs structures. Les enregistrements de vibrations ambiantes sont particulièrement importants pour l'étude du bâti existant en maçonnerie non renforcée pour lequel les propriétés des matériaux et même la géométrie ne sont pas connues *a priori*. Les vibrations ambiantes dans les centres historiques, dont les murs sont souvent mitoyens, ont beaucoup à nous apprendre sur le comportement sous séisme de ces structures vulnérables. Par extension, la vulnérabilité des monuments historiques bénéficiera de ces enregistrements.

L'analyse du comportement modal des structures sur une large plage d'amplitudes, comme nous l'avons fait dans la partie 2.4.1, doit permettre de réconcilier l'approche sismologique sous vibrations ambiantes et le génie parasismique. Une étude systématique des essais en laboratoire de structures réalisées avec différents matériaux en suivant la méthode proposée devra permettre de mieux comprendre la variation des propriétés modales avec l'amplitude. On peut citer l'exemple des structures en bois étudiées par Sugino *et al.* (2012).

La problématique de l'interaction sol-structure s'avère également déterminante dans de nombreux cas et l'analyse modale classique permet difficilement de la traiter. Elle peut en outre avoir une influence à la fois dans le domaine linéaire et pour le comportement non-linéaire des structures. Le développement de l'interférométrie sismique pourrait permettre de résoudre ce problème (p. ex. Michel *et al.*, 2011a) car elle pourrait permettre de séparer la contribution de différentes parties de la structure.

Par ailleurs, les mesures temporaires permettent de collecter un grand nombre de données quantitatives, notamment les fréquences de résonance qui peuvent être utilisées pour une analyse à grande échelle. Il est cependant nécessaire de développer des bases de données géospatiales pour archiver ces données dans un objectif d'analyse du risque sismique. Dans le cadre du projet COGEAR (Fäh *et al.*, 2012), nous avons créé de telles bases, contenant en particulier des données collectées visuellement sur le bâti de plusieurs villes en Suisse. Elles devront être pérennisées à un niveau européen, voire mondial, et inclure les résultats de tests sous vibrations ambiantes et sous séismes.



## Chapitre 3

# Données sismologiques pour l'analyse post-sismique

La survenance d'un tremblement de terre s'accompagne de la nécessité de collecter un grand nombre d'informations, dont une partie importante peut être fournie par la sismologie de l'ingénieur :

1. Les autorités locales, nationales, voire supra-nationales, ont rapidement besoin d'informations sur l'étendue des dégâts (quelques minutes à quelques jours) afin de diriger les équipes de sauvetage et déblaiement et d'organiser l'aide d'urgence. Pour cela, les modèles de prédiction du mouvement du sol, les données des stations accélérométriques transmises en temps réel et les témoignages sur l'intensité ressentie, permettent de générer des cartes de l'intensité du mouvement sismique, aujourd'hui standardisées par le logiciel ShakeMap de l'USGS. Des modèles de pertes à l'échelle mondiale ou plus locale fournissent également des informations sur les pertes humaines et financières attendues (p. ex. les logiciels PAGER de l'USGS ou QLARM de WAPMERR). En Suisse, dans le cadre d'un accord avec le corps d'aide humanitaire (SKH), le sismologue d'astreinte du SED (Service Sismologique Suisse) prévient le SKH en cas de séisme important dans le monde et évalue les dégâts à l'aide des informations dont il dispose et de son expérience afin de déclencher, ou non, une mission humanitaire.
2. Dans les quelques jours à semaines (voire mois) qui suivent l'événement, les autorités de protection civile ont besoin d'experts du génie civil pour évaluer l'habitabilité des bâtiments afin de gérer le logement des sinistrés. Nous proposons dans la partie 3.3 une idée dans laquelle la sismologie de l'ingénieur pourrait accélérer cette analyse : un schéma d'analyse probabiliste (Bayésien) de l'habitabilité à partir de données de capteurs accélérométriques bon marché disposés dans chaque bâtiment (Goulet *et al.*, 2015).
3. Dans le même temps, les travaux scientifiques des sismologues et des ingénieurs doivent démarrer : la collecte des témoignages et l'observation des dégâts permettent d'améliorer la cartographie préliminaire des intensités (p. ex. Schlupp *et al.*, 2008) et l'installation de stations temporaires permet de mieux localiser les répliques (sismomètres) et d'enregistrer des mouvements forts (accéléromètres). Par ailleurs, d'autres disciplines scientifiques peuvent bénéficier des techniques géophysiques en mission post-sismique : l'observation de traces de failles en surface (p. ex. avec notre proposition dans Baumann *et al.*, 2013), d'effets géotechniques (glissements de terrain voir p. ex. Larose *et al.*, 2015) et surtout l'observation des dégâts aux constructions (voir partie 3.2 (Régner *et al.*, 2013)).
4. Enfin, après quelques semaines et mois, les évaluations précises des dégâts par les exploitants

et les assureurs finalisent la collecte de données post-sismiques. Ce sont également des sources précieuses pour l'analyse du risque.

Cela témoigne de la nécessité de l'expertise en sismologie de l'ingénieur en période de crise suite à un séisme et du besoin de développement de nouveaux outils de prédiction toujours plus précis.

### 3.1 La multidisciplinarité en mission post-sismique

Les missions post-sismiques traditionnelles, avec une mission "ingénieurs" observant les dégâts et une mission "sismologues" installant des stations pour observer les répliques, font désormais de plus en plus place à des missions multidisciplinaires où chaque spécialiste fait bénéficier les autres de ses connaissances. Lors de la mission du Bureau Central Sismologique Français (BCSF) suite au séisme de Nord-Martinique du 29 Novembre 2007 (Schlupp *et al.*, 2008), nous avons voyagé avec des sismomètres afin d'enregistrer des vibrations ambiantes sur des sites où l'origine de dégâts particuliers n'apparaissait pas clairement (voir partie 3.2 (Régner *et al.*, 2013)). Nous sommes restés en contact permanent avec l'observatoire de Martinique qui coordonnait les enregistrements des répliques et avec les missions de l'Association Française de Génie Parasismique en quête de retour d'expérience. Nous avons ainsi pu focaliser nos recherches aux endroits les plus intéressants et faire bénéficier ces autres institutions de nos résultats. Par ailleurs, en 2009, suite au séisme de l'Aquila, j'ai participé à une mission regroupant des chercheurs, des ingénieurs de génie civil, un architecte, un expert des assurances et des sauveteurs du SKH, là encore avec un sismomètre (Michel et Oropeza, 2009). Chaque spécialiste a pu apporter sa vision sur les sites observés. Nous avons étudié en détail 6 bâtiments modérément endommagés afin de valider des modèles pour l'analyse du bâti existant (Michel et Oropeza, 2009).

Depuis à la mission de 2007, je collabore avec le BCSF afin de former les futurs participants à des missions post-sismiques dans le cadre du Groupe d'Intervention Macrosismique (GIM). Je me charge de la partie de la formation comprenant une introduction à la dynamique des structures, à l'analyse de la vulnérabilité et des dégâts sismiques. J'ai pu constater un vif intérêt de la part des sismologues pour mieux comprendre les dégâts sismiques. Des formations ont été organisées en mai 2011 à Niederbronn (Alsace), avril 2012 (Martinique), juin 2012 (Mont-Ste-Odile, Alsace), mars 2013 (Lyon) et mai 2013 (Wickerschwihr, Alsace). Plus de 60 membres du GIM ont été formés. En outre, j'ai proposé une version courte de cette formation au SED en 2012.

L'INSARAG (International Search and Rescue Advisory Group), organisme dépendant de l'Organisation des Nations Unies, est chargé de la coordination des secours lorsque le pays touché n'est pas en mesure d'assurer cette mission (p. ex. Haïti en 2010). En outre, l'INSARAG a défini un standard international pour les équipes de sauvetage et déblaiement, avec une certification sans laquelle elles ne sont pas autorisées à intervenir. Ce standard définit notamment la composition d'une équipe dont le management doit inclure un ingénieur structure qui agit en conseiller du chef d'équipe. Par ailleurs, le SKH inclut dans son propre organigramme, fondé sur celui de l'INSARAG, un sismologue du SED en soutien. J'ai également eu la chance d'intervenir lors de la formation du SKH (ingénieurs structures et chefs d'équipe), qui s'entraîne aux interventions dans un village de décombres particulièrement réaliste à Epeisses (Suisse, Fig. 3.1). La problématique des sauveteurs est différente de celle de l'analyse de l'habitabilité détaillée dans la partie 3.3. Alors que cette dernière s'intéresse surtout aux bâtiments modérément endommagés (dommages 2 et 3 EMS-98) afin de déterminer s'ils sont habitables ou non (les bâtiments peu endommagés et effondrés ne posent pas de problème), les sauveteurs ne travaillent que dans des bâtiments au moins partiellement effondrés (dommages 4 et 5 EMS-98). Il s'agit donc d'être capable d'évaluer la sécurité des décombres instables en cas de réplique. Aucun modèle mathématique

n'est en mesure de faire cette évaluation ; seule l'expérience, l'observation et quelques bases d'analyse des structures sont utiles.



**Figure 3.1** – *Entraînement à l'intervention post-sismique avec le SKH dans les décombres du village d'Epeisses.*

Il y a donc un besoin et une demande de multidisciplinarité suite à un événement sismique. Ingénieurs de génie civil, sismologues, autorités et secouristes doivent partager leurs données et leur expérience afin de limiter les conséquences de la catastrophe. Dans la suite, je présente deux articles développant des idées fondées sur des enregistrements sismiques, afin de déterminer l'origine des dégâts en un site particulier et de quantifier ces dégâts à l'échelle d'une ville.

### 3.2 Contribution de l'enregistrement de vibrations ambiantes en mission post-sismique (Régnier *et al.*, 2013)

Les Antilles françaises (Guadeloupe et Martinique) constituent la zone avec le plus fort aléa sismique en France. Hayes *et al.* (2014) estiment qu'un séisme de magnitude  $M_w=8.2$ , du même ordre que celui de 1843, pourrait intervenir prochainement compte tenu de l'énergie accumulée dans la zone de subduction au large de la Guadeloupe. Le 29 novembre 2007, un séisme de magnitude  $M_w=7.3$  touchait le Nord-Martinique avec une distance hypocentrale de l'ordre de 150 km. Des dégâts légers (intensité VI) sont constatés dans environ la moitié de l'île, certains sites montrant des dégâts plus importants, dont quelques effondrements complets de structures très vulnérables. Les enregistrements accélérométriques montrent 1 site dépassant un PGA de  $4 \text{ m/s}^2$ , 7 sites au-delà de  $2 \text{ m/s}^2$  et 24 sites supérieurs à  $1 \text{ m/s}^2$ , soit 70% des sites instrumentés en Martinique (dont quasiment tous les sites implantés sur des sédiments) (Schlupp *et al.*, 2008). 10% des sites instrumentés dépassent le PGA des normes parasismiques ( $3 \text{ m/s}^2$ ) qui correspond à une probabilité de dépassement de 10% en 50 ans.

Dans l'article Régnier *et al.* (2013), nous montrons l'apport des enregistrements de vibrations ambiantes afin de mieux comprendre les dégâts observés suite à un séisme (Fig. 3.2). En effet, il est souvent difficile, juste par l'observation des dommages, de déterminer s'ils sont dus à un mouvement sismique plus fort (p. ex. effet de site) ou à une vulnérabilité particulière, voire d'une combinaison de ces deux phénomènes. Des données quantitatives mesurées *in situ* doivent permettre de mieux comprendre les

phénomènes à l'œuvre. Nous avons enregistré des vibrations en champ libre afin de déterminer la présence d'éventuels effets de site en observant leur fréquence de résonance (voir la partie 1.5), mais aussi dans des bâtiments (voir la partie 2.3) afin d'observer une éventuelle concordance entre résonance des structures et résonance des sites. Si ces mesures sont simples, rapides et peu coûteuses, l'interprétation des résultats doit être effectuée avec la plus grande prudence. La technique H/V permet de déterminer la fréquence de résonance d'un site, mais pas de quantifier l'amplification à la résonance ni, *a fortiori*, pour les fréquences supérieures. Cette mesure permet donc de déterminer à partir de quelle fréquence une amplification est attendue et de donner une information qualitative sur l'importance de l'effet de site (un pic H/V très net est synonyme de forte amplification). Par ailleurs, comme on l'a vu à la partie 2.4.1, la fréquence de résonance des structures évolue sous séisme, ce qui complique l'interprétation.

L'intégralité des mesures effectuées peut être trouvée dans Régnier et Michel (2008) et les plus intéressantes sont détaillées dans l'article suivant. Le cas de l'école Anne Marc est assez caractéristique des Antilles françaises. Le bâtiment, avec une structure très souple (ossature béton armé), présente une irrégularité de ses contreventements, préjudiciable pour sa résistance sismique. Il est fondé sur une ancienne mangrove avec un effet de site marqué à basse fréquence. La concordance des fréquences de résonance du sol et du bâtiment ont conduit à une sollicitation sismique forte qui a provoqué l'endommagement important (degré 3 EMS-98) du bâtiment. De nombreuses écoles ont été renforcées dans les Antilles suite au séisme de 2007.



**Figure 3.2** – *Enregistrements de vibrations ambiantes devant l'hôpital de la Trinité (Martinique).*

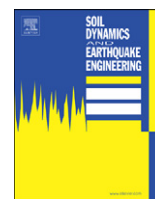
Si des enregistrements avant le séisme sont disponibles, il est particulièrement intéressant de regarder si des changements dans les caractéristiques modales ont eu lieu. C'est le cas pour les sols qui ont pu montrer un comportement non-linéaire, mais surtout pour les structures endommagées. Il faut toutefois être en mesure de différencier les variations dues à l'endommagement des variations naturelles par exemple dues à la température (p. ex. Clinton *et al.*, 2006). Nous avons comparé les spectres H/V avant et après le séisme près de l'hôpital de la Trinité sans observer de changement. En revanche, nous avons mis en évidence une baisse des fréquences de résonance du bâtiment sous vibrations ambiantes de l'ordre de 20% alors que les dommages observés était de degré 2 (dommages modérés) sur l'échelle de l'EMS-98 (Grünthal *et al.*, 2001). Une telle variation ne peut être due qu'à l'endommagement. Pour mémoire, le PGA enregistré à proximité par la station MATR était de l'ordre de  $1.5 \text{ m/s}^2$ . La baisse significative des fréquences de résonance montre que ce paramètre est très sensible aux dommages et peut être utilisé pour les quantifier (voir partie 3.3).



ELSEVIER

Contents lists available at SciVerse ScienceDirect

## Soil Dynamics and Earthquake Engineering

journal homepage: [www.elsevier.com/locate/soildyn](http://www.elsevier.com/locate/soildyn)

## Technical Note

## Contribution of ambient vibration recordings (free-field and buildings) for post-seismic analysis: The case of the Mw 7.3 Martinique (French Lesser Antilles) earthquake, November 29, 2007

J. Régnier<sup>a,\*</sup>, C. Michel<sup>c</sup>, E. Bertrand<sup>a</sup>, P. Guéguen<sup>b</sup><sup>a</sup> ERA "risque sismique", LRPC Nice, CETE Méditerranée, France<sup>b</sup> ISTERre, CNRS/IRD/IFSTTAR, Université Joseph Fourier, Grenoble 1, France<sup>c</sup> Swiss Seismological Service, ETH Zürich, Switzerland

## ARTICLE INFO

## Article history:

Received 15 January 2013

Received in revised form

11 March 2013

Accepted 13 March 2013

## Keywords:

Ambient vibrations

Site effect

Resonance

Post-earthquake survey

Damage

Martinique earthquake

## ABSTRACT

Following the Mw 7.3 Martinique earthquake, November 29<sup>th</sup>, 2007, a post-seismic survey was conducted by the Bureau Central Sismologique Français (BCSF) for macroseismic intensities assessment. In addition to the inventories, ambient vibration recordings were performed close to the particularly damaged zones in the free-field and the buildings. The objective of the paper is to show the relevancy of performing ambient vibration recordings for post-earthquake surveys. The analyses of the recordings aim at explaining the variability of the damages through site effects, structure vulnerability or resonance phenomena and to help the characterization of the post-seismic building integrity. In three sites prone to site effects, we suspect damage to be related to a concordance between soil fundamental frequency and building resonance frequency. Besides, the recordings of ambient vibrations at La Trinité hospital before and after the earthquake allow us to quantify the damage due to earthquake in terms of stiffness loss.

© 2013 Elsevier Ltd. All rights reserved.

## 1. Introduction

A large part of knowledge in the fields of earthquake engineering and engineering seismology has been accumulated during post-seismic surveys all around the world. These surveys have many different objectives: (1) estimate the buildings safety right after the earthquake, (2) characterize the ground motion by establishing macroseismic maps, (3) provide feedback for earthquake engineering by studying damage features and, eventually (4) help urban planning in defining zones with ground motion amplification and induced effects (liquefaction, landslides...). However, the knowledge of the structural damage causes is prior information necessary to relevantly reach these objectives. For a given deformation capacity, e.g. associated to a building class, damage will only depend on the building response to the ground motion. The building response depends on the incident seismic motion (that can be largely affected by the site response) and its representing parameters (maximal amplitude, frequency content...) with regard to the structure and its dynamic properties (e.g. [7]). Thus, two key parameters among those influencing the

seismic demand can be considered: (1) the resonance frequencies of the site and (2) the building resonance frequencies.

Seismic noise recordings in free-field and ambient vibration recordings in buildings are robust and low cost methods for estimating the soil and structure low-strain resonance frequencies. Since the 1990s and the widespread studies for site effects based upon the Horizontal to Vertical Noise Spectral Ratio (HVNSR), several papers have shown the relevancy of HVNSR to partially explain damage locations and/or grades (e.g. [1,9,14,29]). However, other studies show that HVNSR alone cannot be directly linked to damage distribution ([20,21,27,28],) and the damage variability can also be related to the building capacity rather than the site characteristics ([6]).

Besides, ambient vibration recordings in buildings have gained more and more interest for last decades, for earthquake engineering and civil engineering applications. The elastic fundamental frequency is a key-parameter in earthquake engineering for building response assessment (e.g. [18,19]) and structural health monitoring (e.g. [4,8]).

The joint approach (i.e. free-field and building investigation) can be relevant for post-seismic evaluation of the origin of the damage variability and building integrity. Gallipoli et al. [10], Gosar and Martinec [11] and Mucciarelli et al. [21,22] showed by ambient vibrations applications that soil–structure resonance could play a major role in damage location.

\* Correspondence to: CETE Méditerranée, 56 Boulevard de Stalingrad, 06359 Nice, France. Tel.: +33 492 008 157.

E-mail address: [julie.regnier@developpement-durbale.gouv.fr](mailto:julie.regnier@developpement-durbale.gouv.fr) (J. Régnier).

Following the 29th November 2007  $M_w=7.3$  Martinique earthquake, a post-seismic survey was set up to collect macroseismic data by the Bureau Central Sismologique Français in charge of the definition of the macroseismic intensities after earthquakes [26]. During this survey, the authors performed ambient vibration recordings in highly damaged zones.

The scope of this paper is to show a case study of the usefulness of the joint utilization of ambient vibration recordings in free-field and building to (1) improve the evaluation of the damages, (2) understand the origins of the damage variability by understanding the low-strain response of the soil and building and (3) show the relevancy of these information to complete a macroseismic study such as the one led by the BCSF.

## 2. Description of the case study

The 29th November 2007 Martinique earthquake occurred at rather great depth (152 km) with a moment magnitude of 7.3 [15] located in the northwest at 30 km of the island. The French Accelerometric network (RAP <http://www-rap.obs.ujf-grenoble.fr>, [23]) recorded ground motions due to the main shock in 34 stations in Martinique (Fig. 1). The horizontal Peak Ground Accelerations (PGA) is ranging from 0.3 to  $4 \text{ m s}^{-2}$  through the island. The local variability is large, e.g. in Fort-de-France from 0.4 to  $2 \text{ m s}^{-2}$  over several hundred meters, indicating the importance of local soil conditions. Macroseismic intensities using EMS98 ([12]) on the island were estimated between V and VI–VII (Fig. 1). We performed ambient vibration recordings in free-field and in buildings in three sites (Fig. 1), selected for the high level of structural damages compared to the macroseismic intensities estimated in the town.

*Site 1.* In Le Francois, damage due to the earthquake did not exceed grade 2 (EMS98) except for two school buildings, which suffered damage up to grade 3. The building A of Anne Marc school (Fig. 2) is a two-storey building with reinforced concrete (RC)

frames built in 1973 without earthquake-resistant design on ancient mangrove, sedimentary deposit prone to site effects [13]. It exhibits a low lateral stiffness in the longitudinal direction and a soft story at the ground floor. After the earthquake, we observed cracks at the bottom of several columns of the ground floor as well as numbers of cracks in partition walls and falls of mortar (damage grade 3 EMS98).

*Site 2.* In La Trinité, the AFPA buildings (E and H) were strongly damaged. Both structures, built in the 1970s without earthquake-resistant design, were studied but this paper focuses on building E. It is a two-storey building with RC frames and a soft ground floor (Fig. 2). This building is divided by thin filled joints into 4 L-shaped blocks, sensitive to torsion due to the eccentricity of the rigidities. Moreover, infill brick walls are not symmetrically distributed. It suffered slight structural damage (small cracks in columns at the ground floor) and moderate non-structural damage (large cracks in partition walls). According to soil studies during the construction, these buildings are founded on sedimentary deposits.

*Site 3.* The hospital of La Trinité is a RC infilled frames structure built in 1974. Excluding low-rise aisles, three high-rise blocks (called A, B and C) are respectively 9, 8 and 7 stories above the ground level and separated by 5 cm joints filled by Styrofoam (Fig. 2). After the earthquake, small cracks appeared in the structural system, larger cracks and plaster falls in the infill walls and false ceiling pieces fell down, associated to moderate damage (grade 2).

## 3. Experiments, processing and results

Ambient vibration recordings in free field and in structures were at least 15 min. long with seismometers (Lennartz 3D 5s and LITE) and a 24-bits Cityshark digitizer [5] at a sampling frequency of 150 Hz to 200 Hz. The N component of sensors, were oriented in one of the main direction of the studied building. The free-field recordings were analyzed using Horizontal to Vertical Noise Spectral Ratio (HVNSR) method where the Fourier Transforms of at least 30 s windows selected with an anti-triggering STA/LTA (Short Term Averaging, Long Term Averaging) algorithm are averaged and smoothed following Konno and Ohmachi [16] procedure ( $b=40$ ). The HVNSR is given by the ratio of the quadratic mean of the horizontal spectra by the vertical one and interpreted following the SESAME project recommendations [2]. If the SESAME criteria are fulfilled, the frequency of the peak is likely to be related to the fundamental frequency of the site.

Depending on the importance of the building, on the complexity of the structure and on the severity of the damages, one must adapt the experimental procedure. Ambient vibrations in buildings were recorded with one or two sensors simultaneously. Several processing techniques were used depending on the number and position of the recording points. For single station recordings at the building top, the Power Spectral Density (PSD) spectra have been estimated (square of the Fourier Transform amplitude) using the same procedure as for the ground without smoothing. Interpretation of these spectra in terms of building dynamic properties may be ambiguous and were done with caution. For simultaneous recordings at different points, the Frequency Domain Decomposition (FDD, [3]) is used as in Michel et al. [18]. Peaks in the first singular values can be interpreted as resonance frequencies and singular vectors as modal shapes. The knowledge of modal shapes is crucial for the interpretation of structural modes, but their quality depends on the number and position of recording points.

For both ground and structure, the resonance frequencies obtained from ambient vibration recordings are valid for low strains. During strong motion, nonlinear response of the soil

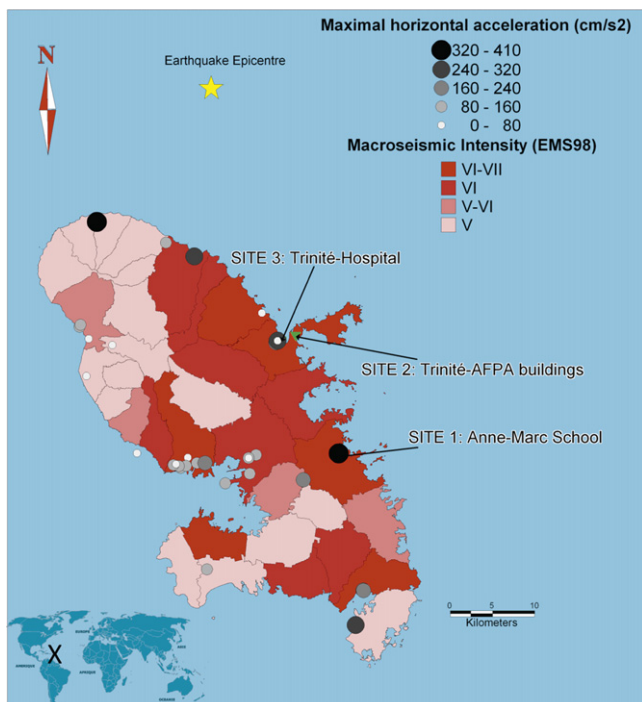


**Fig. 1.** Map of the macro seismic intensity at the Martinique island after the 28<sup>th</sup> November 2007 earthquake. The circles indicate the position of the RAP stations that recorded the earthquake (size scale is function of the maximal PGA on the three components in  $\text{cm/s}^2$ ), and location of the sites that were studied.

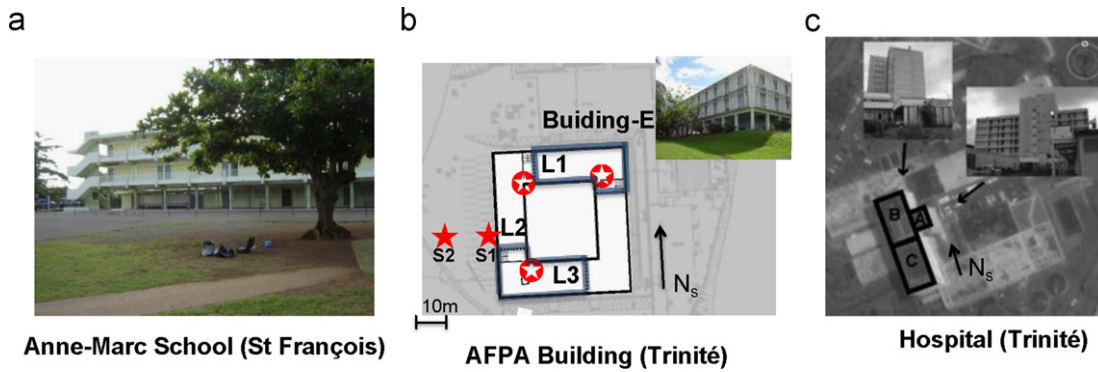


**Fig. 2.** (a) Site 1—location of the recordings performed at the Anne-Marc School in Le François. The building ambient vibration recording is performed at the second floor half length. (b) Site 2—AFPA Building E at the Trinité district. (c) Site 3—the La Trinité Hospital site (aerial view) with study-blocks A, B and C. The Sensors were oriented in the transverse direction of the buildings (the N component of the sensors is called  $N_s$ ).

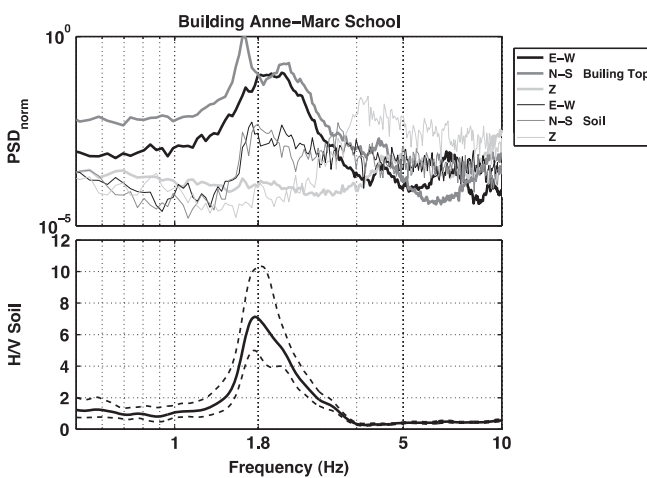


**Fig. 3.** Site 1—top: normalized Power Spectral Density of the recordings in the structure (solid lines) and the recordings in the soil (dashed lines) in the 3 directions East (E) North (N) and Vertical (Z). Bottom: HVNSR of the free field recording (mean, 16 and 84 percentiles).

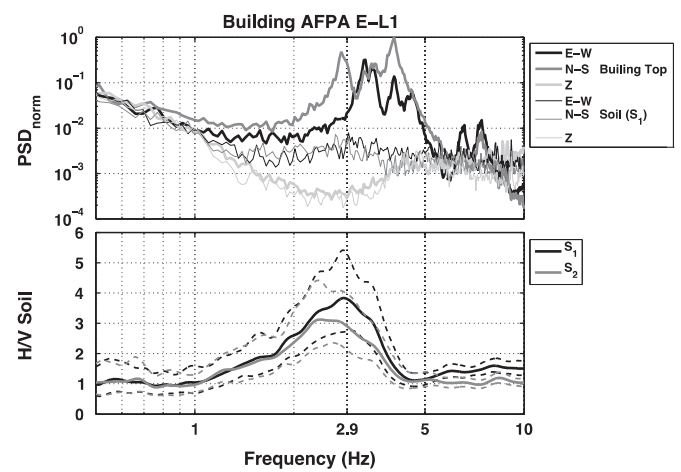


**Fig. 4.** Site 2—top: normalized Power Spectral Density of the recordings in the structure (solid lines) and the recordings in the soil (dashed lines) in the 3 directions East (E) North (N) and Vertical (Z). Bottom: HVNSR of the free field recording (mean, 16 and 84 percentiles).

(e.g. [25]), the building (e.g. [17]) and the soil–structure interaction can temporarily make the observed natural frequencies shifting to lower frequencies. Nonetheless, [24] showed that the frequencies variations due to nonlinear soil behavior were not relevant (during the l'Aquila earthquake for which acceleration up to 0.7 g were recorded) from building design standpoint. In this article, we study the link between damage and the similarity in the natural linear frequencies of the soil and the structure.

In the Anne Marc School (site 1), both soil and structure recordings were performed to evaluate and compare the soil and structure responses. The analysis of the recordings (Fig. 3) shows that the peak frequency of the HVNSR in free field (1.75 Hz) and the first peaks of the PSD in the structure in both directions (1.6 and 1.8 Hz in the longitudinal and transverse directions, respectively) are very close. It indicates that the structure is sensitive at low strain to the 1D resonance frequency of the soil and, thus, that a resonance between soil and structure eventually occurred during the Martinique earthquake, inducing higher damage.

In the AFPA building (site 2), the same procedure was followed but with more recording points. Free-field recordings were performed at different ground levels ( $S_1$ , 3 m from the building at the same level,  $S_2$ , 15 m from the building downhill, Fig. 2). Frequency peaks are clearly observed at 2.4 and 2.8 Hz in the HVNSR for  $S_1$  and  $S_2$ , respectively (Fig. 4), the difference of the frequencies being certainly due to the variation of the deposit thickness.

In three of the 4 L-shaped blocks of the building (named L1, L2 and L3), we recorded ambient vibrations simultaneously at the ground floor, the first and the second stories. The chosen sensor placement, however, did not allow to fully understand the dynamic behavior of the building. The fundamental modes appear between 2.7 and 4.3 Hz and include bending and torsion. These modes are quite close to the fundamental frequency of the ground found previously (2.4 to 2.8 Hz). However, the other AFPA building (building H), not detailed here, has higher resonance frequencies (3.5 to 4.5 Hz) and was therefore less prone to resonate with the ground but was more damaged than building E (damage grade 3) also with typical damage due to torsion. In this case, the design of the structure (lack of symmetry in the load bearing system) was therefore probably the main cause of damage during the earthquake.

Finally, in the hospital building (site 3), full-scale ambient vibration recordings have been performed several months before the event. After the Martinique earthquake, we recorded ambient vibrations in the building to analyze the evolution of its dynamic behavior related to damage.

As illustrated in Fig. 5, the soil at his site is prone to site effect with a clear peak at 2.4 Hz. The Fourier transform of the recordings at the top of the block A shows that the building resonance frequencies are close to the HVNSR peak around 2.5 Hz.

Data recorded in 93 points of the structure before the earthquake has been reprocessed using FDD technique [3] (Fig. 6).

In this dataset, two close clear peaks carried by the 2 first singular values indicate the presence of 2 modes around 2.5 Hz. The first mode at  $2.45 \pm 0.03$  Hz is the first longitudinal bending mode of the whole building (Fig. 6). The second mode at  $2.56 \pm 0.03$  Hz is

the first transverse bending mode of the structure. The modal shape indicates that these modes are partly coupled to torsion but with differences for each block. The amplitudes of the higher modes are lower and are not detailed here.

The PSD of the ambient vibration recordings in the structure at the same position before and after the earthquake have been calculated (Fig. 7). Assuming only a moderate frequency decrease, the knowledge of the pre-earthquake structural behavior allows interpreting the peaks of the post-earthquake recordings. The first longitudinal mode has shifted from  $2.45 \pm 0.03$  Hz to  $2.00 \pm 0.05$  Hz, i.e.  $18 \pm 4\%$  frequency drop. Moreover, the first transverse mode has shifted from  $2.56 \pm 0.03$  Hz to  $2.15 \pm 0.05$  Hz, i.e.  $16 \pm 4\%$  frequency drop. Dunand et al. [8] already used this technique at a larger scale after the Mw=6.8 Boumerdes, Algeria earthquake (May 21, 2003) and suggests a value of 40% frequency drop as a limit for the building to be impossible to retrofit (difference between orange and red classification). The observed damage is therefore noticeable but not critical as denoted by the assigned damage grade 2 EMS. However, such comparisons are still lacking in the literature to propose a relationship between frequency drop and damage grade.

Ambient vibration recordings in free field were as well performed before and after the earthquake. The soil fundamental frequency at 2.4 Hz is found to be the same. The resonance of the building before the earthquake (2.45 Hz for the first mode) is very close from the soil fundamental frequency. Resonance between the

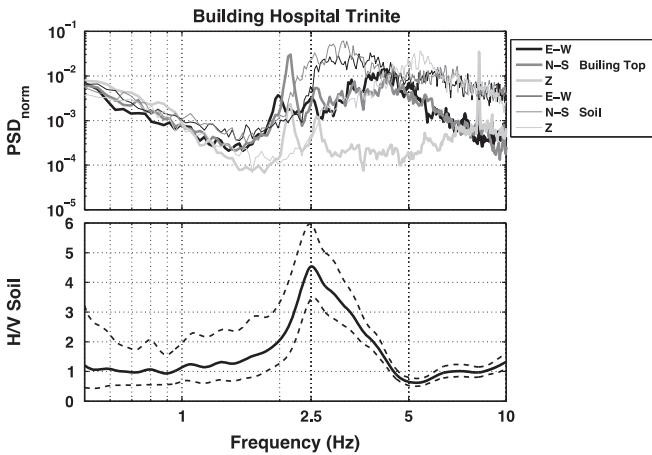


Fig. 5. Site 3—top: normalized Power Spectral Density of the recordings in the structure (solid lines) and the recordings in the soil (dashed lines) in the 3 directions East (E) North (N) and Vertical (Z) of the recording at the top of the block A. Bottom: HVNSR of the free field recording the mean, 16 and 84 percentiles.

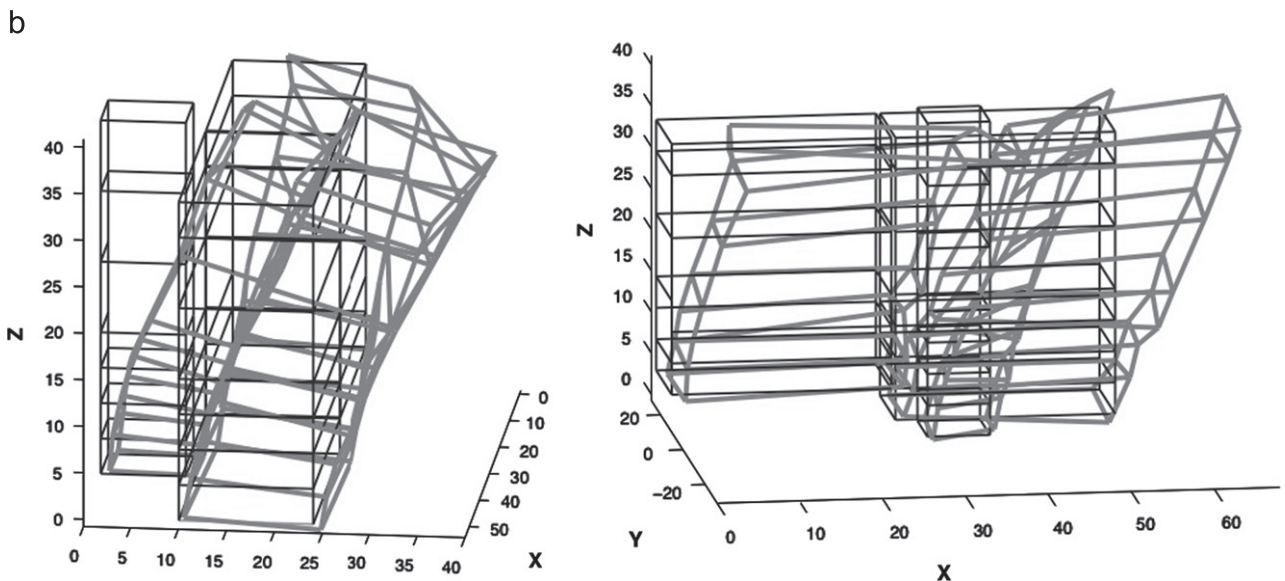
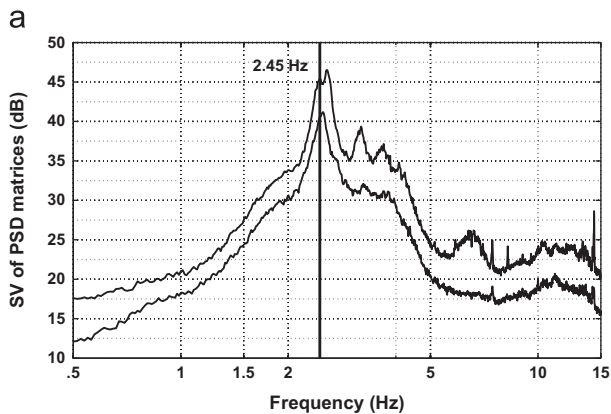


Fig. 6. Site 3—pre-earthquake modal analysis results. (a) FDD spectrum, (b) Modal shapes of the first transverse and longitudinal modes at 2.56 and 2.45 Hz, respectively.



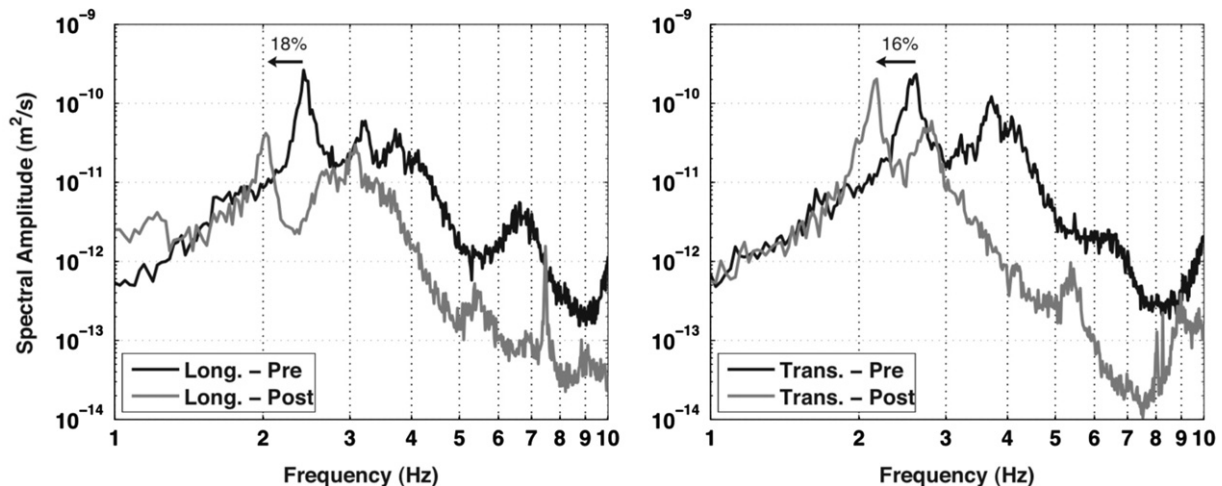


Fig. 7. Site 3—pre- and post-earthquake PSD spectra in block A in the longitudinal (left) and transverse (right) directions.

soil and the building response increased the seismic demand of the structure, which explains most probably the damage.

#### 4. Conclusions

Through these examples, we illustrated how to use ambient vibration recordings in soil and structure in post seismic survey. This approach helps to understand the possible causes of damaged zones distribution. Moreover, ambient vibrations recordings are low cost and can be rapidly set up after an earthquake.

With soil recordings, we investigated the possibility of soil to be prone to site effect. Link with damage is however not straightforward: site effect only increases the seismic demand around the soil resonance frequency. However, using both soil and structure recordings, the sensitivity of the structure to the 1D linear soil resonance can be checked. Thus, conclusions can be made on the possibility of having a resonance between soil and structure, which increases the seismic demand in the building and can induce higher damage.

In the three study-sites, the free field ambient vibration recordings indicate the occurrence of site effects. We found similarities between soil and structures resonance frequencies. It appears that resonance played a role in damage distribution.

In the La Trinité hospital, the fundamental frequency suffered a shift of 15–20% during the earthquake. Besides, the permanent frequency shift was related to a loss of stiffness of the structure that can be associated to a damage grade 2 EMS98. To analyze temporary frequency shift, structure permanent monitoring is necessary.

According to this case study, we can make some recommendations for the use of these recordings in post seismic survey. These recommendations should be adapted to the building importance, damage level and the objectives of the recordings. In our experience, such post-seismic survey should be focused on important buildings (importance class III and IV in Eurocode 8).

- Objective 1: Looking at potential concordance between soil and structure frequencies. In this case only one recording at the top of the structure and one on the free field (in the same geological context as the soil under the structure) are sufficient. Such measurements are interesting to understand the sources of damage. Analysis of such measurements could be used as one support (among others) to make decision on whether the building should be retrofitted (so as the resonance frequency of the building is different from the soil one).

- Objective 2: Having the modal shape associated to the predominant frequency. It requires simultaneous recordings at different storeys of the building. Such information could be very useful to constrain the numerical simulation of the dynamic behavior of the structure and to test retrofitted solutions. Besides it can also be used to evaluate the evolution of the damaged structure behavior during the aftershock sequences.
- Objective 3: Evaluate the stiffness loss of the structure and evaluate damage grade. It requires recordings at the top of the building before and after the earthquake. It is very useful in crisis management and is a support to emergency diagnosis of the building and visual screening of damages state. It is a quantitative measurement that is complementary to expert advises. Such measurements should be performed for high stake buildings of class IV in Eurocode 8.

For risk mitigation and to anticipate post earthquake crisis management, recordings of ambient vibrations should be performed in structures of high importance. Although permanent monitoring has a heavy cost, it should be considered for a small number of typical buildings.

#### Acknowledgments

This work has been supported by the ANR National Research Agency as part of its RiskNat program (URBASIS project, no. ANR-09-RISK-009). The authors thank Bertrand Pilot and Thierry Vassail (Bureau Veritas) who provided the pre-earthquake recordings in site 3.

#### References

- [1] Anderson JG, Bodin P, Brune JN, Prince J, Singh SK, Quaaas R, et al. Strong ground motion from the Michoacan, Mexico, earthquake. *Science* 1986;233(4768):1043–9.
- [2] Bard PY and SESAME participants. Guidelines for the implementation of the H/V spectral ratio technique on ambient vibrations: measurement, processing and interpretation, (<http://sesame-fp5.obs.ujf-grenoble.fr>); 2004.
- [3] Brincker R, Zhang L, Andersen P. Modal identification of output-only systems using Frequency Domain Decomposition. *Smart Materials and Structures* 2001;10:441–5.
- [4] Carden PE, Fanning P. Vibration based condition monitoring: a review. *Structural Health Monitoring* 2004;3(4):355–77.
- [5] Chatelain JL, Guéguen P, Guillier B, Fréchet J, Bondoux F, Sarrault J, et al. Cityshark: a user-friendly instrument dedicated to ambient noise (microtremor) recording for site and building response studies. *Seismological Research Letters* 2000;71(6):698–703.

- [6] Chatelain JL, Guillier B. False site effects: The Anjar Case, following the 2001 Bhuj (India) earthquake. *Seismological Research Letters* 2008;79(6):816–9.
- [7] Clough RW, Penzien J. *Dynamics of structures*. New York: McGraw-Hill; 1993.
- [8] Dunand F, Ait Meziane Y, Guéguen P, Chatelain JL, Guillier B, Ben Salem R, et al. Utilization du bruit de fond pour l'analyse des dommages des bâtiments de Boumerdès suite au séisme du 21 mai 2003. *Bulletin du Service Géologique de l'Algérie* 2004;12:177–91.
- [9] Duval A-M, Bertrand, E, Vidal, S. Combined survey of site effects and damage in Les Saintes, Guadeloupe. In: *Proceedings of the third international symposium on the effects of surface geology on seismic motion*. Grenoble; 2006.
- [10] Gallipoli MR, Mucciarelli M, Castroc RR, Monachesi G, Contrie P. Structure, soil–structure response and effects of damage based on observations of horizontal-to-vertical spectral ratios of microtremors. *Soil Dynamics and Earthquake Engineering* 2004;24:487–95.
- [11] Gosar A, Martinec M. Microtremor HVSR study of site effects in the Ilirska Bistrica Town Area (S. Slovenia). *Journal of Earthquake Engineering* 2009;13(1):50–67.
- [12] Grünthal G, Musson, RMW, Schwarz, J, Stucchi, M. *European Macroseismic Scale 1998*, EMS-98. Luxembourg; 1998.
- [13] Guéguen P, Langlais M, Foray P, Rousseau C, Maury J. A natural seismic isolating system: the buried mangrove effects. *Bulletin of the Seismological Society of America* 2011;101(3):1073–80.
- [14] Guéguen P, Chatelain J-L, Guillier B, Yepes H, Egred J. Site effect and damage distribution in Pujili (Ecuador) after the 28 March 1996 earthquake. *Soil Dynamics and Earthquake Engineering* 1998;17:329–34.
- [15] Guéguen P. Experimental analysis of the seismic response of one base-isolation building according to different levels of shaking: example of the Martinique earthquake (2007/11/29) Mw 7.3. *Bulletin of Earthquake Engineering* 2012;10(4):1285–98.
- [16] Konno K, Ohmachi T. Ground motion characteristics estimated from spectral ratio between horizontal and vertical components of microtremor. *Bulletin of the Seismological Society of America* 1998;88(1):228–41.
- [17] Michel C, Guéguen P. Time–frequency analysis of small frequency variations in civil engineering structures under weak and strong motions using a reassignment method. *Structural Health Monitoring* 2010;9(2):159–71.
- [18] Michel C, Guéguen P, El Arem S, Mazars J, Kotronis P. Full scale dynamic response of a RC building under weak seismic motions using earthquake recordings, ambient vibrations and modelling. *Earthquake Engineering and Structural Dynamics* 2010;39(4):419–41.
- [19] Michel C, Guéguen P, Lestuzzi, P, Bard P-Y. Comparison between seismic vulnerability models and experimental dynamic properties of existing buildings in France. *Bulletin of Earthquake Engineering* 2010;8(6):1295–307.
- [20] Mucciarelli M, Monachesi G. A quick survey of local amplifications and their correlation with damage observed during the Umbro-Marchesan (Italy) earthquake of September 26, 1997. *Journal of Earthquake Engineering* 1998;2(2):325–37.
- [21] Mucciarelli M, Monachesi G. The Bovec (Slovenia) earthquake, April 1998: preliminary quantitative association among damage, ground motion amplification and building frequencies. *Journal of Earthquake Engineering* 1999;3(3):317–27.
- [22] Mucciarelli M, Bianca M, Ditommaso R, Gallipoli MR, Masi A. Far field damage on RC buildings: the case study of Navelli during the L'Aquila (Italy) seismic sequence, 2009. *Bulletin of Earthquake Engineering* 2010;9(1):263–83.
- [23] Péquegnat C, Guéguen P, Hatzfeld D, Langlais M. The French Accelerometric Network (RAP) and National Data Centre (RAP-NDC). *Seismological Research Letters* 2008;79(1):79–89.
- [24] Puglia, R, Ditommaso, R, Pacor, F, Mucciarelli, M, Luzi, L, Bianca M. Frequency variation in site response as observed from strong motion data of the L'Aquila (2009) seismic sequence; 2011.
- [25] Régnier, J, Cadet, H, Bonilla, F-L, Bertrand, E, Semblat, J-F. Assessing nonlinear behavior of soils in seismic site response: statistical analysis on KiK-net strong motion data. *Bulletin of Seismological Society of America* 2013;103(3).
- [26] Schlupp A, Sira, C, Cara, M, Bazin, S, Michel, C, Régnier, J, et al. Séisme de Martinique du 29 novembre 2007, rapport du BCSF: synthèse sismologique et étude macrosismique, BCSF2008-R1, 132p, 266 fig, 3 tableaux, 5 annexes; 2008 [in French].
- [27] Tertulliani A, Leschiutta I, Bordonni P, Milana G. Damage distribution in L'Aquila City (Central Italy) during the 6 April 2009 earthquake. *Bulletin of the Seismological Society of America* 2012;102(4):1543–53.
- [28] Trifunac MD, Todorovska MI. Long period microtremors, microseisms and earthquake damage: Northridge, CA, earthquake of 17 January 1994. *Soil Dynamic and Earthquake Engineering* 2000;19(4):253–67.
- [29] Theodoulidis N, Cultrera G, De Rubeis V, Cara F, Panou A, Pagani M, et al. Correlation between damage distribution and ambient noise H/V spectral ratio: the SESAME project results. *Bulletin of Earthquake Engineering* 2008;6:109–40.

### 3.3 Analyse post-sismique rapide grâce à l'instrumentation de bâtiments (Goulet *et al.*, 2015)

A la suite d'un tremblement de terre, même modéré, le doute sur la stabilité des bâtiments endommagés conduit à leur évacuation préventive. Ils ne peuvent être réintégrés qu'une fois qu'un expert ou un groupe d'experts, mandaté par les autorités, a examiné le bâtiment et l'a jugé sûr. Cette sûreté est relative, car une analyse sismique telle qu'elle peut être réalisée hors temps de crise est exclue, car trop coûteuse en temps et en personnel, compte tenu du grand nombre de structures à traiter. Les experts se prononcent donc sur la perte de la résistance sismique de la structure par rapport à son état initial, et donc sa capacité à résister à des secousses moins fortes que le choc principal (répliques). Ils se concentrent donc uniquement sur le niveau de dommage, en particulier de la structure porteuse. Une analyse comporte en général les éléments suivants :

- Importance du bâtiment (utilisation, nombre d'occupants...)
- Vulnérabilité initiale du bâtiment (dimensions, type de structure porteuse, répartition des éléments porteurs...)
- Dangers secondaires (effets géotechniques, désordres sur les réseaux - eau, gaz, électricité -, menace des structures alentour...)
- Dommages à la structure porteuse et aux éléments non-structuraux
- Décision sur l'habitabilité et mesures de sécurité à prendre

Les photos sur la Fig. 3.3 montrent le bien-fondé du périmètre de sécurité (ignoré par le personnage) mis en place suite à l'analyse post-sismique d'une église après le choc principal du séisme d'Emilie-Romagne en 2012. Les experts avaient observé le détachement de la façade (photo a) qui s'est poursuivi jusqu'à l'effondrement du fronton lors de la réplique intervenant quelques jours plus tard (photo b).



**Figure 3.3** – Eglise à Tramuschio (Emilie-Romagne, Italie) (a) suite au séisme du 20 mai 2012 et (b) après la réplique du 29 mai (Photos T. Wenk).

Cette expertise de plusieurs heures pour une structure demande du temps et du personnel qualifié. Le coût des structures non-analysées est également élevé, d'un point de vue humain et financier : d'une part les habitants doivent être relogés tant que leurs habitations ne sont pas analysées, d'autre part les entreprises ne peuvent pas fonctionner (y compris pour la reconstruction) tant que leurs

locaux professionnels ne sont pas sûrs. L'Office Fédéral de Protection de la Population suisse souhaite que cette analyse puisse être conduite par des praticiens du génie civil quel que soit leur niveau de formation (maçons. . .) en raison du faible nombre d'ingénieurs qualifiés dans le pays, alors que la plupart des pays confie cette tâche à des ingénieurs et architectes. La question de la formation préalable de ces professionnels est également cruciale. J'ai ainsi donné en 2013 avec la Société Suisse du Génie Parasismique et de la Dynamique des Structures (SGEB) une formation d'analyse de l'habitabilité post-sismique pour les experts des assurances de la compagnie GVB (Berne).

Dans Goulet *et al.* (2015) nous soutenons l'idée que cette problématique peut être traitée en partie à l'aide de l'instrumentation des structures et d'algorithmes de décision fondés sur des données *in situ*. Les structures de génie civil sont de plus en plus équipées de capteurs intégrés, par exemple des jauges de déformation dans les tabliers de ponts (voir l'article de revue de Smith, 2016). L'avènement d'accéléromètres à bas coût basés sur des microsystèmes électromécaniques (MEMS) et de nano-ordinateurs bon marché (de type *Raspberry Pi*) permettra bientôt d'équiper à grande échelle les bâtiments en stations accélérométriques et même d'enregistrer leurs vibrations ambiantes. Ce type d'instrumentation permettra non-seulement l'étude de la sécurité suite à un séisme, mais aussi le suivi des structures (effet du vieillissement, d'événements climatiques etc.). En Californie, les bâtiments de 10 étages et plus doivent déjà être instrumentés par un accéléromètre.

Dans cet article, nous assimilons la sécurité post-sismique à un niveau de dommage atteint par la structure. L'un des moyens de quantifier ce niveau de dommage est d'étudier la baisse de fréquence avant et après l'événement sous vibrations ambiantes, comme nous l'avons fait dans Régnier *et al.* (2013) (voir partie 3.2). Nous supposons que les capteurs en place dans une ville, par exemple San Francisco, nous permettent d'avoir accès à ces données avant et après un séisme. Nous avons réalisé une revue de littérature montrant les données disponibles avant et après séisme. Si la corrélation entre baisse de fréquence et niveau de dommage est évidente, l'incertitude liée à cette relation l'est aussi. La quantité de données actuellement disponible est trop faible pour pouvoir déterminer une relation prenant en compte le type de bâtiment, les spécificités locales de la construction, etc. Nous proposons donc un algorithme fondé sur une approche bayésienne permettant d'apprendre cette relation entre baisse de fréquence et dommage, à partir de quelques expertises réalisées sur place. L'objectif n'est donc pas de remplacer les experts, mais d'accélérer et de valoriser leur travail. Il est très important que l'algorithme évite les faux-positifs (bâtiments jugés sûrs mais qui ne le sont pas), alors que les faux-négatifs sont moins problématiques. L'algorithme proposé permet, avec environ 5% de structures visitées par les experts, de déterminer la sécurité de près de 50% des structures considérées. Par ailleurs, il peut facilement être relancé suite à une réplique, évitant aux experts un deuxième passage. Enfin, cet algorithme peut s'appliquer à d'autres indicateurs de dommage pouvant être mesurés, comme la déformation inter-étage, et même les combiner.

# Data-driven post-earthquake rapid structural safety assessment

J. A. Goulet<sup>\*,†1</sup>, C. Michel<sup>2</sup> and A. Der Kiureghian<sup>1</sup>

<sup>1</sup>*Department of Civil and Environmental Engineering, University of California, Berkeley, Berkeley, CA, USA*

<sup>2</sup>*Swiss Seismological Service, ETH Zurich, Zurich, Switzerland*

## SUMMARY

Earthquake-prone cities are exposed to important societal and financial losses. An important part of these losses stems from the inability to use structures as shelters or for generating economic activity after the event of an earthquake. The inability to use structures is not only due to collapse or damage; it is also due to the lack of knowledge about their safety state, which prohibits their normal use. Because a diagnosis is required for thousands of structures, city-scale safety assessment requires solutions that are economically sustainable and scalable. Data-driven algorithms supported by sensing technologies have the potential to solve this challenge. Several ambient vibration monitoring studies of buildings, before and after earthquakes, have shown that the extent of damage in a building is correlated with a decrease in the natural frequency. However, the observed worldwide data may not be representative of specific cities due to factors such as construction type, quality, material, and age. In this paper, we propose a framework that is able to progressively learn the relationship between frequency shift and damage state as a small number of buildings in a city are inspected after an earthquake, and to use that information to predict the safety state of uninspected but monitored buildings. The capacity of the proposed framework to learn and perform prognosis is validated by applying the methodology to a city with 1000 buildings having simulated frequency shifts and damage states. Copyright © 2015 John Wiley & Sons, Ltd.

Received 24 January 2014; Revised 8 August 2014; Accepted 20 November 2014

KEY WORDS: resilience; earthquake; safety; statistical learning; sensors; condition assessment

## 1. INTRODUCTION

Earthquake-prone cities are exposed to important societal and financial losses. A part of these losses is attributed to the inability to use structures as shelters or for generating economic activity after the event of an earthquake. The inability to use structures is not only due to collapse or damages; it is also due to the lack of knowledge about their safety state, which prohibits their normal use. When relying on qualified inspectors alone, inspecting structures at the scale of a city can take weeks, if not months (e.g. [1]). Not knowing the safety of buildings might force people out of their homes and companies out of business, further delaying the recovery and adding to the societal and economic impact of the earthquake. Several countries have developed procedures for visual inspection for post-earthquake assessment of buildings, for example, the USA [2], Italy [3], and New Zealand [4]. The main challenge for inspectors is to state if a building can withstand aftershocks without performing a detailed seismic analysis.

Because a diagnosis is required for thousands of structures, city-scale safety assessment requires solutions that are economically sustainable and scalable. An alternative to using inspections alone is to employ sensors to monitor characteristic structural responses that are related to damage [5, 6]. In the earthquake engineering community, the inter-story drift computed from strong-motion monitoring is a

\*Correspondence to: J. A. Goulet, Department of Civil and Environmental Engineering, University of California, Berkeley, Berkeley, CA, USA.

†E-mail: james.a.goulet@gmail.com

common damage parameter [5]. Researchers have proposed alternative approaches to post-earthquake safety assessment using either models-based approaches, for example, [7–9], or vibration-based condition monitoring [6, 10, 11]. In this paper, in order to obtain an economically sustainable and scalable solution, we choose not to rely on models of the structures studied. Also, we use the shift in the natural frequency computed from ambient vibration measurements as the damage parameter. This choice is motivated by the increasing interest and ease in ambient vibration monitoring and the amount of existing data.

As early as in 1922, Omori [12] showed that the damage caused by an earthquake affected the natural frequencies of a building. Since then, several ambient vibration monitoring (AVM) studies of buildings, before and after an earthquake, have confirmed Omori's observation [13–17]. These experimental studies are further described in Section 2. When taken alone, existing data are not sufficient to support post-earthquake safety assessment applications where lives and billions of dollars worth of infrastructure are involved. This is in part because the relationship between the natural frequency shift and observed damage may not be representative of specific cities due to factors such as construction type, quality, material, and age. A solution to this challenge is to use statistical techniques capable of learning the relationship between damage and frequency shift, as structures in the city are inspected after an earthquake.

In this paper, we propose a framework that is able to learn and predict, at the scale of a city, the safety state of structures based on observed shifts in the frequencies and a limited number of inspections. Section 2 reviews a collection of experimental investigations, reporting shifts in the frequencies of buildings before and after an earthquake and the corresponding identified damage states. Section 3 presents the statistical learning and prognosis methodologies in two parts. The first part consists in progressively learning, as inspections are performed, the conditional probability of observing a frequency shift given the damage state of a structure. The second part consists in using the learned relationship and observed frequency shifts to predict the safety state of the population of uninspected buildings. Section 4 describes how the proposed methodology can be integrated into a city-scale structural health monitoring framework for post-earthquake rapid structural safety assessment. Finally, Section 5 uses simulated data to validate the capacity of the proposed method to learn and predict the safety state of buildings at the scale of a city.

## 2. COLLECTION AND CHARACTERIZATION OF EXISTING DATA

### 2.1. Ambient vibration monitoring and safety state classification

Ambient vibration monitoring (AVM) consists in recording the natural vibrations of a structure, mostly because of ground ambient vibrations (or seismic noise) or wind (e.g. [18]). Assuming input vibrations are broad band, observed resonance peaks in the Fourier transform of the structural response correspond to its natural frequencies. These frequencies characterize the state of the structure, including those of the load-bearing system and stiff nonstructural elements, and the effect of soil–structure interaction. In the next section, we review a collection of existing AVM experimental studies reporting the frequencies of buildings before and after an earthquake. Neither strong-motion recordings nor laboratory tests are selected, because the observed modal properties under these conditions can be substantially different from those recorded for real structures under ambient vibrations. We wish to relate the frequency shift to the observed damage in the corresponding buildings. One challenge is that existing studies did not all use a common metric for damage.

For loss estimation, it is common to use discrete or continuous damage scales that can be related to visual inspections. Hill and Rossetto [19] reviewed several damage scales, highlighting the advantages and disadvantages of each scale. For post-earthquake safety assessment, a three-grade scale designated by color coding (green, yellow/orange, and red) is generally used. The Applied Technology Council guidelines ATC-20 [2], has defined them as follows:

- green: “no restriction on use or occupancy”
- yellow: “limited entry, entry is permitted only by the owner for emergency purposes, at his or her own risk”
- red: “unsafe, the structure poses an obvious safety hazard”

In this study, we employ the European Macroseismic Scale (EMS) 98 [20] damage scale to conform with the scale used by most of the available datasets described in the following section. This scale has 5 damage indices (1 to 5) plus index 0 for no damage. Up to damage index 1, the building is classified as *safe*. Buildings with damage indices 2 and above are classified as *unsafe*; these buildings do not meet the conditions for normal occupancy. For the purpose of this paper, we also define a subclass labeled *marginally unsafe* to designate unsafe buildings for which restricted entrance may be allowed; this subclass corresponds to damage indices 2 and 3. In terms of the color designations described earlier, an approximate mapping is *green* = {0, 1}, *yellow* = {2, 3}, and *red* = {4, 5}.

## 2.2. Existing datasets

The earliest data used are the ambient vibration experiment conducted by F. Omori on the Marunouchi building in Tokyo, Japan, before and after the 1922 earthquake [12]. This building was a steel-brick structure and suffered moderate damage (diagonal cracks in curtain walls) that is classified as damage index ( $d$ ) 2.

Another building is the Millikan Library on the campus of the California Institute of Technology in Pasadena. Clinton *et al.* [13] reviewed tests performed on this building, which has experienced several earthquakes. The building is a shear wall reinforced concrete (RC) structure. During the 1970 San Fernando earthquake, slight structural damage was noted [13], corresponding to  $d = 2$ . The building was subsequently repaired. No evidence of damage was found after the 1987 Whittier Narrows, 1991 Sierra Madre, 1994 Northridge, and 2001 Beverly Hills earthquakes ( $d = 0$  assumed), although slight frequency shifts were observed.

In Italy, Mucciarelli *et al.* [15] recorded ambient vibrations before and after a damaging aftershock of the 2002 Molise earthquake on an RC frame structure in Bonefro. The building was already damaged ( $d = 3$ ) because of the mainshock and suffered additional damage ( $d = 4$ ) during the recorded aftershock.

In Algeria, Dunand *et al.* [14] and Dunand [21] recorded ambient vibrations in several buildings after the 2003 Boumerdès earthquake. Because the frequencies of similar undamaged buildings were measured, they were considered by the authors to represent the states of the damaged buildings before the earthquake. Dunand *et al.* [14] reported the damage classification by the local inspectors following the color-coded damage scale presented in Section 2.1. These damage indices were transferred into the EMS98 using original pictures provided by Dunand. Six 5-story RC frame structures were moderately to heavily damaged, four 5-story RC shear wall buildings sustained lighter damage, and four 10-story RC shear wall buildings experienced moderate damage. The last three groups of buildings, as well as the building studied by Mucciarelli *et al.* [15], were already damaged when the earthquake occurred. Therefore, for these buildings, the frequency shifts before and after the earthquake are considered as lower-bound observations for the corresponding total frequency shifts.

The La Trinité Hospital in Martinique (French Lesser Antilles) was studied by Régnier *et al.* [16] before and after the 2007 moderately damaging earthquake. This structure was an irregular RC frame structure with 9 stories and suffered damage up to  $d = 2$ . Finally, the most extensive dataset comes from a recent study by Vidal *et al.* [17]. It consists in 34 RC frame buildings with 2 to 13 stories from Lorca, Spain, with ambient vibration recordings performed before and after the 2010 earthquake. Damage indices ranging from 1 to 4 were estimated by Vidal *et al.* [17].

Figure 1 summarizes the results of the previous studies. It shows the frequency shifts  $x$  expressed as the ratio of the post-earthquake and pre-earthquake frequencies of the building. Frequencies used are the larger of the two frequency shifts recorded in the longitudinal and transverse directional modes, and the corresponding damage index for 45 buildings. Arrowheads indicate lower-bound observations of frequency shifts. Note that a lower-bound observation for a frequency shift corresponds to an upper-bound observation for  $x$ .

A clear relationship between the frequency shift and damage index is noticeable within and across the datasets. This collection of data is used in Section 5 to characterize the conditional probability density function (PDF) of observing a frequency shift given the damage index. The PDF is subsequently used to simulate frequency shifts and damage indices for the population of buildings in a city. The simulated data are then used to validate the learning and prognosis capacity of the proposed methodology.

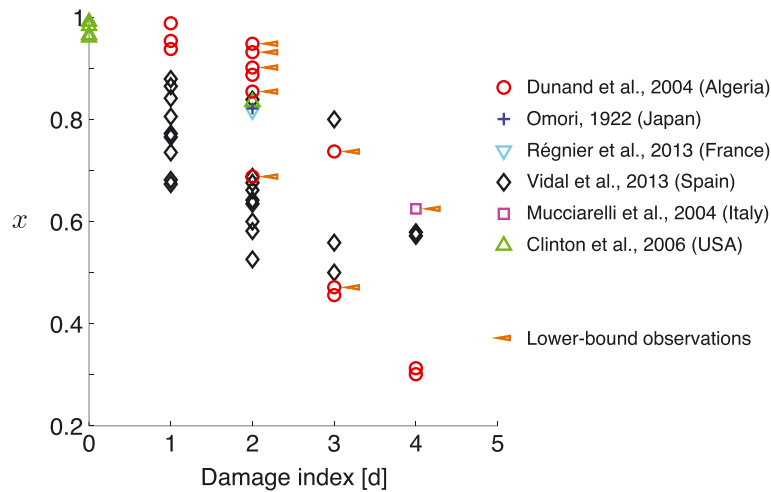


Figure 1. Collection of existing datasets reporting the corresponding frequency shifts  $x$  expressed as the ratio of the post-earthquake and pre-earthquake frequencies of the building, and damage index data obtained from AVM experiments and visual inspections. Arrowheads indicate lower-bound observations of frequency shifts.

### 3. DATA-DRIVEN LEARNING AND PROGNOSIS

The methodology proposed in this paper is divided into two parts: First, by using data for a collection of  $n$  buildings with known damage indices and frequency shifts, we learn about the conditional PDF of the frequency shift given the damage index. Second, for each uninspected building, we compute the probability that the building has a specific damage index given the observed frequency shift after an earthquake.

#### 3.1. Data-driven learning

Let  $D \in \{0, \dots, 5\}$  denote a discrete random variable representing the damage index of a building after an earthquake. The domain of  $D$  is based on the EMS98 damage scale presented in Section 2.1. Also let  $X \in (0, 1)$  denote a continuous random variable, describing the ratio of the post-earthquake and pre-earthquake frequencies. The range of possible values of  $X$  is determined by assuming that structural frequencies are strictly positive, and that damage can only decrease the frequency of a building. We consider  $D$  and  $X$  as dependent variables so that  $f_{X|D}(x|d)$  is the conditional PDF of  $X$  given  $D = d$  and  $p_{D|X}(d|x)$  is the conditional probability mass function of  $D$  given  $X = x$ . For the conditional PDF of  $X$ , we employ the beta distribution:

$$f_{X|D}(x|d) = \frac{x^{a(d)-1}(1-x)^{b(d)-1}}{B(a(d), b(d))} \tag{1}$$

where  $\{a(d), b(d)\}$  are the conditional shape parameters to be estimated and  $B(\cdot, \cdot)$  is the beta function. This choice of distribution is motivated by the physical constraints on the frequency ratio  $X$ . The conditional mean,  $\mu(d)$ , and conditional standard deviation,  $\sigma(d)$ , of  $X$  are related to the shape parameters by

$$\mu(d) = \frac{a(d)}{a(d) + b(d)} \tag{2}$$

and

$$\sigma(d) = \left( \frac{a(d)b(d)}{(a(d) + b(d))^2(a(d) + b(d) + 1)} \right)^{1/2} \tag{3}$$



We learn the joint posterior PDF of  $\mu(d)$  and  $\sigma(d)$  by using data on  $n$  buildings for which the frequency shifts and corresponding damage indices,  $(\hat{x}_j, d_j)$ ,  $j = 1, \dots, n$ , are observed. Considering that the true frequency shift for the  $j$ th building is  $X_j \in (0, 1)$ , we assume  $X_j \sim f_{X_j}(x)$  has a beta distribution with mean  $\hat{x}_j$  and known standard deviation  $\sigma_j$ . The corresponding parameters of the distribution,  $a_j$  and  $b_j$ , are obtained in terms of  $\hat{x}_j$  and  $\sigma_j$  by inverting relations similar to Equations 2 and 3. The damage indices  $d_j$  are assumed to consist in error-free observations. The joint posterior PDF of  $\mu(d)$  and  $\sigma(d)$  is computed from Bayes rule

$$f''(\mu(d), \sigma(d)) \propto \mathcal{L}(\mu(d), \sigma(d)) f'(\mu(d), \sigma(d)) \tag{4}$$

where  $\mathcal{L}(\cdot, \cdot)$  is the likelihood function and  $f'(\cdot, \cdot)$  is the prior distribution. The likelihood function  $\mathcal{L}(\mu(d), \sigma(d))$  is computed from  $\mathcal{L}(a(d), b(d))$  using Equations 2 and 3. The latter is the likelihood function for the parameters  $\{a(d), b(d)\}$  and, assuming observations are statistically independent, is given by

$$\mathcal{L}(a(d), b(d)) \propto \prod_{j=1}^n \mathcal{L}_j(a(d_j), b(d_j)) \tag{5}$$

where  $\mathcal{L}_j(a(d_j), b(d_j))$  is the likelihood for the  $j$ th observation. When the frequency shift is directly observed, the likelihood is given by

$$\begin{aligned} \mathcal{L}_j(a(d_j), b(d_j)) &\propto \int_0^1 f_{X|D}(x|d_j) f_{X_j}(x) dx \\ &\propto \int_0^1 \frac{x^{a(d_j)-1} (1-x)^{b(d_j)-1}}{B(a(d_j), b(d_j))} \cdot \frac{x^{a_j-1} (1-x)^{b_j-1}}{B(a_j, b_j)} dx \end{aligned} \tag{6}$$

where  $f_{X_j}(x)$  is the beta PDF of  $X_j$ . When the observed value is a lower bound of the frequency shift, such as the observations marked by an arrowhead in Figure 1, the conditional PDF  $f_{X|D}(x|d)$  in the previous expression is replaced by the complement of corresponding conditional CDF, that is,  $1 - F_{X|D}(x|d)$ .

We assume that no prior information about parameters  $\{\mu(d), \sigma(d)\}$  is available, except for the constraint that  $\mu(0) > \mu(1) > \dots > \mu(5)$ . These constraints on the mean represent our domain-specific knowledge, whereas we expect the mean frequency ratio to be decreasing with increasing values of  $d$ . Thus, using diffuse priors for  $\mu(d)$  in the applicable domain and non-informative priors proportional to  $1/\sigma(d)$  for  $\sigma(d)$ , the posterior distribution of all 12 parameters  $\{\mu(d), \sigma(d), d = 0 : 5\}$  is given by

$$f''(\mu(0), \sigma(0), \dots, \mu(5), \sigma(5)) \propto \frac{\mathcal{L}(\mu(0), \sigma(0))}{\sigma(0)} \dots \frac{\mathcal{L}(\mu(5), \sigma(5))}{\sigma(5)}, \quad \mu(0) > \dots > \mu(5) \tag{7}$$

Note that  $\sigma(d)$  terms are not coupled in the previous equation. However, the  $\mu(d)$  terms are coupled through the boundary of their applicable domain. To find the posterior distribution  $f''(\mu(d), \sigma(d))$  for a particular  $d$ , we integrate Equation (7) over the parameters  $\{\mu(k), \sigma(k)\}$  for all  $k \neq d$ :

$$\begin{aligned} f''(\mu(d), \sigma(d)) &\propto \frac{\mathcal{L}(\mu(d), \sigma(d))}{\sigma(d)} \prod_{k < d} \int_{\mu(k+1)}^1 \int_0^\infty \frac{\mathcal{L}(\mu(k), \sigma(k))}{\sigma(k)} d\sigma(k) d\mu(k) \\ &\dots \prod_{d < k} \int_0^{\mu(k-1)} \int_0^\infty \frac{\mathcal{L}(\mu(k), \sigma(k))}{\sigma(k)} d\sigma(k) d\mu(k) \end{aligned} \tag{8}$$

Let  $F(\mu(d))$  denote the posterior marginal CDF of  $\mu(d)$  if each  $\mu(d)$  is assumed to have a diffuse prior over  $(0, 1)$ . This is equivalent to neglecting the constraint  $\mu(0) > \mu(1) > \dots > \mu(5)$ , in which case, the pairs of parameters  $\{\mu(d), \sigma(d)\}$  are statistically independent for different  $d$  values so that

$$F(\mu(d)) \propto \int_0^{\mu(d)} \int_0^\infty \frac{\mathcal{L}(\mu(d), \sigma(d))}{\sigma(d)} d\sigma(d) d\mu(d) \quad (9)$$

It follows that

$$f''(\mu(d), \sigma(d)) \propto \frac{\mathcal{L}(\mu(d), \sigma(d))}{\sigma(d)} \prod_{k < d} (1 - F(\mu(k))) \prod_{d < k} F(\mu(k)) \quad (10)$$

When  $d = 0$ , the second product term drops out, whereas when  $d = 5$ , the first product term drops out.

### 3.2. Data-driven prognosis

Suppose that we compute from measurements the ratio of the post-earthquake and pre-earthquake frequencies  $X$  for a building after an earthquake. The updated distribution of  $D$  for the building is

$$p_{D|X}(d|x) = \frac{\tilde{f}_{X|D}(x|d)p_D(d)}{\tilde{f}_X(x)} = \frac{\tilde{f}_{X|D}(x|d)p_D(d)}{\sum_{d=0}^5 \tilde{f}_{X|D}(x|d)p_D(d)} \quad (11)$$

where  $p_D(d)$  is the prior probability mass function of  $d$  and  $\tilde{f}_{X|D}(x|d)$  is the predictive conditional distribution of  $X$  given  $D = d$ , which incorporates the uncertainty in the estimation of the parameters  $\mu(d)$  and  $\sigma(d)$  and the latter is given by

$$\tilde{f}_{X|D}(x|d) = \int_{\mu(d)} \int_{\sigma(d)} f_{X|D}(x|d) f''(\mu(d), \sigma(d)) d\sigma(d) d\mu(d) \quad (12)$$

Let  $S \subset \{0, \dots, 5\}$  denote a subset of the damage indices. We have

$$\Pr(D \in S | X = x) = \sum_{d \in S} p_{D|X}(d|x) \quad (13)$$

For an uninspected structure, we label the damage state as belonging to set  $S$  when

$$\int_0^1 \Pr(D \in S | x) \cdot f_X(x) dx > \phi_{\text{class}} \quad (14)$$

Here,  $\phi_{\text{class}}$  is a prescribed threshold probability. To select an optimal value for  $\phi_{\text{class}}$ , one should define a utility function

$$U = g(\mathbf{Z}, \phi_{\text{class}}) \quad (15)$$

where  $\mathbf{Z}$  is a set of variables defining performance metrics. For post-earthquake structural safety assessment,  $\mathbf{Z}$  should contain metrics related to the rate of false-positive and false-negative classification, as well as a metric capturing the fraction of structures assessed as a function of time. The optimal value  $\phi_{\text{class}}^*$  is computed by maximizing the expected utility:

$$\phi_{\text{class}}^* = \arg \max_{\phi_{\text{class}}} E[g(\mathbf{Z}, \phi_{\text{class}})] \quad (16)$$

Equations 2–13 can be extended for cases where frequency shifts are monitored for multiple modes and for cases where other structural characteristic responses, such as inter-story drifts or tilts, are also recorded. In such a case,  $X$  is replaced by a vector of random variables  $\mathbf{X}$ . Furthermore, it is possible to condition  $X$  on features such as structural type, height, material, or year of construction. In this paper, such a refined categorization is not used because of lack of data. But as data on characteristic structural responses versus damage index are gathered for different types of structures, more refined

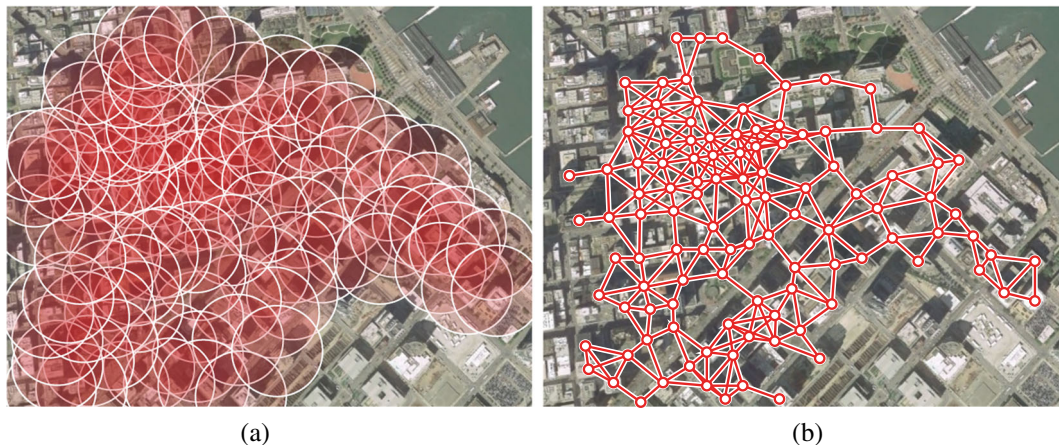


Figure 2. (a) Range of each sensing node antenna and (b) interconnectivity between sensing nodes.

categorization will be possible. It is also noted that the posterior distribution of  $\mu(d)$  and  $\sigma(d)$  obtained for a city after an earthquake can be used as the prior distribution for subsequent earthquakes affecting the city, including aftershocks. In this way, safety assessment can be made prior to conducting any inspections.

#### 4. MONITORING FRAMEWORK

The application of the methodology presented in Section 3 requires knowing the natural frequencies for a population of buildings in near-real time after an earthquake. For each building, a minimum requirement is to have a two-axis accelerometer positioned on the rooftop. For the system to survive an earthquake, the power supply and communication channel of each sensor node should not rely on existing infrastructure. One solution would be to use solar panels with a small battery for supplying power and to use a wireless local area network to enable communication between sensing nodes placed on different buildings. In recent applications, similar approaches have been used to install arrays of sensors on single structures [22–25]. In dense urban areas, using consumer-grade antennas with a range of 100 m would allow having a redundant communication network across a city. Only a few of the sensing nodes need to be connected to the Internet in order to send a continuous stream of data during the periods before and after an earthquake. In the event where internet connection is not available after an earthquake, the data for the entire population of instrumented buildings can be fetched at any time via a local connection to the wireless network. The wireless network can be accessed in the neighborhood of any instrumented building. Figure 2 illustrates an example of interconnectivity for the city center of San Francisco. In Figure 2a, each circle corresponds to the range of the antenna of a sensing node placed on the rooftop of a building, and links in Figure 2b represent the interconnectivity of the sensing nodes.

Continuously monitoring the frequency of structures would allow knowing the frequency shift of buildings, minutes after the event of an earthquake. Then, hours after the event, teams of engineers could start inspecting buildings based on priorities established using observed frequency shifts. Once the knowledge of  $p_{D|X}(d|x)$  is available, it becomes possible to perform prognoses for the safety of buildings that have not yet been inspected. In the event of a strong aftershock, it could become necessary to reassess the safety of the buildings. In such a case, the posterior distributions obtained from the main shock can be used immediately to perform prognoses for the entire population of buildings.

#### 5. VALIDATION OF LEARNING AND PROGNOSIS CAPACITY

This section contains three parts. In Section 5.1, we use the methodology presented in Section 3 to estimate the posterior PDF of  $\{\mu(d), \sigma(d)\}$ , using the existing data reported in Section 2. In Section 5.2,

we use  $f_{X|D}(X|D)$  to generate a city-scale post-earthquake scenario for the purpose of illustrating the utilization and viability of the proposed data-driven safety assessment methodology. Finally, in Section 5.3, we estimate the expected performance of the framework with respect to its capacity to quickly and correctly classify uninspected structures as either safe or marginally unsafe/unsafe.

### 5.1. Estimation of $f''(\mu(d), \sigma(d))$

To estimate the posterior joint distribution of  $\mu(d)$  and  $\sigma(d)$  for the dataset reported in Section 2, we assume that the standard deviation of  $X_j$  is  $\sigma_j = 0.02$ . In order to obtain valid parameter values for the beta distribution, each observed frequency shift (the mean of the distribution) is assumed to lie within the range (0.001–0.999). Theoretically, the standard deviation  $\sigma(d) \in \mathbb{R}^+$ . However, because of lack of data for buildings having a damage index  $d = 5$ , considering the entire domain of  $\sigma(5)$  would lead to an improper PDF. To avoid this problem, we impose the constraint  $\sigma(d) \leq 0.25$ . Judging from the spread of data in Figure 1, the upper limit of 0.25 for  $\sigma(d)$  appears reasonable.

Figure 3 shows contour plots of  $f''(\mu(d), \sigma(d))$  computed using Equation 10. As expected,  $\mu(d)$  is decreasing with the damage index  $d$ . Note that despite not having data for  $d = 5$ , it is possible to obtain an estimate for  $\{\mu(5), \sigma(5)\}$  using the knowledge that  $\mu(d) < \mu(d - 1)$ . Without these constraints, the prior knowledge for a damage index could only be modified by data corresponding to that index. Figure 4 shows the predictive conditional PDF of  $X$  for each value of  $d$ . These predictive PDFs are in good agreement with the data presented in Figure 1.

### 5.2. Example: progressive learning and structural condition assessment

Assume that for a population of 1000 buildings in a city, we know the frequency shifts right after an earthquake. As in the previous section, we assume the standard deviation of  $X_j$  is  $\sigma_j = 0.02$ . The set of damage indices for the population of buildings is simulated using the Binomial distribution

$$p(d) = \frac{5!}{d!(5-d)!} p^d (1-p)^{5-d}, d \in (0:5) \quad (17)$$

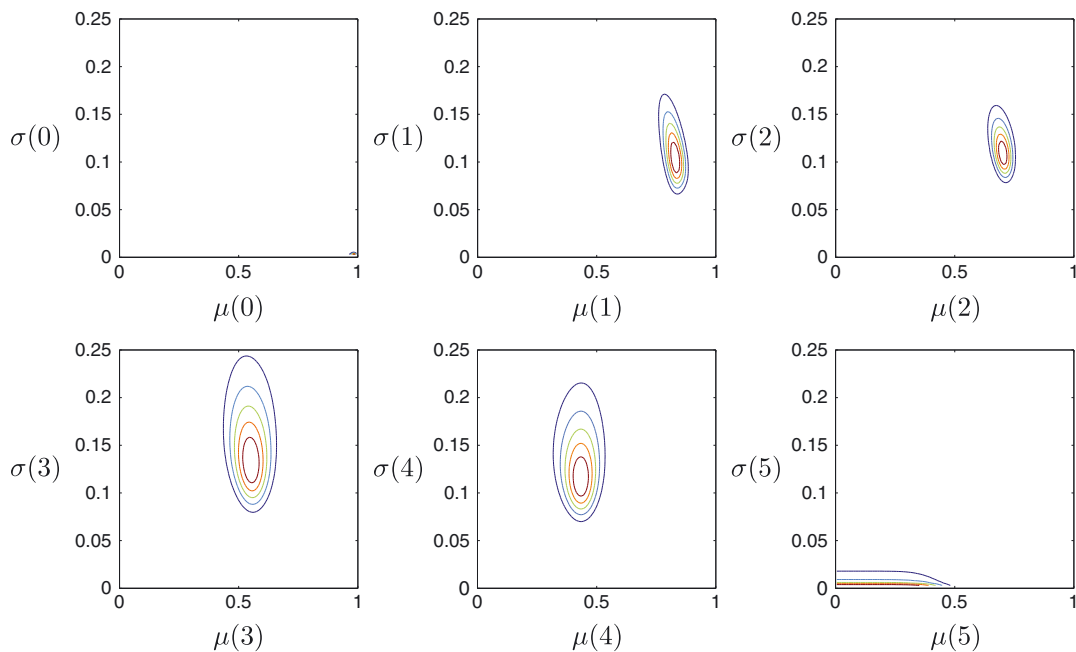


Figure 3. Contour plot of the joint PDFs  $f''(\mu(d), \sigma(d))$  computed using Equation 10 for damage indices  $d = \{0, 1, \dots, 5\}$ .

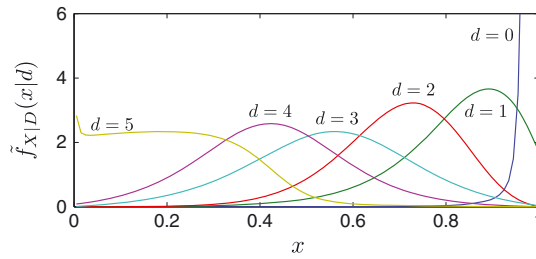


Figure 4. Predictive PDFs of the frequency shifts  $X$  given damage indices  $d = \{0, 1, \dots, 5\}$ .

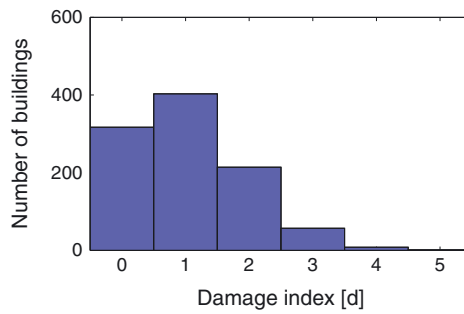


Figure 5. Apportionment of damage indices among the population of buildings.

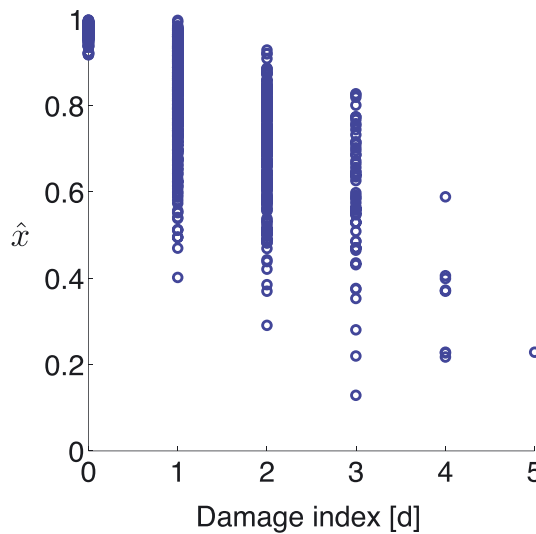


Figure 6. Simulated frequency shifts  $\hat{x}_j$  and damage indices  $d_j$  for the population of buildings.

with  $p = 0.2$ . This distribution has a mean of  $\mu_D = 1$  and standard deviation of  $\sigma_D = 0.894$ . Figure 5 shows the apportionment of damage indices among the simulated population of buildings. The number of buildings in each damage category is as follows: 317 in  $d = 0$ , 403 in  $d = 1$ , 214 in  $d = 2$ , 57 in  $d = 3$ , 8 in  $d = 4$ , and 1 in  $d = 5$ . The “observed” ratio of post-earthquake and pre-earthquake frequencies for each building is obtained by simulating from the conditional distribution  $f_{X|D}(x|d)$  using one realization of  $f''(\mu(d), \sigma(d))$  of the parameters, as estimated in Section 5.1 based on the existing data. Figure 6 shows the simulated measured frequency shifts  $\hat{x}_j$  and damage indices  $d_j$  for the simulated population of buildings. Our purpose is to classify buildings either as *safe*, *marginally unsafe*, or *{marginally unsafe, unsafe}*. That is, we wish to categorize buildings in damage classes  $S_1 \in \{0, 1\}$  and  $S_{2\&3} \in \{2 : 5\}$ . However, we also explore the possibility of considering three damage

classes:  $S_1 \in \{0, 1\}$ ,  $S_2 \in \{2, 3\}$ , and  $S_3 \in \{4, 5\}$ . For the sake of simplicity, the combined damage state  $\{\textit{marginally unsafe/unsafe}\}$  is hereafter denoted as the *combined unsafe* state.

We assume no prior knowledge about  $\mu(d)$  and  $\sigma(d)$ , except for the constraint described in Section 3.1 and the assumed upper bound of 0.25 on  $\sigma(d)$ . We use the methodology presented in Section 3 to learn  $f_{D|X}(d|x)$  as inspections are conducted and damage indices are determined. For the classification probability threshold, we assume that  $\phi_{\text{class}} = 1$  up to 10 inspections and  $\phi_{\text{class}} = 0.97$  thereafter. We assumed that once a prognostic is made for a building, it can only be modified by an inspection of the building. This assumption is made so that the classification of buildings is not constantly changing as data are collected. The latency of  $\phi_{\text{latency}} = 10$  inspections is introduced to avoid early misclassifications attributed to lack of knowledge. In order to speed up the assessment, buildings inspected are chosen so that their frequency shifts are evenly distributed and inspections are prioritized for buildings for which prognosis is not yet possible. The prior distribution  $p_D(d)$  is assumed to be equiprobable for all  $d$ .

Figure 7a shows the evolution of the percentages of buildings in three categories as inspections are performed: (1) those whose damage states are identified through inspection (darkly shaded area), (2) those whose damage states are predicted according to the rule following Equation (14) (lightly shaded area), and (3) the remaining buildings whose damage states cannot be identified with the current state of knowledge and the specified value of the threshold  $\phi_{\text{class}}$  (white area). The height of the vertical axis represents the entire population of buildings, and the height of each area represents the proportion of buildings classified as *inspected*, *not inspected but with known damage state*, or *not inspected with unknown damage state*. Without inspections, 100% of the buildings fall in the last class. Up to the inspection of the 10th building, only buildings that have been inspected have a known damage state. Then, having learned the distribution  $f_{X|D}(x|d)$  based on the information gained from the 10 inspections, it is possible to make a prognosis for 320 additional buildings. This number grows with additional inspections. After collecting the results of 50 inspections, it is possible to predict the damage states of 396 buildings, of which 389 are in the safe state and seven are in the combined unsafe state. Also, no unsafe buildings classified as safe (i.e. false positive) and three safe buildings classified as combined unsafe (i.e. false negative). Thus, the proposed data-driven approach is capable of classifying the damage states of buildings much faster than using inspections alone. However, beyond 50 inspections, the percentage of buildings whose damage states can be predicted does not increase significantly. It indicates that our capacity to perform a prognosis is limited by the *aleatory uncertainty* associated with the variability of frequency shifts for each damage state.

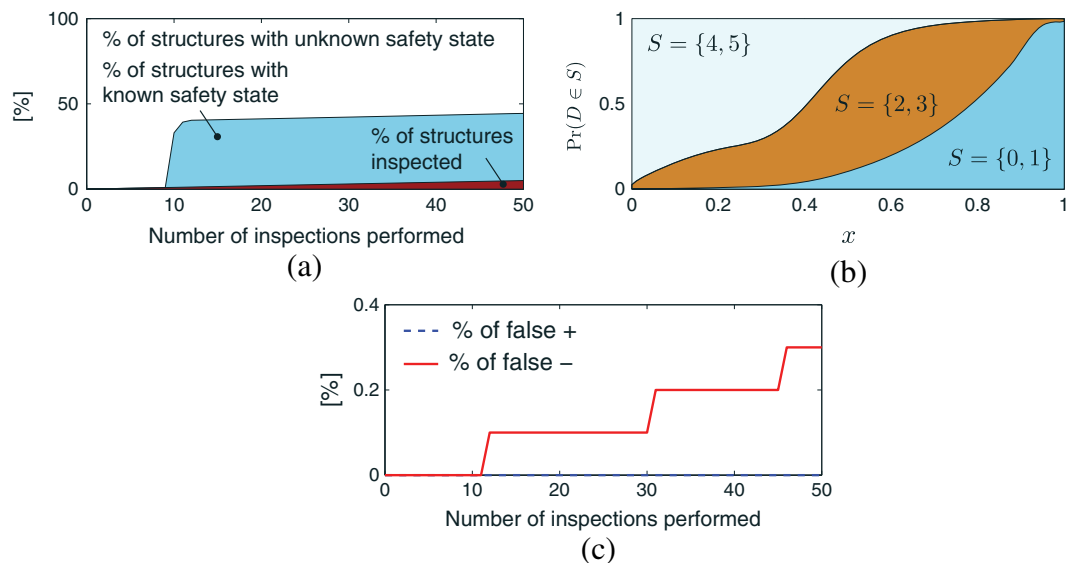


Figure 7. Prognosis of damage states: (a) Percent of buildings with identified damage states with increasing number of inspections. (b) Prognosis tool after 50 inspections. (c) Percent false-positive and false-negative classifications.

Note that the small number of unsafe buildings where a prognosis is possible is due to two factors: First, the variability in the conditional distribution of frequency shifts is smaller for safer states. The second is the distribution of damage states that is strongly skewed toward safer buildings. With such a distribution of damage, there are fewer damaged buildings to learn from and fewer on which to perform a prognosis. When using a distribution of damage that is skewed toward unsafe buildings, the effect is reversed and a better prognosis can be made for these buildings. Finally, we note that in this case, one way to address false negatives is to prioritize the inspection of buildings that have been identified as unsafe.

Figure 7b shows the prognosis tool derived from  $f_{D|X}(d|x)$  after it is updated with the results of 50 inspections. For a given  $x$ , the height of each area represents the probability that the building is in damage classes  $S_1 \in \{0, 1\}$ ,  $S_2 \in \{2, 3\}$ , and  $S_3 \in \{4, 5\}$ . Here, we have made a distinction between the classes *marginally unsafe* and *unsafe*. With the assumed  $\phi_{\text{class}} = 0.97$ , buildings with  $\hat{x} > 0.937$  are classified as *safe* and buildings with  $\hat{x} < 0.370$  are classified in the *combined unsafe* state. The available information for damage class  $S_2$  (*marginally unsafe*) is too vague to identify buildings in this category. (This is why we combined the marginally unsafe and unsafe classes.) One could use a smaller (larger) value for  $\phi_{\text{class}}$  to allow a more (less) refined classification, but that would result in higher (lower) rates of false negatives and false positives. A better option would be to refine the prediction model  $f_{X|D}(x|d)$  by developing it for different types of buildings, an effort that can be realized as post-earthquake monitoring data are gathered and analyzed.

Figure 7c shows the evolution of false-positive and false-negative classifications. A false positive is defined as classifying a building as safer than it is; for example, classifying an *unsafe* building as *safe*. A false negative is the opposite: classifying a building as less safe than it is. False positives are more critical than false negatives because human casualties may result from occupying an unsafe building. False negatives only have economic or social impact. As Figure 7c shows, for the present example, both rates are small, but the rate of false positives is smaller than that of false negatives. Note that the illustrated example is just one realization of a stochastic process. In the following section, we study the influence of the classification threshold  $\phi_{\text{class}}$  and of the classification latency  $\phi_{\text{latency}}$  (the number of inspections before prediction is performed) on the expected value of metrics quantifying the performance of the proposed framework.

### 5.3. Estimation of the expected performance

We evaluate the expected performance of the proposed framework by estimating, for the previous example, the expected values of what follows: (1) the percentage of buildings not yet inspected but with identified damage states, (2) the percentage of false positives, and (3) the percentage false negatives, after 50 simulated inspections. We estimate the expected values of the three metrics using 100 randomly generated populations of buildings and damage scenarios obtained following the procedure presented in Section 5.2. For each population of buildings, a different binomial distribution of damage indices is used having parameters  $n = 5$  and  $p$ , the latter generated from a beta distribution with mean 0.2 and 20% coefficient of variation. Moreover, for each scenario, we use a different realization of the parameters of the conditional distribution  $f_{X|D}(x|d)$  for generating frequency shifts given damage indices. The expected values of the three performance metrics are estimated for the classification threshold values  $\phi_{\text{class}} = \{0.90, 0.92, 0.95, 0.97, 0.99\}$  and the latency threshold values  $\phi_{\text{latency}} = \{0, 5, 10, 15, 20\}$ .

Figure 8 shows the expected performance of the proposed methodology in terms of the three metrics as a function of parameters  $\phi_{\text{class}}$  and  $\phi_{\text{latency}}$ . Each point corresponds to the expected result obtained from 100 simulations, and the meshed grid corresponds to the sample mean plus one standard deviation. The surface is a second-degree polynomial function fitted to the simulation results by minimizing the mean-square error. The results indicate that it is possible to control the safety assessment capacity and the rate of false classifications by adjusting the two parameters. Optimal values  $\phi_{\text{class}}^*$  and  $\phi_{\text{latency}}^*$  could be obtained from

$$\{\phi_{\text{class}}^*, \phi_{\text{latency}}^*\} = \arg \max_{\{\phi_{\text{class}}, \phi_{\text{latency}}\}} E[g(\mathbf{Z}, \phi_{\text{class}}, \phi_{\text{latency}})] \quad (18)$$

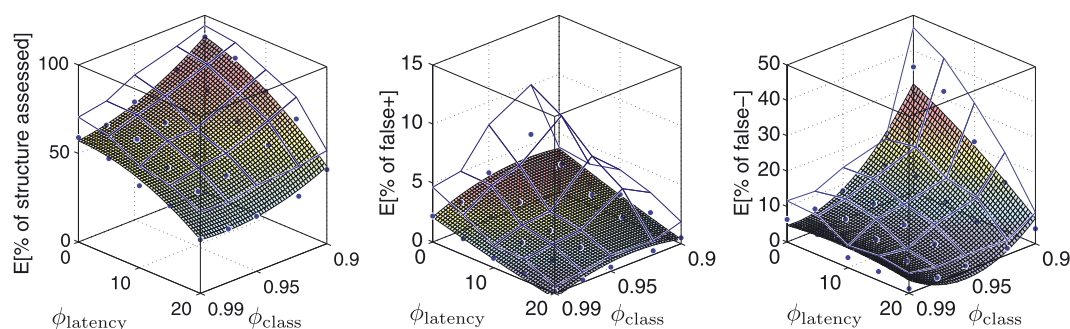


Figure 8. Expected performance as a function of classification threshold  $\phi_{\text{class}}$  and classification latency  $\phi_{\text{latency}}$ . Each point corresponds to the expected result obtained from 100 simulations, and the meshed grid corresponds to the sample mean plus one standard deviation. The surface is a second-degree polynomial function fitted to the simulation results by minimizing the mean-square error.

This optimization can be performed from a trivial search operation on the results presented in Figure 8.

Note that the low values of  $\phi_{\text{class}}$  and  $\phi_{\text{latency}}$  produce large percentages of structures assessed, however, with unacceptable rates of false negatives. For more reasonable parameter values such as  $\phi_{\text{class}} = 0.97$  and  $\phi_{\text{latency}} = 10$ , the expected percentage of structures assessed after 50 inspections is 50% with an expected percentage of false positive and false negative respectively equal to 1.3% and 4.7%. Results indicate that the expected performance reaches levels sufficient to justify consideration of the proposed framework as a candidate for improving the resilience of earthquake-prone cities.

## 6. DISCUSSION AND LIMITATIONS

With the framework proposed in this paper, we intend to take advantage of the frequency data collected on a large number of buildings across a city. Despite requiring a minimal number of sensors, such instrumentation can nowadays still be expensive because of the small amplitudes of building oscillations under ambient vibration, which determines the required sensitivity of the sensor. Notwithstanding recent developments in wireless sensor nodes for structural health monitoring applications [22–26], the cost of instrumenting one building is currently of the order of thousands of US dollars. However, recent advances in open-source hardware [27, 28] such as Raspberry Pi, Arduinos, and MinnowBoard, as well as in microelectromechanical-based sensor technologies [29, 30], allows us to expect significant cost reductions. As cost should decrease, public agencies in earthquake-prone areas might follow the example of California that requires the instrumentation of new buildings having 10 stories or more [31]. In addition to monitoring buildings for post-earthquake safety assessment, recording characteristic responses of structures during their service life would contribute to understanding their long-term behavior as well as guarantee their integrity in-between routine inspections. Moreover, it should be possible to improve the performance of the methodology by further categorizing buildings according to materials, usages, and structural systems.

This paper focuses on the technical aspects allowing learning the relationship between post-earthquake frequency shifts and a damage index. The details of what occupants should do with the information provided by the system remain to be established in collaboration with emergency response authorities.

## 7. SUMMARY AND CONCLUSIONS

A collection of data available in the literature demonstrates the potential of using the frequency shift to infer the damage state of a structure. Using this information, this paper proposes a data-driven framework for predicting the damage states of structures in a city in the hours following an earthquake. In this framework, Bayesian updating allows learning, as inspection data are collected, the relationship between the shift in the structure frequency and the corresponding damage index obtained from



each inspection. This information is then used to classify the damage states of uninspected structures, for which frequency shifts are measured by monitoring devices. The illustrative application shows that, when generating city-scale simulated scenarios using existing data, we expect to be able to predict the safety states of 50% of the monitored structures after having performed inspections only for 5%. The corresponding expected percentages of false positives and false negatives is respectively 1.3% and 4.7%. The proposed method leverages the information provided by visual inspections and frequency shifts to speed up the safety assessment process, valorize the assessment performed by qualified personnel, and support the prioritization of building inspections.

#### ACKNOWLEDGEMENTS

The authors thank Prof. Manuel Navarro and Dr François Dunand for sharing part of the data used in this project. The first author thanks the Swiss National Science Foundation and the Quebec Research Fund for Nature and Technology for funding this research. Additional support was provided by the US National Science Foundation under grant no. CMMI-1130061.

#### REFERENCES

1. Rapporto attività di sopralluogo effettuate al: 26/06/2009. *Technical Report*, Dipartimento della Protezione Civile: L'Aquila, Italy, 2009.
2. Rojahn C. Procedures for post-earthquake safety evaluation of buildings, ATC-20. *Technical Report*, Applied Technology Council (ATC), Redwood City, CA, 1989.
3. Baggio C, Bernardini A, Colozza R, Corazza L, Bella MD, Pasquale GDI, Dolce M, Goretti A, Martinelli A, Orsini G, *et al.* Field manual for post-earthquake damage and safety assessment and short term countermeasures (AeDES). *Technical Report*, European Commission, Joint Research Centre, 2007.
4. Marshall JD, Jaiswal K, Gould N, Turner F, Lizundia B, Barnes JC. Post-earthquake building safety inspection: lessons from the Canterbury, New Zealand, earthquakes. *Earthquake Spectra* August 2013; **29**(3):1091–1107.
5. Çelebi M, Sinclair ASM, Gallant S, Radulescu D. Real-time seismic monitoring needs of a building owner and the solution – a cooperative effort, *13th World Conference on Earthquake Engineering*, Vol. 3104, Vancouver, B.C., Canada, 2004.
6. Porter KA, Beck JL, Ching J, Mitrani-Reiser J, Miyamura M, Kusaka A, Kudo T, Ikkatai K, Hyodo Y. Real-time loss estimation for instrumented buildings. *Technical Report EERL 2004-08*, Earthquake Engineering Research Laboratory, California Institute of Technology, Kajima Corporation, Pasadena (California), 2004.
7. Iervolino I, Giorgio M, Chioccarelli E. Closed-form aftershock reliability of damage-cumulating elastic-perfectly-plastic systems. *Earthquake Engineering & Structural Dynamics* September 2013; **43**(4):613–625.
8. Mosquera V, Smyth AW, Betti R. Rapid evaluation and damage assessment of instrumented highway bridges. *Earthquake Engineering & Structural Dynamics* 2012; **41**(4):755–774.
9. Wu S, Beck JL. Synergistic combination of systems for structural health monitoring and earthquake early warning for structural health prognosis and diagnosis. *SPIE Smart Structures and Materials + Nondestructive Evaluation and Health Monitoring*, Vol. 8348, International Society for Optics and Photonics, 2012; 83481Z–83481Z–10.
10. Carden EP, Fanning P. Vibration based condition monitoring: a review. *Structural Health Monitoring* 2004; **3**(4):355–377. DOI: 10.1177/1475921704047500.
11. Rodríguez Ramsés, Escobar JA, Gómez R. Damage detection in instrumented structures without baseline modal parameters. *Engineering Structures* June 2010; **32**(6):1715–1722. DOI: 10.1016/j.engstruct.2010.02.021.
12. Omori F. The semi-destructive earthquake of April 26. *Seismological Notes (Imperial Earthquake Investigation Committee)* 1922; **3**:1–30.
13. Clinton JF, Bradford SC, Heaton TH, Favela J. The observed wander of the natural frequencies in a structure. *Bulletin of the Seismological Society of America* 2006; **96**(1):237–257.
14. Dunand F, Meziane YA, Guéguen P, Chatelain JL, Guillier B, Salem RB, Hadid M, Hellel M, Kiboua A, Laouami N, Machane D, Mezouer N, Nour A, Oubaiche E, Remas A. Utilisation du bruit de fond pour l'analyse des dommages des bâtiments de Boumerdes suite au séisme du 21 mai 2003. *Mémoires du Service Géologique de l'Algérie* 2004; **12**:177–191.
15. Mucciarelli M, Masi A, Gallipoli Maria Rosaria, Harabaglia P, Vona M, Ponso F, Dolce M. Analysis of RC building dynamic response and soil-building resonance based on data recorded during a damaging earthquake. *Bulletin of the Seismological Society of America* 2004; **94**(5):1943–1953.
16. Régnier J, Michel C, Bertrand E, Guéguen P. Contribution of ambient vibration recordings (free-field and buildings) for post-seismic analysis: The case of the Mw 7.3 Martinique (French Lesser Antilles) earthquake, November 29, 2007. *Soil Dynamics and Earthquake Engineering* 2013; **50**:162–167.
17. Vidal F, Navarro M, Aranda C, Enomoto T. Changes in dynamic characteristics of Lorca RC buildings from pre- and post-earthquake ambient vibration data. *Bulletin of Earthquake Engineering* 2013:1–16.
18. Goulet JA, Michel C, Smith IF. Hybrid probabilities and error-domain structural identification using ambient vibration monitoring. *Mechanical Systems and Signal Processing* May 2013; **37**(1–2):199–212, DOI 10.1016/j.ymssp.2012.05.017.

19. Hill M, Rossetto T. Comparison of building damage scales and damage descriptions for use in earthquake loss modelling in Europe. *Bulletin of Earthquake Engineering* Jan 2008; **6**(2):335–365. DOI: 10.1007/s10518-007-9057-y.
20. Grünthal G, Musson RMW, Schwartz J, Stucchi M. *European Macroseismic Scale 1998*, Vol. 15, Cahiers du Centre Européen de Géodynamique et de Séismologie: Luxembourg, 1998.
21. Dunand F. Pertinence du bruit de fond sismique pour la caractérisation dynamique et l'aide au diagnostic sismique des structures de génie civil. *Ph.D Thesis*, Université Joseph-Fourier-Grenoble I, 2005.
22. Cho S, Yun CB, Lynch JP, Zimmerman AT, Spencer Jr BF, Nagayama T. Smart wireless sensor technology for structural health monitoring of civil structures. *International Journal of Steel Structures* 2008; **8**(4):267–275.
23. Kurata M, Kim J, Zhang Y, Lynch JP, Van der Linden GW, Jacob V, Thometz E, Hipley P, Sheng LH. Long-term assessment of an autonomous wireless structural health monitoring system at the new Carquinez suspension bridge, Vol. 7983: Proceedings of SPIE, 2011.
24. Kurata N, Spencer BF, Ruiz-Sandoval M. Risk monitoring of buildings with wireless sensor networks. *Structural Control and Health Monitoring* 2005; **12**(3-4):315–327.
25. Lynch J, Loh K. A summary review of wireless sensors and sensor networks for structural health monitoring. *Shock and Vibration Digest* 2006; **38**(2):91–130.
26. Clayton RW, Heaton T, Chandy M, Krause A, Kohler M, Bunn J, Guy R, Olson M, Faulkner M, Cheng M, Strand L, Chandy R, Obenshain D, Liu A, Aivazis M. Community seismic network. *Annals of Geophysics* 2011; **54**(6): 728–747.
27. Pearce JM. Building research equipment with free, open-source hardware. *Science* 2012; **337**(6100):1303–1304.
28. Pearce JM. *Open-source Lab: How to Build Your Own Hardware and Reduce Research Costs*, Newnes: Waltham, MA, USA, 2013.
29. D'Alessandro A, D'Anna G. Suitability of low-cost three-axis MEMS accelerometers in strong-motion seismology: tests on the LIS331DLH (iPhone) accelerometer. *Bulletin of the Seismological Society of America* 2013; **103**(5):2906–2913.
30. Milligan DJ, Homeijer BD, Walmsley RG. An ultra-low noise MEMS accelerometer for seismic imaging. *Sensors, 2011 IEEE*, IEEE, 2011; 1281–1284.
31. CBSC. *California Building Code, Appendix L*. California Building Standards Commission: Sacramento, CA, 2013.

## 3.4 Perspectives

La recherche en sismologie de l'ingénieur trouve des applications évidentes pendant les périodes de crise suivant un séisme destructeur. Les enregistrements de vibrations ambiantes fournissent facilement et rapidement des données *in situ* afin d'affiner des modèles prédictifs et de quantifier les dommages aux structures. Des stations sismologiques devraient donc trouver leur place dans toute mission post-sismique.

Les modèles de prédiction du mouvement du sol, complétés avec les données des stations permanentes, permettent de délimiter la zone des dégâts. Ces cartes ShakeMap sont désormais largement répandues. Cependant, il est nécessaire d'étendre les modèles au calcul des pertes, qui donneront un avantage décisif aux secours juste après un séisme. Les méthodes actuelles sont pour la plupart fondées sur l'intensité macrosismique et des analyses de la vulnérabilité robustes mais grossières. Pour affiner ces modèles, il faut aller vers des méthodes mécaniques qui nécessitent cependant un plus grand nombre de données sur la géologie locale et le bâti. Nous sommes allés dans cette direction en proposant un modèle pour les écoles de la ville de Bâle (Michel *et al.*, 2017b).

# Conclusions et perspectives générales

Le rôle des chercheurs en sciences de la Terre et en mécanique dans l'analyse du risque sismique, c'est-à-dire des pertes humaines et matérielles attendues à cause des séismes, consiste en la prédiction des dommages dus au mouvement du sol et aux dangers secondaires (mouvements de terrain, liquéfaction, tsunami). Cette estimation s'effectue en deux phases : la prédiction du mouvement du sol et le calcul de la réponse des structures à ce mouvement. Comme je l'ai souligné dans ce document, la prédiction du mouvement du sol doit être locale en prenant en compte la géologie des dernières centaines de mètres du sous-sol. J'ai montré que les données sismologiques collectées *in situ* (vibrations ambiantes et séismes) étaient nécessaires pour déterminer correctement les propriétés mécaniques et la géométrie de la sub-surface. J'ai également proposé une procédure pour détecter les effets 2D/3D qui a permis de mettre en évidence qu'une évaluation 1D était suffisante dans la plupart des cas. J'ai aussi montré que l'analyse modale empruntée à l'ingénierie mécanique et civile permettait d'évaluer plus précisément la résonance 2D/3D.

J'ai également prouvé que, comme pour les sols, la prédiction de la réponse des structures existantes au mouvement sismique pouvait être améliorée grâce à des enregistrements sous vibrations ambiantes et l'étude des propriétés dynamiques expérimentales. C'est en particulier vrai pour le bâti en maçonnerie pour lequel ni la géométrie, ni les propriétés mécaniques ne sont en général bien connues. Réalisées en grand nombre, ces mesures m'ont permis une analyse statistique des propriétés du bâti existant. Elles permettent en outre de prédire l'importance de la torsion sur la réponse du bâti et de donner des informations sur l'interaction sol-structure. En ce qui concerne les ponts pour lesquels les matériaux sont en général mieux connus, nous avons vu que les données expérimentales permettent de fixer les hypothèses de modélisation. En revanche, la détermination des propriétés mécaniques à partir des propriétés modales est plus difficile à cause des incertitudes de modélisation. J'ai également mis en évidence et surtout quantifié le comportement élastique non-linéaire des structures de génie civil, en particulier en maçonnerie, sous mouvement modéré à fort. La quantification de la baisse de la fréquence fondamentale permet de faire le lien entre les données sismologiques et les calculs du génie parasismique, ce qui constitue sans doute le point le plus innovant de ma contribution.

Après un séisme ayant causé des dommages, j'ai aussi montré que les données sismologiques étaient nécessaires afin de mieux comprendre les dommages pour éviter qu'ils ne se reproduisent et aider à l'analyse de l'habitabilité.

J'ai montré que la collecte de données sismologiques par les réseaux d'excellente qualité, en champ libre et en structures, était donc nécessaire pour améliorer la prédiction du mouvement sismique local et de la réponse des structures. En complément, on constate déjà, et on peut imaginer que la tendance va se poursuivre, le développement de réseaux très denses avec des capteurs à bas coût du type de ceux contenus dans les téléphones mobiles. Cela permettra d'augmenter la densité spatiale des données pour mieux comprendre la variabilité du mouvement sismique et le comportement des structures et des groupes de structures. Ce sont des données de ce type qu'il faudra intégrer dans les analyses futures.

Dans les années à venir, je poursuivrai la transition entre les méthodes empiriques d'analyse du

risque sismique, fondées uniquement sur la statistique du retour d'expérience, vers des méthodes mécaniques, calculées, intégrant les données sismologiques locales. Cette transition est nécessaire pour permettre la prédiction objective (c.-à-d. pas uniquement fondée sur un avis d'expert) des dommages dus à des séismes ne s'étant jamais produits, en particulier dans les régions à sismicité modérée. En effet, celles-ci présentent nécessairement des caractéristiques géologiques et de bâti propres, différentes de celles des régions à forte sismicité où les méthodes empiriques ont été développées. L'accent sera mis sur la robustesse des analyses et leur vérification afin d'éviter une surestimation des dommages que nous avons constatée dans un premier temps dans le projet d'analyse du risque à Bâle (Michel *et al.*, 2017b).

Je m'intéresserai à la prédiction probabiliste du mouvement sismique en prenant en compte la composante spatiale (corrélation spatiale), en relation avec la géologie locale, qui a un rôle déterminant pour le calcul du risque sur des structures distribuées spatialement. Dans un premier temps, cette étude se fera à l'aide des outils de la géostatistique sur des données existantes de réseaux de stations denses à l'échelle d'un bassin sédimentaire (p. ex. Bâle) et dans un second temps à l'aide de données temporaires à acquérir à l'aide d'un réseau très dense. L'objectif sera de quantifier la corrélation du mouvement sismique en fonction de la fréquence et d'expliquer d'où vient cette corrélation (effets de source ou de site) afin d'améliorer les équations de prédiction du mouvement du sol. En parallèle, j'étudierai le champ d'ondes sous vibrations ambiantes et sous séisme à cette même échelle et avec les mêmes données en utilisant et en développant des techniques d'analyse du signal comme WaveDec (Maranò *et al.*, 2012) et MUSIQUE (Hobiger *et al.*, 2016). L'objectif est de mettre en évidence la génération d'ondes de surface en bord de bassin et de la relier à l'amplification mesurée sous séisme. Je souhaite également déterminer si l'anisotropie de sédiments lacustres peu consolidés peut jouer un rôle dans le mouvement sismique. Je poursuivrai l'étude modale des structures géologiques comme les bassins sédimentaires et les glissements de terrains afin de proposer de nouvelles techniques pour caractériser leur géométrie et leurs propriétés mécaniques, y compris l'atténuation. Enfin, je poursuivrai la collecte de données de profils de vitesse à l'échelle de la Suisse afin d'aider au développement d'un modèle national d'amplification de la géologie locale pour l'analyse du risque.

Dans le domaine des structures, je continuerai à développer leur étude à l'aide des outils de la sismologie (analyse en réseau, déconvolution). Un objectif central sera de caractériser l'interaction sol-structure et ses variations (en terme de fréquence et d'amortissement), afin de les découpler des variations des propriétés de la structure elle-même. Je souhaite mieux relier les caractéristiques des structures à leurs fréquences de résonance et leurs variations sous mouvement fort. Je m'attacherai aussi à montrer l'importance de la géométrie sur le comportement dynamique afin d'améliorer la connaissance sur le comportement sismique des structures existantes. Cela passe par des comparaisons avec des modèles numériques, en collaboration avec des chercheurs en mécanique. Les bâtiments existants en maçonnerie, les îlots de centre-ville et les structures historiques remarquables seront particulièrement étudiés. Enfin, pour l'analyse de la vulnérabilité et du risque, je proposerai de nouveaux outils méthodologiques pour conduire des analyses prenant en compte les incertitudes de façon rationnelle, sans double comptage, en particulier pour les incertitudes épistémiques, liées aux hypothèses de modélisation. Les courbes de fragilité sont l'outil actuellement choisi pour ce calcul, qu'il faudra sans doute dépasser. Pour les études de risque, j'aborderai en particulier le risque financier lié aux séismes modérés à proximité des agglomérations, par exemple liés à la géothermie. Les dommages aux éléments non-structuraux, encore mal caractérisés, ont alors un rôle prépondérant dans l'analyse. Ces outils doivent pouvoir être implémentés à différentes échelles (agglomération, pays) et en temps réel, peu de temps après un événement. Pour cela, le logiciel Openquake sera utilisé et développé en collaboration avec le *Global Earthquake Model* (GEM).

Je développerai également les outils d'analyse post-sismique, afin que chaque événement permette de réduire l'impact des suivants. La collecte de données avant et après séisme est déterminante dans ce développement, en collaboration avec les organismes qui travaillent lors d'une crise (protection civile, sociétés savantes, laboratoires de recherche, etc.).

Ces travaux ont donc pour ambition de réduire les incertitudes dans l'étude du risque sismique dans le but de mieux calibrer la prévention (normes de construction, information à la population), l'alerte (modèles de pertes en temps réel) et d'améliorer la réponse à une crise sismique.

# Activités scientifiques

## Encadrement d'étudiants (Master et doctorat)

- Co-encadrant du travail de Master de Marlen Bigler avec P. Lestuzzi à l'EPFL en Génie Civil : « Vérification de la sécurité parasismique de la tour du Bürgerheim à Berne » en 2009.
- Encadrant du travail de Master de Yoon Jung Choi à l'ETHZ dans le département de Sciences de la Terre, « Soil-structure interaction from a building in a sedimentary basin » en 2012.
- Co-encadrant du doctorat de Marcelo Oropeza à l'EPFL avec P. Lestuzzi : « Fragility functions for seismic risk in regions with moderate seismicity » soutenue en décembre 2011.
- Aide à l'encadrement du doctorat de James-Alexandre Goulet à l'EPFL (direction I. Smith) : « Probabilistic Model Falsification for Infrastructure Diagnosis » soutenue en juillet 2012. Nous avons co-signé trois articles de journaux.
- Encadrant principal à l'ETHZ du doctorat d'Elena Manea (direction Mircea Radulian, National Institute of Earth Physics, Bucarest – Roumanie – bourse Sciex de 16 mois à l'ETHZ en 2015) : soutenue en septembre 2016. Un article publié, un en préparation.

## Enseignement et formations

- Remplacement de P. Lestuzzi pour les cours de génie parasismique et de mécanique des structures à l'EPFL.
- Création et enseignement du cours « Advanced Earthquake Engineering » avec P. Lestuzzi pour l'école doctorale « Structures » de l'EPFL (2008/2009), invité à enseigner pour les sessions 2012 et 2016.
- Travaux pratiques « Résonance et vibrations ambiantes » pour les étudiants en Bachelor en Sciences de la Terre à l'ETHZ (2010-2012). Formation pour des professeurs du secondaire participant au projet *seismo@school* (« SISMOS à l'École » en France).
- Création de la formation pour les membres du Groupe d'Intervention Macrosismique (GIM) « Expertise des effets et estimation des intensités macrosismiques sur le terrain après séisme et procédures de sécurité en zone sinistrée » pour l'Université de Strasbourg en collaboration avec le Bureau Central Sismologique Français (BCSF). 5 sessions entre 2011 et 2013.
- Création et enseignement des formations « Etude macrosismique et analyse des bâtiments après séisme » au Service Sismologique Suisse (2012) et « Analyse du bâti après un séisme : présentation du manuel de l'Office Fédérale pour la Protection Civile » avec l'Association de Génie Parasismique et Dynamique des Structures (SGEB) pour les experts de la compagnie d'assurance GVB Berne (2013).

## Responsabilités administratives

- Coordination et mise en œuvre du projet de renouvellement du réseau accélérométrique suisse (phase 1, 2009-2013) : sélection des sites d’implantation de 30 nouvelles stations, supervision de l’installation et caractérisation géophysique des sites. Grâce au succès de la première phase, la seconde phase à laquelle j’apporte un soutien opérationnel, a été financée ; Coordination des travaux du SED sur le projet de prévention du risque sismique du canton de Bâle-Ville (Basel Erdbebenvorsorge, 2013-2015) : installation de 6 stations supplémentaires.
- Membre de l’équipe d’astreinte du SED (Duty Seismologist) depuis 2011. Il s’agit du groupe chargé de la gestion en cas de crise sismique, répondant aux autorités et aux médias. Je participe en outre activement aux tâches de communications du SED (site web, interviews, conférences, etc.), en particulier pour le public francophone.
- Développement, en coordination avec le service informatique et le réseau sismologique, de nouvelles bases de données regroupant les informations sur les sites d’implantation des stations et les données géophysiques collectées par le SED depuis le début de ses activités.

## Autres activités

- Expert pour le projet de l’Office Fédéral de l’Environnement « Risque sismique du bâti existant » (2010-2014). Dans ce projet, les bases scientifiques pour une mise à jours des normes sismiques pour le bâti existant ont été étudiées par l’EPFL et le bureau Risk&Safety.
- Conférence invitée « Vibrations ambiantes et mouvements forts dans les structures : le rôle des réseaux dans la recherche sur la vulnérabilité sismique » aux 2e Rencontres Scientifiques et Techniques RESIF, octobre 2015
- Conférence invitée « Incertitudes et vulnérabilité sismique » au symposium Vulnérabilités, Risques et Catastrophes, Ecole des Mines de Nancy, Novembre 2014.
- Conférence invitée au symposium « Bauwerksdynamik und Erschütterungsmessungen » (Dynamique du bâti et mesures de vibrations) sur le séisme de Zoug (2012) [en allemand].
- Revue d’articles pour les journaux spécialisés : Bulletin of the Seismological Society of America, Geophysical Research Letters, Earthquake Engineering and Structural Dynamics, Soil Dynamics and Earthquake Engineering, Pure and Applied Geophysics, Earthquake Engineering and Engineering Vibrations, Bulletin of Earthquake Engineering, etc.

## Publications de rang A

24 articles rang A dont 10 en premier auteur et 4 articles d’étudiants encadrés. H-index ISI : 9 ; Scopus : 11. Liste complète avec liens sur [http://mercalli.ethz.ch/~clmichel/Clotaire\\_Michel\\_Homepage/Publications.html](http://mercalli.ethz.ch/~clmichel/Clotaire_Michel_Homepage/Publications.html).

24. **Michel, C.**, Hannewald, P., Lestuzzi, P., Fäh, D., Husen, S. “Probabilistic mechanics-based loss scenarios for school buildings in Basel (Switzerland)” *Bulletin of Earthquake Engineering*, 15(4), 1471-1496, 2017.

23. Manea E. F., **Michel C.**, Poggi V., Fäh, D., Radulian M., Balan F. “Improving the shear wave velocity structure beneath Bucharest (Romania) using ambient vibrations”, *Geophysical Journal International*, 207(2),



848-861, 2016.

22. **Michel C.**, Fäh D., Edwards B., Cauzzi C. “Site amplification at the city scale in Basel (Switzerland) from geophysical site characterization and spectral modelling of recorded earthquakes.” *Physics and Chemistry of the Earth, Special Issue “Advances in seismic site response : standard-practice and innovative methods”*, in press, 2016.

21. Poggi V., Ermert L., Burjānek J., **Michel C.**, Fäh D. “Modal analysis of 2-D sedimentary basin from frequency domain decomposition of ambient vibration array recordings”, *Geophysical Journal International*, 200(3), 615-626, 2015.

20. Goulet J.-A., **Michel C.**, Der Kiureghian A., “Data-driven post-earthquake rapid structural safety assessment”, *Earthquake Engineering and Structural Dynamics*, 44(4), 549-562, 2015.

19. **Michel C.**, Edwards B., Poggi V., Burjānek J., Roten D., Cauzzi C., Fäh D., “Assessment of site effects in Alpine regions through systematic site characterization of seismic stations”, *Bulletin of the Seismological Society of America*, 104(6), 2809-2826, 2014.

18. Diehl T., Clinton J., Kraft T., Husen S., Plenkers K., Guilhem A., Behr Y., Cauzzi C., Kästli P., Haslinger F., Fäh D., **Michel C.**, Wiemer S. “Earthquakes in Switzerland and surrounding regions during 2013”, *Swiss Journal of Geosciences*, 107(2-3), 359-375, 2014.

17. Psimoulis P. A., Houlié N., **Michel C.**, Meindl M., Rothacher M. “Long-period surface motion of the multi-patch Mw9.0 Tohoku-Oki earthquake”, *Geophysical Journal International*, 199(2), 968-980, 2014.

16. **Michel C.**, Lestuzzi P., Lacave C. “Simplified non-linear seismic displacement demand prediction for low period structures”, *Bulletin of Earthquake Engineering*, 12(4), 1563-1581, 2014.

15. Goulet J.-A., Texier M., **Michel C.**, Smith I.F.C., Chouinard L. “Quantifying the effects of modeling simplifications for structural identification of bridges”, *Journal of Bridge Engineering*, 19(1), 59-71, January 2014.

14. Diehl T., Deichmann N., Clinton J., Husen S., Kraft T., Plenkers K., Edwards B., Cauzzi C., **Michel C.**, et al. “Earthquakes in Switzerland and surrounding regions during 2012”, *Swiss Journal of Geosciences*, 106(3), 543-558, October 2013.

13. Baumann C., Burjanek J., **Michel C.**, Fäh D., Dalguer L. A. “Fault zone signatures from ambient vibration measurements : a case study in the region of Visp (Valais, Switzerland)”, *Swiss Journal of Geosciences*, 106(3), 529-541, October 2013.

12. Régnier J., **Michel C.**, Bertrand E. and Guéguen P., “Contribution of ambient vibration recordings (free-field and buildings) for post-seismic analysis : the case of the Mw 7.3 Martinique (French Lesser Antilles) earthquake, November 29, 2007”, *Soil Dynamics and Earthquake Engineering*, 50, 162-167, July 2013.

11. Edwards B., **Michel C.**, Poggi V., Fäh D., “Determination of Site Amplification from Regional Seismicity : Application to the Swiss National Seismic Networks”, *Seismological Research Letters*, 84(4), 611-621, July-August 2013.

10. Goulet J.-A., **Michel C.**, Smith I.F.C., “Hybrid probabilities and error-domain structural identification using ambient vibration monitoring”, *Mechanical Systems and Signal Processing*, 37(1-2), 199-212, May-June 2013.

9. Fäh D., Moore J. R., Burjanek J., Iosifescu I., Dalguer D., Dupray F., **Michel C.** et al., “Coupled

seismogenic geohazards in alpine regions”, *Bollettino di Geofisica Teorica ed Applicata*, 53, 485-508, December 2012.

8. **Michel C.**, Guéguen P., Causse M. “Seismic vulnerability assessment to slight damage based on experimental modal parameters”, *Earthquake Engineering and Structural Dynamics*, 41(1), 81-98, January 2012.

7. **Michel C.**, Zapico B., Lestuzzi P., Molina F., Weber F. “Quantification of fundamental frequency drop for unreinforced masonry buildings from dynamic tests”, *Earthquake Engineering and Structural Dynamics*, 40(11), 1283-1296, September 2011.

6. **Michel C.**, Guéguen P., Lestuzzi P., Bard P.-Y. “Comparison between seismic vulnerability models and experimental dynamic properties of existing buildings in France”, *Bulletin of Earthquake Engineering*, 8(6), 1295-1307, December 2010b.

5. **Michel C.**, Guéguen P. “Time–Frequency Analysis of Small Frequency Variations in Civil Engineering Structures Under Weak and Strong Motions Using a Reassignment Method”, *Structural Health Monitoring*, 9(2), 159-171, March 2010.

4. **Michel C.**, Guéguen P., El Arem S., Mazars J., Kotronis P. “Full Scale Dynamic Response of a RC Building under Weak Seismic Motions Using Earthquake Recordings, Ambient Vibrations and Modelling”, *Earthquake Engineering and Structural Dynamics*, 39(4), 419-441, 2010a.

3. Guéguen P., Jolivet V., **Michel C.**, Schweitzer A.-S. “Comparison of velocimeter and coherent LIDAR measurements for building frequency assessment”, *Bulletin of Earthquake Engineering*, 8(2), 327-338, April 2010.

2. **Michel C.**, Guéguen P., Bard P.Y. “Dynamic parameters of structures extracted from ambient vibration : an aid for the seismic vulnerability assessment of existing buildings”, *Soil Dynamics and Earthquake Engineering*, 28(8), 593-604, August 2008.

1. Guéguen P., **Michel C.**, LeCorre L. “A simplified approach for vulnerability assessment in moderate-to-low seismic hazard regions : application to Grenoble (France)”, *Bulletin of Earthquake Engineering*, 5(3), 467-490, August 2007.

## Chapitres d’ouvrages

**Michel C.**, Guéguen P., “Méthode expérimentale : utilisation des vibrations ambiantes pour réduire l’incertitude des courbes de vulnérabilité”, in *Vulnérabilité sismique des constructions*, Hermes Science publication et Lavoisier Eds, ISBN 978-2-7462-3814-5, April 2013.

**Michel C.**, Guéguen P., “Experimental method : Contribution of Ambient Vibration Recordings to the Vulnerability Assessment”, in *Seismic Vulnerability of Structures*, John Wiley & Sons, Inc., USA, ISTE Ltd, UK, ISBN 978-1-84821-524-5, 161-212, February 2013.

Clinton J., Cauzzi C., Fäh D., **Michel C.**, Zweifel P., Olivieri M., Cua G., Haslinger F. and Giardini D. “The current state of strong motion monitoring in Switzerland”, in *Earthquake Data in Engineering Seismology : Predictive Models, Data Management and Networks*, S. Akkar, P. Gülkan, and T. V. Eck (Editors), Springer, Dordrecht, 14, 219-233, 2011.

## Actes de conference (depuis 2008)

**Michel C.**, Hannewald P., Lestuzzi P., Fäh D., Husen S., Roth M., "Earthquake scenarios for school buildings in the city of Basel (Switzerland)", in Proceedings of 16th World Conference on Earthquake Engineering (16WCEE), paper 1491, Santiago (Chile), January 2017.

Hobiger M., Fäh D., Scherrer C., **Michel C.**, Duvernay B., Clinton J., Cauzzi C., Weber F., "The renewal project of the Swiss Strong Motion Network SSMNet", in Proceedings of 16th World Conference on Earthquake Engineering (16WCEE), paper 433, Santiago (Chile), January 2017.

Hobiger M., Fäh D., **Michel C.**, Burjánek J., Maranò S., Poggi V., Pilz M., Kleinbrod U., Edwards B., Imperatori W. and Roten D., "Site Characterization in the Framework of the Renewal of the Swiss Strong Motion Network (SSMNet)", in Proceedings of the 5th IASPEI / IAEE International Symposium : Effects of Surface Geology on Seismic Motion (ESG 2016), Taipei, Taiwan, August 2016.

Fäh D., Burjanek J., Hobiger M., **Michel C.**, Maranò S., Poggi V., Pilz M., Kleinbrod U., Edwards B., Imperatori W. and Roten D., "Assessment of the complex seismic response of geological structures", in Proceedings of the 5th IASPEI / IAEE International Symposium : Effects of Surface Geology on Seismic Motion (ESG 2016), Taipei, Taiwan, August 2016.

**Michel C.**, Fäh D., Lestuzzi P., Hannewald P., Husen S., "Detaillierte Erdbeben-Schadenszenarien für die Schulgebäude im Kanton Basel-Stadt", in Dokumentation SIA D 0255 Erdbeben und bestehenden Bauten, 14. D-A-CH-Tagung, Zürich, August 2015, in German.

Guéguen P., Gallipoli M.R., Navarro M., Masi A., **Michel C.**, Guillier B., Karakostas C., Lekidis V., Mucciarelli M., Ponzio F., Spina D., "Testing buildings using ambient vibrations for earthquake engineering : a European review", in Proceedings of the 2nd European Conference on Earthquake Engineering and Seismology (2ECEES), Paper 569, Istanbul, Turkey, 25-29 August 2014.

**Michel C.**, Edwards B., Poggi V., Fäh D., "Ground motion amplification in alpine regions : new insights from the Swiss Strong Motion Network", in Proceedings of Vienna Congress in Recent Advances of Earthquake Engineering and Structural Dynamics (VEESD 2013), Paper No. 264, Vienna, Austria, 28-30 August 2013.

**Michel C.**, Cauzzi C., Fäh D., Clinton J., Zweifel P., Kästli P., "The Swiss strong-motion network : high-quality strong-motion monitoring in a region of low-to-moderate seismicity", in Proceedings of 15th World Conference on Earthquake Engineering (15WCEE), paper 1470, Lisbon (Portugal), September 2012.

**Michel C.**, Guéguen P., "Seismic vulnerability assessment based on vibration data at the city-scale", in Proceedings of 15th World Conference on Earthquake Engineering (15WCEE), paper 2826, Lisbon (Portugal), September 2012.

Burjanek J., Fäh D., **Michel C.**, Dalguer L. A., Baumann C., Gassner-Stamm G., Poggi V., Roten D., Laue J., Marin A., Lestuzzi P., Karbassi A., "Earthquake damage scenario in Visp (Switzerland) : from active fault to building damage", in Proceedings of 15th World Conference on Earthquake Engineering (15WCEE), paper 5472, Lisbon (Portugal), September 2012.

**Michel C.**, Cauzzi C., Deichmann N., Grolimund R., Husen S., Clinton J., Kästli P., Haslinger F., Fäh D., "Lessons from the 2012 ML=4.2 earthquake in Zug", in 15. Symposium Bauwerksdynamik und Erschütterungsmessungen, Dübendorf, June 2012, invited paper.

Guéguen P., **Michel C.**, Jolivet V., Augère B., Valla M., Totems J., Schweitzer A.-S., "Remote assessment of building frequencies using LIDAR", Proceedings of the 4th International Conference on Experimental Vibration Analysis for Civil Engineering Structures (EVACES), Varenna, Italy, 3-5 October 2011, p547-552.

Guéguen P., **Michel C.**, “Time-frequency analysis of small frequency variations in civil engineering structures under weak and strong motion under reassignment methods”, Proceedings of the 4th International Conference on Experimental Vibration Analysis for Civil Engineering Structures (EVACES), Varenna, Italy, 3-5 October 2011, p399-406.

**Michel C.**, Lestuzzi P., Guéguen P., “Quantification de la chute de fréquence dans le bâti en maçonnerie moderne : des vibrations ambiantes aux mouvements forts”, actes du 8e colloque de l’Association Française de Génie Parasismique (AFPS), Ecole des Ponts-et-Chaussées, Paris, France, Septembre 2011, paper 29.

**Michel C.**, Fäh D., Poggi V., Burjanek J., Cauzzi C., Kästli P. and Clinton J. “Site characterization strategy for the Swiss Strong Motion Network”, Proceedings of 4th IASPEI / IAEE International Symposium Effects of Surface Geology on Seismic Motion (ESG 2011), Santa Barbara, California, August 23–26, 2011.

**Michel C.**, Guéguen P., Lestuzzi P., “Observed non-linear soil-structure interaction from low amplitude earthquakes and forced-vibration recordings”, Proceedings of the 8th International Conference on Structural Dynamics, EURO DYN 2011, Leuven, Belgium, 4-6 July 2011, G. De Roeck, G. Degrande, G. Lombaert, G. Müller (eds.), ISBN 978-90-760-1931-4, pp. 601-606.

**Michel C.**, Oropeza M., Lestuzzi P., Kölz E., Duvernay B. “Probabilistic seismic risk analysis of existing buildings in regions with moderate seismicity”, in Proceedings of 14th European Conference on Earthquake Engineering (14ECEE), Ohrid (Macedonia), September 2010.

Oropeza M., **Michel C.**, and Lestuzzi P. “A simplified analytical methodology for fragility curve estimation in existing buildings”, in Proceedings of 14th European Conference on Earthquake Engineering (14ECEE), Ohrid (Macedonia), September 2010.

Oropeza M., **Michel C.**, and Lestuzzi P. “Fragility Functions for Seismic Risk in regions with Moderate Seismicity”, in Proceedings of 9th US National and 10th Canadian Conference on Earthquake Engineering (9USN/10CCEE), 7, 5684-5693, Toronto (Canada), July 2010.

**Michel C.**, and Guéguen P. “Full scale dynamic behaviour of a RC-building under low-to-moderate seismic motions”, in Proceedings of 9th US National and 10th Canadian Conference on Earthquake Engineering (9USN/10CCEE), 2, 1571-1580, Toronto (Canada), July 2010.

Oropeza M., **Michel C.**, Bigler M. and Lestuzzi P. “New Analytical fragility curves for existing URM buildings in regions with moderate seismicity”, in Proceedings of 8th International Masonry Conference, Dresden (Germany), July 2010.

**Michel C.**, Lattion E., Oropeza M. and Lestuzzi P. “Erdbebenverletzbarkeitsfunktionen von einem typischen Schweizer Mauerwerksgebäude”, in Erdbeben und Mauerwerk, Proceedings of the 11. D-A-CH Tagung, SIA Dokumentation D 0231, Zürich, September 2009, in German.

**Michel C.**, Lattion E., Oropeza M. and Lestuzzi P. “Vulnerability assessment of existing masonry buildings in moderate seismicity areas using experimental techniques”, in Proceedings of the 2009 Asian-Pacific Network of Centers for Earthquake Engineering Research (ANCER) Workshop, Urbana IL, August 2009.

Régnier J., **Michel C.** “Contribution of ambient vibration recordings (soil and buildings) in post-seismic survey : 29 November 2007 Martinique earthquake”, in Proceedings of Provence’ 2009, Aix-en-Provence (France), July 2009.

**Michel C.**, Lestuzzi P., Guéguen P. "Analyse de vulnérabilité du bâti existant à l’aide d’enregistrements de vibrations in situ pour les régions à sismicité modérée", actes des VIIIe rencontres Archéologie Pathologie Sismicité (APS), Manosque, Décembre 2008.

Jolivet V., Guéguen P., **Michel C.**, Schweitzer A.-S. “On the full-scale dynamic behaviour of RC-buildings using coherent laser radar vibrometer”, in Proceedings of 14th World Conference on Earthquake Engineering (14WCEE), Beijing, October 2008.

**Michel C.**, Guéguen P. “Seismic vulnerability analysis of moderate seismicity areas using in situ experimental techniques : from the building to the city scale – Application to Grenoble and Pointe-à-Pitre (France)”, Proceedings of Seismic Risk 2008 – Earthquakes in North-Western Europe, 321-328, Liège, Belgium, September 2008.

## Rapports, bases de données (depuis 2008)

**Michel C.** and Fäh D. (2016). Basel earthquake risk mitigation – Computation of scenarios for school buildings, Technical Report, ETH-Zürich, Zürich, Switzerland, 69 pp. doi : 10.3929/ethz-a-010646514

Swiss Seismological Service (SED) at ETH Zurich (2015). The Site Characterization Database for Seismic Stations in Switzerland. Zurich : Federal Institute of Technology. doi : 10.12686/sed-stationcharacterizationdb <http://stations.seismo.ethz.ch>

Schweizerischer Erdbebendienst (SED), “Erneuerung des Starkbebennetzwerkes in der Schweiz, Jahresbericht 2013“, Report SED/SSMNet\_R/R/004/20131030, ETH Zürich, October 2013, in German.

Schweizerischer Erdbebendienst (SED), “Erneuerung des Starkbebennetzwerkes in der Schweiz, Jahresbericht 2012“, Report SED/SSMNet\_R/R/003/20121030, ETH Zürich, October 2012, in German.

Schweizerischer Erdbebendienst (SED), “Erneuerung des Starkbebennetzwerkes in der Schweiz, Jahresbericht 2011“, Report SED/SSMNet\_R/R/002/20111028, ETH Zürich, October 2011, in German.

Schweizerischer Erdbebendienst (SED), “Erneuerung des Starkbebennetzwerkes in der Schweiz, Jahresbericht 2010“, Report SED/SSMNet\_R/R/001/20101029, ETH Zürich, October 2010, in German.

**Michel C.**, Oropeza M., Lestuzzi P. “Seismic Vulnerability of Existing Masonry Buildings : Final Research Report 2009“, Research Report, n°10, EPFL-IMAC, Lausanne, December 2009.

**Michel C.**, Oropeza M., Lestuzzi P. “COGEAR Project Module 1c : Vulnerability and Risk“, COGEAR Deliverables 1c.1.1 & 1c.1.2 : Validate the building inventory and important infrastructure in the test area ; Development of theoretical fragility functions, EPFL-IMAC, Lausanne, December 2009.

**Michel C.**, Oropeza M. “Post-earthquake survey in L’Aquila (Italy). Ambient vibration experiment report“, Research Report, n°9, EPFL-IMAC, Lausanne, October 2009.

**Michel C.**, Lestuzzi P., Oropeza M., Lattion E. “Seismic Vulnerability of Swiss Masonry buildings : Findings and issues“, Research Report, n°8, EPFL-IMAC, Lausanne, December 2008.

Schlupp A., C. Sira, M. Cara, S. Bazin, C. Michel, J. Régnier, C. Beauval, N. Feuillet, J.-B. De Chabaliér, A.-V. Barras, S. Auclair, M.-P. Bouin, C. Duclos, M. Granet (2008) - Séisme de Martinique du 29 novembre 2007, rapport du BCSF : synthèse sismologique et étude macrosismique, BCSF2008-R1, 132 p.

Régnier J., **Michel C.**, Compte rendu de mission post-sismique en Martinique - Séisme du 29 novembre 2007, CETE Méditerranée, Mai 2008.

# Remerciements

Je remercie les membres du jury qui ont accepté de prendre DU temps pour évaluer mon travail, en particulier les rapporteurs de ce document : Françoise Courboux, Fabrice Cotton et Guido de Roeck ainsi que les examinateurs Helle Pedersen et Frédéric Dufour. Un grand merci à Christine Bigot de l'Ecole Doctorale pour son assistance sans faille.

Je tiens également à remercier les personnes qui ont relu tout ou partie de ce document contribuant ainsi à son amélioration : Anne Bouscasse, Philippe Guéguen et Remo Grolimund ainsi que Thomas Wenk pour avoir fourni la Fig. 3.3. Je remercie également les instituts qui m'ont accueilli et ainsi permis de réaliser ces travaux (ISTERRE Grenoble, IMAC-EPFL Lausanne et ETHZ-SED Zurich) ainsi que les organismes qui les ont financés et plus particulièrement Philippe Guéguen, Pierino Lestuzzi et Donat Fäh. Enfin, je remercie mes co-auteurs sans lesquels ces travaux n'auraient pu être menés à bien.

# Bibliographie

- AKKAR, S., SANDIKKAYA, M. a. et AY, B. O. (2014a). Compatible ground-motion prediction equations for damping scaling factors and vertical-to-horizontal spectral amplitude ratios for the broader Europe region. *Bulletin of Earthquake Engineering*, 12:517–547.
- AKKAR, S., SANDIKKAYA, M. a. et BOMMER, J. J. (2014b). Empirical ground-motion models for point- and extended-source crustal earthquake scenarios in Europe and the Middle East. *Bulletin of Earthquake Engineering*, 12:359–387.
- ALFORD, J. L. et HOUSNER, G. W. (1953). A dynamic test of a four-story reinforced concrete building. *Bulletin of the Seismological Society of America*, 43(1):7–16.
- ARDHUIN, F., GUALTIERI, L. et STUTZMANN, E. (2015). How ocean waves rock the Earth : Two mechanisms explain microseisms with periods 3 to 300s. *Geophysical Research Letters*, 42(3):765–772.
- BAUMANN, C., BURJÁNEK, J., MICHEL, C., FÄH, D. et DALGUER, L. a. (2013). Fault zone signatures from ambient vibration measurements : a case study in the region of Visp (Valais, Switzerland). *Swiss Journal of Geosciences*, 106(3):529–541.
- BAUMANN, C. et DALGUER, L. A. (2014). Evaluating the compatibility of dynamic rupture-based synthetic ground motion with empirical ground-motion prediction equation. *Bulletin of the Seismological Society of America*, 104(2):634–652.
- BEN-MENACHEM, A. (1995). Review A Concise History of Mainstream Seismology : Origins, Legacy, and Perspectives. *Bulletin of the Seismological Society of America*, 85(4):1202–1225.
- BERTIL, D. (2013). Réseau accélérométrique du BRGM en Guadeloupe et Martinique. Rapport technique, Bureau des Recherches Géologiques et Minières (BRGM), Orléans, France.
- BETTIG, B., BARD, P. Y., SCHERBAUM, F., RIEPL, J., COTTON, F., CORNOU, C. et HATZFELD, D. (2001). Analysis of dense array noise measurements using the modified spatial auto-correlation method (SPAC) : Application to the Grenoble area. *Bollettino di Geofisica Teorica ed Applicata*, 42(3-4):281–304.
- BLUME, J. A. (1935). A machine for setting structures and ground into forced vibrations. *Bulletin of the Seismological Society of America*, 25(4):361–379.
- BONNEFOY-CLAUDET, S., COTTON, F. et BARD, P. (2006). The nature of noise wavefield and its applications for site effects studies. *Earth-Science Reviews*, 79(3-4):205–227.
- BOWDEN, D. C., TSAI, V. C. et LIN, F. C. (2015). Site amplification, attenuation, and scattering from noise correlation amplitudes across a dense array in Long Beach, CA. *Geophysical Research Letters*, 42(5):1360–1367.
- BRADY, A. G. (2009). Strong-motion accelerographs : Early history. *Earthquake Engineering and Structural Dynamics*.
- BRUNE, J. N. (1970). Tectonic stress and the spectra of seismic shear waves from earthquakes. *Journal of Geophysical Research*, 75(26):4997–5009.
- BURJÁNEK, J., EDWARDS, B. et FÄH, D. (2014). Empirical evidence of local seismic effects at sites with pronounced topography : a systematic approach. *Geophysical Journal International*, 197(1):608–619.
- BYERLY, P., HESTER, J., MARSHALL, K. et MARSCHALL, K. (1931). The natural periods of vibration of some tall buildings in San Francisco. *Bulletin of the Seismological Society of America*, 21(4):268–276.
- CARDER, D. S. (1936a). Observed vibrations of buildings. *Bulletin of the Seismological Society of America*, 26(3):245–277.
- CARDER, D. S. (1936b). Observed vibrations of steel water towers. *Bulletin of the Seismological Society of America*, 26(1):69–81.
- CARDER, D. S. (1936c). *Vibration observations*, chapitre 5, pages 49–106. Numéro Spec. Publ. 201. U.S. Coast and Geodetic Survey.

- CARDER, D. S. (1937). Observed vibrations of bridges. *Bulletin of the Seismological Society of America*, 27(4):267–289.
- CAUZZI, C., EDWARDS, B., FÄH, D., CLINTON, J., WIEMER, S., KASTLI, P., CUA, G. et GIARDINI, D. (2015). New predictive equations and site amplification estimates for the next-generation Swiss ShakeMaps. *Geophysical Journal International*, 200:421–438.
- CAUZZI, C. et FACCIOLI, E. (2008). Broadband (0.05 to 20 s) prediction of displacement response spectra based on worldwide digital records. *Journal of Seismology*, 12(4):453–475.
- CHOPRA, A. K. et WANG, J.-T. (2010). Earthquake response of arch dams to spatially varying ground motion. *Earthquake Engineering and Structural Dynamics*, 39:887–906.
- CLINTON, J., BRADFORD, S. C., HEATON, T. H. et FAVELA, J. (2006). The Observed Wander of the Natural Frequencies in a Structure. *Bulletin of the Seismological Society of America*, 96(1):237–257.
- CLINTON, J., CAUZZI, C., FÄH, D., MICHEL, C., ZWEIFEL, P., OLIVIERI, M., CUA, G., HASLINGER, F. et GIARDINI, D. (2011). The Current State of Strong Motion Monitoring in Switzerland. In AKKAR, S., GÜLKAN, P. et van ECK, T., éditeurs : *Earthquake Data in Engineering Seismology*, volume 14 de *Geotechnical, Geological, and Earthquake Engineering*, pages 219–233. Springer Netherlands, Dordrecht.
- COBURN, A. et SPENCE, R. (2002). *Earthquake Protection*. John Wiley & Sons, Ltd., second édition.
- DARBRE, G. R., DE SMET, C. A. M. et KRAEMER, C. (2000). Natural frequencies measured from ambient vibration response of the arch dam of Mauvoisin. *Earthquake Engineering and Structural Dynamics*, 29:577–586.
- DE BIASIO, M., GRANGE, S., DUFOUR, F., ALLAIN, F. et PETRE-LAZAR, I. (2014). A simple and efficient intensity measure to account for nonlinear structural behavior. *Earthquake Spectra*, 30(4):1403–1426.
- de QUERVAIN, A. (1922). Der transportable Seismograph mit drei Komponenten (System Quervain-Piccard). Rapport technique, Erdbebendienst der Schweizerischen Meteorologischen Zentralanstalt, Zürich, Switzerland.
- DERLETH, C. (1921). Vibration of the Sather Tower. *Bulletin of the Imperial Earthquake Investigation Committee*, 9(3):106–109.
- DOLCE, M., NICOLETTI, M., DE SORTIS, A., MARCHESINI, S., SPINA, D. et TALANAS, F. (2017). Osservatorio sismico delle strutture : the Italian structural seismic monitoring network. *Bulletin of Earthquake Engineering*, 15(2):621–641.
- DOUGLAS, J. et EDWARDS, B. (2016). Recent and future developments in earthquake ground motion estimation. *Earth-Science Reviews*, 160(1):203–219.
- EDWARDS, B. et FÄH, D. (2014). Ground Motion Prediction Equations. Rapport technique, Swiss Seismological Service, ETH Zurich, Zürich, Switzerland.
- EDWARDS, B., KRAFT, T., CAUZZI, C., KASTLI, P. et WIEMER, S. (2015). Seismic monitoring and analysis of deep geothermal projects in St Gallen and Basel, Switzerland. *Geophysical Journal International*, 201(2):1020–1037.
- EDWARDS, B., MICHEL, C., POGGI, V. et FÄH, D. (2013). Determination of Site Amplification from Regional Seismicity : Application to the Swiss National Seismic Networks. *Seismological Research Letters*, 84(4):611–621.
- EGEN, P. N. C. (1828). Ueber das Erdbeben in den Rhein- und Niederlanden vom 23. February 1828. *Annalen der Physik und Chemie*, 13:153–163.
- ERI (1965). Strong Motion Earthquake Records in Japan Volume 2. Rapport technique, Earthquake Research Institute, University of Tokyo, Tokyo, Japan.
- ESPOSITO, S. et IERVOLINO, I. (2012). Spatial Correlation of Spectral Acceleration in European Data. *Bulletin of the Seismological Society of America*, 102(6):2781–2788.
- FAENZA, L. et MICHELINI, A. (2010). Regression analysis of MCS intensity and ground motion parameters in Italy and its application in ShakeMap. *Geophysical Journal International*, 180:1138–1152.
- FÄH, D., MOORE, J. R., BURJÁNEK, J., IOSIFESCU, I., DALGUER, L. A., DUPRAY, F., MICHEL, C., WOESSNER, J., VILLIGER, A., LAUE, J., MARSCHALL, I., GISCHIG, V., LOEW, S., MARIN, A., GASSNER-STAMM, G., ALVAREZ-RUBIO, S., BALDERER, W., KÄSTLI, P., GIARDINI, D., IOSIFESCU, C., HURNI, L., LESTUZZI, P., KARBASSI, A., BAUMANN, C., GEIGER, A., FERRARI, A., LALLOUI, L., CLINTON, J. et DEICHMANN, N. (2012). Coupled Seismogenic Geohazards in Alpine Region. *Bolletino di Geofisica Teorica ed Applicata*, 53(December):485–508.
- FIELD, E. H. (1996). Spectral Amplification in a Sediment-Filled Valley Exhibiting Clear Basin-Edge-Induced Waves. *Bulletin of the Seismological Society of America*, 86(4):991–1005.
- FOREL, F.-A. (1884). Les tremblements de terre étudiés par la commission sismologique suisse pendant l'année 1881. *Archives des sciences physiques et naturelles*, 11:147–182.



- FREEMAN, J. R. (1932). *Earthquake Damage and Earthquake Insurance*. McGraw-Hill, New-York.
- GAROFALO, F., FOTI, S., HOLLENDER, F., BARD, P., CORNOU, C., COX, B., DECHAMP, A., OHRNBERGER, M., PERRON, V., SICILIA, D., TEAGUE, D. et VERGNAULT, C. (2016a). InterPACIFIC project : Comparison of invasive and non-invasive methods for seismic site characterization. Part II : Inter-comparison between surface-wave and borehole methods. *Soil Dynamics and Earthquake Engineering*, 82:241–254.
- GAROFALO, F., FOTI, S., HOLLENDER, F., BARD, P., CORNOU, C., COX, B., OHRNBERGER, M., SICILIA, D., ASTEN, M., DI GIULIO, G., FORBRIGER, T., GUILLIER, B., HAYASHI, K., MARTIN, A., MATSUSHIMA, S., MERCERAT, D., POGGI, V. et YAMANAKA, H. (2016b). InterPACIFIC project : Comparison of invasive and non-invasive methods for seismic site characterization. Part I : Intra-comparison of surface wave methods. *Soil Dynamics and Earthquake Engineering*, 82:222–240.
- GISLER, M., KOZAK, J. et VANEK, J. (2008). The 1855 Visp (Switzerland) Earthquake : A Milestone in Macroseismic Methodology ? In FRÉCHET, J., MEGHRAOUI, M. et STUCCHI, M., éditeurs : *Historical Seismology*, pages 231–247. Springer.
- GOULET, J.-A., MICHEL, C. et DER KIUREGHIAN, A. (2015). Data-driven post-earthquake rapid structural safety assessment. *Earthquake Engineering and Structural Dynamics*, 44(4):549–562.
- GOULET, J.-A., MICHEL, C. et SMITH, I. F. (2013). Hybrid probabilities and error-domain structural identification using ambient vibration monitoring. *Mechanical Systems and Signal Processing*, 37(1-2):199–212.
- GOULET, J.-A., TEXIER, M., MICHEL, C., SMITH, I. F. et CHOUINARD, L. E. (2014). Quantifying the Effects of Modeling Simplifications for Structural Identification of Bridges. *Journal of Bridge Engineering*, 19(1):59–71.
- GRÜNTAL, G., MUSSON, R. M. W., SCHWARTZ, J. et STUCCHI, M. (1998). *European Macroseismic Scale 1998*, volume 15. Cahiers du Centre Européen de Géodynamique et de Séismologie, Luxembourg.
- GRÜNTAL, G., MUSSON, R. M. W., SCHWARTZ, J., STUCCHI, M. et LEVRET, A. (2001). *L'Echelle Macrosismique Européenne*, volume 19. Cahiers du Centre Européen de Géodynamique et de Séismologie, Luxembourg.
- GUÉGUEN, P. (2012). Experimental analysis of the seismic response of one base-isolation building according to different levels of shaking : example of the Martinique earthquake (2007/11/29) Mw 7.3. *Bulletin of Earthquake Engineering*, 10(4):1285–1298.
- GUÉGUEN, P., JOLIVET, V., MICHEL, C. et SCHVEITZER, A.-S. (2010). Comparison of velocimeter and coherent lidar measurements for building frequency assessment. *Bulletin of Earthquake Engineering*, 8(2):327–338.
- GUIDOBONI, E. et EBEL, J. E. (2009). *Earthquakes and Tsunamis in the Past : a Guide to techniques in historical seismology*. Cambridge University Press.
- HALL, E. E. (1912). Vibrations of Buildings Due to Street Traffic. *Engineering News*, 68(5):198–201.
- HANS, S., BOUTIN, C., IBRAIM, E. et ROUSSILLON, P. (2005). In situ experiments and seismic analysis of existing buildings. Part I : experimental investigations. *Earthquake Engineering and Structural Dynamics*, 34(12):1513–1529.
- HASHEMI, A. et MOSALAM, K. M. (2006). Shake-table experiment on reinforced concrete structure containing masonry infill wall. *Earthquake Engineering and Structural Dynamics*, 35(14):1827–1852.
- HAYES, G. P., MCNAMARA, D. E., SEIDMAN, L. et ROGER, J. (2014). Quantifying potential earthquake and tsunami hazard in the Lesser Antilles subduction zone of the Caribbean region. *Geophysical Journal International*, 196(1):510–521.
- HOBIGER, M., CORNOU, C., BARD, P.-Y., LE BIHAN, N. et IMPERATORI, W. (2016). Analysis of seismic waves crossing the Santa Clara Valley using the three-component MUSIQUE array algorithm. *Geophysical Journal International*.
- HOLDEN, E. S. (1888). Note on Earthquake-Intensity in San Francisco. *American Journal of Science*, 35(210):427–431.
- HOUSNER, G. W. et BRADY, A. G. (1963). Natural periods of vibration of buildings. *Journal of Engineering Mechanics*, 89:31–65.
- HUDSON, D. E. (1962). Dynamic tests of buildings and special structures. In *Experimental techniques in shock and vibration*, pages 81–91, New York. ASME.
- HUDSON, D. E., ALFORD, J. L. et HOUSNER, G. W. (1952). Reponse of a structure to an explosive-generated ground shock. Rapport technique, Earthquake Engineering Research Laboratory, California Institute of Technology, Pasadena (California).
- ISHIMOTO, M. et TAKAHASI, R. (1929). Mesures des mouvements d'un bâtiment dans des conditions tranquilles. *Bulletin of the Earthquake Research Institute, Tokyo*, 7(1):175–184.
- KANAI, K. et TANAKA, T. (1951). Vibration test of actual reinforced concrete building. *Bulletin of the Earthquake Research Institute, Tokyo*, 29(4):617–626.
- KANAI, K., TANAKA, T. et SUZUKI, T. (1949). Vibration experiments with the actual buildings. *Bulletin of the Earthquake Research Institute, Tokyo*, 27(1-4):91–95.

- KANAI, K. et YOSHIZAWA, S. (1952). On the damping of vibration of actual buildings I. *Bulletin of the Earthquake Research Institute, Tokyo*, 30(2):121–126.
- KIKUCHI, D. (1904). Recent Seimological Investigations in Japan. *Publications of the Earthquake Investigation Committee in Foreign Languages*, 19.
- LAROSE, E., CARRIÈRE, S., VOISIN, C., BOTTELIN, P., BAILLET, L., GUÉGUEN, P., WALTER, F., JONGMANS, D., GUILLIER, B., GARAMBOIS, S., GIMBERT, F. et MASSEY, C. (2015). Environmental seismology : What can we learn on earth surface processes with ambient noise? *Journal of Applied Geophysics*, 116:62–74.
- LEMOINE, A., DOUGLAS, J. et COTTON, F. (2012). Testing the Applicability of Correlations between Topographic Slope and VS30 for Europe. *Bulletin of the Seismological Society of America*, 102(6):2585–2599.
- LESUEUR, C., CARA, M., SCOTTI, O., SCHLUPP, A. et SIRA, C. (2013). Linking ground motion measurements and macroseismic observations in France : A case study based on accelerometric and macroseismic databases. *Journal of Seismology*, 17:313–333.
- MALLET, R. (1862). *Great Neapolitan Earthquake of 1857 : The First Principles of Observational Seismology*. Chapman and Hall, London, UK.
- MANEA, E. F., MICHEL, C., POGGI, V., FÄH, D., RADULIAN, M. et BALAN, F. S. (2016). Improving the shear wave velocity structure beneath Bucharest (Romania) using ambient vibrations. *Geophysical Journal International*, 207(2):848–861.
- MARANÒ, S., RELLER, C., LOELIGER, H. A. et FÄH, D. (2012). Seismic waves estimation and wavefield decomposition : Application to ambient vibrations. *Geophysical Journal International*, 191(1):175–188.
- MICHEL, C. (2007). *Vulnérabilité Sismique de l'échelle du bâtiment à celle de la ville - Apport des techniques expérimentales in situ - Application à Grenoble*. Thèse de doctorat, UJF Grenoble.
- MICHEL, C., CROWLEY, H., HANNEWALD, P., LESTUZZI, P. et FÄH, D. (2017a). Deriving fragility functions from bilinearized capacity curves using the conditional spectrum. *Earthquake Engineering & Structural Dynamics*, in review.
- MICHEL, C., EDWARDS, B., POGGI, V., BURJÁNEK, J., ROTEN, D., CAUZZI, C. et FÄH, D. (2014a). Assessment of Site Effects in Alpine Regions through Systematic Site Characterization of Seismic Stations. *Bulletin of the Seismological Society of America*, 104(6):2809–2826.
- MICHEL, C., FÄH, D., EDWARDS, B. et CAUZZI, C. (2016). Site amplification at the city scale in Basel (Switzerland) from geophysical site characterization and spectral modelling of recorded earthquakes. *Physics and Chemistry of the Earth, Parts A/B/C*.
- MICHEL, C. et GUÉGUEN, P. (2008). Seismic vulnerability analysis of moderate seismicity areas using in situ experimental techniques : from the building to the city scale - Application to Grenoble and Pointe-à-Pitre (France). In *Seismic Risk 2008 - Earthquakes in North-Western Europe*, pages 321–328, Liège, Belgium.
- MICHEL, C. et GUÉGUEN, P. (2010). Time-Frequency Analysis of Small Frequency Variations in Civil Engineering Structures Under Weak and Strong Motions Using a Reassignment Method. *Structural Health Monitoring*, 9(2):159–171.
- MICHEL, C., GUÉGUEN, P. et BARD, P. (2008). Dynamic parameters of structures extracted from ambient vibration measurements : An aid for the seismic vulnerability assessment of existing buildings in moderate seismic hazard regions. *Soil Dynamics and Earthquake Engineering*, 28(8):593–604.
- MICHEL, C., GUÉGUEN, P. et CAUSSE, M. (2012). Seismic vulnerability assessment to slight damage based on experimental modal parameters. *Earthquake Engineering and Structural Dynamics*, 41(1):81–98.
- MICHEL, C., GUÉGUEN, P., EL AREM, S., MAZARS, J. et KOTRONIS, P. (2010a). Full-scale dynamic response of an RC building under weak seismic motions using earthquake recordings, ambient vibrations and modelling. *Earthquake Engineering and Structural Dynamics*, 39(4):419–441.
- MICHEL, C., GUÉGUEN, P. et LESTUZZI, P. (2011a). Observed non-linear soil-structure interaction from low amplitude earthquakes and forced-vibration recordings. In DE ROECK, G., DEGRANDE, G., LOMBAERT, G. et ÄMÜLLER, G., éditeurs : *8th International Conference on Structural Dynamics, EURO DYN 2011*, pages 601–606, Leuven, Belgium.
- MICHEL, C., GUÉGUEN, P., LESTUZZI, P. et BARD, P. (2010b). Comparison between seismic vulnerability models and experimental dynamic properties of existing buildings in France. *Bulletin of Earthquake Engineering*, 8(6):1295–1307.
- MICHEL, C., HANNEWALD, P., LESTUZZI, P., FÄH, D. et HUSEN, S. (2017b). Probabilistic mechanics-based loss scenarios for school buildings in Basel (Switzerland). *Bulletin of Earthquake Engineering*, 15(4):1471–1496.
- MICHEL, C., LESTUZZI, P. et LACAVER, C. (2014b). Simplified non-linear seismic displacement demand prediction for low period structures. *Bulletin of Earthquake Engineering*, 12(4):1563–1581.

- MICHEL, C. et OROPEZA, M. (2009). Post-earthquake survey in L'Aquila (Italy) - Ambient vibration experiment report. Rapport technique 9, Ecole Polytechnique Fédérale de Lausanne, Applied Computing and Mechanics Laboratory (EPFL-IMAC), Lausanne, Switzerland.
- MICHEL, C., OROPEZA, M. et LESTUZZI, P. (2010c). Probabilistic seismic risk analysis of existing buildings in regions with moderate seismicity. In *14th European Conference on Earthquake Engineering (14ECEE)*, Ohrid, Macedonia.
- MICHEL, C., ZAPICO, B., LESTUZZI, P., MOLINA, F. J. et WEBER, F. (2011b). Quantification of fundamental frequency drop for unreinforced masonry buildings from dynamic tests. *Earthquake Engineering and Structural Dynamics*, 40:1283–1296.
- MILNE, J. (1888). The Movement produced in certain Buildings by Earthquakes. *Transactions of the Seismological Society of Japan*, 12:67–75.
- NAKAMURA, Y. (1989). A method for dynamic characteristics estimation of subsurface using microtremor on the ground surface. *Quarterly Report of the Railway Technical Research Institute*, 30(1):25–33.
- OMORI, F. (1900). Earthquake Measurement in a Brick Building. *Publications of the Earthquake Investigation Committee in Foreign Languages*, 4:7–11.
- OMORI, F. (1902). On the Deflection and Vibration of Railway Bridges. *Publications of the Earthquake Investigation Committee in Foreign Languages*, 9:1–61.
- OMORI, F. (1903a). Motion of a Brick Wall Produced by Earthquakes. *Publications of the Earthquake Investigation Committee in Foreign Languages*, 12:57–65.
- OMORI, F. (1903b). Note on the Vibration of Chimneys. *Publications of the Earthquake Investigation Committee in Foreign Languages*, 12:29–37.
- OMORI, F. (1903c). Note on the Vibration of Railway Bridge Piers. *Publications of the Earthquake Investigation Committee in Foreign Languages*, 12:39–55.
- OMORI, F. (1905). Earthquake Measurement in a Brick Building 3rd Paper. *Publications of the Earthquake Investigation Committee in Foreign Languages*, 20:73–83.
- OMORI, F. (1907a). The Deflection and Vibration of Railway Bridges. 2nd Paper. *Bulletin of the Imperial Earthquake Investigation Committee*, 1(4):172–190.
- OMORI, F. (1907b). Vibrations of a Railway Bridge Pier. *Bulletin of the Imperial Earthquake Investigation Committee*, 1(3):155–157.
- OMORI, F. (1910). Application of Seismographs to the Measurement of the Vibrations of Railway Bridge Piers. 3rd Paper. *Bulletin of the Imperial Earthquake Investigation Committee*, 4:33–93.
- OMORI, F. (1918). Vibration of Reinforced Concrete Chimneys. *Bulletin of the Imperial Earthquake Investigation Committee*, 9(1):1–29.
- OMORI, F. (1921a). Measurement of Vibration of Gojunotos, or 5-Story Buddhist Stupas (Pagodas). *Bulletin of the Imperial Earthquake Investigation Committee*, 9(3):110–152.
- OMORI, F. (1921b). Measurement of Vibration of the 660-foot Wireless Telegraph Station Tower at Haranomachi. *Bulletin of the Imperial Earthquake Investigation Committee*, 9(3):77–99.
- OMORI, F. (1921c). Vibration of a 12-story Brick Tower. *Bulletin of the Imperial Earthquake Investigation Committee*, 9(3):100–105.
- OMORI, F. (1922). The Semi-Destructive earthquake of April 26, 1922. *Seismological Notes (Imperial Earthquake Investigation Committee)*, 3:1–30.
- OROPEZA, M., MICHEL, C., BIGLER, M. et LESTUZZI, P. (2010). New analytical fragility curves for existing URM buildings in regions with moderate seismicity. In *8th International Masonry Conference*, pages 1491–1499.
- OTANI, S. (2008). The Dawn Of Structural Earthquake Engineering In Japan. In *14th World Conference on Earthquake Engineering (14WCEE)*.
- PARK, C. B., MILLER, R. D. et XIA, J. (1999). Multichannel analysis of surface waves. *Geophysics*, 64(3):800–808.
- PEER (2010). Concrete Column Blind Prediction Contest 2010.
- POGGI, V., EDWARDS, B. et FÄH, D. (2011). Derivation of a Reference Shear-Wave Velocity Model from Empirical Site Amplification. *Bulletin of the Seismological Society of America*, 101(1):258–274.

- POGGI, V., ERMERT, L., MICHEL, C. et FÄH, D. (2015). Modal analysis of 2-D sedimentary basin from frequency domain decomposition of ambient vibration array recordings. *Geophysical Journal International*, 200:615–626.
- POGGI, V. et FÄH, D. (2010). Estimating Rayleigh wave particle motion from three-component array analysis of ambient vibrations. *Geophysical Journal International*, 180(1):251–267.
- PSIMOULIS, P. A., HOULIE, N., MICHEL, C., MEINDL, M. et ROTHACHER, M. (2014). Long-period surface motion of the multipatch Mw9.0 Tohoku-Oki earthquake. *Geophysical Journal International*, 199(2):968–980.
- RÉGNIER, J. et MICHEL, C. (2008). Compte rendu de mission post- sismique en Martinique. Séisme du 29 novembre 2007. Rapport technique, CETE Méditerranée.
- RÉGNIER, J., MICHEL, C., BERTRAND, E. et GUÉGUEN, P. (2013). Contribution of ambient vibration recordings (free-field and buildings) for post-seismic analysis : The case of the Mw 7.3 Martinique (French Lesser Antilles) earthquake, November 29, 2007. *Soil Dynamics and Earthquake Engineering*, 50:162–167.
- RICHTER, C. F. (1935). An instrumental earthquake magnitude scale. *Bulletin of the Seismological Society of America*, 25:1–32.
- ROTEN, D., FÄH, D., OLSEN, K. B. et GIARDINI, D. (2008). A comparison of observed and simulated site response in the Rhône valley. *Geophysical Journal International*, 173(3):958–978.
- SCHLUPP, A., SIRA, C., CARA, M., BAZIN, S., MICHEL, C., RÉGNIER, J., BEAUVAL, C., FEUILLET, N., DE CHABALIER, J.-B., BARRAS, A.-V., AUCLAIR, S., BOUIN, M.-P., DUCLOS, C. et GRANET, M. (2008). Séisme de Martinique du 29 novembre 2007, rapport du BCSF : synthèse sismologique et étude macrosismique. Rapport technique, Bureau Central Sismologique Français (BCSF), Strasbourg, France.
- SCHWAB, P. et LESTUZZI, P. (2007). Assessment of the seismic non-linear behavior of ductile wall structures due to synthetic earthquakes. *Bulletin of Earthquake Engineering*, 5(1):67–84.
- SILVA, V., CROWLEY, H. et BAZZURRO, P. (2016). Exploring Risk-Targeted Hazard Maps for Europe. *Earthquake Spectra*, 32(2):1165–1186.
- SMIT, P. (1996). *Datenerfassung und Bestimmung der Abminderung der Bodenbewegung bei Erdbeben in der Schweiz*. Thèse de doctorat, Eidgenössische Technische Hochschule Zürich (ETHZ).
- SMITH, I. F. C. (2016). Studies of Sensor Data Interpretation for Asset Management of the Built Environment. *Frontiers in Built Environment*, 2:1–9.
- SPARKS, N. R. (1935). Building vibrations. *Bulletin of the Seismological Society of America*, 25:381–386.
- SUGINO, M., TAKIYAMA, N. et HAYASHI, Y. (2012). Maximum Response Evaluation of Traditional Wooden Buildings Based on Amplitude Dependency of Vibration Characteristics. In *World Conference on Timber Engineering (WCTE 2012)*, pages 12–19.
- TRIFUNAC, M. D. (2008). Early history of the response spectrum method. *Soil Dynamics and Earthquake Engineering*, 28(9):676–685.
- TRIFUNAC, M. D. (2009). 75th anniversary of strong motion observation - A historical review. *Soil Dynamics and Earthquake Engineering*, 29(4):591–606.
- VALLA, M., GUEGUEN, P., AUGÈRE, B., GOULAR, D. et PERRAULT, M. (2015). Remote Modal Study of Reinforced Concrete Buildings Using a Multipath Lidar Vibrometer. *Journal of Structural Engineering*, 141(1):D4014005.
- VELETSOS, A. S. et NEWMARK, N. M. (1960). Effect of inelastic behavior on the response of simple systems to earthquake motion. In *2nd World Conference on Earthquake Engineering*, volume 2, pages 895–912, Tokyo, Japan.
- WALD, D. J. et ALLEN, T. I. (2007). Topographic slope as a proxy for seismic site conditions and amplification. *Bulletin of the Seismological Society of America*, 97(5):1379–1395.
- WATHELET, M. (2008). An improved neighborhood algorithm : Parameter conditions and dynamic scaling. *Geophysical Research Letters*, 35(9):1–5.
- WORDEN, C. B., WALD, D. J., ALLEN, T. I., LIN, K., GARCIA, D. et CUA, G. (2010). A Revised Ground-Motion and Intensity Interpolation Scheme for ShakeMap. *Bulletin of the Seismological Society of America*, 100(6):3083–3096.

# Annexe : le spectre de réponse

Document préparé avec Felicitas Stein et Valerio Poggi.

Le spectre de réponse, inventé par Biot en 1932 (Trifunac, 2009), est utilisé en routine en sismologie de l'ingénieur et en génie parasismique depuis plusieurs décennies. Or, sa signification et les nuances entre le spectre en accélération et en déplacement et entre spectre et pseudo-spectre ne sont pas toujours bien comprises ni décrites dans les ouvrages spécialisés. Ce document a donc pour but de détailler ces définitions et de montrer quelles sont les limites des spectres et leur lien avec les autres mesures d'intensité du mouvement du sol comme le PGA, le PGV, etc.

## Definition of the response spectrum

The response spectrum at each angular frequency  $\omega$  with damping parameter  $\zeta$  is defined as the maximum response of the single-degree-of-freedom (SDOF) system with those characteristics.

**Equation of motion.** The equation of motion for the relative displacement of the SDOF system  $x$  under the ground acceleration  $\ddot{x}_g(t)$  is written as follows :

$$\frac{\partial^2 x}{\partial t^2} + 2\zeta\omega \frac{\partial x}{\partial t} + \omega^2 x = -\frac{\partial^2 x_g}{\partial t^2}$$

or

$$\ddot{x} + 2\zeta\omega\dot{x} + \omega^2 x = -\ddot{x}_g$$

The solution of this equation, i.e. the relative displacement of the SDOF system can be written as follows, using the Duhamel integral :

$$x(t) = -\frac{1}{\omega_D} \int_0^t \ddot{x}_g(\tau) \cdot e^{-\zeta\omega(t-\tau)} \cdot \sin(\omega_D(t-\tau)) d\tau$$

with  $\omega_D = \omega\sqrt{1-\zeta^2}$  the "damped" angular frequency. The displacement of the SDOF system corresponds to the convolution of the ground acceleration  $\ddot{x}_g(t)$  with a damped oscillator  $e^{-\zeta\omega t} \cdot \sin(\omega t)$ .

**Definition.** The displacement, velocity and acceleration response spectra are defined as the maximum **relative** displacement  $S_d(\omega, \zeta) = |x|_{max}$ , the maximum **relative** velocity  $S_v(\omega, \zeta) = |\dot{x}|_{max}$  and the maximum **absolute** acceleration  $S_a(\omega, \zeta) = |\ddot{x} + \ddot{x}_g|_{max}$  of the SDOF system, respectively. Using relative displacement and absolute acceleration is purely for engineering reasons : the relative displacements are related to the strains experienced by the structure, while the absolute acceleration is related to the seismic coefficient (elastic force in the SDOF system, see section 3.4). The absolute acceleration is also the one recorded by an accelerometer at the top of a structure.

In order to simplify the expressions of the response spectrum, one generally assumes  $\omega \approx \omega_D$ , which is true for low damping, and that the phase shifts do not change the maxima. The quantity  $\mathcal{S}_v$  is first defined :

$$\mathcal{S}_v(\omega, \zeta) = \left| \int_0^t \ddot{x}_g(\tau) \cdot e^{-\zeta\omega(t-\tau)} \cdot \sin(\omega(t-\tau)) d\tau \right|_{max}$$

The displacement, velocity and acceleration response spectra are then classically computed as follows :

$$\begin{aligned} S_d(\omega, \zeta) = |x|_{max} &\approx \frac{1}{\omega} \left| \int_0^t \ddot{x}_g(\tau) \cdot e^{-\zeta\omega(t-\tau)} \cdot \sin(\omega(t-\tau)) d\tau \right|_{max} = \frac{1}{\omega} \cdot \mathcal{S}_v(\omega, \zeta) \\ S_v(\omega, \zeta) = |\dot{x}|_{max} &\approx \left| - \int_0^t \ddot{x}_g(\tau) \cdot e^{-\zeta\omega(t-\tau)} \cdot \cos(\omega(t-\tau)) d\tau \right|_{max} \approx \mathcal{S}_v(\omega, \zeta) \\ S_a(\omega, \zeta) = |\ddot{x} + \ddot{x}_g|_{max} &\approx \omega \left| \int_0^t \ddot{x}_g(\tau) \cdot e^{-\zeta\omega(t-\tau)} \cdot \sin(\omega(t-\tau)) d\tau \right|_{max} = \omega \cdot \mathcal{S}_v(\omega, \zeta) \end{aligned}$$

Note that in this expression of  $S_a$ ,  $\ddot{x}_g$  has been neglected, which is not valid if  $\omega$  is large (see section 3.4).

## Pseudo-response spectra

Going back to the SDOF system with its mass  $m$  and stiffness  $k$ , the elastic force in the SDOF  $f_S(t) = k \cdot x(t)$ , can be written as  $f_S(t) = M \cdot \omega^2 \cdot x(t) = M \cdot A(t)$ , with  $A$  the pseudo-acceleration defined as  $A(t) = \omega^2 \cdot x(t)$ . The equation of motion can be rewritten as follows :

$$\ddot{x} + \ddot{x}_g = -\omega^2 x - 2\zeta\omega\dot{x} = -A - 2\zeta\omega\dot{x}$$

The pseudo-acceleration  $A(t)$  is therefore close, in absolute value, to the absolute acceleration of the SDOF if  $\zeta$  is small enough. Similarly, one defines the pseudo-velocity as  $V(t) = \omega \cdot x(t)$ , that is however different from the velocity of the SDOF :  $\dot{x} = -\frac{1}{2\zeta}\omega x - \frac{1}{2\zeta\omega}(\ddot{x} + \ddot{x}_g) = -\frac{1}{2\zeta}V - \frac{1}{2\zeta\omega}(\ddot{x} + \ddot{x}_g)$ .

The pseudo-spectral acceleration and velocity are then defined as follows :

$$\begin{aligned} PSA(\omega, \zeta) &= |A|_{max} = \omega^2 \cdot S_d(\omega, \zeta) \\ PSV(\omega, \zeta) &= |V|_{max} = \omega \cdot S_d(\omega, \zeta) \end{aligned}$$

The maximum elastic force in the system is therefore  $f_S = M \cdot PSA$ , which explains the interest of earthquake engineering in PSA, while  $S_a$ ,  $S_v$  and  $PSV$  are of minor interest.

PSA and  $S_a$  are very similar, but PSV and  $S_v$  can be quite different. In general, in the literature, spectral acceleration refers to pseudo-spectral acceleration.

### Limit when $\omega \rightarrow \infty$ ( $T \rightarrow 0$ )

For infinitely rigid oscillators ( $\omega \rightarrow \infty$ ), in the Duhamel integral,  $\frac{e^{-\zeta\omega t}}{\omega t} \rightarrow 0$  and  $\sin(\omega t)$  is finite, so  $S_d \rightarrow 0$ . The relative response of the SDOF system, including its displacement, velocity and acceleration tends to 0. Therefore,  $S_d$  and  $S_v$  tend to 0.

Similarly, using the Duhamel integral,  $PSV = \omega \cdot S_d$  tends to 0, because  $e^{-\zeta\omega t} \rightarrow 0$  and  $\sin(\omega t)$  is finite.

However, the (absolute) spectral acceleration  $S_a = |\ddot{x} + \ddot{x}_g|_{max} \rightarrow |\ddot{x}_g|_{max} = PGA$ , the Peak Ground Acceleration. Moreover, in the equation of motion  $\ddot{x} + 2\zeta\omega\dot{x} + \omega^2x = -\ddot{x}_g$ , the relative acceleration  $\ddot{x}$  and the pseudo-velocity  $\omega\dot{x}$  tend to 0 (see above), so that the equation tends to  $\omega^2x = -\ddot{x}_g$ . Therefore, the pseudo-spectral acceleration  $PSA \rightarrow |\ddot{x}_g|_{max} = PGA$ .

As a conclusion, for infinitely rigid oscillators ( $\omega \rightarrow \infty$ ,  $T \rightarrow 0$ ), the displacement, velocity and pseudo-velocity response spectra tend to 0 whereas the spectral and pseudo-spectral accelerations tend to the Peak Ground Acceleration (PGA). The SDOF system is fully attached to the ground and follows its motion without inertia.

### Limit when $\omega \rightarrow 0$ ( $T \rightarrow \infty$ )

For infinitely soft oscillators ( $\omega \rightarrow 0$ ),  $e^{-\zeta\omega t} \rightarrow 1$  and  $\frac{\sin(\omega t)}{\omega} \rightarrow t$ , so  $\ddot{x} \rightarrow \int_0^t \ddot{x}_g(\tau) \cdot (t - \tau) d\tau$ . This last integral can be calculated by parts :

$$\begin{aligned} \int_0^t \ddot{x}_g(\tau) \cdot (t - \tau) d\tau &= [\dot{x}_g(\tau) \cdot (t - \tau)]_0^t - \int_0^t \dot{x}_g(\tau) \cdot (-1) d\tau \\ &= \int_0^t \dot{x}_g(\tau) d\tau \\ &= x_g(t) \end{aligned}$$

The relative displacement tends therefore to the opposite of the ground displacement, so the relative velocity tends to the opposite of the ground velocity, as well as the relative acceleration

tends to the opposite of the ground acceleration. Therefore the absolute acceleration ( $\ddot{x} + \ddot{x}_g$ ) tends to 0. For such an infinitely soft oscillator, the system is not moving due to an extremely large inertia, whereas the ground is moving so that the relative displacement of the system is equal to the opposite of the displacement of the ground.

Finally, when  $\omega \rightarrow 0$ ,  $S_d \rightarrow |x_g(t)|_{max} = PGD$ , the Peak Ground Displacement and  $S_v \rightarrow |\dot{x}_g(t)|_{max} = PGV$ , the Peak Ground Velocity. However,  $PSA = \omega^2 \cdot S_d \rightarrow 0$  and  $PSV = \omega \cdot S_d \rightarrow 0$ .  $PSV$  and  $S_v$  are therefore diverging when  $\omega \rightarrow 0$ .

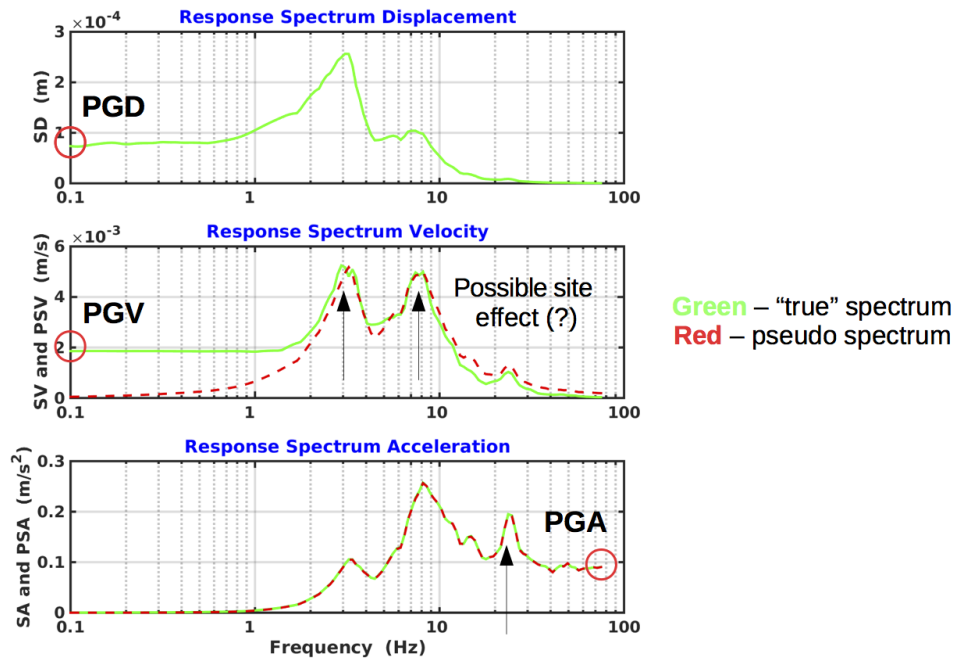


Figure 4 – Example of response spectra and pseudo response spectra.